AN OPTICAL STUDY OF HUMAN OCULAR DIMENSIONS

MARK CARDIFF MICHAEL DUNNE
Doctor of Philosophy

THE UNIVERSITY OF ASTON IN BIRMINGHAM
July 1987

The University of Aston in Birmingham

AN OPTICAL STUDY OF HUMAN OCULAR DIMENSIONS

Mark Cardiff Michael Dunne

Ph.D Thesis

July 1987

SUMMARY

Many workers have studied the ocular components which occur in eyes exhibiting differing amounts of central refractive error but few have ever considered the additional information that could be derived from a study of peripheral refraction.

Before now, peripheral refraction has either been measured in real eyes or has otherwise been modelled in schematic eyes of varying levels of sophistication. Several differences occur between measured and modelled results which, if accounted for, could give rise to more information regarding the nature of the optical and retinal surfaces and their asymmetries. Measurements of ocular components and peripheral refraction, however, have never been made in the same sample of eyes.

In this study, ocular component and peripheral refractive measurements were made in a sample of young near-emmetropic, myopic and hyperopic eyes. The data for each refractive group was averaged. A computer program was written to construct spherical surfaced schematic eyes from this data. More sophisticated eye models were developed making use of a linear algebraic ray tracing program. This method allowed rays to be traced through toroidal aspheric surfaces which were translated or rotated with respect to each other. For simplicity, the gradient index optical nature of the crystalline lens was neglected. Various alterations were made in these eye models to reproduce the measured peripheral refractive patterns.

Excellent agreement was found between the modelled and measured peripheral refractive values over the central 70° of the visual field. This implied that the additional biometric features incorporated in each eye model were representative of those which were present in the measured eyes. As some of these features are not otherwise obtainable using in vivo techniques, it is proposed that the variation of refraction in the periphery offers a very useful optical method for studying human ocular component dimensions.

2

To my wife,

FIONA

ACKNOWLEDGEMENTS

CHAPTER FIVE

A SCHEME FOR MODELLING PERIPHERAL REFRACTION
IN SCHEMATIC EYES USING THE LINEAR ALGEBRAIC
RAY TRACING PROGRAM

CHAPTER SIX

APPLICATION OF THE COMPUTING SCHEME FOR

MODELLING PERIPHERAL REFRACTION IN REAL EYES

CHAPTER SEVEN

DISCUSSION

11

12

13

14

15

17

18

CHAPTER ONE

THE HUMAN EYE.

1.1 INTRODUCTION.

In this chapter, the complexities of the ocular structures are studied emphasising the way in which they combine to produce different amounts of refractive error and how they contribute to various ocular asymmetries.

Detailed anatomical descriptions of the eye are available in many text books (Duke-Elder and Wybar, 1961; Davson, 1980). A brief account of the general ocular anatomy will be given using the schematic horizontal section of the human eye (fig. 1.1) as a guide.

Fig. 1.1   Schematic horizontal section of the eye.
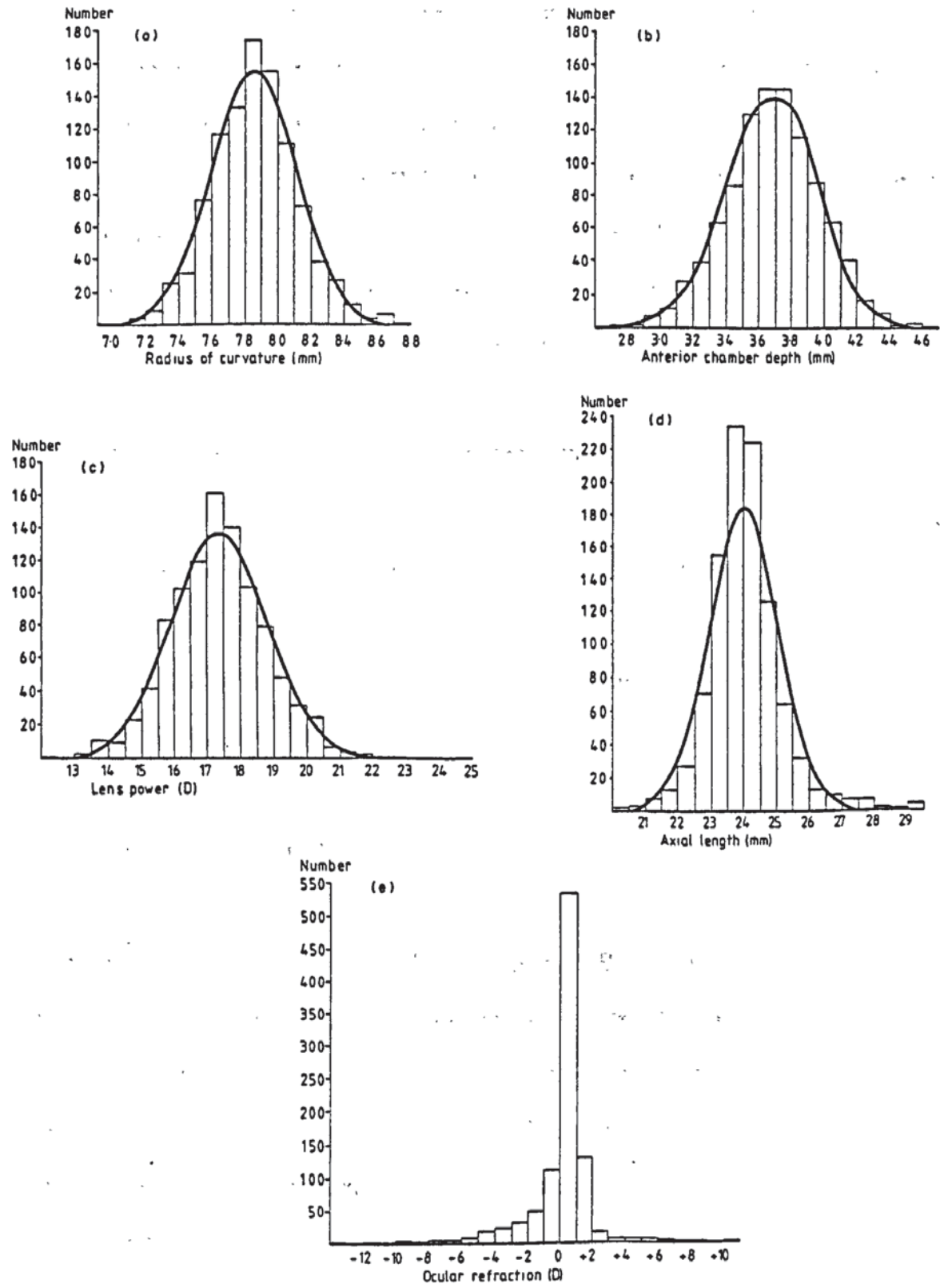
Fig. 1.2   (a) Distribution of corneal radius. (b) Distribution of anterior chamber depth. (c) Distribution of lens power. (d) Distribution of axial length. (e) Distribution of refractive error. [Redrawn by McBrien and Barnes (1984) after Stenstrom (1946)]. DISTRIBUTIONS a—c FIT A NORMAL DISTRIBUTION, WHILE DISTRIBUTIONS d AND e DO NOT.

25

Fig. 1.2 serves to illustrate the general distribution of ocular component dimensions in the population. Some indication will be given as to the influence of age and sex on these components. Very useful reviews on this area are provided by Borish (1970), Weale (1982) and Bennett and Rabbetts (1984). As this study deals with the human eye, much of the work performed on animals will not be included. Neither is a vast amount of literature relating to the research carried out in the last century which has already been extensively reviewed by Duke-Elder and Wybar (1961).

1.2 SUPPORTING STRUCTURES OF THE EYE.

The shape of the eye is maintained by intra-ocular pressure acting against its relatively inelastic walls. The latter are composed of the outer fibrous coat and the uveal tract. Both influence the relative positions of the refracting surfaces as well as the retinal profile.

1.2.1 THE FIBROUS COAT.

The fibrous coat consists of the sclera and cornea. Both provide considerable physical protection whilst the latter also possesses remarkable transparency and will be described later. Le Grand and El Hage (1980) pointed out that the human eye is roughly composed of two spheres. The sclera forms the larger, opaque, posterior segment with an external radius of 12 mm. This is continuous with the smaller transparent anterior segment, the cornea, which has an external radius of approximately 8 mm. In actual fact neither segment is perfectly spherical as the eye is normally somewhat flattened posteriorly and conical anteriorly.

The sclera varies in thickness from 1 mm at the optic nerve head to 0.3 mm behind the insertions of the extraocular muscles, 0.5 mm at the equator and 0.7 mm at its junction with the cornea. Its strength and opacity is attributable to the bands of collagen fibres which branch and interdigitate in a complex manner. However, numerous small apertures pierce the sclera through which various vessels, nerves and lymphatics pass but the weakest point arises where the optic nerve fibres enter and leave the back of the eye. Experimental evidence (Greene, 1980) shows that the extraocular muscles, which make their insertions in the sclera, are able to exert considerable pressure on the eyeball. This may have the effect of stretching the posterior segment thereby altering the retinal profile.

At birth, both the equatorial and axial diameters of the eye are between 17 and 18 mm respectively (Scammon and Wilmer, 1950; Sorsby and Sheridan, 1960; Larsen, 1971d; Gordan and Donzis, 1985). Growth of the eye occurs mostly in the first year and a half of life and proceeds more slowly until approximately 13 years of age (Sorsby and Sheridan, 1960; Sorsby et al., 1961; Larsen, 1971d). Once fully grown, the eye assumes an equatorial diameter of approximately 23 mm and an axial length of about 24 mm (Deller et al. 1947; Sorsby, 1948).

The axial length shows greater variation than any other component (Hirsch, 1966). Indeed, variations of between 21 and 38 mm have been reported (Tron, 1934; Stenstrom, 1948a; Sorsby et al., 1957). The range of axial lengths throughout the population shows a skewed and leptokurtotic distribution (fig. 1.2 d) but is binomial if eyes showing fundus changes, mostly found in high myopia, are excluded (Stenstrom, 1946, 1948a, b; Sorsby et al., 1957).

There is a high correlation between axial length and central refraction (Stenstrom, 1946, 1948a, b; Sorsby et al., 1957; Jansson 1963b; Larsen, 1971d). In general, myopic eyes tend to be longer and hyperopic eyes shorter than those of emmetropes. However, axial length only seems to be the exclusive determinant of ocular refraction in high ametropia (over 4 D) whereas the axial lengths of emmetropes and ametropes possessing less refractive error have similar values (Sorsby et al., 1957). Males tend to have longer eyes than females, the difference being of the order of 0.4 mm (Jansson, 1963b; Gernet, 1964a; Larsen, 1971d; Francois and Goes, 1977).

1.2.2 THE UVEAL TRACT

The choroid, ciliary body and iris are all components of the uveal tract, so named as it resembles a brown grape (uva) on a stalk (the optic nerve) when the fibrous coat is removed. Nutrients and support are provided for the retina by the highly vascular choroid. Anteriorly, the choroid runs continuously with the ciliary body and the iris. The ciliary body, which supports the crystalline lens by means of membrane-like zonules, possesses radial and circular smooth muscle fibres which are involved in accommodation. In the iris similar muscles allow pupil dilatation and constriction.

There is evidence (Van Alphen, 1986) that the uveal tract behaves like a solid sheet of smooth muscle and may provide some resistance to the intra-ocular pressure in addition to that of the fibrous coat.

1.3 TRANSPARENT STRUCTURES OF THE EYE.

1.3.1 CORNEA.

Fig.1.3 shows the microscopic structure of the cornea in transverse section. Light microscopy reveals that it is composed of 5 layers. These are the anterior epithelium, Bowman's membrane, the stroma, Descemet's membrane and the posterior endothelium. Each contribute to small variations in the corneal refractive index.

Fig. 1.3 The microscopic structure of the cornea in transverse section.

The anterior corneal surface is covered by a very thin tear film. Precise measurement of its thickness is difficult as it varies between individuals, for different head positions and between blinks of the eyelid. A thickness of between 7-9 μm is normal (Ehlers, 1965; Maurice, 1967). These values are too small to warrant specific consideration but if variations of greater than 100 μm were to occur due to abnormalities in tear flow, the dioptric effect would be both noticeable and measurable (Ehlers, 1965).

Some 88% of the corneal thickness is taken up by the stroma which is about 480 μm thick. It is made up of collagen fibres arranged in the form of 200-250 parallel lamellae (Maurice, 1957). The collagen fibres vary from 25-30 nm in diameter (compared to scleral fibres of 30-300 nm) and are separated by approximately 50 nm within a mucopolysaccharide matrix. Fibres are nearly always at right angles to each other in adjacent lamellae. The apparent resemblence between the corneal and scleral stroma has stimulated considerable research efforts to determine why the former is transparent. Maurice (1957) found the refractive index of the corneal collagen fibres and matrix to be 1.47 and 1.345 respectively (at 500 nm wavelength) which he felt would give the cornea an opaque appearance. Despite this difference, he believed that the corneal would still be transparent if the collagen fibres were of constant size, orientation and spacing thus forming a regular lattice structure. Maurice's explanation was questioned by Smith (1969) who found the fibre and matrix indices to be 1.384 and 1.369 respectively and concluded that these values were sufficiently similar for a lattice theory to be unnecessary. Nevertheless, subsequent theoretical and experimental studies (Cox et al., 1970; Feuk, 1970; Benedek, 1971; Farrell et al., 1973) confirm that transparency depends on an ordered arrangement of collagen fibres. Hart and Farrell (1969) have shown that complete regularity of the lattice is not necessary to ensure transparency but that a pseudo-random arrangement would suffice.

Numerous early measurements of the general corneal dimensions (Duke-Elder and Wybar, 1961) indicate that it has an average width of 11.6 mm horizontally and 10.6 mm vertically. The radius of its anterior surface is about 7.8 mm whilst that of its posterior surface is 6.5 mm.

Corneal thickness has recieved much attention. According to Von Bahr (1948) the first measurements were taken from post-mortem material and correspond to the thickness

of maximally swollen corneae. Blix (1880) performed the first direct optical measurements on living eyes but more simple methods have since been devised which provide an average value for central corneal thickness of approximately 0.55 mm. (Von Bahr, 1948; Maurice and Giardini, 1951; Mishima, 1968; Mishima and Hedbys, 1968; Mandell and Polse, 1969; Lowe, 1969; Kruse-Hansen, 1971; Tomlinson, 1972; Olsen et al., 1980; Olsen and Ehlers, 1984; Edmund and La Cour, 1986). Peripherally, the corneal thickness increases to about 0.7 mm (Steindorff, 1947; Maurice and Giardini, 1951; Martola and Baum, 1968; Mandell and Polse, 1969; Tomlinson, 1972; Hirji and Larke, 1978).

The development of contact lenses has resulted in many studies into corneal contour. The pioneer work of Senff and Helmholtz (Helmholtz, 1924) revealed that the cornea flattens peripherally in an ellipsoidal fashion. Mattheissen (1902) reached a similar conclusion using data obtained by other investigators. More recent work supports this (Noto, 1961; Holden, 1970; Mandell and St Helen, 1971; Kiely et al., 1982, 1984; Guillon et al., 1986). However, a range of mathematical surfaces have been used such as a catenary (Aebly, 1922), an asymmetric catenary (Nordenson, 1956), a cartesian ovaloid (Watkins, 1972) a hyperbola (Mandell, 1962a), an asymmetric conicoid (Kiely et al., 1982) and various other curve fitting equations (Berg, 1927; Bonnet and Cochet, 1962).

Others workers have described the cornea in qualitative terms (Aubert, 1885; Sulzer, 1892; Eriksen, 1893; Gullstrand, 1924; Bier, 1956; Knoll, 1961a). Gullstrand (1924) concluded that the cornea possesses an approximately spherical central optical zone which extends horizontally about 4 mm and is decentred temporally and slightly inferiorly from the line of sight. Peripheral parts are flattened more on the nasal than the temporal side, and usually more superiorly than inferiorly.

The existence of an optic zone varying from 3 to 9 mm in diameter finds support in the literature (Bier, 1956; Obrig, 1957; Knoll, 1961a; Grosvenor, 1961; Soper, et al., 1962; Jenkins, 1963; Girard, 1970; Fujii et al., 1972; Clark, 1974a, b; Rubin, 1975). Its shape has been described as horizontally ovoid by Grosvenor (1961) whereas Clark (1974a) finds such an irregular outline that the true margins are difficult to identify. Bier (1956) provided evidence that the optic zone was surrounded by a shallow, depressed annulus which he called the negative zone. Other workers have found no evidence for the existence of such a zone (Knoll et al., 1957; Evershed-Martin, 1959; Clark, 1974a).

Although there is general agreement that the corneal apex is decentred by as much as 0.5 mm from the line of sight, the results of studies into the direction of this displacement are by no means consistent. Some workers have found this to be predominantly temporal (Grosvenor, 1961; Bonnet and Cochet, 1962; Jenkins, 1963; Tomlinson, 1976; Tomlinson and Schwartz, 1979) whilst others find no directional trend (Mandell and St Helen, 1969, 1971). There is also little evidence for any directional bias superiorly or inferiorly. Bier's (1956) results are almost entirely opposite to those of Gullstrand (1924). Grosvenor (1961) pointed out that this could be partially resolved if it was understood that Bier (1956) used the geometric centre of the cornea as a reference point rather than the line of sight. The amounts of decentration found by Bier (1956) were small, which support the observations of Knoll (1980), who deduced that the corneal apex was very close to its geometric centre.

In agreement with Gullstrand (1924), most workers have found the cornea to be flatter on the nasal side than than the temporal side (Bier, 1956; Knoll, 1961a; Grosvenor, 1961; Jenkins, 1963; Clark, 1974b). It has also been found to be flatter superiorly

(Knoll, 1961a, b; Clark 1974a, b) but Bier's (1956) findings are to the contrary and Jenkins (1963) finds no difference.

From the above it would appear that the cornea shows considerable asymmetry. However, Ludlam and Wittenberg (1966a, b) commented that measurement of the corneal contour with reference to the line of sight, as performed by most workers, leads to the ambiguous conclusion that the corneal surface is asymmetrical. They added that a tilted ellipsoidal surface would produce the same corneal asymmetries as described by Gullstrand (1924). Other workers have since used tilted and decentred ellipses to represent the corneal profile (Holden, 1970; Kiely et al., 1982).

The posterior corneal surface has received far less attention as it is not readily accessible to measurement. However, Tomlinson's (1972) studies into the variation of corneal thickness in the periphery led him to the conclusion that the posterior surface is fairly constant in shape, relative to the anterior corneal surface, in most eyes.

Both corneal surfaces are known to be toroidal to some extent. According to Reading (1972), Nordensen (1883) was the first to establish this for the anterior corneal surface. This is normally steeper vertically than horizontally and therefore commonly possesses between 0.5 D and 0.75 D of with-the-rule astigmatism (Hirsch, 1963; Mohindra et al., 1978; Fledelius and Stubgaard, 1986). Ludlam and Wittenberg (1966a, b) believed that even if the apex of the cornea was non-toroidal, the combined effect of tilt and decentration would give rise to with-the-rule astigmatism along the line of sight. Indeed, less astigmatism is found at the corneal apex than down the line of sight (Ludlam et al., 1967; Mandell and St Helen, 1969). Much less is known of the contribution from the posterior corneal surface but Tscherning (1904) reported values of between 0.24 and 0.57 D of against-the-rule astigmatism in 3 people.

The majority of corneal growth occurs prenatally (Fletcher and Brandon, 1955). Premature babies are found to have steeper corneae than full term babies (Fledelius, 1976). At birth, the cornea has a diameter of about 9.5 mm with an anterior surface radius of around 6.0 to 7.5 mm (Ellerbrock, 1963; Baldwin, 1964). As the cornea increases in diameter it tends to flatten (Peter, 1924). A full diameter is reached within the first or second year of life (Keeney, 1951; Baldwin, 1964; Gordan and Donzis, 1985; Fledelius and Stubgaard, 1986). The anterior corneal radius then fluctuates by about 0.2 mm, accompanied by power changes of around 0.5 D, up to approximately 20 years of age (Sorsby et al., 1961; Sorsby and Leary, 1970). The corneal power increases up to approximately 30 years of age, decreases to about 70 years at which point it increases again (Heim, 1941; Saunders, 1982; Bennett and Rabbetts, 1984). These changes very closely match the overall variations in ocular refraction (Saunders, 1981, 1982). Anterior corneal asphericity does not vary substantially with age (Kiely et al., 1984). Astigmatism of the anterior cornea tends to be with-the-rule in young subjects and reduces, even becoming against-the-rule, with advancing age (Fischer, 1948; Phillips, 1952; Lyle, 1971; Reading, 1972; Kiely et al., 1984; Fledelius and Stubgaard, 1986). There are few research articles on the changes with age of the posterior corneal surface. Lowe and Clark (1973a) found no correlation between the radius of the posterior corneal surface and age. They did, however, find a strong relationship between the anterior and posterior corneal radii and so the latter would presumably reflect the changes described above for the former.

The range of corneal anterior radius values (fig.1.2 a) in normal eyes is about 7.0 to 8.6 mm (Stenstrom, 1946). Both its power and radius follow a normal distribution (Steiger, 1913; Stenstrom, 1946; Sorsby et al., 1957). Despite the already described similarity between corneal and ocular refractive changes with age, there is no strong correlation between the corneal power and refractive status (Steiger, 1913; Gardiner,

1962; Baldwin, 1964). A better relationship, however, is found with low ametropia (Tron, 1934; Baldwin, 1964) where corneal power is probably as significant as axial length (Sorsby et al., 1957). In this case, the anterior corneal surface is steeper in myopes and flatter in hyperopes than found in emmetropic eyes (Tron, 1934; Baldwin, 1964; Sorsby et al., 1957). This may not necessarily be the case in high ametropia due to the relative influences of either the cornea or axial length (Baldwin, 1962, 1964).

Another source of corneal variability is diurnal variation (Fujita, 1980). Female corneae are also more variable due to menstruation (Kiely et al., 1983). On average, females have steeper corneae than males, the difference in the means being about 0.1 to 0.15 mm (Sorsby et al., 1961; Fledelius, 1976). However, both have similar asphericities (Kiely et al., 1984).

It is worth considering that in vivo measurements of corneal refractive index reveal a value of around 1.377 at a wavelength of 589 nm (Mishima, 1968). As the corneal refractive index differs so much from that of air (1.000) it contributes to about 80% of the total refractive power of the eye. For this reason its aspheric nature is instrumental in the reduction of spherical aberration with large pupils. Any asymmetry in its profile will also have a profound effect on the retinal image.

1.3.2 AQUEOUS HUMOUR.

The anterior and posterior chambers, which lie between the cornea and crystalline lens, are filled with a watery fluid called the aqueous humour. This fluid provides nutrients for the avascular cornea and lens tissues and is the source of the intra-ocular pressure which maintains ocular geometry. Its transparency and refractive index is much the same as that of water. Although the refractive index has only ever been measured in

non-living eyes, a value of about 1.377 is generally adopted by most workers (Borish, 1970).

Aqueous fluid is produced at a rate of approximately 2 µl min^{-1} from the crypts of the ciliary body and the posterior surface of the iris. It flows from the posterior chamber and through the iris aperture to the anterior chamber thus occupying a total volume of 0.5 ml (Heim, 1941; Steindorff, 1947). It then leaves the eye mainly at the filtration angle where it drains away via the canal of Schlemm and aqueous veins. Continued production of aqueous humour maintains the intra-ocular pressure.

Measurements made from either the anterior or posterior surfaces of the cornea to the front of the lens and are referred to as anterior chamber depth. As estimates taken from the posterior corneal surface depend on corneal thickness most studies include the latter in the final value. The anterior chamber depth, including corneal thickness, is usually around 3.6 mm (Goldmann, 1940; Heim, 1941; Stenstrom, 1946; Von Bahr, 1948; Jaeger, 1952; Tornquist, 1953; Calmettes et al., 1958; Sorsby et al., 1961, 1963; Jansson, 1963b; Giglio and Ludlam, 1967; Brown, 1969; Larsen, 1971a; Fledelius, 1976).

At birth, the anterior chamber (including cornea) is approximately 2.5 mm in depth (Ellerbrock, 1963; Larsen, 1971a). It increases rapidly up to 1.5 years of age followed by a slower growth phase to the age of 7. Growth is slower still up to the age of 13 (Sorsby et al., 1961; Larsen, 1971a). At this point the anterior chamber is at its full size, although Calmettes et al. (1958) believed this to occur at closer to 20 years of age. It then decreases, with advancing age, to a value of about 3.0 mm (Raeder, 1922; Stenstrom, 1948a; Tornquist, 1953; Calmettes et al., 1958; Weekers and Grieten, 1961; Jansson, 1963b; Luyckx-Bacus and Weekers, 1966; Lowe, 1970, Weekers et

al., 1973), which is attributable to increase of size and some forward movement of the crystalline lens (see section 1.3.4).

Stenstrom (1946), found the anterior chamber to vary from 2.8 mm to 4.5 mm in depth, following a normal distribution (fig. 1.2 b). Several investigators show an increase in depth from hyperopia to myopia (Stenstrom, 1946; Calmettes et al., 1958; Larson, 1971a). A correlation with the degree of hyperopia is commonly found but with myopia such a clear relationship does not exist (Raeder, 1922; Stenstrom, 1946; Calmettes et al.,1958; Sorsby et al., 1961; Larson, 1971a).

Other factors effecting the anterior chamber are accommodation, which decreases its depth (section 1.3.4), and sex. Regarding the latter, males normally have deeper anterior chambers than females (Calmettes et al., 1958; Sorsby et al., 1961; Jansson, 1963b; Larsen, 1971a; Fledelius, 1976). This may be not be apparent at birth but the growth rate in males, in the first 2 years of life, is greater than that of females (Larsen, 1971a) so giving rise to a difference of about 1.5 mm which remains unchanged in subsequent age groups (Larsen, 1971a; Fledelius, 1976).

1.3.3 PUPIL.

The pupil, an opening in the iris, forms the aperture stop for the eye's optical system and lies approximately tangentially to the anterior crystalline lens surface. Smooth muscles in the iris are able to control its diameter either by constriction (sphincter pupillae) or dilation (dilator epithelium).

The diameter of the pupil normally varies between 2 mm and 5 mm with values ranging from 0.5 mm to 9 mm in extreme cases (Zinn, 1972). It appears magnified through the cornea (entrance pupil). According to Gullstrand (1924) the pupil is usually decentred temporally and inferiorly with respect to the line of sight by approximately the same amount as the corneal apex (see section 1.3.1). More recent studies confirm that the pupil is decentred temporally but do not include any vertical observations (Spring and Stiles, 1948; Jay, 1962; Jennings and Charman, 1978).

Illumination is the main factor *a*ffecting pupil size (Reeves, 1918; Crawford, 1936; Alpern and Campbell, 1962) although emotion, accommodation and drugs also bring about fluctuations (Hess, 1965; Lowenstein and Loewenfeld, 1969; Zinn, 1972; Janisse, 1973).

In infancy the pupil tends to be constricted, possibly due to the relatively advanced developement of the sphincter pupillae compared to that of the dilator epithelium. The pupil is largest during childhood and adolescence but becomes smaller again with advancing age (Zinn, 1972). It is also known that myopes tend to have larger pupils than hyperopes (Zinn, 1972).

A variable pupil has considerable advantage over a static one. The optimum pupil size is a compromise between retinal illumination requirements and ocular aberrations (Woodhouse, 1975). Changing of the pupil size also serves to provide protection against excessive illumination (Barlow, 1972), to increase depth of focus (Campbell, 1957) and to optimise the visual acuity over a wide range of illuminances (Campbell and Gregory, 1960).

It is important to consider that the pupil appears to be roughly ellipsoidal in shape when viewed obliquely (Spring and Stiles, 1948; Jay, 1962; Jennings and Charman, 1978). This and the fact that the iris is about 0.5-0.6 mm thick means that cross-sections of image pencils of light are reduced in the periphery (Charman, 1983) thereby influencing the peripheral dioptrics and aberrations.

1.3.4 CRYSTALLINE LENS.

Fig. 1.4 shows the structure of the crystalline lens. In general it is a transparent, deformable, biconvex elastic body. It is encased within an elastic capsule which contains collagen and possesses around 2000 times more elasticity than the underlying lens material (Fisher, 1969a, 1971; Fisher and Wakely, 1976). Variations in the thickness of this layer play an important role in governing the overall shape of the lens (Fincham, 1937).

Aston University

Illustration removed for copyright restrictions

Fig. 1.4   Transverse section of part of the crystalline lens

At the anterior pole it is approximately 14 μ thick but reaches a maximum of 21 μ at about mid-way towards the periphery. Posteriorly, the capsule is relatively thin, varying from 4 μ at the posterior pole to 23 μ near the equator. The thickness at the equator is 17 μ and in this region zonules arising from the ciliary body are attached to the capsule to provide support for the lens.

Immediately inside the lens capsule is the epithelium which is a cellular layer of 5-8 μ thick. This is confined to the anterior and equatorial surfaces of the lens. At the equator, in a region called the nuclear bow, the epithelial cells elongate to form lens fibres. The youngest of these are the most superficial and comprise the lens cortex whilst the oldest form the lens nucleus.

Lens fibres are 8-12 μ long, 7 μ wide and 2.5μ thick. In cross-section their shape is hexagonal and they interlock with each other (Kuck, 1970) thereby providing a certain amount of intrinsic elasticity (Wanko and Gavin, 1958; Weale, 1962; Kuck, 1970; Fisher, 1969a, b, 1971). Through the continued addition of new lens fibres a layered structure arises. Regions of differential growth such as the embryonal, foetal and adult nucleus can be observed in cross-section and are depicted in fig. 1.4. The internal lens tissue also becomes progressively compressed and the resulting protein concentration leads to a variable and relatively high lenticular refractive index. This has a value of approximately 1.41 in the region of the nucleus which drops to about 1.38 in the equatorial and surface layers of the cortex (Freytag, 1907; Helmholtz, 1924; Tagawa, 1928; Huggert, 1948; Nakao et al.,1969a, b). The lens therefore has a gradient index optical structure (Marchand, 1978) which confers a refractive power equivalent to that of a homogenous lens with the same surface curvatures but with a higher refractive index of about 1.42 (Gullstrand, 1924; Charman, 1983).

Smooth mathematical curves have been used to describe the gradient index optical structure of the human lens (Gullstrand, 1924; Nakao et al., 1969a, b; Watkins, 1972; Blaker, 1980; Pomerantzeff et al., 1971, 1972, 1984). However, the results of Van Den Brink (1962) suggest that the focusing system of the eye has an optically heterogenous structure. Nakao et al. (1968) considered that this implied an irregular distribution of lenticular refractive index but felt that other factors such as the relative positions of the cornea, lens and retina could also play a part.

The adult lens has an equatorial diameter of 9.1 mm, a thickness of 3.6 mm and an anterior and posterior radius of 10 mm and 6 mm respectively (Ellerbrock, 1963). Both lens surfaces are flattened peripherally and take the form of an hyperbola anteriorly and a parabola posteriorly (Parker, 1972; Howcroft and Parker, 1977) although more complicated mathematical curves have also been used (Watkins, 1972; El Hage and Berny, 1973). This aspheric flattening together with the gradient index optical structure of the lens is important in reducing spherical aberration (Charman, 1983). Considerable variations in lens dimensions occur in order to provide the variable refractive power required for accommodation and this together with the continual increase in size of the lens throughout life (Weale, 1963, 1979) means that the above dimensions are only representative.

The detailed mechanism of accommodation is not considered here but has been extensively reviewed by Hogan (1985). Of interest, however, are the structural changes which occur with accommodation. On contraction of the ciliary body the tension on the zonules is released and the the lens assumes a more spherical shape (Fincham, 1937). During this process the lens cortex remains more or less the same thickness whilst that of the nucleus increases (Gallati, 1923; Patnaik, 1967; Brown, 1973). The resulting axial thickening of the lens brings about a forward shift of its

41

anterior pole, reducing the anterior chamber depth, and a smaller backward shift of the posterior pole (Helmholtz, 1924; Gullstrand, 1924; Fincham, 1926, 1937; Brown, 1973; Storey and Rabie, 1983). As the posterior shift is so small, Coleman (1970) was of the opinion that the vitreous body plays a supportive role in accommodation. Both lens surfaces increase in curvature but this change is greater for the anterior surface and very little for the posterior surface.

The actual shape which the anterior surface assumes during accommodation is subject to considerable dispute. It is the opinion of some workers that the anterior surface bulges centrally whilst its curvature in the periphery is little altered (Tscherning, 1904; Fincham, 1937; Brown, 1973). This is caused by the lens cortex moulding around the thickened nucleus (Fincham, 1937). Such a conicoid surface serves to explain the observation of previous studies that reduction in spherical aberration occurs with accommodation (Koomen et al., 1949; Ivanhoff, 1956). Other workers, however, believe that the conicoid shape is the result of observing the lens through the cornea and that in reality an ellipse adequately describes the anterior lens surface shape during accommodation (Nordensen, 1943; Fisher, 1969b, 1971). Brown (1973), however, found that the anterior surfaces of young lenses became practically spherical with accommodation which he explained by the fact that the nucleus makes up the bulk of the lens in childhood thereby confering a change in curvature throughout the peripheral and central regions. That this was observed through the cornea led Brown (1973) to the conclusion that corneal distortion played no significant role, otherwise the young lenses too would have appeared to be conicoidal. The diameter of the lens does not decrease substantially during accommodation as the increase in lens thickness is offset by the previously described peripheral flattening of the anterior surface to maintain volume constancy (Gullstrand, 1924; Fincham, 1926). Storey and Rabie (1985) found an average reduction of 0.08 mm per dioptre of stimulus to accommodation.

At birth, the lens is approximately 6.7 mm in equatorial diameter, 3.7 mm in thickness and has surface radii of 5 mm anteriorly and 4 mm posteriorly (Ellerbrock, 1963). The thickness of the lens diminishes up to approximately 15 years of age (Larsen, 1971b). From then on, it increases at a rate of about 0.02 mm per year (Raeder, 1922; Luyckx-Bacus and Weekers, 1966; Luyckx-Bacus and Delmarcelle, 1969; Francois and Goes, 1969a, b; Lowe, 1970, Weekers et al., 1973, 1975; Howcroft and Parker, 1977) resulting in an equal amounts of shift, forwards and backwards, at the anterior and posterior poles respectively (Weekers et al., 1973). This increase is almost entirely due to the continual addition of new lens fibres to the lens cortex, whereas the lens nucleus shows no consistent change with age, apart from a tendency to reduce in volume due to sclerosis (Brown, 1973; Weekers et al., 1973). Although sclerosing of the nucleus begins in infancy, this continues more rapidly with advancing age bringing about a rise in refractive index. The refractive index of the lens cortex, however, shows no such age related change (Freytag, 1907; Huggert, 1948). There appears to be some difference in opinion with regard to the change in shape of the lenticular surfaces with age. Some have found that the lens surfaces become flatter with increasing age (Nakajima, 1968; Howcroft and Parker, 1977) while others have shown that they become steeper (Brown, 1973; Lowe and Clark, 1973b). It is worth noting that Weale (1982) considered that there must be some forward movement of the entire lens with age as its increase in thickness, due to continued growth, does not entirely account for the reduction of the anterior chamber depth (see section 1.3.2).

Throughout the population, the crystalline lens power follows a normal distribution (fig. 1.2 c) with values varying from 15-25 D and averaging at just above 20 D (Stenstrom, 1946; Sorsby et al., 1957). Unlike the variations due to accommodation and growth, lens dimensions vary little with sex and refraction. Most investigators have found females to have thicker lenses than males, although the difference has

never attained statistical significance (Sorsby et al., 1961; Larsen, 1971b; Fledelius, 1976). Whereas some authors have shown that the lens tends to become progressively thicker from myopia to hyperopia (Zeeman, 1911; Raeder, 1922; Janssen, 1963b), others find no direct relationship but agree that slightly thinner lenses exist in myopes (Francois and Goes, 1977; Larsen, 1971b).

The lens is often considered to be the source of against-the-rule astigmatism (residual astigmatism) which may account for the commonly observed differences between the corneal and total ocular astigmatism. Although the latter may also be explained by the misalignment of corneal apex from the line of sight (see section 1.3.1), it has been long noticed that some astigmatism persists even when the power of the cornea is neutralised (Young, 1807). Some studies show that lens tilt can produce small amounts of against-the-rule astigmatism but that most residual astigmatism must arise from the toricity of the surfaces themselves (Le Grand and El Hage, 1980; Bennett, 1984). Indeed, Tscherning (1904) found that the astigmatism from the anterior surface was approximately 1 D with-the-rule astigmatism whilst the posterior surface exhibited nearly 2 D against-the-rule. Furthermore, the relaxed lens appears to be poorly held in place by the zonules, as it sinks by about 0.3 mm with gravity and oscillates after cessation of head movements (Hess, 1929). There is also evidence that the ciliary muscle contracts asymmetrically leading to prismatic distortion effects from the lens during accommodation (Hess, 1929; Park, 1936).

1.3.5. VITREOUS

The vitreous body comprises about two thirds of the total length of the eye (Francois and Goes, 1969a). By occupying a volume of approximately 5 ml it can be described as the largest constituent of the eye which has a total volume of 7-8 ml (Le Grand and

El Hage, 1980). It provides mechanical and nutritive support to the retina as well as being transparent.

An extensive network of fine collagen fibres (10-25 nm) with fluid (liquid vitreous) filled interstices gives the vitreous its gel like consistency. The liquid vitreous is composed mainly of water. At the edges of the vitreous body a membrane like structure is formed by collagen fibres which lie parallel to each other which in the vicinity of the ciliary body attain a thickness of 3μ (Le Grand and El Hage, 1980). In the latter position, as well as around the edges of the optic disc, attachments are made to the retina. Less firm attachments also occur at the back of the crystalline lens.

At birth, the vitreous length is between 10 and 11 mm (Gernet, 1964b, c; Luyckx-Bacus, 1966; Larsen, 1971c). Growth proceeds rapidly in the first half year of life and more slowly to approximately 13 years of age (Gernet and Holwich, 1969; Larsen, 1971c). At that age the vitreous is fully grown and has a length of around 16 mm (Jansson, 1963b; Gernet, 1964b, c; Nover and Grote, 1965; Larsen, 1971c). With advancing age the length reduces (Weekers et al., 1973), which is attributable to the increase in size of the lens (see section 1.3.4).

Accommodation, sex and refractive status influence the vitreous length. The effects of accommodation have been discussed (Section 1.3.4). Males tend to have longer vitreous lengths than females (Jansson, 1963b; Gernet, 1964b, c; Nover and Grote, 1965; Luyckx-Bacus, 1966; Larsen, 1971a, c) and the length of the vitreous tends to increase from hyperopia to myopia (Janssen, 1963b; Larsen, 1971a, c).

The vitreous humour shows changes with age. In early life it has an homogenous consistency but in adulthood it becomes more gelatinous from lens to retina and from

centre to periphery (Le Grand and El Hage, 1980). It has a refractive index of about 1.336 (Tagawa, 1928; Le Grand, 1967) but there is evidence to suggest that this increases with age (Millodot, 1976).

1.3.6 RETINA

The retina is a transparent, purplish structure whose thickness increases from 0.1 mm anteriorly to 0.3 mm posteriorly. Because it is limited by the outer layers of the eye its radius is approximately 12 mm (Le Grand and El Hage, 1980) and it lacks rotational symmetry (Deller, et al., 1947; Sorsby, 1948). It has been hypothesised that the retinal axis of symmetry lies temporal to the visual line (Hallden, 1956). It has also been described as being flatter temporally (Le Grand and El Hage, 1980) and flatter nasally (Tschermak, 1942). These conflicting results offer no satisfactory evidence for the expected retinal asymmetry. Further irregularities in the retinal surface are caused by the fovea (Polyak, 1941) and the optic disc (Barrett, 1945).

The photoreceptors, consisting of rods and cones, are to the outside of the retina so that light must pass through the inner layers before reaching them. Rods are about 60 μ long and 2 μ thick. They are distributed over most of the retina, except for the fovea, and are sensitive to monochromatic light with a maximum sensitivity at 505 nm. The cones are usually shorter and thicker and provide high visual acuity and colour vision with a maximum sensitivity at 555 nm. They also exhibit a marked directional sensitivity (Stiles and Crawford, 1933). Although they are fewer in number than rods, modified cones are the sole type of receptor at the functional centre of the retina, the fovea, which is a shallow depression of about 1.5 mm in diameter (Emsley, 1952). The latter region contains a yellow pigment which partially absorbs light of 400-500 nm wavelength (Fry, 1959) and modifies the spectral energy distribution at the

46

receptors. Receptors synapse with bipolar cells and these in turn synapse with ganglion cells whose axons form the optic nerve fibres and leave the eye at the optic disc. This cupped region is devoid of receptors, has a diameter of about 2 mm and lies at approximately 4 mm temporally from the fovea, centre to centre.

The shape of the retina with age, sex and refraction would naturally be influenced by the variations already described for the eyeball. Its consideration is important as the function of the eye is to produce optimum image quality and the ability to do this is influenced by the spatial position of the retinal receptors (Charman, 1983).

1.4 CENTRAL REFRACTION

Refraction is measured as the distance, in dioptres, of the image focus (or line foci, in the case of astigmatism) from the retinal surface. It is important to distinguish this from the total refracting power of the eye. Only the refraction at the fovea will be regarded in this section whilst its variation over the peripheral retina will be discussed later.

There have been several major studies on the distribution of refraction which show an undue proportion of emmetropes and near-emmetropes throughout the population (Kronfield and Devney, 1931; Stenstrom, 1946). The distribution curve is shown in fig 1.2e (Stenstrom, 1946).

Some workers have found that the refractive errors of newborn babies ARE normally distributed with a mean of about 2.0 D of hyperopia (Slataper, 1950; Spooner, 1957; Howland et al., 1978). Mohindra and Held (1981), however, reported that newborns are relatively myopic. Their results indicated that the distribution of refractive errors

47

are normal at birth but that the degree of variance reduces and approaches the adult value close to one year of age. Over this period there is also a hyperopic shift. The earlier work indicates that during normal development there are two hyperopic shifts, the first in early infancy and the second in middle age, and two myopic shifts, between adolescence and 30 years of age and then again in old age (Brown, 1938; Slataper, 1950; Spooner, 1957). Although some recent studies show a similar trend, they find no support for a hyperopic shift in early infancy (Saunders, 1981, 1986; Ashton, 1985; Gordon and Donzis, 1985; Fledelius and Stubgaard, 1986).

Females tend to be more hyperopic than males at birth (Saunders, 1981). This persists through their teens (Hirsch, 1964; Saunders, 1981) although Sorsby et al (1961) found the decrease in hyperopia to be more in females than males over the same period. Both sexes show the same values in the middle years but females show greater hyperopia in old age (Saunders, 1981).

Large amounts of astigmatism are present at birth (Mohindra et al., 1978; Howland et al., 1978; Braddick et al., 1979; Ingram and Barr, 1979; Atkinson et al., 1980; Fulton et al. 1980; Mohindra and Held, 1981; Howland, 1982; Howland and Sayles, 1984) due almost entirely to the cornea (Howland and Sayles, 1985). A considerable reduction then occurs within the first two years of life falling to adult levels by about 18 months of age. In youth, astigmatism is predominantly with-the-rule (Hirsch, 1963; Saunders, 1981) but becomes against-the-rule with increasing age (Hirsch, 1959; Saunders, 1981). The rate of change of the latter differs slightly for males and females (Saunders, 1981).

Exhaustive studies have been conducted on the aetiology of refractive errors by observing the distribution and correlation of ocular components. Major contributors in

this area are Stenstrom (1946), Sorsby et al. (1957) and Van Alphen (1961, 1967). A review of these studies and the theories of refractive development which have arisen as a result of them is given by McBrien and Barnes (1984). Most research has been carried out on the genesis of myopia. Three main theories arise from the vast amount of work done: the biological-statistical theory, the use-abuse theory and the theory of emmetropization. These will now be very briefly outlined.

The biological-statistical theory attempts to show that all errors of refraction are due to the way in which the components of the eye combine. Steiger (1913) put forward that all ocular components followed a normal distribution and that free association of these gives rise to emmetropia and ametropia falling upon a normal curve. Subsequent studies showed that there was an abundance of near-emmetropes in the population (fig. 1.2 e). Sorsby postulated that the ocular components were highly correlated giving rise to a high incidence of near-emmetropia (Sorsby, 1967; Sorsby et al., 1957, 1981). Thus eyes with large axial lengths have surfaces with large radii of curvature, while small eyes have small radii. Some ametropia naturally occurs due to insufficient correlation (correlation ametropia). However, the more extreme refractive errors (exceeding -4 D or +6 D) are the result of a component (component ametropia), usually axial length, falling outside the range seen in emmetropia (Sorsby et al., 1962a, b; Sorsby and Benjamin, 1973). These studies also suggested that emmetropia, correlation ametropia and component ametropia were genetically determined (Sorsby, 1967).

The use-abuse theory emphasises the role of environmental stress. It was first proposed by Cohn (1886) and attempts to explain the onset of myopia as an adaptation to use and misuse of the eyes in prolonged close work. More recently, Young (1961, 1967, 1975, 1977, 1981) has systematically evaluated many of the theories of myopia

49

finding only the amount of time spent reading to be a major influence. He induced myopia in monkeys by placing them in a near point environment (Young, 1967) and found an increased incidence of myopia in an Eskimo population due to the effects of close work brought on by school work and television (Young et al., 1969, 1973; Young and Leary, 1972). The evidence of longitudinal studies led Young to the belief that a child went into myopia due to an inability to relax accommodation during long periods of close work (Young, 1977). This continuous state of accommodation increased vitreous pressure and ultimately led to axial elongation. Indeed, paralysis of accommodation is known to reduce myopic progression (Bedrossian, 1966) and increase in vitreous pressure with accommodation has been demonstrated (Coleman, 1970; Young, 1975). Young (1981) suggested that this increase in lens power and vitreous pressure was the mechanism behind the progression from hyperopia at birth to emmetropia in adulthood. If this continued, myopia resulted.

The theory of emmetropization includes both genetic and environmental influences. Although first conceived by Straub (1909), Van Alphen (1961) has offered the most comprehensive theory to date. This involves a self-focusing model and was inspired by the results of a detailed statistical analysis which he performed on the data of Stenstrom (1946). He believed that growth was determined by genetic factors and stretch by intraocular pressure. The latter was evident as an eye without intraocular pressure does not enlarge during body growth (Coulombre and Coulombre, 1956). To produce the high proportion of emmetropes which occur in the population it was proposed that the stretch of the eye must be controlled. Regulation of stretch was assumed to occur via the tonus of the ciliary muscle and choroid, which run continuously with each other (see section 1.2.2), and behave as a continuous sheet of smooth muscle able to resist, in part, the intra-ocular pressure. In support of this Van Alphen (1986) demonstrated that the ciliary body stretched when the globe was

inflated. It was also assumed that information concerning the degree of hyperopia was fed back from the fovea and brain leading to subcortical adjustment of the activity of the autonomic nerve input. Ciliary muscle tone is indeed found to increase and decrease with parasympathetic and sympathetic stimulation respectively (Van Alphen, 1979). Because the stretch of the sclera would be under cortical and subcortical control, the implications were that interruption of the feedback loop would interfere with emmetropization giving rise to ametropia. Such interruptions can occur at the fovea which is demonstrated by the fact that the physical act of covering all or part of the human eye results in myopia (Rabin et al., 1981). On the other hand, environmental effects causing stress and emotion (e.g. studying, giving rise to "school myopia") or extreme autonomic endowment (e.g. excess parasympathetic activity in newborns) might influence emmetropization at the subcortical level.

The above theories show that both genetic and environmental factors can influence the development of refractive errors but the relative involvment of either is still not clear. Goldschmidt (1968) considers that myopia caused by environmental factors develops later in life than myopia of genetic origin (although myopia which is late in onset does not necessarily preclude genetic factors).

As both the use-abuse theory and the theory of emmetropization propose that accommodation is one of the causative factors of myopia various workers have recently attempted to assess the accommodative difference between refractive groups. In the absence of adequate visual stimuli the eye adopts an intermediate resting position of accommodation (Campbell and Primrose, 1953; Leibowitz and Owens, 1975). The eye becomes more myopic in this position which may be appropriately termed tonic accommodation (TA). There is some evidence for a relationship between TA and refractive error showing lower values in myopes (Maddock et al, 1981; Ramsdale,

1982). TA is found to increase with sustained periods of close work (Ebenholtz, 1983, 1985; Hogan, 1985; Gilmartin and Hogan, 1985). This phenomenon is due to increased tonus of the ciliary muscle and is referred to as accommodative hysteresis, the harmful effects of which maybe a precursor to myopia. Gilmartin and Hogan (1985) demonstrated that a subject's TA is determined by the balance of excitatory parasympathetic and inhibitory sympathetic innervation of the ciliary muscle. They suggested that the inhibitory input served to attenuate such myopic shifts in TA and that certain forms of myopia may be the result of inadequate sympathetic activity. The findings of Gilmartin and Bullimore (1986) predict that these individuals have low TA values. Indeed, late-onset myopes have significantly lower values of TA than emmetropes and this may render them susceptible to accommodative hysteresis and myopia (McBrien, 1986; Bullimore and Gilmartin, 1987).

Many of these studies are still in progress and will hopefully provide more insight into refractive error development in the future, particularly with regard to the relative influences of accommodation and convergence. Regarding the latter, Greene (1980) proposed that the extraocular muscles involved with convergence could increase the vitreous pressure. This, in addition to the weakpoint at the back of the eye where the optic nerve enters (see section 1.2.1), would give rise to axial elongation and hence myopia. That accommodative convergence may play a major role has also been implied by Rosenfield and Gilmartin (1987).

1.5 AXES OF THE EYE

One of the consequences of attempting to design simplified mathematical models of the eye is the requirement for a common axis about which each refracting surface is centred. Bearing in mind the considerable amounts of asymmetry that the optical

52

components are known to exhibit, it comes as no surprise that in general the eye possesses no such axis. This section describes the axes which have been used by various workers.

It is logical to first consider the axis which represents the chief or principal ray travelling from the object of regard, through the eye and striking the fovea. This is referred to as the the *visual line* if it passes through the schematic anterior and posterior nodal points. It is otherwise known as the *line of sight* if it passes through the centre of the entrance pupil.

The refracting surfaces are found to be approximately centred upon an *optical axis*. The angle between this and the visual line is called *angle alpha* (Tscherning, 1904; Emsley, 1952). Alternatively, the angle that the optical axis makes with the line of sight is called *angle gamma* .

Other workers consider the optical axis and its associated angles to be imaginary and fictitious but at the same time accept that such a concept is indispensible. As an acceptable approximation they have used the *pupillary axis*, a line perpendicular to the cornea which passes through the centre of the entrance pupil (Gullstrand, 1924; Lancaster, 1943). Landolt called the angle between the pupillary axis and the visual line *angle kappa* (according to Lancaster, 1943). In clinical practice the separation between the pupillary axis and the line of sight is measured at the centre of the entrance pupil and is often erroneously called angle kappa but which Fry (according to Lancaster, 1943) called *angle lambda* .

Similarly to Gullstrand (1924), many of the earlier workers used the position of the corneal apex, or otherwise its geometric centre, to define the optic axis but made

reference to a confusing assortment of angles (Knapp, 1860; Donders, 1864; Helmholtz, 1924).

As the visual axes are very close together, angles alpha and gamma as well as angles kappa and lambda are practically identical. It is also evident that a similar estimate is obtained for either definition of the angle between the optical and visual axes and, therefore, each amount to the same thing (Emsley, 1952). As this is the case, all of these angles will be collectively refered to as angle alpha.

Angle alpha shows considerable variation in the population. In hyperopes and myopes it is found to be higher and lower, respectively, than observed in emmetropes (Donders, 1864; Emsley, 1952). The average value of angle alpha is 5° in the horizontal plane and 1.5° vertically. Consequently the optic axis does not intersect the retina at the fovea but 1.5 mm nasally and 0.5 mm superiorly to it (Emsley, 1952).

The variation of angle alpha within individual observers has been reported and attributed to unequal action of the ciliary muscle causing distortion or decentration of the lens (Park, 1936). Furthermore, there is evidence to suggest that angle alpha disappears altogether in aphakics (Park, 1936; Stimson, 1957). The latter prompts the question as to whether angle alpha is entirely attributable to the crystalline lens. However, decentration of the lens with respect to the cornea is normally negligible (Tscherning, 1904) and ray tracing through schematic eyes indicates that large amounts of lens tilt are required to account for angle alpha (Watkins, 1972).

There are several interesting effects of angle alpha. Residual astigmatism, as previously described, is the observed difference between corneal and ocular astigmatism. If angle alpha is due purely to eye rotation then the occurrence of residual

astigmatism would be explained by the obliquity, with respect to the line of sight, of all of the refracting surfaces and particularly the cornea (see section 1.3.1). However, a certain amount of additional lens tilt or decentration could also play a role (see section 1.3.4). The relative contributions of the cornea and lens are as yet unknown and as there appears to be no direct correlation between angle alpha and residual astigmatism (Loper, 1959) further research in this area would be of interest.

Furthermore, if the optical axis does not strike the retina at the fovea then the most acute optical imagery cannot be expected to lie there either. Indeed, research evidence has shown that the deterioration in image quality with peripheral angle is symmetrical about a position which is decentred nasally with respect to the fovea and seems to be the result of angle alpha (Jennings and Charman, 1978, 1981).

1.6 SUMMARY

The human eye is more or less fully grown by 13 years of the age although the crystalline lens continues to grow throughout life. Each ocular component is distributed normally which also applies to the axial length provided that eyes showing fundus changes are excluded. Free association of these components would give rise to a similar distribution of refractive errors. This does not occur, however, as there is an abundance of near-emmetropes in the population. This has led to the conclusion that growth of the eye is a coordinated process which is probably mostly controlled by genetic factors although environmental factors play an important part as well.

It is clear that the eye is highly adaptable to a variety of visual environments. This is attributable to the accommodative facility as well as having a variable aperture pupil whose size is a compromise between retinal illumination requirements and the ocular

aberrations caused by large pupils. Aspheric optical surfaces and the gradient index optical nature of the crystalline lens contribute to optimising the system by reducing the spherical aberration which results from large pupils.

Despite the apparent coordination and adaptability of the eye's optical system, it possesses considerable asymmetry. The position of the corneal apex and the asymmetry of its surface profile are consistent with the decentration of the pupil suggesting that the eye is rotated away from the line of sight and may be regarded as approximately symmetrical about the pupillary axis. This would explain why residual astigmatism and asymmetry in the degradation of the peripheral optical imagery have been observed when measurements are taken with respect to the line of sight and not the pupillary axis. As well as this, the lens is known to oscillate with head movements and may be susceptible to the effects of unequal ciliary muscle contraction during accommodation. The latter would deviate the principal ray representing the line of sight and explain the fluctuations in angle alpha that have sometimes been observed.

Studies on the refractive condition of the eye have concentrated on the measurement of the ocular components and the central refraction that results from them. However, the refraction in the periphery of the eye is also effected by the nature of the optical surfaces and their asymmetries and may well give some further insight into the way in which they combine. This is discussed in the next chapter.

CHAPTER TWO

PERIPHERAL REFRACTION

2.1 INTRODUCTION

The state of the refraction in the periphery of the human eye can be explained in terms of a simple positive lens (fig. 2.1 a). When light strikes its surfaces obliquely the object rays converge to form two line foci. Rays in the plane of oblique incidence converge first and produce the tangential line foci. Beyond this point, rays travelling at right angles to the plane of oblique incidence converge to produce the sagittal line foci. The space between the sagittal and tangential foci is called the interval of Sturm whose magnitude represents the peripheral astigmatism. Although the image at either of these focal points is a line, at different positions between them it assumes various ellipsoidal shapes and at half way between them becomes a circle which is appropriately named the circle of least confusion. For a given object distance, separate foci arising from pencils of light coming from all directions lie on two curved surfaces called image shells (fig. 2.1 b) which resemble a teacup (tangential) and saucer (sagittal). Figure 2.1 b depicts the orientation of the tangential and sagittal line foci.

What is measured in the human eye is the variation with field angle in the position of the sagittal and tangential line foci with respect to the retina. A simplified diagram of the astigmatic image shells in the human eye (fig. 2.2 a) shows that the retinal surface normally lies between them. As field angle increases, the tangential image shell falls progressively further in front of the retina and thus becomes more myopic. At the same time the sagittal image shell falls further behind the retina and becomes more hyperopic. This may be represented as in fig. 2.2 b where refraction is plotted as a function of field angle. Here, the horizontal line representing zero on the vertical scale corresponds with the position of the retina. The vertical line representing zero on the horizontal scale may correspond with the line of sight or the optic axis.

(a)

Interval of Sturm

Sagittal line focus

Positive lens

Circle of least confusion

Optic axis

Tangential line focus

Off-axis object point

(b)

"Saucer" Sagittal image shell

"Teacup" Tangential image shell
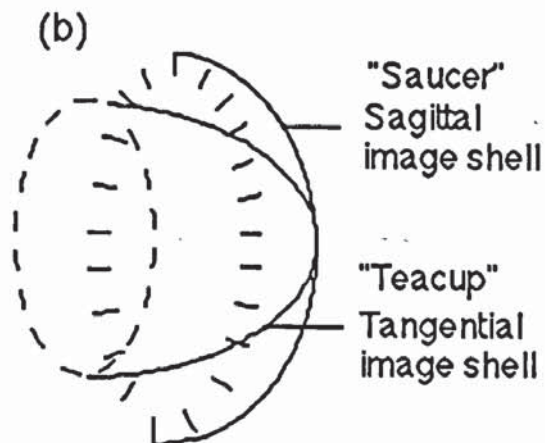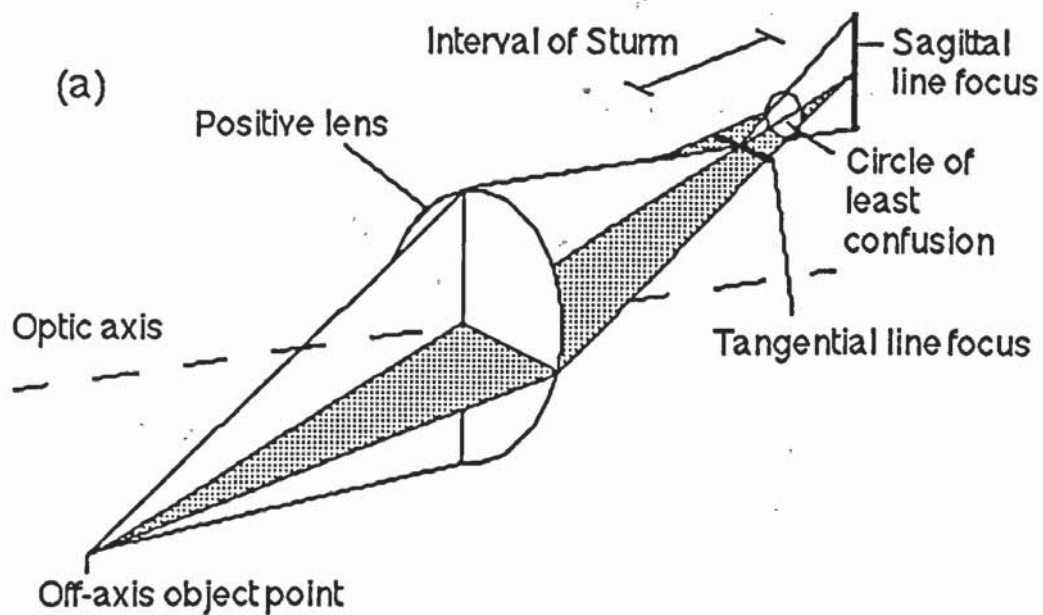
(After Bennett and Rabbetts, 1984)

Fig. 2.1 (a) Diagrammatic representation of the tangential and sagittal line foci, the circle of least confusion and the interval of Sturm. (b) A three-dimensional diagram of the "teacup and saucer" formation of the image shells. The orientation of the tangential and sagittal line foci are depicted in the diagram.
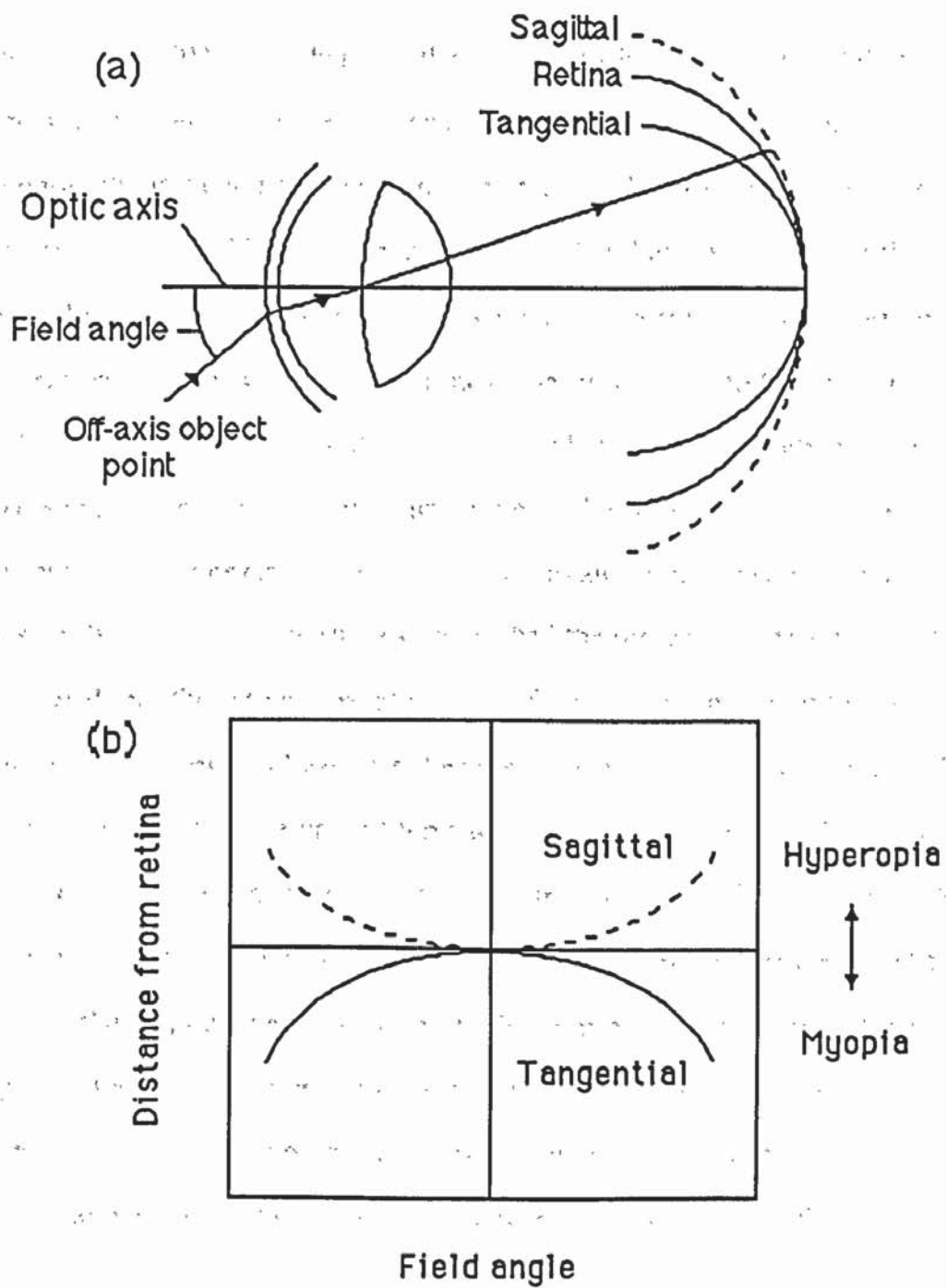
Fig. 2.2   (a) A simplified diagram showing the positions of the tangential and sagittal image shells in the human eye. (b) A graphical representation showing the distance of the sagittal and tangential image shells from the retina as a function of field angle.

60

2.2 HISTORICAL STUDIES ON PERIPHERAL REFRACTION.

Since Young (1801) first calculated the relative positions of the sagittal and tangential image shells, there have been many other theoretical and experimental studies throughout the last century. Ames and Proctor (1921) provide an extensive review of this work which considers the variation of peripheral astigmatism over the horizontal plane. Three experimental methods were used. Some workers determined the peripheral refraction with an ophthalmoscope by using it to focus on retinal blood vessels which lay in the tangential or sagittal planes. Others made measurements by retinoscopy. Those who employed subjective methods moved a grating, or a black line of various orientations drawn on a white card, to and from the subject until it was seen to be sharply focused. These studies established the presence of peripheral astigmatism and showed that the retina normally lies half way between (i.e. at the circle of least confusion) or otherwise closer to either the tangential or sagittal image shell. It was noted by some that the interval of Sturm was larger over the temporal retina than on the nasal side. The same was reported by Ames and Proctor (1921) who considered this to be due to either the effects of angle alpha or to a lopsidedness in the shape of the retina or the crystalline lens or both. In summary, Ames and Proctor (1921) recognised the need for larger studies on both emmetropic and ametropic eyes. They also felt that observations of the relationship between angle alpha and the positions of the astigmatic image shells with respect to the retina would be of value.

2.3 RECENT MEASUREMENTS OF PERIPHERAL REFRACTION

Ferree et al. (1931) considered that previous attempts to measure peripheral refraction involved methods which were too cumbersome or presented the results in a form that had no practical meaning. They therefore conducted what is considered to be the first

major study in this area. By modifying a Zeiss coincidence optometer so that it could be rotated around a stationary eye, they were able to measure the peripheral refraction in 21 eyes to an eccentricity of 60° nasally and temporally in 5 or 10° intervals.

Of the eyes measured, 57% became more myopic in the tangential meridian and more hyperopic in the sagittal meridian as the field angle increased. This gave rise to higher values for the interval of Sturm in the periphery with an average of about 5.5 D at 50° field angle. These were classified as type A. In an emmetrope, the retina would lie between the astigmatic image shells thus exhibiting mixed astigmatism in the periphery as depicted in fig. 2.2 b. They noted, however, that the sagittal image shell lay closer to the retina than the tangential one.

In 29% of the eyes, both astigmatic image shells became more hyperopic as the field angle increased. Consequently, the interval of Sturm did not change significantly in the periphery and a value of approximately 1.5 D was found at 50° field angle. These were classified as type B. In an emmetrope, both astigmatic image shells would fall behind the retina thus exhibiting compound hyperopic astigmatism in the periphery.

Small amounts of asymmetry were found in both types of eye. Here, the tangential image shell was more myopic and the sagittal more hyperopic over the temporal half of the retina compared to the nasal half. The interval of Sturm was thus larger over the temporal retina. In 14% of the eyes, however, considerable amounts of asymmetry were found and these were classified as type C.

Ferree et al. (1932) considered that the major factors influencing the shape of the sagittal and tangential image shells were the retinal profile and the symmetry of action of the refracting system respectively. In one type C eye, asymmetry was only evident

in the tangential image shell which became more myopic on one side of the retina compared to the other. As a result, the interval of Sturm at 45° field angle varied from approximately 8.5 D over the temporal retina to about 4 D nasally. Because the sagittal image shell was more or less symmetrical, they concluded that this form of asymmetry was probably the result of a tilted crystalline lens. In another type C eye, with high central myopia, both astigmatic image shells showed large amounts of asymmetry. The irregular shape of the sagittal image shell led them to believe that this form of asymmetry was largely due to the profile of the retina resulting from the type of axial elongation associated with high myopia.

Ferree and Rand (1933) believed that the breadth of the interval of Sturm and its rate of increase yielded important information as to the strength of the refracting system. Consideration of the latter in relation to the refractive condition at the centre of the field also gave some indication of the length of the eyeball. Such inferences could be used, with a fair degree of certainty, to assess the relative importance of the length of the eyeball and its refractive strength as causal factors in the refractive defect in hyperopic and myopic eyes. Furthermore, they pointed out that only slight variations of the retinal profile are required to produce several dioptres of shift of the peripheral astigmatic image shells. Therefore, information regarding the ellipsoidal nature of the retina could also be derived from the refraction in the periphery.

It is worth noting that Ferree et al. (1931) observed temporary myopic shifts with prolonged viewing. A change in the convexity of the lens or otherwise an elongation of the eyeball, due to the action of the extraocular muscles, were put forward as the cause. They were of the opinion that the former would be in opposition to one of the eyes strongest reflex incentives, as this would blur the retinal image, and so favoured the latter as an explanation. However, neither by keeping the eye stationary or by the

63

use of cycloplegia could this effect be entirely removed. It is possible that both mechanisms could have been responsible to some extent. Indeed, with regard to the role of lens convexity, such effects as accommodative hysteresis (see section 1.4), probably not known to Ferree and his co-workers, could have been involved.

In the light of the above studies, it would almost be possible to bring this chapter to an end were it not for the fact that later workers have substantiated many of the ideas that Ferree and his co-workers put forward. By far the largest of the studies that followed was that of Rempt et al. (1971). The peripheral refraction in 442 pairs of eyes was measured using a retinoscope. Readings were taken over the horizontal plane out to 60° nasally and temporally in 20° intervals. Based on the peripheral refractive variations observed, five classes of eye were described (fig. 2.3).
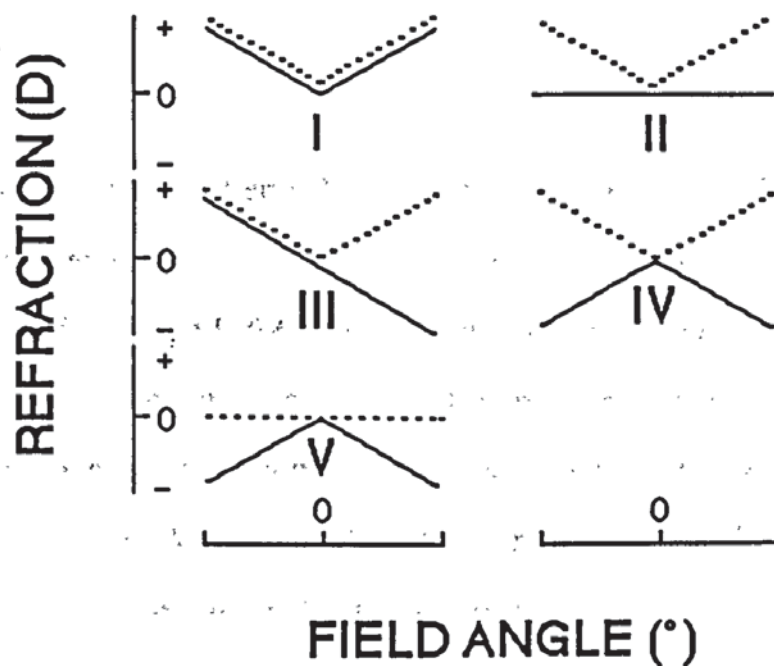
Fig. 2.3   The five kinds of eye described by Rempt et al. (1971) based on the variation with field angle of the sagittal (broken lines) and tangential (solid lines) image shells over the horizontal plane. In this diagram zero degrees field angle coincides with the line of sight.

64

Similar results were usually found in the corresponding right and left eyes. 51% of these were of the type IV pattern which resembled the type A eyes found by Ferree et al. (1931). As these were most frequent and had the highest incidence in emmetropic and hyperopic eyes they were taken to represent the normal condition. 24% of the eyes were of the type I pattern which resembled the type B eyes found by Ferree et al. (1931). These were more commonly found in myopic eyes.

The interval of Sturm was approximately the same over the nasal and temporal halves of the retina in the vast majority of eyes. 3%, however, showed a marked difference. The form of these type III eyes resembled the type C pattern which Ferree et al. (1932) believed to be the result of asymmetries in the refracting system. From the results of Rempt et al (1971) it appears that this pattern, with a larger interval of Sturm over the temporal side of the retina, was the more common asymmetric form and was only found in near-emmetropic eyes.

In addition to the astigmatic patterns described by Ferree et al. (1931), Rempt et al. (1971) found type II and type V eyes which they considered to be intermediate forms. 14% of eyes were of the Type II form in which the tangential image shell was flatter than the sagittal i.e. the former image shell had more or less the same profile as the retina. These were found in emmetropic and myopic eyes. Conversely, 8% of the eyes measured were of the type V form in which the sagittal image shell was the flatter. These were present in emmetropic and hyperopic eyes.

From the previous study, it was noted that eyes exhibiting small values for the interval of Sturm (type I) were characteristic of myopia. Hoogerheide et al. (1971) therefore studied the development of myopia in young pilots. The central and peripheral refraction was first measured when they commenced training (age 18-20 years) and

65

followed up several years later (exact time not specified). The frequency of the type I pattern, in eyes which showed myopic shifts, was found to be 40% in those which progressed from hyperopia to emmetropia, 45% in those which progressed from hyperopia to myopia and 77% in those which progressed from emmetropia to myopia. In contrast, only 5% of those of either group which showed no shift at all were of the type I form. They argued that because the peripheral astigmatic form of an eye may be inborn and changes little during lifetime, it may provide an indication as to whether that eye belongs to a group in which the shift of the refraction towards myopia is a greater or lesser probability. The above is of considerable interest in the light of the research carried out on late-onset myopia (see section 1.4). They also recognised that late shifts towards myopia are rare at 18 years of age and that perhaps the high gravitational forces that pilots are normally exposed to may be causative. The latter was ruled out, however, as fighter pilots are exposed to high gravitational effects but commercial pilots are not and yet both showed myopic shifts.

Millodot (1981, 1984) performed some very interesting studies on peripheral refraction. He compared the peripheral refractive results, obtained on 3 subjects, using a coincidence optometer, retinoscopy and subjective methods (Millodot and Lamont, 1974). Each method, despite its own inherent innaccuracies, produced reasonably similar readings. Because the coincidence optometer was considered to produce the most reliable results, an observation also made by Ferree et al. (1931), Millodot (1981) used it to make further measurements into the effect of ametropia on peripheral refraction. It is worth mentioning here that Millodot (1981) and Ferree et al. (1931) found that the use of cycloplegic drugs to control possible fluctuations in accommodation whilst using the optometer confounded the accuracy of peripheral refractive results due to the aberrations caused by the mydriatic effects of such drugs. They therefore favoured measurements obtained without paralysis of accommodation.

Millodot (1981) made peripheral refractive measurements on 32 pairs of eyes out to 60° nasally and temporally in 10° intervals. The central refraction of the 30 myopic, 13 near-emmetropic and 19 hyperopic eyes ranged between -8 D and +4.5 D spherical equivalent. The results are shown in fig. 2.4. where each datum point represents the mean of all eyes in each group.
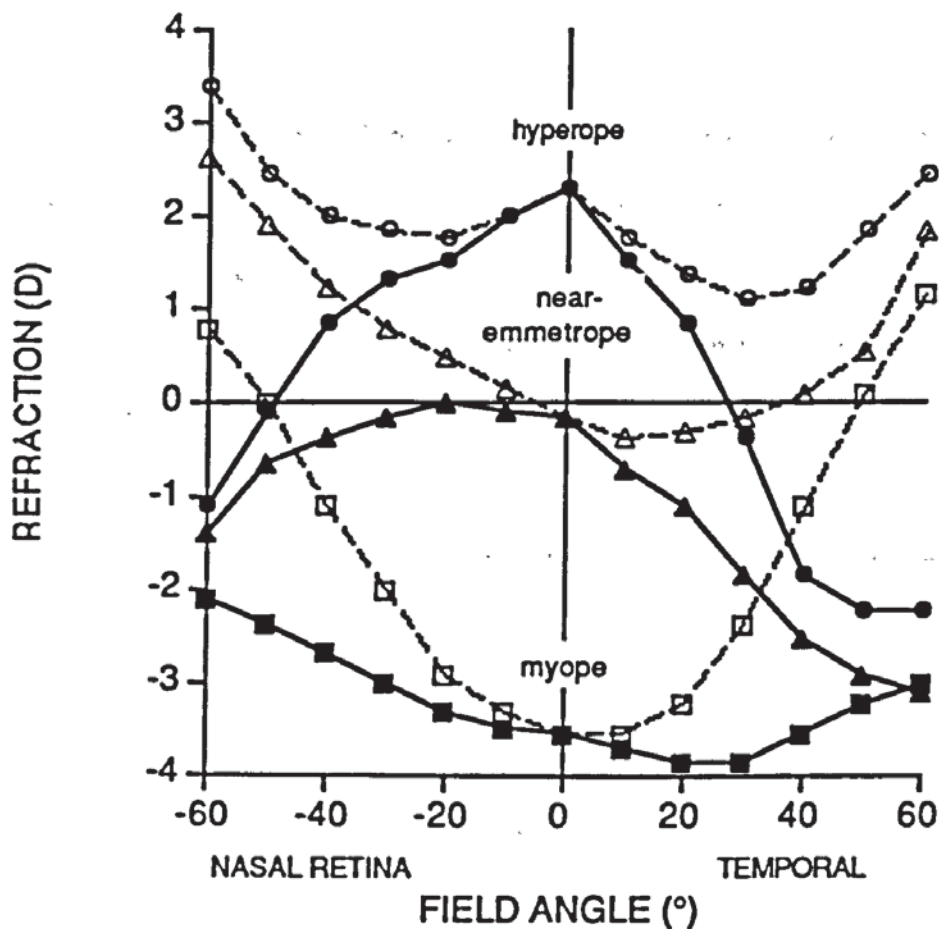
Fig. 2.4   Peripheral refraction for hyperopes (circles), near-emmetropes (triangles) and myopes (squares) plotted as a function of field angle. Each datum point represents the mean of all eyes in each group. Sagittal (broken lines) and tangential (solid lines) are shown separately for clarity (after Millodot, 1981). In this diagram zero degrees field angle coincides with the line of sight.

He found that the interval Sturm in 92% of the eyes was characteristic of the type IV pattern whilst only 8% showed the characteristics of type I (fig. 2.3). Nearly all showed slight asymmetry with a larger interval of Sturm on the temporal side which he believed was due, to some extent, to angle alpha causing the values on the temporal retina to be obtained from a slightly more eccentric position relative to the optic axis. This asymmetry became significantly large in 14% of the eyes (presumably those which he classified as being type IV) thus resembling the type III pattern.

The type of astigmatism differed significantly with each refractive group. Although the interval of Sturm values were more or less the same, myopes exhibited compound myopic astigmatism, emmetropes mixed astigmatism and hyperopes compound hyperopic astigmatism (fig. 2.4). Charman and Jennings (1982) pointed out that this was to be expected as the similarity in the interval of Sturm values showed that the dioptric power of the eyes in each group was approximately equal. Then, if ametropia was purely due to differences in axial length this would produce the different types of astigmatism found for each group. They added that if the retinae in all eyes occupied approximately the same position in the region of the equator of the eyeball, as suggested by Lotmar (1971) and Drasdo and Fowler (1974), there would be a convergence of refractions at large peripheral angles. Charman and Jennings (1982) observed this in the results of Millodot (1981) in which the central refractions differed markedly for the three refractive groups whilst the tangential and sagittal astigmatic image shells had nearly the same values at field angles of 60° (fig. 2.4). Indeed, the resulting flattening of the tangential image shell in the myopes and the sagittal image shell in the hyperopes bears a resemblance to the patterns of the intermediate types II and V eyes of Rempt et al. (1971) (fig. 2.3) and suggests that these are largely due to the shape and position of the retina.

Considering that Ferree and Rand (1933) pointed out that the size of the interval of Sturm was governed by the dioptric strength of the eye, there has been little work on the relative contributions of the cornea and lens. Millodot (1984), however, measured the peripheral refraction in 2 young and 16 old aphakic eyes. He compared the former with the results of his previous study on young eyes (Millodot, 1981) and the latter with the results of 10 normal old eyes. His results indicated that the contribution of the crystalline lens to peripheral astigmatism was more than that of the cornea, despite the fact that the cornea has more than twice the dioptric power. More peripheral astigmatism was found in old eyes than young ones and yet old and young aphakics showed the same values. He concluded from this that the corneal contribution remained fairly constant with age whilst that of the lens increased. The latter, he considered, was due to the lens surfaces becoming more spherical with age. As evidence for this, he pointed out that the peripheral astigmatism found in old eyes was nearly the same as predicted in schematic eyes with spherical surfaces (section 2.4). This is of interest in view of the previously mentioned conflicting evidence for lenticular surface changes with age (section 1.3.4).

From the studies that have been described it is clear that such factors as the shape of the eye and its dioptric power have a great influence on peripheral refraction. Charman (1983) summarised that while the type II, IV and V eyes could be attributed to differences in retinal shape and position, subtleties in the optics were likely to be the cause of reduced astigmatism in type I eyes and asymmetries in type III eyes. Work on schematic eyes, however, has also provided some very useful information and some of the mathematical attempts to model peripheral refraction will now be discussed.

2.4 RECENT ATTEMPTS TO MODEL PERIPHERAL REFRACTION.

Given a knowledge of the typical ocular geometry and refractive indices it is possible to produce a model whose imaging properties approximate those of real eyes. Such models have been used to calculate peripheral refraction. Because of the difficulties in reproducing non-uniformities in the index of the cornea and lens and the asymmetries often present in the human eye, most authors have used schematic eyes with restricted numbers of spherical surfaces, all centred upon common optical axes and separating homogenous optical media (Bennett, 1951; Le Grand, 1967). The schematic eye used by Le Grand (1967) is shown in fig. 2.5.
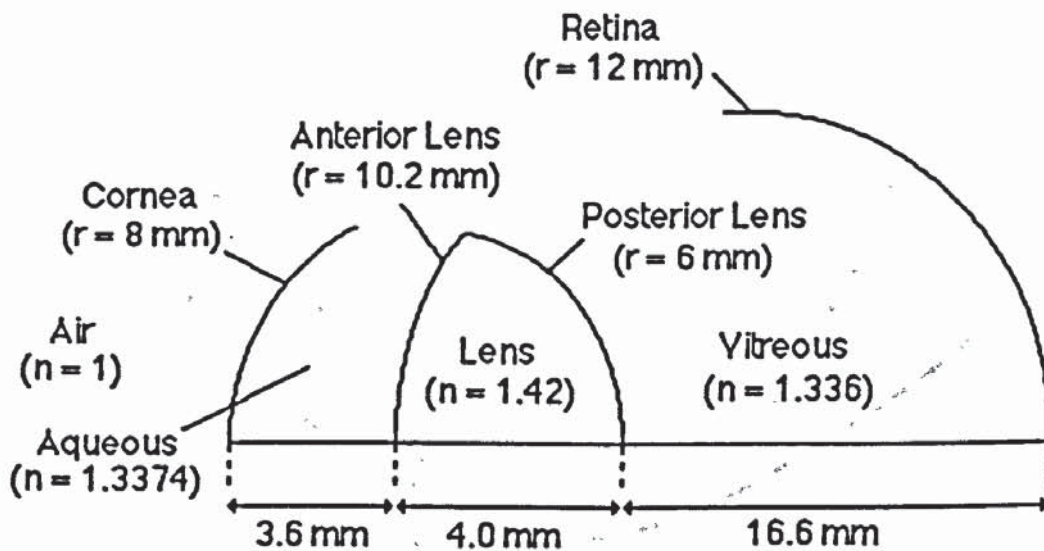
Fig. 2.5   Diagram of the schematic eye used by Le Grand (1967) showing intra-ocular distances, surface radii (r) and assumed refractive indices (n).

These simplified models produce values for the interval of Sturm which are substantially higher than that found experimentally. Figure 2.6 compares the theoretical data of Le Grand (1967) with the curve derived by Lotmar and Lotmar (1974) from the averaged results of 726 of the eyes measured by Rempt et al. (1971).

70

The equation for this curve is:

$$\text{interval of Sturm (D)} = \text{field angle (°)}^{1.5} \times 10^{-2}.$$

To produce larger values for the interval of Sturm over the temporal retina, as observed in real eyes, Le Grand (1967) assumed a value of 5° for angle alpha. He also found it necessary to assume 0.05 D of corneal astigmatism to cancel out the astigmatism that resulted from angle alpha for zero degrees field angle.
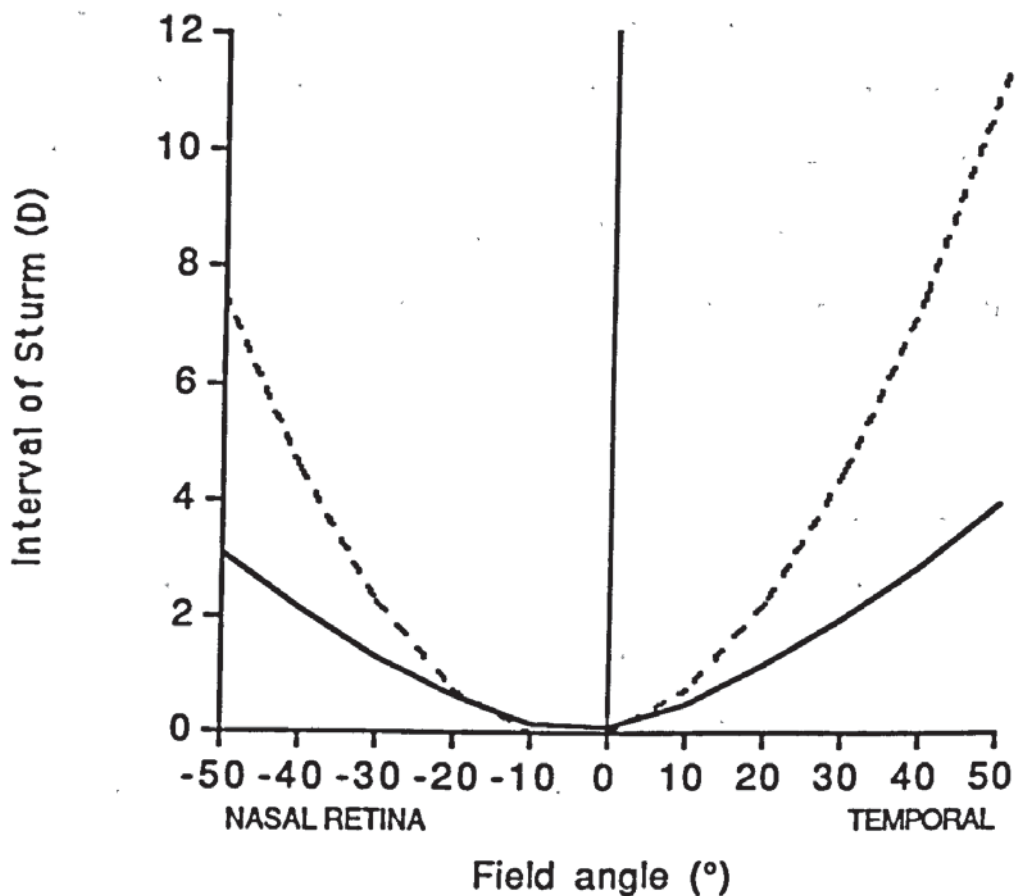
Fig. 2.6   Graph comparing modelled (broken lines) and measured (solid lines) values of the interval of Sturm. Modelled values are taken from Le Grand (1967). Experimental values are those calculated by Lotmar and Lotmar (1974) from 726 of the eyes measured by Rempt et al. (1971). In this diagram zero degrees field angle coincides with the line of sight.

Similarly, Lotmar and Lotmar (1974) found that the axis of their symmetric curve needed to be displaced by 4° from the line of sight in order to reproduce the asymmetries found in the experimental data of Rempt et al. (1971).

Lotmar and Lotmar (1974) considered that the interval of Sturm provided a very sensitive indication of the asymmetries in the eye because measurements made to field angles of 60° are influenced by principal rays which strike the corneal surface as far out as 3.7 mm from the optic axis. Furthermore, they noted that the proportionality of the interval of Sturm to field angle$^{1.5}$, as indicated in their equation, was in contrast to first-order (Seidel) lens aberration theory which predicts proportionality to field angle^2. They pointed out that any model of the peripheral dioptrics of the human eye should account for this difference but noted that some part of it was due to the fact that the Seidel theory only applies to narrow bundles of rays whereas the results of Rempt et al. (1971) were obtained with a full pupil.

As further explanation for the above difference, the research reviewed in chapter one clearly indicates that the corneal and lenticular surfaces are not spherical and that the refractive indices of the optical media, particularly the crystalline lens, are not homogeneous. Several authors have therefore modelled peripheral refraction with more sophisticated schematic eyes aided by recent advances in computer technology.

Lotmar (1971) incorporated aspheric surfaces in a schematic eye resembling the one shown in fig. 2.5 except that it included a two surfaced cornea and the radius of its retina was 12.3 mm. The cornea was assumed to be 0.55 mm thick with a refractive index of 1.3371. Values of 7.8 and 6.5 mm were assumed for the radii of its anterior and posterior surfaces respectively. The front surface of the cornea and the back surface of the crystalline lens were taken to be rotationally symmetric aspherics. A

72

polynomial was used for the front corneal surface, based on the experimental data of Bonnet (see Bonnet and Cochet, 1962), so that the radius at the vertex was the same as specified above but peripherally its surface became flatter. To compensate for the neglect of the gradient index optical structure of the crystalline lens, a second-order parabola was tentatively adopted for its back surface. Again, the vertex radius for the latter remained the same as specified for the spherical model (fig. 2.5) but its surface became flatter peripherally.

Although the above model yielded values for the interval of Sturm (fig. 2.7) which lay within the range of experimental findings, they were still larger than the average results of Rempt et al. (1971). Lotmar (1971) considered that the shape of the cornea had a strong influence on the interval of Sturm and that eyes possessing the type I pattern (fig. 2.3) may be the result of corneae with very flat profiles. With regard to this point, Bennett and Rabbetts (1984) compared the peripheral refraction calculated in a three surfaced (one corneal and two lenticular) schematic eye with a spherical and a parabolic corneal surface. Their results indicate that even when the cornea is flattened to the extent of becoming a parabola, the interval of Sturm is not as small as found in type I eyes. Therefore, as the cornea is normally ellipsoidal in shape (i.e. with peripheral flattening of somewhere between that of a sphere and a parabola) it is only likely to be partially responsible for the low interval of Sturm values found in the human eye. Furthermore, Millodot and Lamont (1974) reported that no appreciable reduction in the interval of Sturm occured in real eyes when the aspheric corneal surface was replaced by a spherical contact lens. They therefore favoured the role of curvature and refractive index variations of the crystalline lens as an explanation for the difference between modelled and experimental results.

Wang et al. (1983) calculated the peripheral refraction in a schematic eye which included two corneal surfaces and up to 400 iso-indicial lenticular surfaces to account for the gradient index optical nature of the lens. Computation of the model, described by Pomerantzeff et al. (1971, 1972, 1984), was based on attributing values for the vertex radii and axial separations of both corneal surfaces and the limiting anterior and posterior lens surfaces together with a curve of the axial spherical aberration with zero accommodation for pupillary apertures up to 4 mm. From these parameters the asphericity of each surface was calculated including the iso-indicial lenticular surfaces. The latter were defined by a third order polynomial to produced a smooth increase in the refractive index from the outside surfaces of the lens to its nucleus.

Although this sophisticated model was designed to produced the correct amounts of axial spherical aberration, Wang et al. (1983) showed that the values it produced for the interval of Sturm in the periphery (fig 2.7) were approximately twice those found by Rempt et al. (1971) for the average eye. It is interesting to note that the schematic eye of Lotmar (1971) also produced more or less the correct amounts of axial spherical aberration although it produced values for the interval of Sturm which were too high.

Figure 2.7 compares the interval of Sturm values predicted by the various schematic eyes described. It can be seen that Lotmar's (1971) model with aspheric surfaces produces more realistic values than the gradient index optical model of Wang et al. (1983). Perhaps this indicates that the asphericity of the refracting surfaces plays a relatively major role in reducing the interval of Sturm.

Lotmar (1971) noted that the tendency for the tangential astigmatic image shell to become strongly myopic in the periphery was preponderantly due to the anterior surface of the crystalline lens. This was explained by the fact that principal rays, traced

74

through the schematic eye, struck the lens surface at greater angles of incidence than at the cornea. To date, no work has been carried out on the effect of the asphericity of the anterior lens surface upon peripheral astigmatism. However, there is evidence that the anterior lens surface flattens peripherally during accommodation (see section 1.3.4) which would have the effect of reducing the interval of Sturm in the periphery. It is therefore interesting that Wang et al. (1983) felt that accommodation may account for the diffence between their results and those found experimentally.
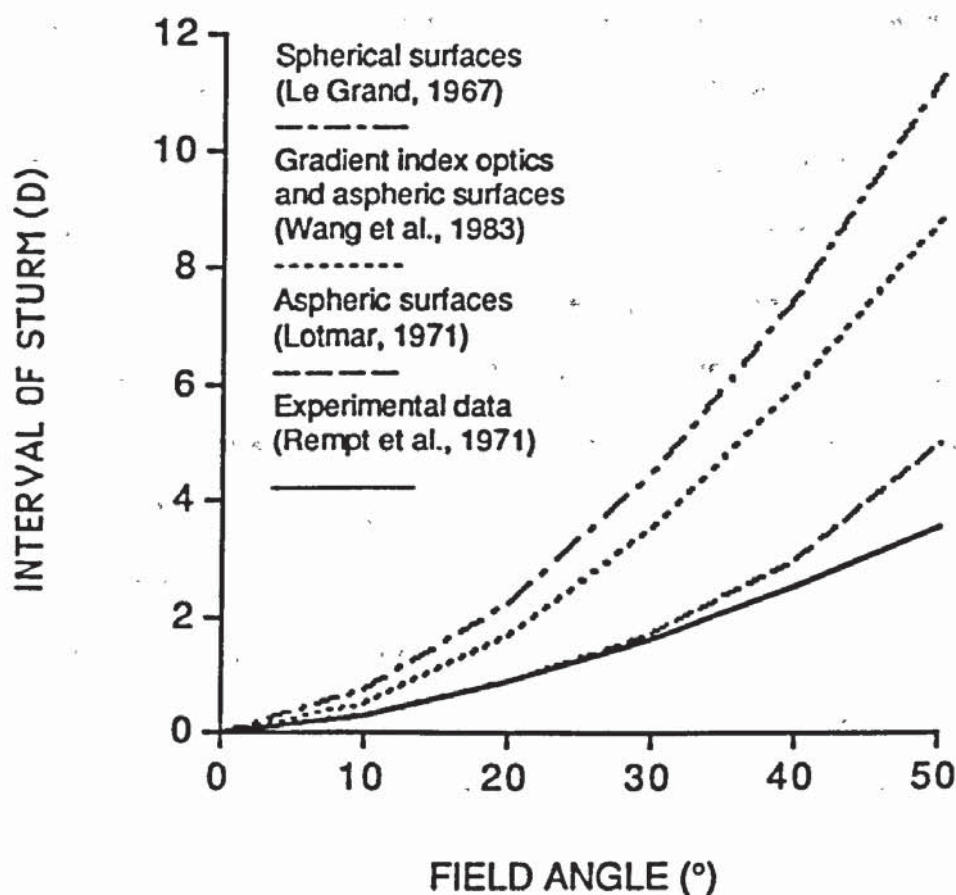
Fig. 2.7   Comparison of the interval of Sturm values predicted by various schematic eyes. The curve representing the experimental data is that derived by Lotmar and Lotmar (1974) from the results of Rempt et al.(1971). In this diagram, zero field angle coincides with the optical axis.

Up to this point, little has been said of the dispositions of the peripheral astigmatic image shells found in schematic eyes. In all of the previously mentioned schematic eyes, an approximately spherical retina of between 12 and 12.3 mm was found to lie between the sagittal and tangential astigmatic image shells (i.e. in the proximity of the circles of least confusion). Schematic eyes are therefore normally of the type IV pattern (fig. 2.3). As already discussed, the intermediate types II and V of Rempt et al. (1971) are likely to be the result of retinae with steeper or flatter curvatures than those specified above. However, the retinal profile is not the only factor that could be involved. Bennett and Rabbetts (1984) pointed out that the disposition of the astigmatic image shells is also governed by one of the properties of aspheric surfaces. As these surfaces, with the same vertex radius, progress from the circular through the ellipses to the parabolic and hyperbolic forms, the sagittal radius of curvature at a given distance from the axis becomes longer. At the same time, the tangential radius of curvature increases at an appreciably faster rate. The result is that both astigmatic image shells move move in the direction of hyperopia, the tangential approximately twice as much as the sagittal. Such an effect could give rise to the types I or II eyes depicted in fig. 2.3 (as was cautioned by Charman and Jennings, 1982). Though this might be construed as further evidence for the role of surface asphericity in eyes showing low values for the interval of Sturm in the periphery, it adds just another complication to the modelling of peripheral refraction in human eyes.

2.5 SUMMARY

This chapter has hopefully pointed out that if there is one technique which can simultaneously yield information regarding such aspects as the relative contributions of axial length and optical power to the refractive status as well as the nature of the asymmetries of the eye, measurement of the peripheral refraction must be a candidate.

Observations of the different patterns of peripheral refraction in individual eyes has led some authors to speculate that whereas the dioptric power of the eye affects the breadth of the interval of Sturm in the periphery, changes in the shape and position of the retina strongly influence the dispositions of the astigmatic image shells. Other authors have investigated the peripheral astigmatic effects of gradient index optical media and aspheric surfaces in schematic eyes of varying levels of sophistication. Despite the amount of work done, it is clear that those who have measured the peripheral refraction have never modelled their results or taken any biometric readings in the same eyes. On the other hand, those who have attempted to model the peripheral refraction have used schematic eyes with "averaged" components which are unlikely to possess the idiosyncracies of the individual eyes from which the original peripheral refractive data was collected.

Regarding measurements of the biometry in living eyes, discussed in the chapter 3, detailed information is only availiable for the profile of the anterior corneal surface whereas simplifying assumptions must be applied to construct the ocular components within. Direct measurements of the crystalline lens surfaces and the refractive indices of the ocular media are only possible in non-living eyes. For this reason, the measurement of peripheral refraction could be a very useful tool if used in conjunction with the former biometric techniques. Here, simplified but representative schematic eyes could be constructed from the biometric data. The manipulation of the schematic surfaces and indices required to model the peripheral refraction would then conceivably lead to some very useful information regarding the nature of the ocular surfaces, their asymmetries and the way in which they combine in individual eyes.

CHAPTER THREE

BIOMETRIC AND PERIPHERAL REFRACTIVE METHODS

3.1 INTRODUCTION

Direct measurements of many of the ocular components are only possible in excised eyes. Such treatment clearly rules out the possibility of further studies on the same eyes. Furthermore, without the support provided by the intra-ocular pressure during life, the excised eye is in a state of mechanical collapse so that the components measured may assume a form which is not necessarily the same as that found in life. Indirect techniques have therefore been employed for studies on living eyes. The limitations of these is that they rely on schematic assumptions which, because of their simplicity, overlook many of the subtleties in the structure of real eyes.

To overcome the above limitations, schematic eyes have been designed, with aspheric surfaces or gradient index optical media (see section 2.4), to simulate various aspects of the optical performance in real eyes. However, as far as the present author is aware, all of the previous studies have attempted to reproduce the optical performance measured in eyes from one population sample with schematic eyes derived from measurements made on other population samples. Although the present study proposes to adopt approximately the same approach as described above, its fundamental difference is that the optical performance and the biometric data are derived from the same sample of eyes so that the idiosyncracies of individual eyes within the sample are accounted for.

For the criterion used to describe optical performance, the variation of refraction in the periphery is chosen because it is so greatly influenced by subtle variations in the shape, power and symmetry of the eye (chapter 2). In this chapter, the methods used to measure the biometry and peripheral refraction are discussed together with the construction of schematic eyes from the raw data. Details regarding subject recruitment

and overall experimental protocol are also outlined.

3.2 TECHNIQUES

In a general review of previously used biometric methods, Ludlam (1967) concluded that future work would benefit from making as many independent determinations of the ocular components as possible in large samples of eyes. He pointed out that multiple measurements in the same eyes, preferably using several different techniques to measure each component, would help to assess the reliability of the data obtained. He also showed that the work carried out by Sorsby et al. (1963), employing ultrasonic and phakometric methods, gave rise to the largest number of independent measurements. For this reason, the present study was constructed along approximately the same lines and will now be discussed in detail.

3.2.1 CORNEAL CURVATURE

(A) OVERVIEW: KERATOMETRY AND KERATOSCOPY

Measurements of the radius of curvature and topography of the anterior corneal surface are made using keratometric and keratoscopic techniques respectively. Clark (1973a, b) presents the most comprehensive review of these and his findings will now be summarised.

Keratometry or ophthalmometry is the method used by most investigators to measure the radius of curvature of the central portion of the anterior corneal surface. Both terms are often used synonymously but Clark (1973a) pointed out that whereas ophthalmometers are suitable for a variety of ocular measurements, keratometers are

80

restricted to the measurement of the anterior surface of the cornea.

Relatively crude opthalmometric determinations were first undertaken by Scheiner (1619). In the late 1700's, Ramsden (Mandell, 1960) improved this technique by adding a doubling device. Helmholtz actually reinvented Ramsden's method but is usually considered to be the original inventor (Helmholtz, 1924). Subsequent adaptations of the instrument, by Javal and Schiotz (Helmholtz, 1924), made it more suitable for the clinical measurement of anterior corneal curvature alone.

Basically, the value for the corneal radius is inferred from the separation of two corneally reflected target mire points which represent the ends of an object imaged by the convex surface of the cornea i.e. the first Purkinje image (see section 3.2.3A). The calibrated doubling device, that allows both mire points to be made coincident, facilitates the measurement of this separation and hence the corneal radius which is directly proportional to it. This method has the advantage of making the results relatively independent of small eye movements and offers the easiest estimation of the principal meridians of corneal astigmatism.

Before discussing the errors involved in making keratometric measurements, it is necessary to distinguish between the accuracy and the precision of a method. Whereas the accuracy is an indication of how close the measured value is to the actual one, the precision refers to the reproducibility of that measurement. Littman (1951) considered that the accuracy of keratometric readings were most seriously effected by imperfect focusing of the mires, incorrect focusing of the eyepeice or accommodation of the observer's eye. Stone (1962) stated that these errors could amount to 0.4 mm in radius measurements. She also indicated that differences in the assumed corneal refractive index values, in keratometers which expressed the results in terms of corneal power,

81

could result in radius errors in the order of ± 0.13 mm. Clark (1973a) noted that there were considerable discrepencies between the values quoted by various authors as to the overall accuracy of keratometry. He estimated, however, that a reasonable figure for the accuracy of central radius readings on human corneae, with conventional two mire keratometers, was ± 0.015 mm. Charman (1972) pointed out that diffraction effects, due to the finite wavelength of light and the limited angular apertures used in keratometry, set the fundamental limit for the precision of this technique. He calculated that even if the various sources of error were controlled, the precision of the surface radii obtained by two mire keratometry would be no better than ± 0.04 mm.

The use of conventional keratometers, for topographic measurements of the peripheral cornea, leads to errors which are proportional to the separation of the mires (Mandell, 1962a, b, 1964, 1969). Many authors have attempted to overcome these errors by modifying keratometers so that the mires are closer together (Berg, 1929; Bonnet and Cochet, 1962; Mandell, 1965; Holden, 1970). However, Charman (1972) has shown that attempts to reduce the area of surface used in making a measurement of the curvature is attended by a reduction in the precision of the measurement. Indeed, for Mandell's (1965) technique of small mire topographic keratometry, Charman (1972) calculated that the lowest limit for precision was 0.1 mm.

The topography of the anterior corneal surface can also be determined by keratoscopy. Although keratometric and most keratoscopic techniques are similar, in that they both involve the measurement of some object's virtual image formed by the cornea, they differ in that keratoscopy measures the radii of concentric target ring images in one or more semi-meridians. Most workers prefer to use photokeratoscopes as these provide instantaneous information over a large area of the cornea in all meridians, with a single photographic exposure. Clark (1973b) provides a detailed review of the designs,

82

errors and mathematical theory involved with various photokeratoscopes, the main points of which will now be summarised.

According to Levene (1965), the keratoscope was invented by Goode in 1847. In 1880, Placido invented the photokeratoscope which was first used to observe pathological irregularities of the corneal surface by Javal in the same year. Gullstrand, however, appears to be the inventor of quantitative photokeratoscopy (Gullstrand, 1924). His method utilised a four ring flat target. To increase the area of the cornea measured, the subject was required to fixate a point in each semi-meridian which meant that four photographs had to be taken. Unfortunately, Gullstrand assumed an incorrect position for the centre of rotation of the eye which made his topographic calculations inaccurate (Wittenberg, 1966). His method also had an error of equivalent to ± 0.07 mm in radius for an 8 mm sphere.

Berg (1929) found that a curved target allowed a much larger area of the cornea to be photographed than was practicable with Gullstrand's plane target photokeratoscope. Berg's targets were located on two semi-circular arcs, one horizontal and the other vertical, and the camera was aimed through a hole at the position where the two arcs intersected. Vignetting by the subject's brows and lids limited the area over which topographic measurements could be made. This technique was found, using a glass lens, to have an error in estimated radius of ± 0.04 mm.

Dekking (1930) realised that the virtual image of a flat target was curved in the same sense as the cornea which prevented the simultaneous focusing of all of the target rings on the photographic plate. He overcame this problem by constructing a keratoscope in which twelve equal sized rings were spaced, in a cylindrical manner, along the optic axis of the camera. Again, vignetting caused by the subject's nose, brows and lids

restricted the coverage when real corneas were observed. Various workers have since used similar cylindrical target designs (Knoll, 1961a, b; Ludlam et al., 1967; Mandell, 1967; Mandell and St. Helen, 1968; El Hage, 1969, 1970). Errors in the estimation of corneal radius of between ± 0.15 mm (Mandell, 1967) and ± 0.061 mm (Ludlam et al., 1967) have been reported when using this method. Clark (1973b) also noted, from Knoll's (1961a, b) photographs, that the vignetting caused by the subjects facial features could be avoided if he fixated 10° to 40° temporally from the straight ahead position.

Ludlam and Wittenberg (1966b) calculated that an ellipsoid target surface would be required to form a flat virtual image, assuming the cornea to be spherical. They believed, however, that such a surface was not directly applicable to the cornea as the latter is normally aspheric. Nevertheless, they later proved that an ellipsoid target surface was appropriate for an ellipsoidal cornea (Wittenberg and Ludlam, 1970). Townsley (1967) described a similar ellipsoid target which was incorporated in the revised Wesley-Jessen Photo Electric Keratoscope (PEK). Wesley (1969) described the errors involved in Townsley's (1967) method in which ellipsoid curves were fitted to the experimental results by the method of least squares. He stated that the typical maximum deviation of the fitted ellipse from the experimental results was 0.0006 mm. Clark (1973b), however, found Wesley's (1969) claim difficult to accept because the value quoted was so much smaller than the errors of radius determination found by Ludlam et al (1967).

Clark (1973b) criticised many of the analytical formulae, intended to represent the observations of real corneae, as being meaningless considering the variation of the corneal surface between individuals and in different semi-meridians. He focused his criticism on Townsley's (1967) method of analysis, stating that the asphericity could

be overestimated by as much as three times, indicating that his assumptions were invalid in practice. In general, he pointed out that the smallest random errors in keratoscopy were two or three times larger than those of keratometry. He added that whereas, for spherical surfaces, the theory of both types of instrument could be made sufficiently exact to allow the systematic errors to become smaller than the random ones, this was not so for the human corneal surface.

Clark (1966, 1971, 1972) described an alternative technique called autocollimating keratoscopy. Although this is not described here, it differs from the previously mentioned keratoscopic techniques in that it depends on the observation of a real image reflected from the cornea. It is interesting to note that the results of Kiely et al. (1982), who used the autocollimating keratoscope to determine the average corneal profile, agree well the findings of a recent study by Guillon et al. (1986) which made use of the PEK and Townsley's (1967) method of analysis.

Although the study of Guillon et al. (1986) was published too late to influence the design of this study, it is somewhat pleasing to report that the approach in both is the same. That is, the central radius of curvature of the anterior corneal surface was measured using a standard keratometric technique and the PEK. The latter provided additional information as to the profile of the cornea in the periphery. The experimental design used by the present author will now be described in more detail.

(B) PRESENT STUDY: KERATOMETRY

The anterior central corneal curvature was measured using a Zeiss keratometer. For this instrument, both of the target mires were collimated and the doubling device was the same as that used by Helmholtz (1924). The above features allowed the

85

keratometer to be used both by emmetropes or ametropes (the author is hyperopic) without eyepiece adjustment. Although the writer made every attempt to focus the instrument correctly, any focusing errors would have led to some blurring but the readings would not have been not be effected (Bennett and Rabbetts, 1984). Hence, the large focusing errors described by Littman (1951) were eliminated. The microscope eyepieces were also arranged such that the corneal images were viewed with the left eye and the scale by the right eye.

Periodical calibration checks were made, in the absence of skew or astigmatic misalignment, by sliding a precision 7.8 mm spherical surface in the position normally occupied by the subjects eye. These checks ensured that the instrument remained correctly calibrated throughout the experiment.

The subject was asked to look towards the fixation target set between the target mires. This ensured alignment of the instrument axis to the subject's line of sight. Measurements were made, in all eyes, of the radii and axes of orientation in the flattest and steepest meridians. A sample of three readings were taken for each parameter from which a mean and standard deviation was calculated.

(C) PRESENT STUDY: PHOTOKERATOSCOPY

Corneal topography was measured using the Wesley-Jessen PEK IIIA, which is fully described elsewhere by Bibby (1976). The photokeratoscope target consisted of seven concentric rings on an ellipsoidal surface; the smallest reflected from a corneal zone of approximately 3 mm in diameter and the largest from a 9 mm diameter zone.

The eyepiece was first set correctly for the experimenter's ametropia. The subject was

86

then asked to look into the PEK with his eyes directed temporally rather than in the straight ahead position. This stopped the nose obstructing the instrument during focusing and increased the area of the cornea available for measurement. By asking the subject to fixate the instrument cross wires, alignment was achieved between the optic axis of the camera and the subject's line of sight.

A Polaroid camera allowed photography of the target image after reflection at the corneal front surface. The photographic results were then inspected, with a 10 D lens, to see whether the rings were in reasonable focus and, if they were not, whether another photograph was required. Only one photograph was taken per person. If the photograph was acceptable, it was sent to Hamblin Contact Lenses Ltd. for analysis.

Wesley (1969) described the "reader" now used in the PEK system; the photograph is projected at a magnification of X 50.8 so that 2 inches on a screen represents 1 mm on the eye; a maximum of 14 points are measured along each of the principal meridians. From this analysis the central radii of curvature and the "shape factor" are determined for both principal meridians as well as the axis orientation of the flattest meridian. The position of the corneal apex relative to the line of sight is also given.

With regard to the "shape factor", Wesley-Jessen define this as being the square of the eccentricity (e^2). For this study, in accordance with Guillon et al. (1986), the notation initially proposed by Barker (1943) and later described in detail by Bennett (1968) is chosen. The following formula, taking the origin of the co-ordinates at the apex of the cornea, gives the relationship between the x (along the optic axis) and y (perpendicular to the optic axis) values for any point of the curve:

$$P\,x^2 - 2xr + y^2 = 0$$

where r is the radius of curvature at the apex and P is the conic constant. The

advantage of this formula is that it is capable of describing all the known conic sections as indicated below:

$$P = -ve = \text{hyperbola}$$
$$P = 0 = \text{parabola}$$
$$P = 0\text{-}1 = \text{prolate ellipse}$$
$$P = 1 = \text{circle}$$
$$P = >1 = \text{oblate ellipse}$$

The relationship between the conic constant and Wesley-Jessen's shape factor is:

$$P = (1 - e^2)$$

3.2.2 AXIAL DISTANCES

(A) OVERVIEW: OPTICAL AND NON-OPTICAL METHODS

Some of the main methods which have been used to measure the axial distances of the eye will be discussed in this section. The axial distances usually measured are the anterior chamber depth, lens thickness, vitreous depth and total axial length. Many workers, however, include the corneal thickness in their estimate of the anterior chamber depth.

Photography of slit lamp sections allows axial distances to be measured by optical means (Sorsby et al., 1961, 1962a and b). The slit lamp generally consists of an illumination system and an observation system which are mounted on a moveable trolley. Both parts are rotatable about the same vertical axis, which also coincides with their respective foci. By this means, the slit image, illuminating the eye, and the observing microscope remain simultaneously in focus on the same part of the eye.

88

With the arms of the latter fixed at an angle of 40°, a photograph can be taken of an illuminated section of the cornea and crystalline lens from which the corneal thickness, anterior chamber depth and lens thickness can be measured. This technique, however, has a few disadvantages.

Firstly, measurements made from the slit lamp sections are apparent depths. To obtain real depths, estimates are required of the corneal surface radii, lenticular surface radii and the central refractive error. Paraxial formulae and assumed refractive indices are then used to calculate the real depths along with the vitreous and axial length. The final values obtained are therefore interdependent and susceptable to schematic assumptions (see section 3.2.3A).

Secondly, the magnification required to obtain a slit image gives rise to a very small depth of field and reduces the quality of the photograph. To overcome this, Goldmann (1940) described an ingenious mechanical method in which both camera and slit lamp are moved forward during exposure whilst the film traverses synchronously behind a slit. The image on the film is thus maintained in constant focus. Brown (1969), applying Scheimpflug's principle (1906), discussed the effects of tilting the camera's objective plane, film plane, or both, so that the the slit image was in focus at all points on the photograph. For biometric measurements, he favoured the results arising from a tilted film plane and built an advanced slit image camera along those lines (Brown, 1972). Unfortunately, attempts made by the present author to construct the latter of these were met with no success and were therefore abandoned.

Finally, even with the above modifications to the slit lamp, the pupil aperture required to produce a slit image showing both crystalline lens surfaces would rule out the possibility of performing measurements on eyes without mydriasis. The latter is

important particularly with respect to the observations of Ludlam et al. (1972) who found that biometric data obtained with natural pupils compared favourably with that under the influence of the mydriatic effect of drugs. Some workers have described methods which use infra-red light to avoid the need for mydriasis (Otsuku et al., 1965; Kabe, 1968). However, the use of such techniques for the present study were limited by the fact that they must either be made in the dark, or otherwise require the use of expensive apparatus such as infra-red teleconverters.

The accurate measurement of corneal thickness and anterior chamber depth have attracted the attention of many workers in connection with contact lens fitting, corneal grafting and the study of such pathological conditions as glaucoma. Consequently, techniques which are specifically used to measure these components are called pachometers. Despite the complications involved in measuring axial distances with slit lamps, the measurement of corneal thickness and anterior chamber depth are relatively easy. This can be achieved by successively focusing the slit lamp microscope on the specular reflexes of the anterior corneal surface, the posterior corneal surface and the anterior lens surface. The respective distances travelled by the microscope then represent the apparent thickness of the cornea and anterior chamber depth. True thicknesses are easily calculated applying the conjugate foci relationship (Bennett and Rabbetts, 1984). Indeed, the first attempts to determine corneal thickness and anterior chamber depth in vivo, used a similar approach to that described above (Blix, 1880; Ulbrich, 1914). However, the successive focusing method is susceptible to involuntary movements of the subject's head during the taking of measurements meaning that measurements could only be made to an accuracy of ±0.1 mm (Von Bahr, 1948).

Von Bahr (1948) developed a pachometer, for the measurement of corneal thickness, in which two glass plates could be rotated about the vertical plane so that, in the field of view of the slit lamp microscope, the reflection of the slit in the corneal endothelium could be made to coincide with that of the corneal epithelium. The angular rotation of the glass plates required for the alignment of the two images could be read from a calibrated scale and related to the true corneal thickness by trigonometric calculations. Because this allowed simultaneous observation of doubled specular reflexes, the problems caused by eye motion were overcome. The standard deviation obtained for corneal thickness readings was found to be ±0.013 mm. Various changes were subsequently made to Von Bahr's (1948) technique to improved the accuracy, subject alignment and measurements of thickness of the cornea in the periphery (Maurice and Giardini, 1951; Donaldson, 1966; Mandell and Polse, 1969; Hirji and Larke, 1978). Hirji and Larke (1978) reported a precision of ±0.03-0.04 mm for measurements of the peripheral corneal thickness by topographic pachometry.

Juillerat and Koby (1928) described a technique for measurement of the apparent thickness of the optical section as seen by diffuse reflection. This technique was later improved by allowing simultaneous observation of the of the anterior and posterior surfaces of the cornea by means of a split ocular (Lobeck, 1937). Jaeger (1952) combined the use of the split ocular with Von Bahr's (1948) method of rotating glass plates to align the anterior and posterior corneal surfaces and produced an attachment to the Zeiss Opton slit lamp. Jaeger's (1952) method was then technically improved and made available for use with the Haag Streit 900 slit lamp (Lowe, 1966). This has now become the standard and most widely used pachometer for convenient and accurate measurements of both the central corneal thickness and the anterior chamber depth. Alsbirk (1974) found the random errors of this method, assessed by taking triple readings and successive examinations over several weeks, to be ±0.02 mm and

± 0.037 mm, respectively, for determinations of the anterior chamber depth (including corneal thickness). For estimates of corneal thickness, the random errors found were ±0.007 mm and ±0.013 mm respectively. Edmund and La Cour (1986) identified three components which effected the precision of pachometric measurements: the day to day variation (±0.006 mm), the variation attributable to slit lamp adjustment (±0.005 mm) and that due to pachometer adjustment (± 0.013 mm). They stated that three pachometric readings should always be made on each occassion.

One of the drawbacks of the Haag Streit 900 slit lamp method is that it makes depth measurements with respect to the line of sight. This can produce a systematically thicker corneal reading for the left eye than the right eye (Kruse-Hansen, 1971), although Alsbirk (1974) found no such difference. Mishima and Hedbys (1968) attempted to increase the accuracy of the Haag Streit 900 attachment by ensuring perpendicular alignment to the corneal surface. This method also allowed subsequent workers to measure the corneal thickness in the periphery (Martola and Baum, 1968; Tomlinson, 1972).

Other pachometric techniques have also been developed such as the electric pachometer (Binder et al., 1977) and an ingenious method involving the use of astigmatic light bundles (Lindsted, 1916; Stenstrom, 1953; Tornquist, 1953). The complexities of these, however, have led many workers to use more conventional pachometers.

Alternatively, there are non-optical methods for the measurement of axial distances. Use of phosphenes produced by X-rays in the retina allows the axial length of the eye to be measured accurately. The fact that X-rays are percieved by the dark adapted eye was noted by Dorn in the late 1890's but was almost forgotten until Taft, in the 1930's, clearly established the visibility of X-rays (Rushton, 1938). Rushton (1938)

92

was the first to apply the use of X-rays in a subjective method of independently measuring the axial length. He projected a thin X-ray beam from the side through the subject's eye, which produced a circular shaped phosphene on the retina. As the beam moved closer to the posterior pole of the eye, the size of this circle diminished and eventually disappeared. The separation between this point and the front of the cornea could then be measured.

It is claimed that this method could locate the posterior pole (i.e. the focal plane of the retina) to a precision of $\pm$ 0.1 to 0.2 mm (Borish, 1970). The accuracy of the technique, however, was found to be less than 0.1 mm (Sorsby and O'Connor, 1945; Stenstrom, 1946) and estimates of the axial length compared well with those made by optical means (Sorsby et al., 1957; Jansson, 1963a).

Although the X-ray technique also offered a method for estimating the total ocular power (Goldmann and Hagen, 1942; Stenstrom, 1946) and the equatorial diameters of the globe (Sorsby and O'Connor, 1945; Deller et al., 1947; Sorsby, 1948), it was not capable of providing a direct measurement of any of the other axial distances.

Ultrasonic techniques offer up to four objective independent measurements of intraocular distances: corneal thickness, anterior chamber depth, crystalline lens thickness and vitreous length. The axial length is taken to be the sum of these distances. The use of ultrasound to make ocular measurements was pioneered by Mundt and Hughes (1956) and Oksala and Lehtinen (1957). Numerous workers have since used this technique (Yamamoto et al., 1960; Leary et al., 1963; Jansson, 1963a; Gernet, 1964a, b, c; Nover and Grote, 1965; Luyckx-Bacus, 1966; Coleman, 1967; Giglio and Ludlam, 1967, 1971; Giglio et al., 1968; Lowe, 1968; Giglio and Meyers, 1969; Gernet and Hollwich, 1969; Larsen, 1971a-d, 1979; Fledelius, 1976; Storey

and Rabie, 1983, 1985; Gordon and Donzis, 1985). Exhaustive reviews have already been published on the theory and application of ultrasound (Jansson, 1963b; Ludlam and Giglio, 1966). Therefore, the following discussion only serves to summarise some of the main approaches made to improve ultrasonic techniques.

The principle is that high frequency longitudinal sound waves are generated by a probe or transducer. When the probe is in contact with the cornea, some energy is reflected back in the form of echoes. From the duration of these echoes, between the time of emission to the time of return, the distance travelled can be calculated. Ultrasonic measurements can be made by either isolated time amplitude (A-scan) or intensity modulated (B-scan) ultrasonograms. In the A-scan mode, only information about axial distances is obtained, whereas in the B-scan mode the equivalent to a transverse section of the eye is given. It is considered that A-scan is the most accurate mode for making linear measurements within the eye. As this is the case, this discussion will be confined to A-scan ultrasonography. Here, the intraocular reflections from the tissue interfaces of the cornea, the anterior and posterior crystalline lens and the vitreo-retinal interface, are normally displayed on an oscilloscope.

The accuracy and resolution of the ultrasonic reflections are increased when a higher frequency probe, producing shorter wavelengths, is used. For instance, at 10 MHz, for measurements in aqueous or vitreous humour, which transmits sound at velocity of 1534 ms^{-1}, each wavelength of sound would be 0.1534 mm. Thus the first quarter cycle, which is the first small recurrent section that can be measured, would be at approximately 0.04 mm. Measuring between two surfaces would give a possible error of about 0.08 mm with an average error of around 0.04 mm. At 20 MHz, the first quarter cycle is halved to 0.02 mm with a correspondingly small value for the average possible error. Frequencies of between 4 MHz (Jansson, 1963a; Leary et al., 1963)

and 20 MHz (Giglio and Ludlam, 1967) have been used, the latter being able to resolve both corneal surfaces and the layers behind the eye. At higher frequencies there is generally not enough energy to show the retinal interface well. High frequencies can also cause ocular injury (Zeiss, 1938; Baum, 1956), which is the reason why most modern ultrasonoscopes, which require such frequencies, generate ultrasound in pulses of short duration so that the intensity is greatly reduced and no risk of tissue damage exists (Jansson, 1963a).

The width of the ultrasound beam is also of importance in producing accurate estimates of the axial length. A wide beam, which would be even wider after dispersion through the crystalline lens, would strike a wide section at the back of the eye. Because of the curvature of the retina, the edges of the beam would be reflected back prior to the central portion, striking the true posterior pole. This would result in the determined axial length being shorter than the actual value. To avoid this, most workers have used a focused transducer which produces a beam of approximately 2 mm at the posterior pole, equivalent to the macula area.

Another factor effecting the measurement accuracy is the assumed value for the velocity of ultrasound through each of the ocular media. Measurements of the velocity of ultrasound have either been performed on isolated tissues (Oksala and Lehtinen, 1958; Yamamoto et al., 1961) or on enucleated and cadaver human eyes (Jansson and Sundmark, 1961; Jansson and Kock, 1962). Velocities of 1639 ms^{-1} for the cornea, 1534 ms^{-1} for the aqueous and vitreous humour, 1640 ms^{-1} for the crystalline lens and 1650 ms^{-1} for the sclera have been reported at 37°C. It is assumed that these are invariant for each different subject which is a little dubious in the case of a complex structure like the crystalline lens whose ultrasonic properties may vary with age and accommodation.

95

Probe application and alignment also *a* effects the accuracy of the results. The probe can either be placed directly on the cornea or separated from it by a water bath. Although the former technique tends to be easier to apply and more rapid, it is less accurate since it compresses the cornea. Compression of the cornea is avoided with the latter method which also has the advantage of preventing the corneal echo from being obscured by the "main bang" of the transducer. The problem with this technique, however, is that the subject needs to wear water filled goggles which is somewhat time consuming and clumsy (Jansson, 1963a; Leary et al. 1963). Giglio and Ludlam (1971) improved the design of the probe by enclosing the water in a cone constructed of silicone rubber and capped with a thin membrane. In general, adequate axial alignment of the probe can be secured by careful visual alignment with the centre of the cornea and by observation of the oscilloscope to ensure that the anterior and posterior crystalline lens echoes are maximised and the maximum posterior lens to vitreo-retinal distance is obtained (Leary et al., 1963). Some workers have increased the accuracy of probe alignment (to the visual axis) by using optotypes or fixation lights (Coleman, 1967). Others have attempted to build automatic probe transport mechanisms (Giglio and Meyers, 1969).

Several methods have been described for the measurement of either time or distance from the A-scan presentation on the oscilloscope. Some authors have used interferometry (Oksala and Lehtinen, 1958; Yamamoto et al., 1960; Jansson and Sundmark, 1961; Jansson and Kock, 1962). Here, sound pulses are directed simultaneously through the test medium and the water column of the interferometer. Adjustment of the reflecting surface of the interferometer is made until the echoes from both coincide. The resulting summation, by interference, of these echoes makes the point of adjustment easily recognisable. With a knowledge of the distance and velocity of ultrasound through the water column, and by knowing either the distance or the velocity of ultrasound through the test medium, the unknown parameter can be

calculated. Other techniques used have been the comparison of photographs of the tissue echoes with known standards (Sorsby et al., 1963; Leary et al., 1963) or the scaling of photographs against a time scale electronically superimposed on the oscilloscope (Giglio and Ludlam, 1967). The use of an electronic interval counter to determine the distances between echoes, however, provides the most accurate and least time consuming method (Coleman, 1967). It is by this method that the more advanced ultrasonic devices make automatic measurements. Furthermore, by continuously monitoring the distances until, for instance, the longest vitreous length is recorded, these instruments can ensure that readings are only taken when the probe is correctly aligned. However, this technique can lead to the measurement of the wrong echoes giving results which are precise but not necessarily accurate.

With the above improvements, the accuracy and precision of ultrasonography has considerably improved. Mundt and Hughes (1956) claimed an accuracy of ±1-2 mm whilst that claimed by Oksala and Lehtinen (1957) was between ±0.4 and ±0.6 mm. Using a better technique, Jansson (1963a) reported measurement errors of ±0.036 mm for the anterior chamber depth and ±0.038 mm for the axial length. Giglio and Ludlam (1967) increased the resolution of the technique such that an accuracy of ±0.03 mm with a precision of ±0.016 mm was reported (Giglio et al., 1968). Many authors have found good agreement between ultrasonic and optical techniques (Jansson, 1963a; Leary et al., 1963; Lowe, 1968).

(B) PRESENT STUDY: ULTRASONOGRAPHY

A-scan ultrasonic measurements of the anterior chamber depth (including corneal thickness), lens thickness, vitreous length and axial length were made with the commercially available Storz Alpha 20/20 Biometric Ruler Soft Probe System (also used by Storey and Rabie, 1985). This instrument was chosen as it offered most of the previously described facilities which aid the retrieval of reliable and convenient measurements.

The hand held probe consisted of a 10 MHz transducer which produced a focused beam of pulsed ultrasound and recieved the resulting echo waves. The design included a built in water bath sealed with a thin silicone reservoir. This apparatus, which was filled with water immediately prior to taking a set of measurements, reduced corneal indentation and optimised probe/corneal coupling by contouring around the cornea.

The instrument automatically monitored the force with which the probe was being applied to the cornea. First of all, the initial length of the water bath was measured using one of the instrument programs. The amount of indentation of the silicone cap, while readings were being taken, could then be continuously recorded. A value for the average probe compression was then given next to each measurement taken. The manufacturer's instructions recommended that rejection of all measurements with probe compressions outside 0 to 1 mm would ensure that the results were reasonably free from errors caused by indentation of the cornea. This recommendation was duly followed.

Probe alignment was also automatically controlled using a preprogrammed algorithm. This required four echoes to be returned (from the cornea, anterior lens, posterior lens and retina) which were at least 80% of their expected maximum height and were spaced in accordance with reasonable human eye parameters. The algorithm also searched for an echo in front of the fourth spike (which may be from the retina or sclera) and if one was detected, it was enhanced and examined for conformity with a retinal echo. The algorithm then either accepted the complete return signal and began a series of readings, or rejected it. If the rejected signal was close to being acceptable, a chirping sound was emmitted by the instrument. By this means, the experimenter could make small adjustments to the alignment of the hand held probe using the chirping signal of the instrument for guidance.

Although the manufacturers state that alignment is made to the line of sight and provide a built in fixation light with the probe, they also indicate that the algorithm ensures ideal alignment of the ultrasonic beam to a line, travelling through the cornea and falling upon the retina at a position between the macula and the optic disc, which resembles the optic axis. This apparent discrepancy was noticed by the present author who frequently failed to obtain any acceptable readings even when the probe fixation light was used. Nevertheless, even if it was accepted that alignment occurred about the optic axis, the latter is only a concept (see section 1.5) and is itself susceptible to the effects of translation and rotation of the ocular surfaces. Therefore, for the present purposes and because of the difficulties in estimating the errors incurred by incorrect alignment to either axis, it was assumed that the difference between the results obtained by alignment to either would be insignificant.

Another feature of the instrument was that it automatically measured the distance between the echoes with an electronic interval counter. An average value of 1550 ms^{-1}

was assumed (by the manufacturer) for the velocity of ultrasound through the whole eye. Once an acceptable echo pattern was obtained, the alpha 20/20 took 60 consecutive readings from which an average value was calculated. It then rechecked for a valid pattern and repeated the process until eight groups of 60 readings were taken. During this time, the instrument made a continuous audible tone, signalling to the experimenter that readings were being taken. A beep was then sounded when the operation was complete. At that point a new average and, for axial length only, a standard deviation was calculated from the eight previously determined averages. All 480 readings could be taken within 0.5 seconds which minimised the influence of head movements whilst also providing a large sample of readings. Values for the standard deviation (for axial length) provided a further check in case any head movements had occured during the retrieval of data. The manufacturer's instructions recommended that averaged readings whose standard deviations exceeded 0.1 mm were rejected. This recommendation was also followed in this study.

A footswitch was provided which, when depressed, initiated the measurement sequence. Continued pressure on the footswitch allowed up to 32 successive blocks of 480 readings to be made which were automatically stored in the instrument's memory. These could be reviewed on completion of data collection so that the readings which failed to meet the previously mentioned rejection criteria could be deleted. A printout of the final results was then obtained for further analysis.

Prior to taking readings from each eye, the probe water bath was filled with tap water, sterilised using Webcol Alcohol Preps (70% isopropyl alcohol) and rinsed in a bowl of sterile contact lens solution. The cornea of the test eye was anaesthetised with 0.4% Benoxinate. A chin and forehead rest was used to keep the subject's head steady in the upright position. To control eye movements and accommodation, the non-test eye

fixated an illuminated target positioned 3 m away (see section 3.4.3). It was also necessary to disable the small fixation light built into the probe as this was found to be of no assistance in aligning the probe and often hindered fixation of the actual target with the non-test eye.

After measuring the initial probe length, the probe was applied to the test eye. The footswitch was depressed and minute adjustments were made, guided by the chirping noises of the instrument, until a continuous tone indicated that readings were being taken. Keeping the probe very steady the beeps, which sounded on completion of each set of 480 readings, were counted until at least 10 readings had been obtained.

The experimenter then quickly reviewed the results to ascertain their suitability in case more readings were required. Here, another criterion for rejection was employed as a result of fluctuations in accommodation. These were evident by the fact that a block of consecutive results would suddenly acquire lenses which were noticeably thicker and anterior chambers which were shallower than the other readings. Great care was taken when deleting these so as not to bias the results in any way. A printout of the accepted results was finally obtained so that the average and standard deviation for each component length could be calculated.

(C) PRESENT STUDY: ANTERIOR CHAMBER PACHOMETRY

A comparison between the axial distances obtained using ultrasonic and optical techniques was required. As previously explained, however, optical techniques such as the photography of slit lamp sections only provide direct measurement of apparent depths and require mydriasis which would automatically rule out any valid comparison between the results. Nevertheless, a pachometer is able to provide convenient (though

101

indirect) measurements of the true anterior chamber depth without mydriasis. Although it could be argued that the complexity of the crystalline lens may lead to the largest errors between both techniques, it must be remembered that the anterior chamber is susceptible to the effects of corneal indentation by the probe as well as variable accommodation. For this reason, comparison of the anterior chamber depth by pachometric and ultrasonic means serves not only to indicate the concordance between the results obtained by both methods but also to check on the control of accommodation throughout the experiment and the effectiveness of the measures taken to prevent corneal indentation with the ultrasonic probe.

Optical determinations of the anterior chamber depth were made with the commercially available Haag Streit 900 Anterior Chamber Pachometer, a full description of which is given elsewhere (Lowe, 1966). Essentially, a slit of light was used to illuminate a section of the eye to be measured. This section was viewed from a fixed angle of 40° to the right hand side (with respect to the experimenter). Two plane glass plates (one above the other) horizontally bisected the reflected light rays passing to the eyepiece of the observation microscope serving the experimenter's right eye. The lower glass plate was set at right angles to the reflected light so that rays passed directly through it. The upper glass plate could be pivoted which deviated the light travelling through. A split ocular was used for the right eyepiece so that the images from the lower and upper glass plates were seen in the lower and the upper halves of the field respectively.

When both plates were parallel a single image could be seen but after rotation of the upper glass plate, the upper set of images appeared deviated. By this means the front surface of the cornea in the lower set of images was aligned with the front surface of the lens in the upper set. The amount of rotation required to do this was a measure of the apparent anterior chamber depth and could be read from a scale which was directly

callibrated in millimeters with 0.1 mm graduations.

Apparent depth readings were converted to real depths using a table supplied by the manufacturer. This assumed a value of 1.336 for the refractive index of the aqueous humour. It also required a value for the corneal curvature. For the latter, the previously discussed keratometric data (section 3.2.1 B) were used. The radii in the two principal corneal meridians were transposed into a spherocylindrical form and a resolved value for the corneal radius in the vertical meridian was calculated as described by Bennett and Rabbetts (1984).

A chin and forehead rest was used to keep the subject's head steady. To ensure alignment to the line of sight, the test eye was required to look directly at the slit beam whilst the non-test eye was occluded. The experimenter made horizontal adjustments to the position of pachometer so that the image of the vertical slit, on the subject's iris, was centred with respect to the pupil. Vertical adjustments were made until the horizontal divide of the split ocular was centred with respect to the pupil. At the same time, the slit image was maintained in focus. It is worth mentioning here that one of the advantages of the design of this pachometer was that the image doubling was unaffected by the magnification of observation (1.6x) and the experimenter's refractive error (Goldmann, 1968).

To control fixation and accommodation, the non-test eye viewed an illuminated target (section 3.4.3), positioned 3 m away, through an angled mirror. Adjustments of the mirror allowed apparent superimposition of the slit, seen by the test eye, with the fixation target seen by the non-test eye. Three readings were then taken of the apparent anterior chamber depth from which, following conversion to real depths, an average and standard deviation was calculated.

3.2.3 CRYSTALLINE LENS RADII

(A) OVERVIEW: PURKINJE IMAGES AND PHAKOMETRIC TECHNIQUES

By far the majority of in vivo measurements of the ocular surface radii have made use of the catoptric images. These images are formed by reflection at each surface, acting rather like a spherical mirror, and are described as being of the "first order" when they are formed by a single reflection and of the "second order" when formed by multiple reflections. The first order catoptric images, which are used for the determination of ocular radii, were discovered in the late nineteenth century by Purkinje and were later redescribed by Sanson (Duke-Elder and Abrams, 1970). For this reason they are often called Purkinje, Purkinje-Sanson or Purkyne images. The present author, however, will refer to them as Purkinje images. Bennett and Rabbetts (1984) provide a full account of the theoretical considerations involved in the derivation of ocular surface radii from their respective Purkinje images which will now be summarised.

The fraction of incident light which is reflected from a refracting surface increases with the difference between the refractive indices of the media on either side of that surface. As the largest index change occurs at the front surface of the eye, the reflection from the anterior corneal surface (Purkinje image I), used for keratometry and keratoscopy (see section 3.2.1A), is very much brighter than any of the others. Light entering the eye undergoes further partial reflections at the corneal rear surface (Purkinje image II) and at the anterior (Purkinje image III) and posterior (Purkinje image IV) surfaces of the crystalline lens. To form each of these images, the incident light is first refracted by all the surfaces in front of the one acting as a mirror and then, after reflection, is refracted again by the same surfaces in reverse order before emerging from the eye.

104

Theoretical calculations of the position and size of these images ~~is~~ *are* made simpler by using the equivalent mirror theorum. This states that a system comprising one or more refracting surfaces followed by a plane or spherical mirror can be simplified for calculation to an equivalent spherical mirror. The vertex and centre of curvature of the equivalent mirror then coincide, respectively, with the images of the vertex and centre of curvature of the actual mirror formed by the refracting elements.

Using the equivalent mirror theorum in a schematic eye made up of typical human ocular dimensions (Le Grand and El Hage, 1980; Bennett and Rabbetts, 1984), Purkinje I is found to be a virtual, erect, diminished image positioned just behind the anterior surface of the lens. Purkinje II is slightly smaller than Purkinje I and just in front of it. It is also virtual, diminished and erect. However, the relative brightness and proximity of Purkinje I normally obscures Purkinje II. Purkinje III is nearly twice the size of Purkinje I. It is situated in the vitreous chamber and is virtual, diminished and erect. Finally, Purkinje IV is real, diminished and inverted so that it lies close to Purkinje I but is about three-quarters of its size.

The theory of equivalent mirrors applied to a three-surface schematic eye provides the simplest basis for the calculations involved in the measurement of the crystalline lens surface radii (phakometry) (Sorsby et al., 1961; Leary and Young, 1968; Bennett and Rabbetts, 1984). In the three-surfaced schematic eye, a single surfaced cornea is assumed so that only Purkinje images I, III and IV are measured. From these, the apparent surface radii (equivalent mirror radii) are determined using either visual ophthalmophakometric or photographic ophthalmophakometric techniques.

Visual ophthalmophakometry was first performed by Tscherning who is also credited with the invention of the ophthalmophakometer (Tscherning, 1904). This consisted of

a graduated circular arc supported on a stand, with an observing telescope mounted in a central aperture. The subject's eye was placed at the centre of curvature of the arc on which various sets of lamps were fixed. This instrument could be used either for determining the approximate position of the optic axis, by alignment of the Purkinje images (I, III and IV), or for phakometric measurements. For the latter, two bright lamps were positioned so that the twin Purkinje images of either one of the lenticular surfaces (III or IV) were visible to the observer. Two dimmer lamps were then adjusted so that their twin Purkinje I images had the same separation between their centres as the lenticular Purkinje image pair under consideration. As both pairs of images were of the same size the separations between the corresponding pairs of lamps (representing conjugate objects of the Purkinje images) were inversely proportional to the apparent radii of their respective surfaces. By measuring the radius of the corneal surface using a keratometer, the apparent radii of the anterior and posterior lens surfaces could thus be calculated. Although this visual ophthalmophakometric technique was also used by many other workers (Awerbach, 1900; Zeeman, 1911; Tron, 1929; Sorsby et al., 1957) it had the disadvantage that its measurements were susceptible to the effects of eye movements.

Photographic ophthalmophakometric techniques overcome the problems of eye movements (Nakajima, 1955; Sorsby et al.,1961, 1962a, b; Francis, 1962; Ludlam et al., 1972). Here, the Purkinje images are photographed from a known angle and the spot separations appearing on the negatives after processing are measured. The apparent radii are then derived by the method of comparison phakometry. This states that the size of the image formed by reflection is proportional to the focal length of the equivalent mirror, which is one half of its radius of curvature. It then follows that the ratio between the height of Purkinje image I to either III or IV is the same as the ratio between their respective apparent radii. The value of the latter are then simply

calculated following determination of the corneal radius by keratometry.

Finally, given a knowledge of the apparent anterior chamber depth and lens thickness obtained using a slit lamp (see section 3.2.2A) and the central refractive error, the true depths and surface radii can be calculated. It is important to note that the equations required for these calculations (Bennett, 1961) assume a limited number of spherical surfaces, homogenous refractive indices and centration of all elements on a common optical axis. Furthermore, the calculated ocular components are all interdependent and are therefore susceptible to the accumulated errors made with each parameter measured (Ludlam et al.,1965; Ludlam, 1967). In an attempt to alleviate some of these problems, Leary and Young (1968) have adapted Bennett's (1961) equations to include independent ultrasonic determinations of axial distances and these will be described in a later section (see section 3.3). Although the errors of opthalmophakometry have been assessed theoretically (Ludlam et al., 1965), the precision of such measurements has never been determined experimentally (Ludlam, 1967).

Some difficulties are encountered in making precise ophthalmophakometric measurements owing to the nature of the Purkinje images themselves. As already described, the Purkinje images do not all lie in the same plane. For photographic ophthalmophakometry there is therefore a need for two photographs to be taken; the first focused in the iris plane to obtain clear Purkinje I and IV images and the second focused in the vitreous chamber to obtain a clear Purkinje III image. Eye movements made between these two settings can therefore give rise to experimental error. Purkinje images arising from the lens surface are also very dim. The high levels of illumination required to photograph these introduce considerable glare particularly from the bright corneal reflection. Some authors have attempted to improve the quality of the Purkinje

images by using monochromatic light (Ludlam et al., 1965) or otherwise infra-red light (Wulfeck, 1955; Otsuku et al., 1965; Kabe, 1968). The precise measurement of Purkinje images III and IV is also made difficult due to the effects of "shagreen" (Weale, 1982). Shagreen describes the optical mottling and dimpling of surfaces as seen by specular reflection. This is present on both anterior and posterior crystalline lens surfaces but is dominant in the former. Purkinje IV is twice as badly effected as III, being the result of light which has passed through the anterior lens surface twice.

Measurements of the lenticular radii can also be made from photographs of a slit lamp section taken applying the Scheimpflug principle (see section 3.2.2A). This is done by using a plane mirror to draw a set of normals to selected areas of the photographed surface, thereby estimating the surface curvature by observing where these normals intersect each other (Brown, 1973).

(B) PRESENT STUDY: PHOTOGRAPHIC OPHTHALMOPHAKOMETRY

A photographic ophthalmophakometer was built by modifying a Zeiss Jena Biomicroscope (photographic slit lamp). The latter was chosen because its observing microscope was coupled with a camera which allowed high quality photographs to be taken; the slit lamp, including a synchronised flash unit for photography, could also be simply modified for ophthalmophakometric measurements; furthermore, the observing microscope and the slit lamp were mounted on support arms which were rotatable to any angle about a point below the test eye, thus facilitating the observation of Purkinje images whilst keeping the subject's head steady in a built in chin and forehead rest. Figure 3.1 shows a photograph and fig. 3.2 a schematic diagram of the photographic ophthalmophakometer.
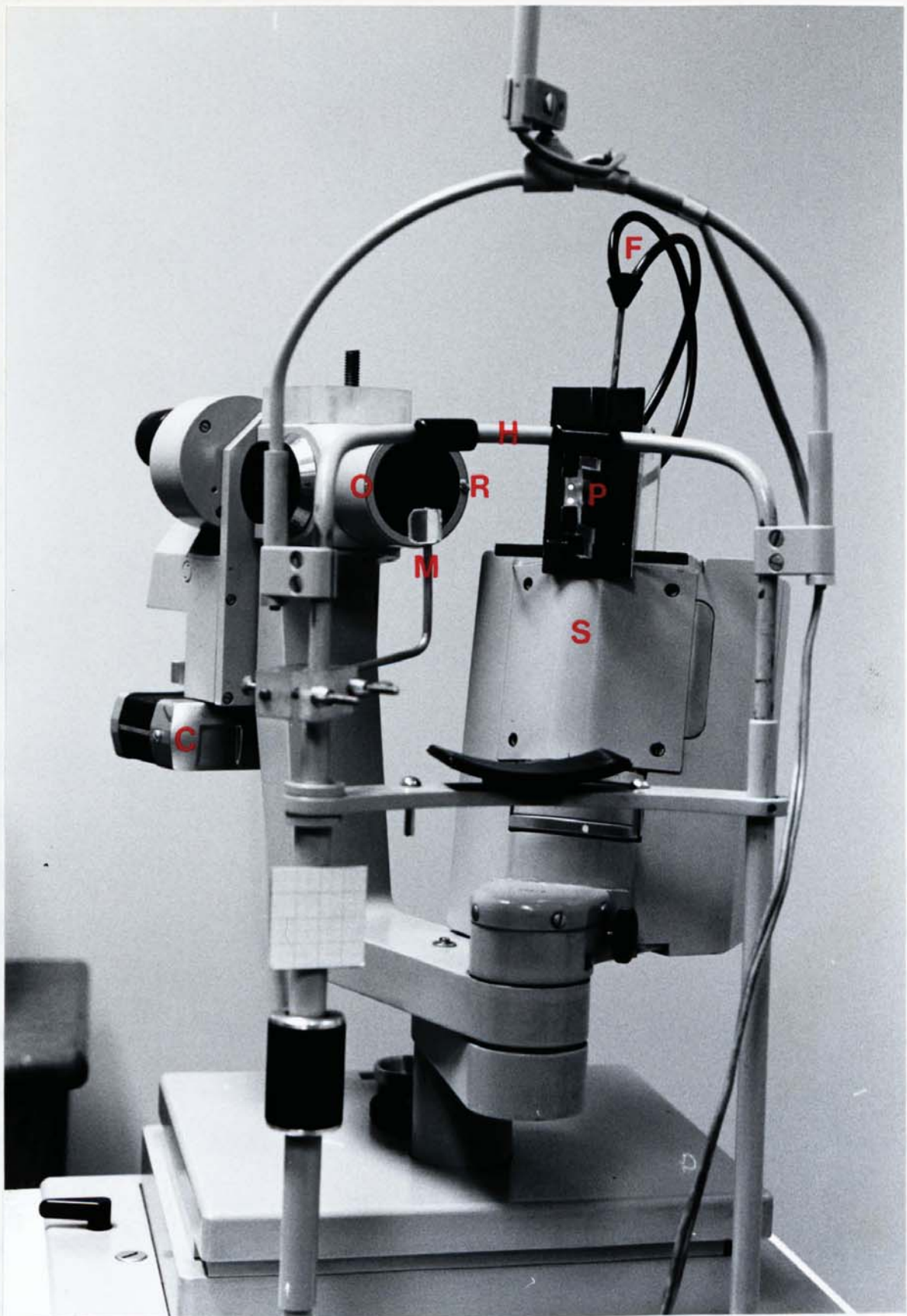
Fig. 3.1 Photograph of photographic ophthalmophakometer. Key: *F* -bifurcated fibre optic cable; *P* -Purkinje image light sources; *S* -slit lamp housing; *C* -camera; *O* -microscope objective; *M* -mirror; *R* -red fixation light and *H* -headrest. See text.
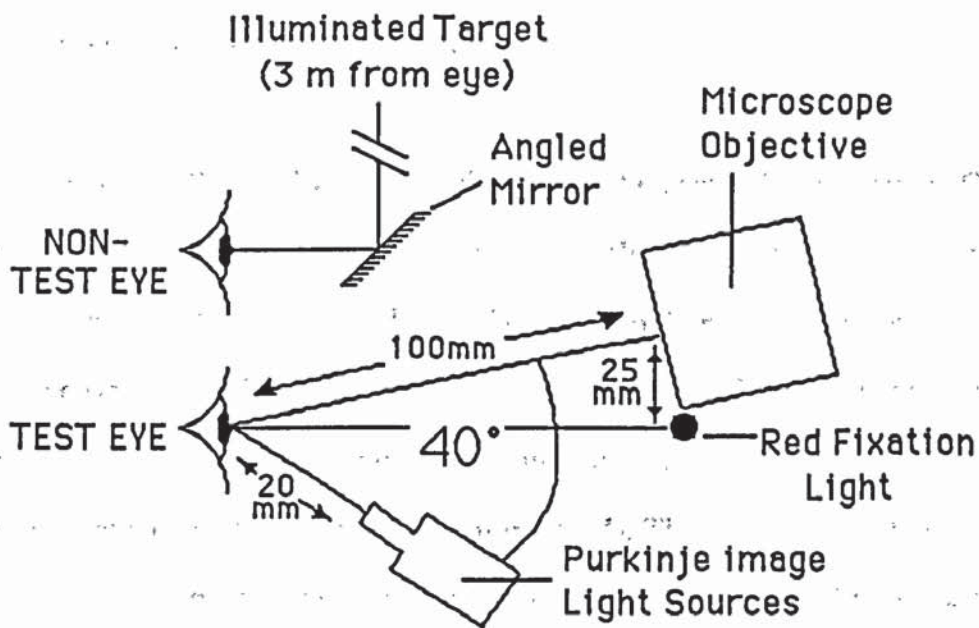
Fig. 3.2   Schematic diagram of photographic ophthalmophakometer.

The slit lamp mirror, which normally served to deflect illumination in the direction of the subject's eye, was removed so that light could be guided down a bifurcated fibre optic cable (F) producing two Purkinje image light sources (P) of 1mm diameter. The distance between the Purkinje image light sources and the test eye was 20 mm. This distance was adopted for two reasons. First of all, limitations were set by the amount of light emerging from the fibre optic cable and that required to produce enough illumination for the formation of visible lenticular Purkinje images. Secondly, the distance employed was the most convenient in terms of mounting the fibre optic cable.

When the Purkinje image light sources were set 6 mm apart, centre to centre, in the vertical plane, the Purkinje images produced never exceeded 2.5 mm in height which was considered to be small enough for measurements to be made in most subjects with natural pupils. Though it would have been desirable to measure the Purkinje images in other planes as well as the vertical one, difficulties encountered in the construction of

the opthalmophakometer prevented this.

Purkinje images I, III and IV were visible when the arms of the camera (C) and slit lamp housing (S) were locked at 40°. The test eye also needed to be directed to a point, illuminated by a red fixation light (R) displaced 25mm horizontally from the axis of the microscope objective (O) and towards the light sources (P). To control fixation and accommodation, the non-test eye fixated an illuminated target (see section 3.4.3), positioned 3 m away, through an angled mirror (M). The mirror was adjusted until the illuminated target seen with the non-test eye and the red fixation light seen with the test eye appeared to be superimposed. A chin and forehead rest (H) was used to keep the subject's head steady.

Purkinje images were located with the slit lamp observation light set at maximum. The camera was focused at the plane of the iris so that Purkinje images I and IV, as well as the edges of the iris, were seen to be in focus. Dimming the lamp prior to taking a photograph reduced the effect of extraneous light on accommodation. To provide enough light output to photograph the faint lenticular Purkinje images, the slit lamp flash unit was set at its maximum intensity (480 watts) and an exposure of 0.04 seconds made.

On the photograph taken, the Purkinje III images would naturally be blurred. As already explained, previous photographic opthalmophakometric studies have required a second exposure in which the observing camera is refocused on these images. This, however, was not possible owing to the fact that focusing of the slit lamp camera was achieved by moving the entire apparatus forwards or backwards on a moveable base. Consequently, the light sources (P) also moved with respect to the subject's eye, making any further measurements of the Purkinje images after refocusing incompatible

111

with the first. To partially overcome the disadvantage caused by image blur, a large number of readings were taken of the Purkinje image separations. Here, three photographs were taken per subject; for each photograph, three estimates were made of the heights of each pair of Purkinje images; an average and standard deviation was then calculated from the nine readings of each image.

Consistently clear photographic results were obtained through an aperture of ratio 1:79 and with a reproduction ratio of 1:1.6 when using Kodak Tri-X pan 400 ASA black and white film processed in I.D. 11 for 7 minutes at 20°C. Photographs were projected against a screen and measured. Magnification and distortion arising from the slit lamp camera, film processing and the projection system were all assessed simultaneously by photographing a 1mm square grid and measuring its dimensions after projection. A travelling microscope could also have been used for making measurements of the Purkinje images but this technique proved to be slower and no more accurate than than the one employed.

Although the design of the ophthalmophakometer had several limitations, it must be added that many designs were unsuccessfully attemped, including that of a slit lamp based on the Scheimpflug principle. Therefore, the method used had the simple advantage in that it worked well and produced repeatable results (see chapter 4). The calculations required for the determination of the lenticular radii from the Purkinje image heights are described in a later section (see section 3.3).

3.2.4 CENTRAL AND PERIPHERAL REFRACTIVE ERROR

(A) OVERVIEW: OPTOMETRIC TECHNIQUES

A vast range of techniques are available for the measurement of refractive error, descriptions of which can be found elsewhere (Henson, 1983; Bennett and Rabbetts, 1984). However, the methods employed by the present author were chosen for the measurement of both central and peripheral refraction. From the previous chapter (see section 2.3) it appears that most workers favour the use of objective optometers, rather than retinoscopy or subjective methods as a means of measuring peripheral refraction. For this reason, central and peripheral refraction were determined using two kinds of optometer; an objective coincidence optometer and an infra-red optometer.

Generally, objective optometers work on the basis that some of the light falling upon the retina will be diffusely reflected by the retinal surface. A problem arises in that the site of the reflecting layer does not necessarily coincide with the subjective focal plane. Research evidence indicates that several layers of the retina are jointly responsible for the reflection and that the dominant one varies according to the wavelength of light used, whether it is polarised and the subject's age (Charman and Jennings, 1976; Millodot and O'Leary, 1978; O'Leary and Millodot, 1978). To overcome this problem, the manufacturers calibrate their instruments using subjective measurements of refraction (Henson, 1983).

Ferree et al. (1931) and Millodot (1981, 1984) both used coincidence optometers for their measurements of peripheral refraction. These studies indicated that the refraction could be determined to a precision of between ±0.25 D centrally, and ±0.50 D peripherally (out to 60°). Millodot and Lamont (1974) also obtained comparable

peripheral refractive results when measurements obtained with an objective coincidence optometer were compared with retinoscopic and subjective methods.

As far as the present author is aware, however, nobody has ever measured peripheral refraction with an infra-red optometer although several workers have compared central refractive readings obtained using these instruments, with subjective techniques. Average differences of ± 0.25 D for the spherical component and ± 0.375 D for the cylindrical component have been found using the Canon R-1 Autoref infra-red optometer (McBrien and Millodot, 1985). The precision of the same technique was found to be ± 0.1 D for successive readings and ± 0.25 D for readings of the spherical and cylindrical components repeated on different days. Successive estimates of the axis of astigmatism revealed a precision of $\pm 6°$ but this decreased markedly when the cylinder power was less than 0.75 D. McBrien and Millodot (1985) also noticed that the infra red optometer produced readings which were slightly more negative (-0.37 D) than those obtained by subjective methods. The latter observation was consistent with the results obtained using other infra-red optometers (French and Wood, 1982; French et al., 1982).

(B) PRESENT STUDY: THE OBJECTIVE COINCIDENCE OPTOMETER

Peripheral and central refraction were measured using a Zeiss Jena Hartinger coincidence optometer. Henson (1983) provides a detailed description of this instrument, a summary of which will now be given.

The Hartinger optometer made use of a small target, composed of three vertical lines divided into two and passed through different parts of the subject's pupil. In an emmetrope the retinal images of both halves of this image would be in alignment but in

an ametrope they would be displaced with respect to one another. The magnitude and direction of this displacement depended on the degree and type (i.e hyperopia or myopia) of ametropia. By adjustment of the vergence of the light entering the eye, the two half images could be aligned and a measure of the refractive error obtained. Readings of the latter could then be read off a scale calibrated in dioptres at intervals of ±0.25 D.

Two horizontal lines also present on the target, enabled the axes of any astigmatism to be determined. These were also divided and sent through different parts of the pupil so that when the instrument was not in alignment with one of the principal astigmatic axes, they did not align. The correct axis, which could be found by rotating the whole instrument about its antero-posterior axis until the lines were aligned, could also read off a scale at intervals of 1°.

With other types of objective optometer difficulties are encountered in judging the exact point at which the target is correctly focused. The Hartinger coincidence optometer, however, assisted in making this judgment by employing the more simple task of aligning target lines, thereby giving rise to more accurate estimates of the refractive error. Correct adjustment of the eyepiece to the experimenters refraction was also important to ensure accurate readings.

Problems associated with the Hartinger optometer were the brightness and the size of its target. The target brightness was a compromise between the illumination requred to produce a visible retinal image and that which would have a minimal effect on pupil size and accommodation. The target size (2 mm) was, likewise, a compromise between the size required to give sensitive readings and that which allowed measurements to be made in subjects with small pupils. Another problem arose due to

the change of vergence of the light from the target during measurements which acted as a stimulus to accommodation. It was therefore necessary to approach the subject's refractive error from the positive side.

For the measurement of refraction at various oblique angles, the Hartinger optometer was modified as shown in fig. 3.3, so that it could be rotated around the test eye. The optometer (O) was supported by a modified arm (A) which allowed it to be rotated about a point (P) set directly below the subject's eye. This point was easily adjusted as the entire apparatus was mounted upon a moveable base (B). Two steel bars were used to construct the new arm. One of these was connected to the moveable base so that it remained in alignment with the instrument's original axis. The other was attached to the optometer and was rotatable. By means of a scale (S), the experimenter could rotate the optometer accurately, up to 60° nasally and temporally.

A chin and forehead rest (H) served to keep the subject's head steady. To control fixation and accommodation, the non-test eye viewed an illuminated target (see section 3.4.3) positioned 3 m away through an angled mirror (M). The instrument was first set in the normal, straight ahead position and the subject asked to look directly into it. Small adjustments were then made to its height and position until the instrument target could be seen in focus by the experimenter. At this point the subject's test eye could also see this target. Adjustment of the angled mirror then allowed the illuminated fixation target, seen in the non test eye, to be made coincident with the instrument target, seen by the test eye, and thereby ensured alignment of the instrument axis with the subject's line of sight (fig. 3.4). The fixation target had the additional advantage of reducing the effect of the instrument target on the subject's accommodation as well as keeping fixation steady whilst the optometer was being moved to different field angles.

116

Fig. 3.3 Photograph of the modified arm built for the Hartinger coincidence optometer. Key: *O* -optometer; *A* -modified arm; *P* -point of rotation; *B* -moveable base; *S* -scale; *H* -headrest; *M* -mirror. See text.
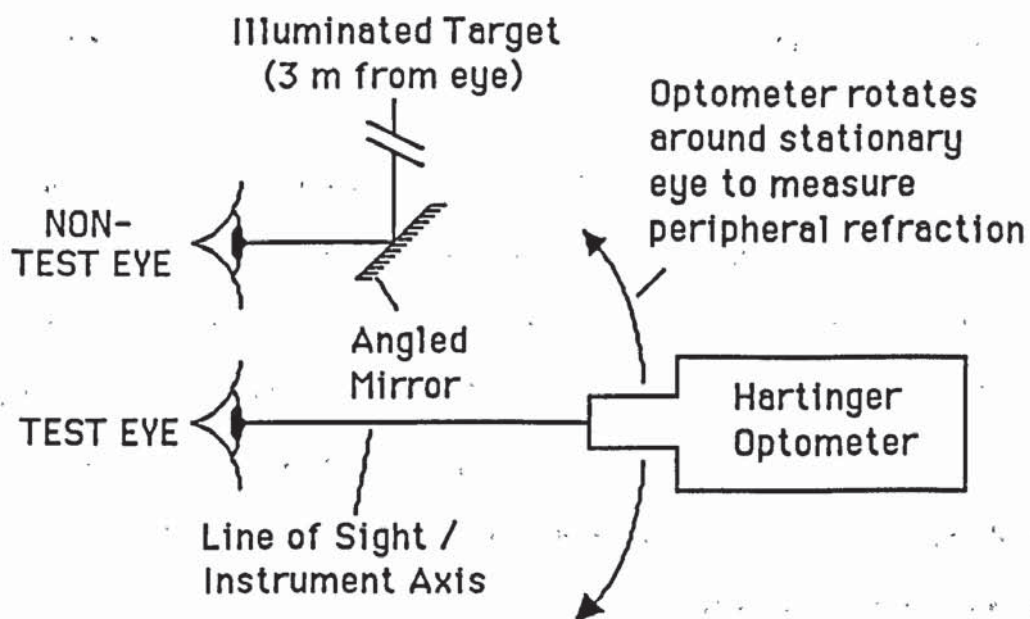
Fig. 3.4 Schematic diagram depicting rotation of Hartinger coincidence optometer around stationary eye and its alignment to the subject's line of sight.

Three readings of the central refractive error and axis of orientation were taken in both principal meridians. The same was repeated for all field angles measured (up to 60° nasally and temporally in 10° intervals). An average and a standard deviation were calculated from each set of values. The total time required to perform these measurements was between 30 to 45 minutes. This meant that the readings taken in the periphery could well be prone to the myopic shifts, possibly due to prolonged fixation, descibed by Ferree et al. (1931) (see section 2.3). For this reason, the results obtained using the Hartinger optometer were compared with those taken using a Canon Autoref R-1 which is an infra-red, objective autorefractor. With the latter, readings could be made more quickly.

118

(C) PRESENT STUDY: THE AUTOMATED INFRA-RED OPTOMETER

A detailed description of the Canon Autoref R-1 is given by McBrien and Millodot (1985). The Canon Autoref R-1 had the advantage that the instrument target was illuminated with infra-red light which, being invisible to the human eye, did not effect the subject's accommodation level. This target was focused automatically with an electronic focus detector, giving rise to accurate and rapid determinations of the refractive error. In addition to the above, light from the instrument was reflected into the test eye via an angled semi-silvered mirror thus affording a largely unrestricted field of view to the subject over the horizontal plane. Using an infra-red teleconverter, the subject's eye could be seen on a monitor screen in visible light. This apparatus not only served to bring the experimenter out of the subject's field of view but also allowed accurate alignment of the instrument to the test eye. Refractive results could be read from the monitor screen or otherwise printed out for permanent record.

For measuring refractive error, the vergence of light entering the subject's eye from the instrument target was continuously altered by the forward and backward movement of a set of lenses. The best focus of the target was determined in three meridians, each separated by 60°, using an array of photodiodes which registered a maximum signal when optimum focus had been achieved. By electronically processing the information, regarding the position of the moveable lenses and the signal being emmitted by the photodiodes, a spherocylindrical refractive result could be computed after applying a $sine^2$ curve. It is assumed that, because infra-red light was being used, the manufacturer calibrated the instrument with subjective measurements of refraction (as is normally done according to Henson, 1983). The spherocylindrical powers were determined in steps of 0.12 D and the axis in steps of 1°. This whole proceedure, ending in a recording on the monitor display, took only 0.2 s.

Limitations of the Canon Autoref R-1 were that it required a minimun pupil diameter of 2.9 mm for measuring purposes and that its readings were the result of an analysis in only three meridians. Although Bennett (1960) has shown that only three meridians are needed to produce a refractive result, Long (1974) pointed out that by confining readings to only three meridians, small measurement errors could give rise to large errors in the final computed result. As already mentioned, McBrien and Millodot (1985) noted that the axis determination became less reliable for subject's with less than 0.75 D astigmatism.

Two additional infra-red lights were shone onto the subject's eye for several purposes: they illuminated the eye so that it could be seen on the monitor screen by the experimenter; by keeping their images (Purkinje I) in focus, the working distance could be kept constant; by aligning them to the edges of an alignment ring displayed on the monitor screen, the subject's eye could be aligned. To align the subject's eye, the alignment ring also had to be centred with respect to the pupil. This was easily achieved as the Canon Autoref R-1 was mounted on a table which allowed vertical and horizontal adjustments to be made to its position. As the Purkinje I images are naturally aligned with the apex of the cornea and because they are further aligned to the centre of the apparent pupil (or entrance pupil) then by using the above method, alignment is made to the pupillary axis (see section 1.5). As the present study required alignment of the instrument to the subject's line of sight, another method of aligning the subject's eye was utilised (described later).

For the measurement of peripheral refraction the subject's head was held still in a chin and forehead rest and the test eye was allowed to rotate to fixate an illuminated target (see section 3.4.3). Figure 3.5 demonstrates how the instrument axis was aligned to the line of sight of the test eye whilst the subject looked straight ahead.
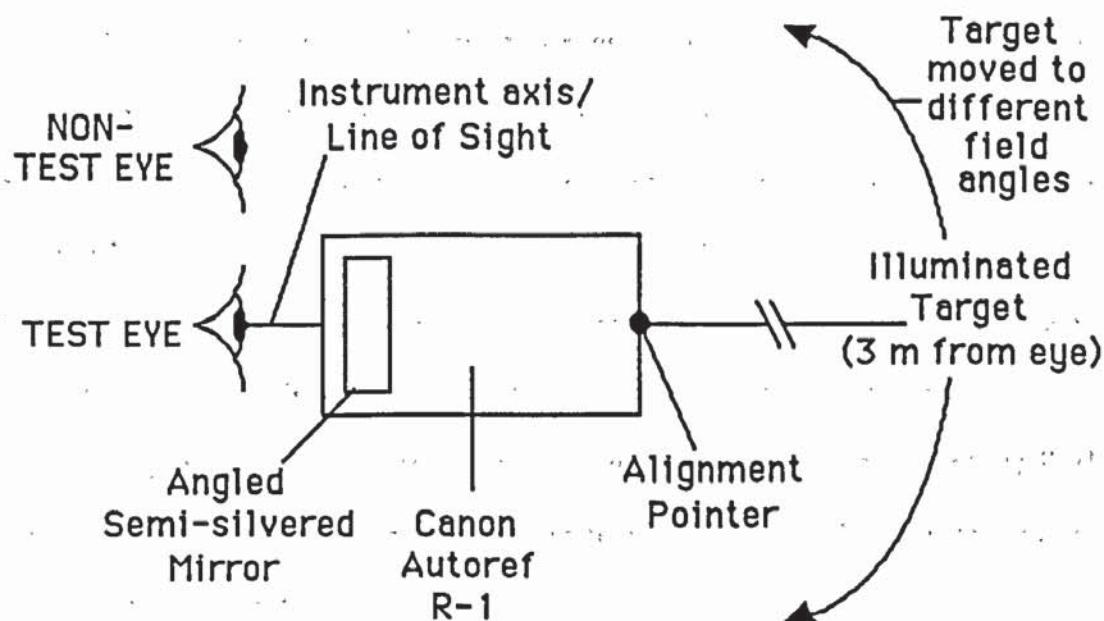
Fig. 3.5 Schematic diagram depicting alignment of Canon Autoref R-1 to the subject's line of sight (in the straight ahead position). The stationary instrument takes readings of the peripheral refraction whilst the test eye is allowed to rotate to fixate the illuminated target which is moved to different field angles.

A pointer was placed down the instrument axis. With the non-test eye occluded, the test eye fixated the illuminated target positioned 3 m away. The instrument was then adjusted until the alignment circle seen on the monitor was centred with respect to the pupil and the subject reported superimposition of the illuminated target and the pointer. The pointer was then moved and the non-test eye uncovered to allow binocular viewing. Five central refractive readings were then taken. Following this, the illuminated target was moved in an arc up to 60° nasally and temporally in 10° intervals. At each position the subject's eyes were allowed to rotate to fixate the illuminated target and five more refractive readings were taken. A small amount of lateral adjustment of the instrument was often necessary to reposition the alignment circle with respect to the centre of the pupil at each eccentric fixation angle. However,

because this movement was only in the order of millimetres, any change that this incurred to the effective field angle was considered to be negligible. It was also necessary to keep the working distance constant. Although the latter is normally carried out by focusing the Purkinje I images of the illuminating sources, this was no longer possible as these were displaced and often not visible during eccentric viewing. Instead, the upper and lower edges of the iris, corresponding to the widest vertical portion of the pupil (i.e. its centre), were kept in focus as it is known that the Purkinje I images are formed close the iris plane (see section 3.2.3A). This ensured a constant working distance from the centre of the pupil.

From each set of five readings an average and standard deviation were calculated. The total time required to obtain a full set of readings per eye was between 5 and 10 minutes thereby reducing the possible effects of prolonged fixation. Although this was the case, it may be argued that the effects of extraocular muscles during eye rotation might influence the results. However, the present author considered that because the eye was never held in any one position for more than one minute at most, such an effect was unlikely.

3.2.5 APPARENT (ENTRANCE) PUPIL DIAMETER

(A) OVERVIEW: PUPILLOMETRY

Bennett and Rabbetts (1984) provide a review of the various techniques employed for the measurement of pupil size, the main points of which are now briefly summarised. Pupil measurements are made difficult by pupillary changes caused by or occurring during the process of measurement. Even if these are controlled, the dimension measured is that of the pupil as seen through the cornea (i.e. the entrance pupil).

The simplest objective methods involve direct comparison of the observed pupil with a graduated series of circles or circular apertures. A subjective approach is the use of twin-pinholes. If held close to the eye, two entoptic images of the pupillary aperture are seen. These may appear separated or partially overlapping but will touch if the pupil diameter is equal to the distance between the pinhole centres. The above methods, however, provide only a modest standard of accuracy.

For research purposes, where a higher degree of accuracy is required, various doubling devices are able to produce an accuracy of approximately ±0.1 mm (Charman, 1980). Some workers have made measurements from photographs (Spring and Stiles, 1948; Jay, 1962). The latter studies have concentrated on the variation of pupillary area when viewed eccentrically and outline errors which can arise, in interpretation of the results, due to the geometry of the cornea through which the natural pupil is viewed and the finite thickness of the iris.

The most complicated techniques include motion picture photography in infra-red light, which is particularly useful for continuous recording of pupillary size (Taylor, 1977). Other workers have developed techniques which involve electronic scanning of the pupil and give rise to analogue or digital displays on closed-circuit television (Lowenstein and Loewenfeld, 1958; Saladin, 1978; Watanabe and Oono, 1982).

(B) PRESENT STUDY: PHOTOGRAPHIC DETERMINATION OF PUPIL SIZE

The size of the entrance pupil was measured from the projected ophthalmophakometric photographs (see section 3.2.3B). As the test eye was directed towards a point which was horizontally displaced from the camera axis, the diameter of the entrance pupil (assumed to be circular) was expected to be slightly smaller horizontally than

123

vertically, the latter being the required value. Three readings, from the vertical plane only, were therefore made from each of the three photographs taken of the test eye. An average and standard deviation was then calculated from the nine readings obtained overall.

The entrance pupil was assumed to be constant in size throughout the experiment. As this depended on the control of ambient illumination and accommodation, the latter were kept constant for every ocular measurement made (see section 3.4.3). Unfortunately, the same cannot be said for extraneous light sources arising from the various instruments used. However, it is the refractive readings which are susceptible to variations in pupil size and readings of the latter, taken with Hartinger optometer, were effected by similar light sources to those used for taking the photographs from which the entrance pupil readings were measured.

3.3 CONSTRUCTION OF SCHEMATIC EYES FROM BIOMETRIC DATA

(A) OVERVIEW: COMBINING ULTRASONIC AND PHAKOMETRIC RESULTS

In section 3.2, the reason given for using ultrasonic and phakometric techniques was that these provided the greatest number of independent determinations of ocular dimensions. Independent ultrasonic measurements of the anterior chamber depth, lens thickness and vitreous length (the sum of which gave the axial length) were described in section 3.2.2A. In Section 3.2.3A a set of equations were described (Bennett, 1961) which calculated true values of the surface radii and axial distances from the apparent dimensions measured using slit lamp and ophthalmophakometric techniques. However, the results obtained from the latter would all have been interdependent. Leary and Young (1968),therefore, developed a new set of equations based on those

of Bennett (1961), which combined ultrasonic and opthalmophakometric measurements.

In the method described by Leary and Young (1968) the true values for anterior chamber depth and lens thickness obtained by ultrasonography were "back calculated" to derive apparent depths. In one set of equations, the heights of Purkinje images I and III provided data which when combined with the apparent depths and the ultrasonically derived axial length, enabled the surface radii of the lens to be calculated. These calculations, however, while making use of a measured axial length rather than a computed one, transfered the possible error to the computed back surface of the lens. Therefore, in a second set of equations, the heights of Purkinje images I, III and IV were combined with the anterior chamber depth and lens thickness obtained by ultrasonography to permit determination of a computed axial length along with the surface radii of the lens.

Although the above equations still produced interdependent values of the lenticular radii, they had the advantage that the computed axial length could be compared with that determined by ultrasonography to provided an estimate of the accumulated experimental error. In other words, they provided a form of "internal validation check". They also did not require the use of a slit lamp to provide apparent depth measurements. For the latter, mydriasis of the subject's eye would have been necessary to make such depth measurements possible (see section 3.2.2A).

(B) COMPUTER PROGRAM: ULTRASONIC OPHTHALMOPHAKOMETRY

The equations used are fully described by Leary and Young (1968). A BASIC program, incorporating these, was written by the present author for use on the

Commodore CBM 3032 computer and is shown in appendix 1.

The program was designed to display the assumed refractive indices on the computer screen. Assumed refractive index values were 1.0 for air, 1.3374 for the aqueous humour, 1.42 for the crystalline lens and 1.336 for the vitreous humour. These refractive indices were also assumed to be homogenous and constant for each individual. The gradient index optical nature of the crystalline lens was neglected. A message on the screen further reminded the operator that a single surfaced cornea was assumed so that its refractive index was also neglected.The screen then prompted the operator for the following data:

1.Subject information.

2.Heights of Purkinje images I, III and IV (see section 3.2.3B).

3.The ultrasonically determined anterior chamber depth, lens thickness, vitreous length and axial length (see section 3.2.2B).

4.The central refraction measured using the Hartinger coincidence optometer (see section 3.2.4B). This was required in spherocylindrical form. To resolve the results to the vertical meridian (as described by Bennett and Rabbetts, 1984), the sine of the angle between the cylinder axis and the vertical (90°) meridian was required.

5.The radius of curvature of the central portion of the anterior corneal surface measured using the PEK (see section 3.2.1C). This was also required in spherocylindrical form. Likewise, the results were resolved to the vertical meridian as described above.

Having stored the data in the computer memory, the program carried out the calculations already described in section 3.3A. For the sake of simplicity, those calculations which made use of the ultrasonically determined axial length will be refered to as "routine 1", whilst those which gave rise to a computed axial length will be refered to as "routine 2". A printout of the results (see appendix 1) was available which included:

1.The original data upon which the results were based, including the anterior corneal radius and the central refractive error, both resolved to the vertical meridian.

2.The radius and power of the anterior and posterior lenticular surfaces in the vertical meridian. Two values were given for the calculated posterior lens surface parameters; the first (denoted "ULTRA" on the printout) were derived using routine 1 and the second (denoted "CALC" on the printout) were derived using routine 2.

3.The vitreous and axial lengths calculated using routine 2 for comparison with those which were determined ultrasonically and used for routine 1.

4.The total power of the eye and the equivalent lens power in the vertical meridian. Two values were given for each of these representing the values derived using routines 1 and 2.

5.A set of cardinal points for the calculated schematic eye. Although the present author made no use these values, they were neverthless included. However, the values calculated were only those derived from routine 1.

127

3.4 OVERALL EXPERIMENTAL PROTOCOL

3.4.1 SCOPE OF STUDY AND SUBJECT DETAILS

The initial intention of this study was to compare the ocular component dimensions found in eyes exibiting different amounts of ametropia and different patterns of peripheral refraction. Because of the variation with age of various ocular components (as described in chapter 1), a narrow age range was considered. A suitable source of subjects, falling within a narrow age range, was the undergraduate population attending the Ophthalmic Optics course at Aston University. From this population, approximately 100 people (200 eyes) were screened.

For screening purposes, the Canon Autoref R-1 was used to make rapid measurements of peripheral refraction in the same manner as described in section 3.2.4C. Because of the amount of data collected, analysis was confined to observing central refraction and the variation of astigmatism with increasing field angle. The outcome was, however, that although varying degrees of ametropia were found, none of the eyes exhibited the low values of peripheral astigmatism or the significant amounts of nasal-temporal peripheral astigmatic asymmetry which (as described in section 2.3) were characteristic of type I and III eyes, respectively. Indeed, every one of the eyes screened possessed the normal, type IV, peripheral astigmatic pattern. At first, this was considered to be a major limitation. However, Millodot (1981) also found that the vast majority (92%) of the emmetropic and ametropic eyes measured in his group exhibited the common type IV pattern. Furthermore, his results revealed some very interesting variations in the profiles of the sagittal and tangential image shells which seemed to be the result of subtle changes in retinal shape and position (see section 2.3). This illustrated that although a study of the more extreme peripheral refractive variations would have been

of great interest, the more subtle variations, as shown in Millodot's (1981) results, were also worth investigating. For this reason, a group of eyes exhibiting a wide range of central refractive errors were chosen for experimentation.

The length of time required to perform measurements on each subject limited the number of subjects recruited. Readings were taken from 10 near-emmetropes (-0.46 to +0.25 D spherical equivalent), 16 myopes (-1.38 to -6.07 D spherical equivalent) and 8 hyperopes (+0.74 to +3.34 D spherical equivalent). Only right eyes were used except in the case of 4 of the hyperopes who were anisometropic. Here, the left eyes were chosen as they exhibited the greatest amount of ametropia. All eyes were healthy, possessed normal binocular vision and demonstrated a visual acuity of at least 6/6 in each eye with correction if necessary. Contact lens wearers were excluded to avoid the possible influence of contact lens wear on the corneal profile. The age range of the subjects was between 19 and 30 years (average and standard deviation: 21.4 ± 3.3 years). Of the subjects chosen, 24 were male and 10 were female.

3.4.2 ORGANISATION OF EXPERIMENTAL SESSIONS

The validity of the anterior corneal curvature and the peripheral refractive data was estimated by comparing the readings taken of each using two different methods. As estimates of the axial distances and Purkinje image heights were only possible using ultrasonic and phakometric techniques respectively, both measurements were performed twice to assess their validity. The latter also served as an indication of how well the illuminated target (see section 3.4.3) controlled accommodation. An additional validation between optical and ultrasonic depth determinations was provided by measuring the anterior chamber depth using ultrasonic and pachometric techniques.

As the total time required to take all 9 sets of measurements was approximately 3.25 hours, each subject was asked to attend three separate sessions. The readings were taken in the same order for every subject and the sessions were organised as follows:

SESSION ONE (approximate duration 45 minutes).

1.Peripheral refraction (Canon Autoref R-1).

2.Axial distances - first readings (Storz Alpha 20/20).

SESSION TWO (approximate duration 75 minutes).

3.Purkinje image heights and entrance pupil diameter - first readings (Photographic Ophthalmophakometer).

4.Anterior chamber depth (Haag Streit slit lamp 900 pachometer).

5.Anterior corneal radius and surface profile (Wesley-Jessen PEK).

6.Axial distances - second readings (Storz Alpha 20/20).

SESSION THREE (approximate duration 75 minutes).

7.Purkinje image heights and entrance pupil diameter - second readings (Photographic Ophthalmophakometer).

8.Peripheral refraction (Zeiss Hartinger coincidence optometer).

9.Anterior corneal radius (Zeiss keratometer).

Because of the difficulties encoutered in booking the subjects and the limited time in which the experimental room was free, the interval of time between the first and last sessions ranged from 9 to 77 days. The duration between the first and the second session ranged from 3 to 48 days whilst that between the second and the last session ranged from 6 to 29 days.

3.4.3 CONTROL OF EXPERIMENTAL CONDITIONS

One of the objectives of the experimental design was to take readings from eyes under "natural" conditions. Therefore none of the measurements were taken with either paralysis of accommodation or mydriasis of the pupil. Furthermore, as already mentioned, the accuracy of some techniques are improved when measurements are made with natural pupils. Therefore, the pupil size and the level of accommodation were controlled by keeping the illuminance of the room and the target constant as well as using the same target, at the same distance, for each set of measurements.

All measurements were made in the same room under a constant ambient illuminance of 45 lux. The target (fig. 3.6) was back illuminated with four 60 watt bulbs (I) which were mounted in such a way that the light from them was evenly distributed over the target plate (P). This consisted of a disc of 360 mm in diameter which was divided into 16 equal segments. The illuminance of the alternate translucent white and opaque black segments was 590 lux and 12 lux respectively. This allowed control over fixation and accommodation for the uncorrected ametropic eyes measured (see section 3.4.1) and adequate contrast against the light often arising from the instruments themselves. By building the target on a stand (S), it could be moved from one instrument to the next and kept at a constant distance of 3 m from the subject. The latter distance was a compromise between positioning the target as far from the subject as possible, in order to relax accommodation, and the limitations set by the size of the room.
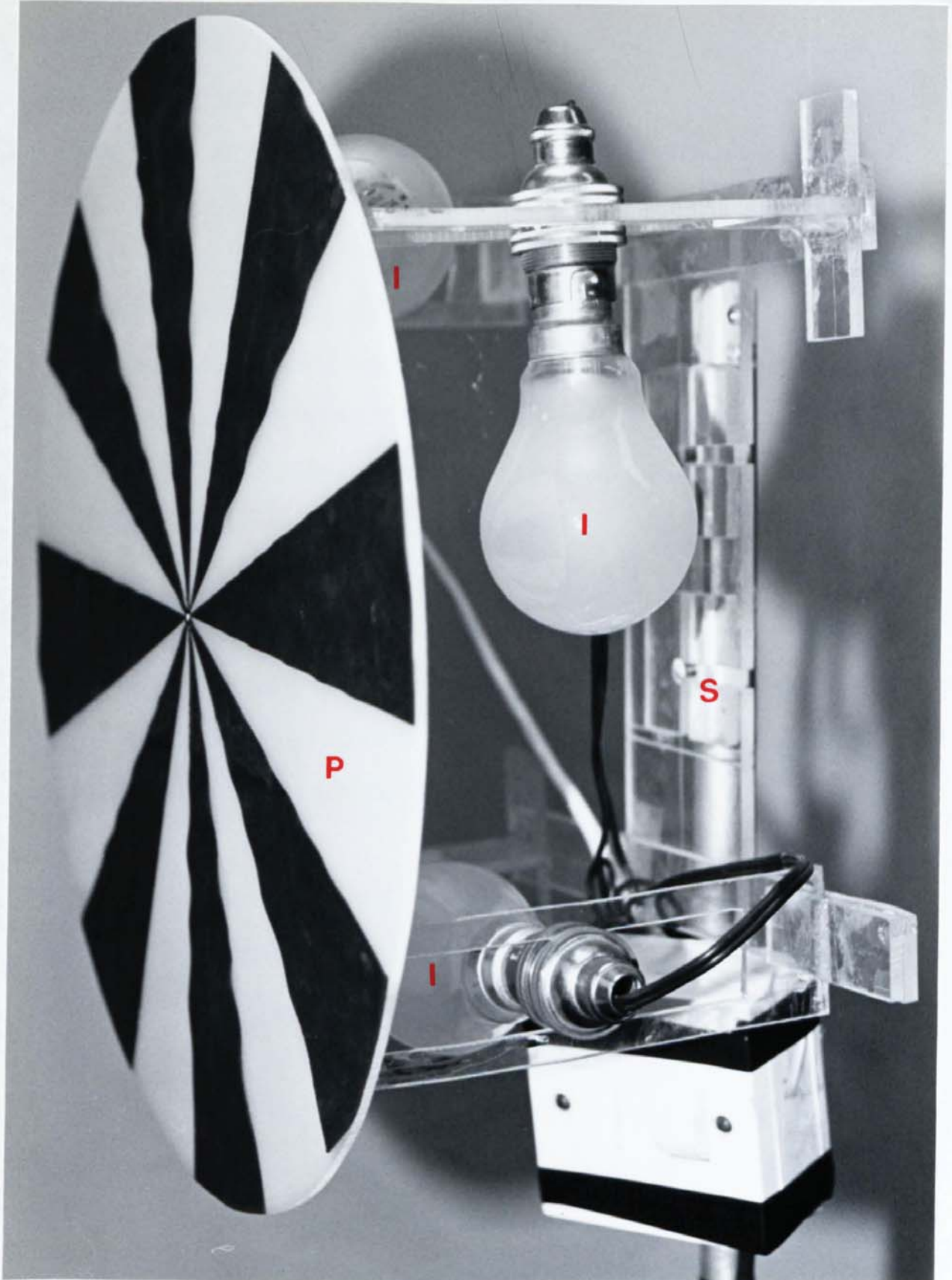
Fig. 3.6 Photograph of the illuminated target used throughout the experiment. Key: *I* -back illuminating bulbs; *P* -target plate; *S* -target stand

3.5 SUMMARY

This chapter has outlined an approach in which the variation of refraction over the peripheral retina and the ocular dimensions were measured in the same sample of eyes.

To measure the ocular component dimensions a method was employed which essentially combined ultrasonic and phakometric techniques. This maximised the amount of independent measurements made which included the anterior corneal radius, anterior chamber depth, lens thickness, vitreous length, axial length and refractive error. The anterior and posterior crystalline lens surface radii were then calculated and schematic eyes constructed from the independently measured data.

The reliability of the readings was assessed by comparing different techniques for measuring the same parameter or otherwise by making repeat measurements using the same technique. Furthermore, an "internal validation check" was provided by the computer program used to construct the schematic eyes.

Several points of criticism arise in connection with the experimental methods used. Firstly, each instrument was aligned to the subject's line of sight. This can lead to such problems as over estimation of the corneal toricity (see section 1.3.1). Nevertheless, alignment to the line of sight has been advocated since the time of Gullstrand as the only logical means of identifying a common axis about which optical measurements should be made (Gullstrand, 1924). Secondly, limitations in the design of the ophthalmophakometer restricted schematic eye calculations to the vertical meridian whilst measurements of the peripheral refraction, were restricted to the horizontal meridian. Attempts to overcome both of these problems, however, are described in a later chapter. Finally, the schematic calculations were susceptible to the correctness of

the assumed invari*a*nt homogenous refractive indices, the assumption that all surfaces were spherical and centred upon a common optic axis and the neglect of the posterior corneal surface.

In later chapters, the subtle ocular component variations found in the ametropic eyes under consideration will be investigated by developing more complex eye models. A description will be given of the construction of these, by modifying the simplified schematic eyes described in this chapter, until the peripheral refractive patterns predicted by them match the measured values. Use will also be made of the measured corneal contour and pupil dimensions. The next chapter, however, concentrates on the results obtained from the previously described techniques and their validity.

.

CHAPTER FOUR

BIOMETRIC AND PERIPHERAL REFRACTIVE RESULTS

4.1 INTRODUCTION

In this chapter the results, measured as described in the chapter 3, are discussed along with their validity in terms of precision and, to a limited extent, accuracy. The precision (repeatability) was assessed by observing the range of standard deviations arising from the repeat readings taken of any given component in one session. Further estimates of the precision were made by correlating repeat readings taken on two separate occasions either by using the same or different instruments. It is understood, of course, that diurnal variations could also play a part. The accuracy of the results (how close they were to the true values) could not be determined as this would require a knowledge of the true component values which, in the case of the living human eye, are unobtainable. Repeat readings taken using different instruments, however, served as some indication of accuracy assuming both methods of measurement were not effected by the same systematic errors. Additionally, repeat readings taken on either one or two occassions served to estimate the control of such random errors as fluctuations of the level of accommodation and poor fixation.

Although to model the observed peripheral refractive patterns, it would have been desirable to construct schematic eyes from each of the 34 eyes measured, the time required to do this made such an approach impractical. The latter would perhaps have been of greater importance had more extreme variations of peripheral refraction been found but, as already explained in section 3.4.1, every one of the eyes measured possessed the normal, type IV, peripheral refractive pattern. Nevertheless, subtle differences in the profiles of the tangential and sagittal astigmatic image shells and small amounts of peripheral refractive asymmetry were evident. Furthermore, the peripheral refractive findings for near-emmetropes, myopes and hyperopes seemed to bear a great resemblance to the results of Millodot (1981) (see fig. 2.4). As this was

the case, the biometric and peripheral refractive data was *ere* averaged to produce three sets of results representing near-emmetropic, myopic and hyperopic eyes in order to provide some experimental corroboration for the ideas put forward to explain Millodot's (1981) peripheral refractive findings (see chapter 2).

The above approach not only saved a vast amount of time but also had the advantage of averaging out some of the experimental random errors so that the components of the final schematic eyes constructed were even closer to those of the eyes from which the peripheral refractive patterns were derived. As previously explained (section 3.3), the "internal validation" check provided by computer program, designed to construct the schematic eyes, served to estimate the extent of the final accumulated experimental error.

4.2 VALIDITY OF MEASUREMENTS

4.2.1 RADIUS AND PROFILE OF ANTERIOR CORNEAL SURFACE

(A) CENTRAL RADIUS

The central radius of curvature and axis orientation of the near horizontal and near vertical meridians of the anterior corneal surface were measured using a Zeiss keratometer (section 3.2.1B) and a Wesley-Jessen PEK photokeratoscope (section 3.2.1C). Only one photograph was taken using the PEK and therefore the precision of its results, taken on one occassion, could not be estimated. Three readings were, however, obtained using the keratometer which allowed the precision of its results to be determined, as descibed in section 4.1, by observing the range of standard deviations which occurred. Table 4.1 shows the results obtained from all 34 eyes

measured and is constructed from the data shown in appendix 2b. The keratometer was calibrated in 0.01 mm steps for radius determinations and 1° steps for axis determinations.

STANDARD DEVIATION		MERIDIAN Horizontal	Vertical
RADIUS	Range	0 - 0.05 mm	0 - 0.06 mm
	Mean	0.015 mm	0.015 mm
AXIS	Range	0 - 12.7°	0 - 19.6°
	Mean	2.884°	2.830°

Table 4.1 The precision of keratometric readings in terms of the range and mean of the standard deviations observed by taking three repeat readings, on one occasion only, on 34 corneae (see appendix 2b).

In section 3.2.1A , it was mentioned that Charman (1972) calculated that the precision of conventional two mire keratometry could be no better than ±0.04 mm. Although this value falls well within the range of standard deviations found in the present study, the mean standard deviation value of ±0.015 mm is somewhat smaller than the error predicted by Charman (1972). Nevertheless, it must be remembered that the present estimate of precision is a standard deviation value and that the spread of 95% of the population is expected to fall within two standard deviations so that the present value is in reasonable agreement with that predicted by Charman (1972).

Figure 4.1 shows a scatter plot of the central corneal radii in the near horizontal meridian, measured using the keratometer and the PEK. A similar scatter plot is shown in Figure 4.2 for determinations of the central corneal radii in the near vertical meridian. It can be seen that the readings obtained from both completely different methods are highly correlated. The latter implied that both methods were very accurate assuming both were not effected by the same systematic errors.

Fig. 4.1 Scatter plot of central corneal radii of curvature (mm) for the near horizontal meridian measured using the keratometer (x) and the PEK (y).
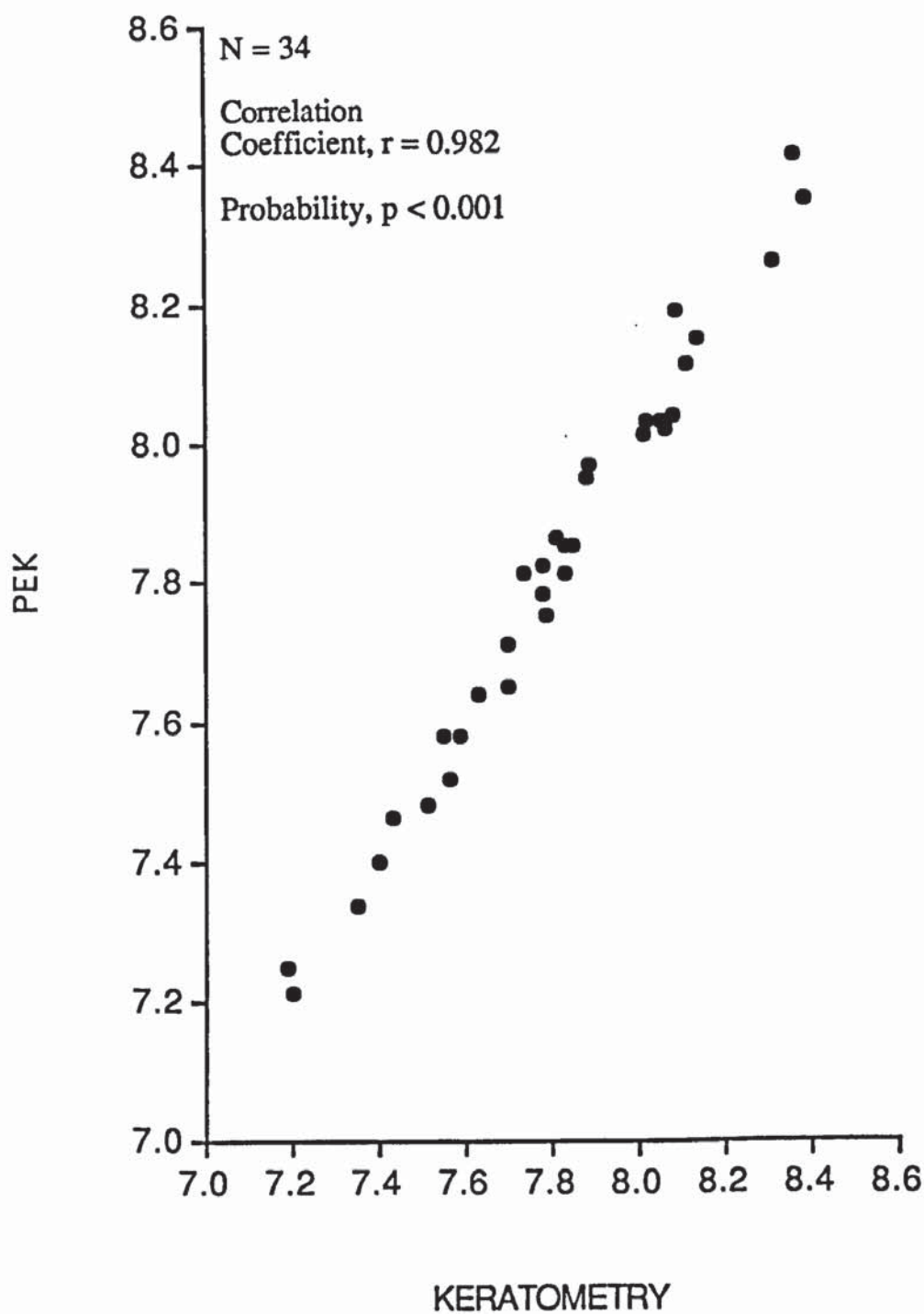
Fig. 4.2 Scatter plot of central corneal radii of curvature (mm) for the near vertical meridian measured using the keratometer (x) and the PEK (y).

It must be remembered, however, that both measurements were taken on separate occasions (see section 3.4.2) so that various biological (e.g. diurnal or menstrual) variations in the corneal curvature may also have played a part in the results. Nevertheless, the high correlation between both sets of readings indicated that any variation that might have occurred had very little influence.

A scatter plot of the axis orientation of the near horizontal and near vertical meridians, as determined using the keratometer and the PEK, is not shown. The reason for this was that the PEK results, analysed by Hamblin Contact Lens Ltd., only indicated the axis orientation of the flattest meridian (see appendix 2a). It was also evident that in two of the near-emmetropes (SB and RD), three of the myopes (DM, MG and MES) and one of the hyperopes (SH), the flattest meridian was found to be vertical indicating against-the-rule corneal astigmatism. The keratometric results (see appendix 2b) showed that for subjects RD and MES the astigmatism was with-the-rule whilst for subject DM the cornea was found to be spherical. The latter discrepancies were probably due to neither of the eyes possessing more than 0.06 mm difference between the horizontal and vertical meridians. Errors in the judgement of axis orientation were therefore likely to occur. Of course, biological variations could also have been causative. Nevertheless, these differences would have reduced any correlation between the two methods of measurement. As for the other subjects, a comparison between the axis orientations as shown in appendices 2a and 2b indicate good agreement between the two methods. Even a correlation between these results would have been poor due to the low spread of the data caused by the axes in both meridians being close to the horizontal and vertical position for most subjects. In only one subject (PCE) were the axes found to be oblique using keratometry, which again seemed to be the result of poor judgement of the axis orientation due to the small difference (0.08 mm) between the corneal radii in the steepest and flattest meridians.

Some months before the main collection of experimental data, a set of PEK readings were taken which conveniently served to indicate the precision of the results for six of the subjects taken on two separate occasions (see appendix 2a). The manufacturer claimed that PEK values of the central corneal radius were given to an accuracy of ±0.02 mm. This was, however, using steel balls as test pieces.

CORNEAL RADIUS		MERIDIAN Horizontal	Vertical
FIRST READING	Mean	7.85 mm	7.82 mm
	SD	0.29 mm	0.32 mm
SECOND READING	Mean	7.86 mm	7.82 mm
	SD	0.28 mm	0.33 mm

Table 4.2   The precision of PEK measurements of the central corneal radius. Mean and standard deviations (SD) were derived from measurements made on six corneae on two occasions (see appendix 2a).

Although table 4.2 shows that estimates of the corneal radius were remarkably consistent, it is also evident (see appendix 2a) that the flattest meridian changed its orientation for subjects RD and MES. Although the reasons for this have already been discussed, it still remains that the axis orientations appear to be unreliable, whereas in actual fact they were reliable enough for the present purposes.

(B) PROFILE AND APEX POSITION

The repeat readings, shown in appendix 2a, also served to indicate the precision of the data relating to the corneal profile and apex position. In Table 4.3, the corneal profile is expressed in terms of the conic constant (P) rather than Wesley-Jessen's "shape factor" (e^2) (see section 3.2.1C). Values of the shape factor were given, according to

the manufacturer, to an accuracy of 0.04 units. The averaged results indicate that repeat readings can be taken of the corneal profile to a reasonable level of precision. It must be added, however, that on an individual basis, the corneal profile did not appear to be as precise as central radius measurements. This outlines one of the advantages of averaging the data in each refractive group in order to minimise the effects of such small errors.

| CONIC | | MERIDIAN | |
CONSTANT (*P*)		Horizontal	Vertical
FIRST READING	Mean	0.74	0.78
	SD	0.10	0.15
SECOND READING	Mean	0.73	0.79
	SD	0.09	0.13

Table 4.3   The precision of PEK measurements of the corneal contour. Mean and standard deviations (SD) for conic constant (*P*) values were derived from measurements made on six corneae on two occasions (see appendix 2a).

In table 4.4, the displacement of the corneal apex from the line of sight is shown. From the analysed PEK results, the distance of the apex from the line of sight measured along a chord was given to the nearest half millimeter and the "apex angle" to the nearest 5° (Tomlinson and Schwartz, 1979). A chord with an apex angle of 0° referred to a horizontal displacement towards the nasal side in the subject's right eye and towards the temporal side of the subject's left eye. A chord with an apex angle of 90° referred to a superior vertical displacement whilst an angle of 270° referred to an inferior vertical displacement. Because the apex angle data in its raw form was cyclical (i.e. falling anywhere between 0° and 359°), statistical analysis was only possible if the data was resolved to displacements in the horizontal and vertical meridians only, as shown in table 4.4.

DISTANCE OF APEX FROM LINE OF SIGHT		DIRECTION OF DISPLACEMENT	
		Horizontal	Vertical
FIRST READING	Mean	0.34 mm NASAL	0.39 mm SUPERIOR
	SD	0.68 mm	1.01 mm
SECOND READING	Mean	0.04 mm TEMPORAL	0.34 mm INFERIOR
	SD	0.11 mm	1.36 mm

Table 4.4   The precision of PEK measurements of the position of the corneal apex with respect to the line of sight. Mean and standard deviations (SD) were derived from measurements made on six corneae on two occasions (see appendix 2a).

As shown above, estimates of the apex position, using the PEK, appeared to be unreliable. Furthermore, displacements of as much as 3 mm were found which led the present author to question the results. It is of interest that Tomlinson and Schwartz (1979) also found similarly high apical displacements. Nevertheless, the data regarding apex position was considered to be too inconsistent to be of use in the present study.

4.2.2 AXIAL DISTANCES

(A) ANTERIOR CHAMBER DEPTH

The anterior chamber depth (measured from the anterior surface of the cornea to the anterior surface of the crystalline lens) was measured using a Storz Alpha 20/20 ultrasound unit (section 3.2.2B) and a Haag Streit 900 anterior chamber pachometer (section 3.2.2C). In table 4.5, the precision of the results are shown in terms of the range of standard deviations which occurred on all 34 eyes from repeat readings taken on one session. The table includes data from the first ultrasonic readings and the

pachometric readings shown in appendix 2c. After the application of the various rejection criteria (see section 3.2.2B), between 7 and 41 repeat ultrasonic readings were used per person, to calculate mean and standard deviation values. Three repeat readings were taken using the pachometer. Anterior chamber depth estimates from both instruments were read to the nearest 0.01 mm.

STANDARD DEVIATION	READINGS Ultrasound (first)	Pachometry
Range	0.01 - 0.31 mm	0 - 0.16 mm
Mean	0.067 mm	0.045 mm

Table 4.5   The precision of ultrasonic and pachometric anterior chamber depth measurements in terms of the range and mean of the standard deviations observed by taking repeat readings, on one occasion only, on 34 eyes (see appendix 2c).

Figure 4.3 shows a scatter plot of the anterior chamber depths measured using ultrasound (first readings) and pachometry. It can be seen that the readings obtained from both completely different methods are highly correlated. As with the corneal data, the latter implied that both methods were very accurate assuming that both were not effected by the same systematic errors. Figure 4.4 shows a scatter plot of the first ultrasonic readings compared with the second. In this case, the high correlation observed further indicated the precision of the ultrasonic method. Repeat ultrasonic measurements were only possible on 28 eyes due to difficulties experienced whilst obtaining ultrasonic data from some subjects. As the data in both scatter plots was taken on separate occasions (see section 3.4.2), the high correlations observed also implied that the various biological (e.g. diurnal or menstrual) variations had little influence on the results. Furthermore, possible fluctuations of the anterior chamber depth resulting from accommodation and compression of the cornea by the ultrasonic probe, appeared to be well under control.

N = 34

Correlation
Coefficient, r = 0.915

Probability, p < 0.001
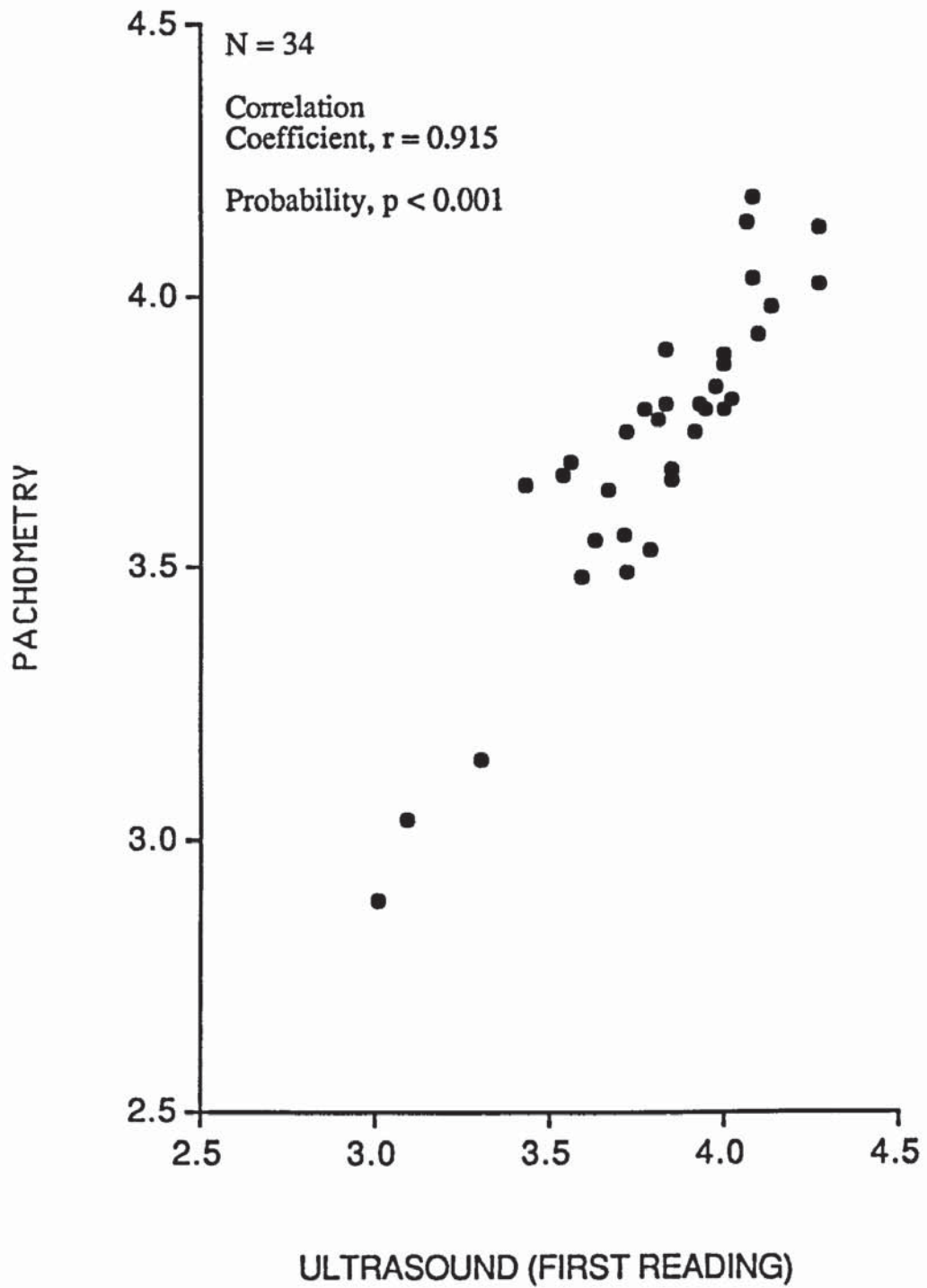
Fig. 4.3 Scatter plot of anterior chamber depth (mm) measured using ultrasound (x) and pachometry (y).

Fig. 4.4 Scatter plot of the first (x) and second (y) ultrasonic measurements of the anterior chamber depth (mm).

147

(B) CRYSTALLINE LENS THICKNESS

The thickness of the crystalline lens was measured, using the Storz Alpha 20/20 ultrasound unit, at the same time as ultrasonic anterior chamber depth measurements were being made. Table 4.6 shows the precision of the results in terms of the range of standard deviations which occurred on all 34 eyes from repeat readings taken on one occasion. As with the anterior chamber depth measurements, the table only includes the first ultrasonic readings (as shown in appendix 2d). After the application of various rejection criteria, between 7 and 41 repeat ultrasonic readings were used per person to calculate mean and standard deviation values. The ultrasound unit gave lens thickness values to the nearest 0.01 mm.

STANDARD DEVIATION	ULTRASOUND (First readings only)
Range	0.01 - 0.19 mm
Mean	0.049 mm

Table 4.6 The precision of ultrasonic lens thickness measurements in terms of the range and mean of the standard deviations observed by taking repeat readings, on one occasion only, on 34 eyes (see appendix 2d).

Figure 4.5 shows a scatter plot of the first (appendix 2d) and the second (appendix 2e) ultrasonic readings of the crystalline lens thickness taken on 28 eyes. The high correlation observed indicated that ultrasonic lens thickness measurements could be made on different occasions to a high degree of precision. As the data in both scatter plots was taken on separate occasions, the high correlations observed also implied that various biological variations had little influence on the results. Possible fluctuations of the lens thickness due to accommodation also appeared to be well under control.
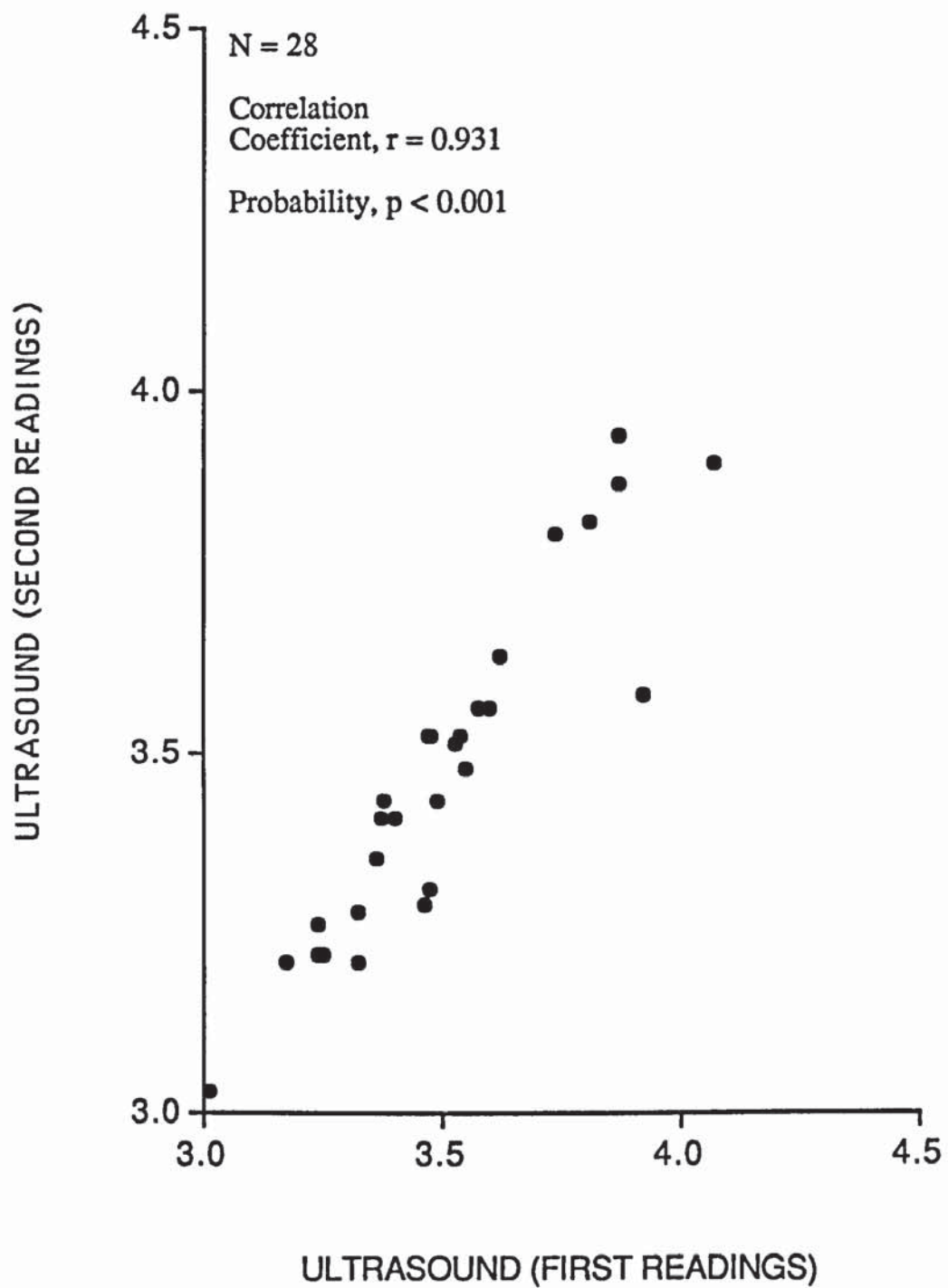
Fig. 4.5 Scatter plot of the first (x) and second (y) ultrasonic measurements of the crystalline lens thickness (mm).

(C) VITREOUS AND AXIAL LENGTH

The vitreous chamber length was also measured using the Storz Alpha 20/20 ultrasound unit, at the same time as anterior chamber depth and lens thickness measurements were made. From the sum of the latter distances the axial length was calculated. Table 4.7 shows the precision of the vitreous and axial length results in terms of the range of standard deviations which occurred on all 34 eyes, from repeat readings taken on one occassion. Again, the table only includes the first ultrasonic readings as shown in appendix 2d. As already mentioned, the application of various rejection criteria left between 7 and 41 repeat ultrasonic readings per person, from which the mean and standard deviation values were calculated. Ultrasonic vitreous and axial length values were also given to the nearest 0.01 mm.

STANDARD DEVIATION Length	ULTRASOUND (First readings only) Vitreous Length	Axial
Range mm	0.01 - 0.47 mm	0.01 - 0.39
Mean	0.083 mm	0.095 mm

Table 4.7   The precision of ultrasonic vitreous and axial length measurements in terms of the range and mean of the standard deviations observed by taking repeat readings, on one occasion only, on 34 eyes (see appendix 2d).

Figure 4.6 shows a scatter plot of the first (appendix 2d) and the second (appendix 2e) ultrasonic readings of the vitreous length carried out on 28 eyes. Figure 4.7 shows a similar scatter plot for axial length determinations. The high correlation shown in both graphs indicated that measurements could be made on different occasions with a high degree of precision. Again, various biological variations seemed to have had little influence on the results.
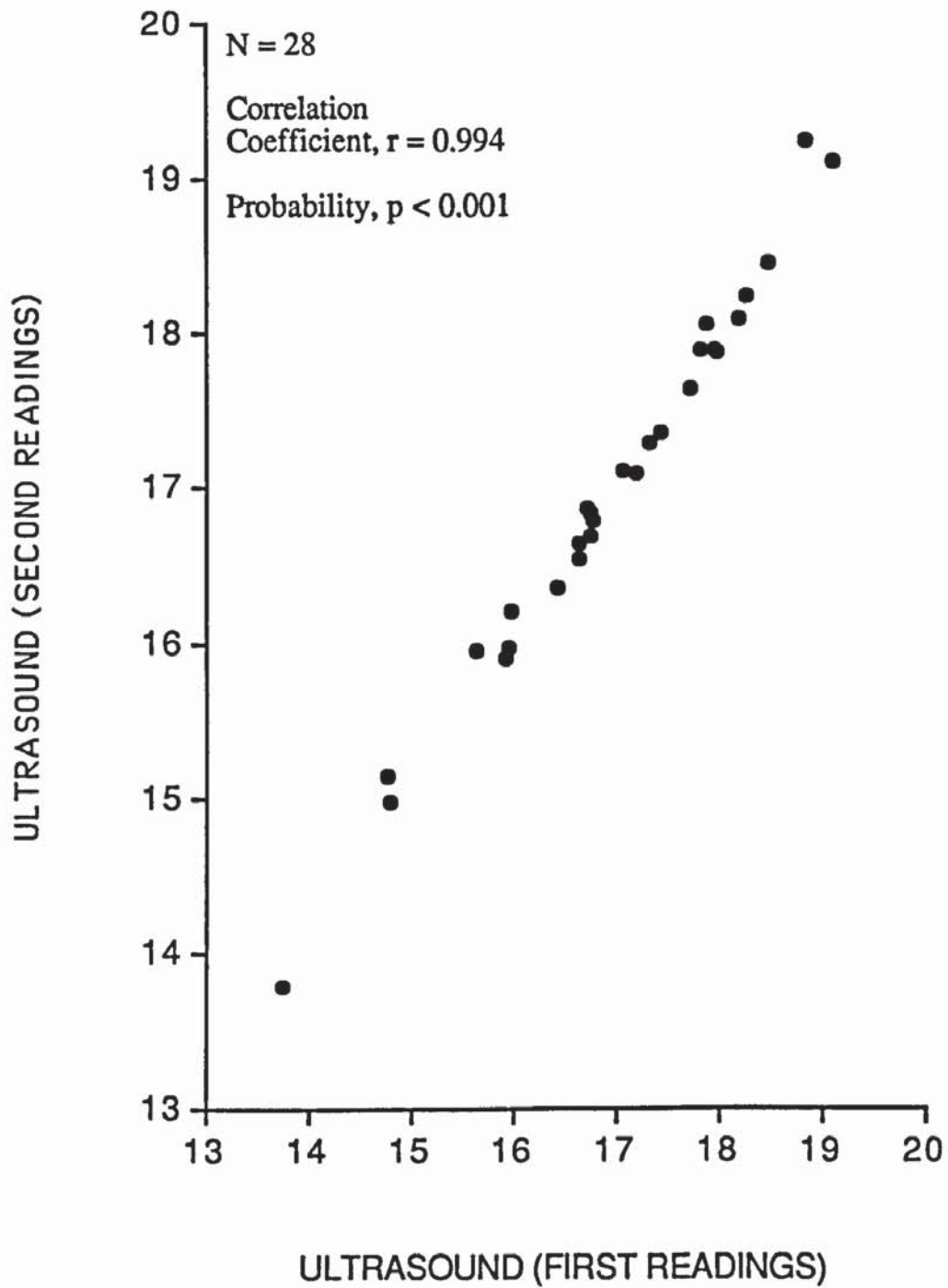
Fig. 4.6 Scatter plot of the first (x) and second (y) ultrasonic measurements of the vitreous chamber depth (mm).
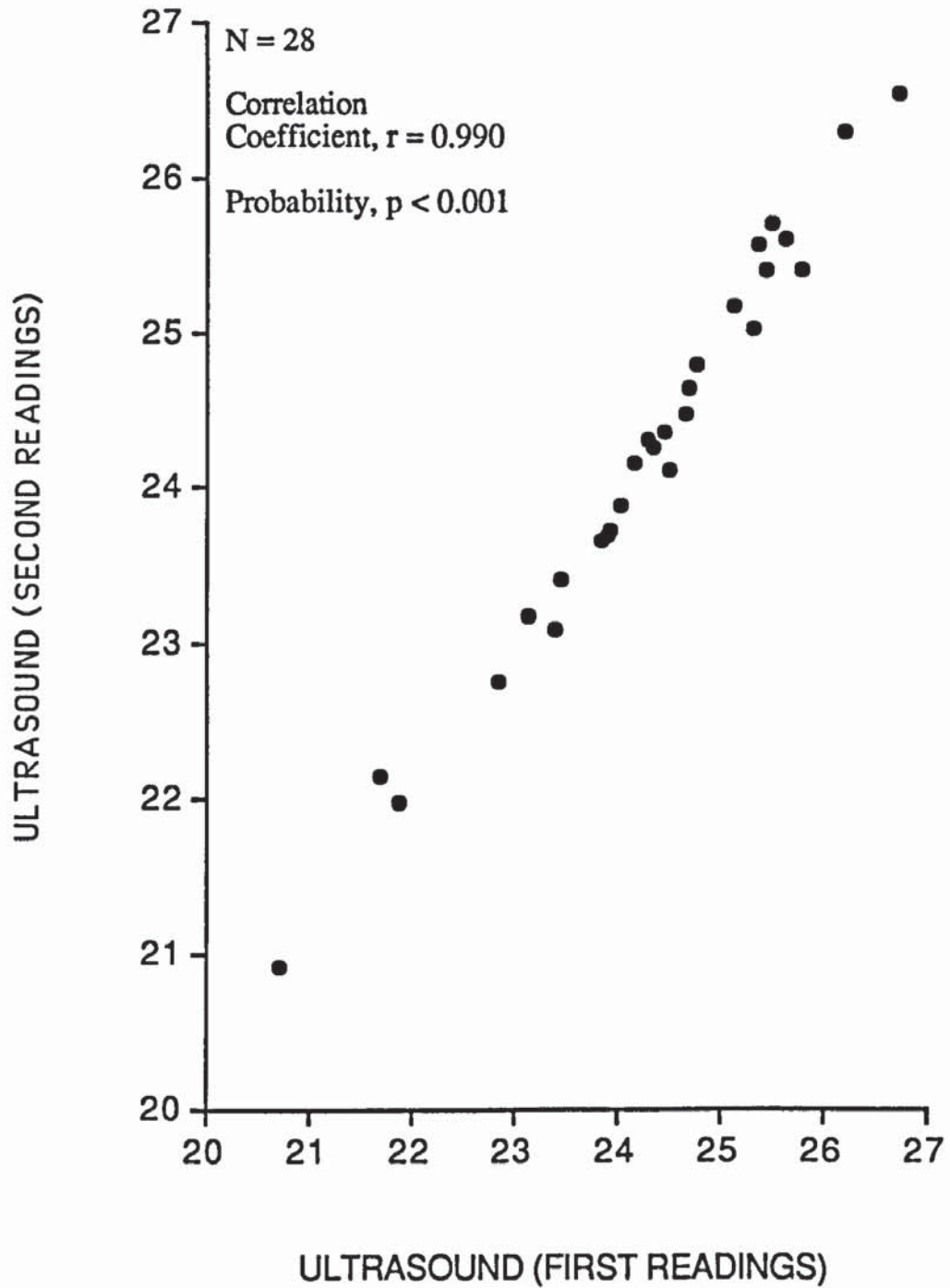
Fig. 4.7 Scatter plot of the first (x) and second (y) ultrasonic measurements of the axial length (mm).

4.2.3 PURKINJE IMAGE HEIGHTS

To illustrate the problems involved with estimating Purkinje image heights, fig. 4.8 shows a typical photograph of the Purkinje images taken using the photographic ophthalmophakometer described in section 3.2.3B.

The slit lamp camera was focused in the plane of the iris so that Purkinje I and IV, as well as the edges of the iris, were seen in focus. The brightness of Purkinje I led to measurement difficulties due to flare. Purkinje III was blurred as its images were formed in the vitreous chamber (see section 3.2.3A). It was also very much dimmer than Purkinje I and IV making measurement difficult. In addition, the presence of "shagreen" (see section 3.2.3A) was very marked in the case of Purkinje III which could be seen from its mottled appearance. Needless to say, this added further difficulties to the precise measurement of this image. Weale (1982) pointed out that Purkinje image IV should also show the effects of shagreen but this does not appear to be the case in fig. 4.8.

(A) ASSESSMENT OF DISTORTION FROM GRID PHOTOGRAPHS

As explained in section 3.2.3B, the magnification and distortion of the ophthalmophakometric photographs arising from slit lamp camera, film processing and projection system, were all assessed simultaneously by photographing a grid and measuring its dimensions after projection. The grid used consisted of fine drawn graph paper showing grid lines of 1 mm separation. For measurement purposes, a horizontal and a vertical line was drawn on the grid. These intersected each other in the centre of the grid which coincided with the centre of the photographic field.

153

Fig. 4.8   Photograph of Purkinje images I, III and IV as taken using the photographic ophthalmophakometer (see section 3.2.3B).

After mounting the grid in the position normally occupied by the test eye, the slit lamp camera was focused on it and 10 photographs taken. These were processed and the negatives projected in exactly the same manner as for the Purkinje image photographs. The interval between successive grid lines, positioned horizontally above and below as well as vertically to the right and to the left of the grid centre, were measured to as far out as 5 mm. The 10 mm field was chosen to allow distortion to be assessed over an area which was larger than that covered by the Purkinje images and the entrance pupil.

Measurements were made, with a steel ruler, to the nearest 0.5 mm and the results are shown in appendix 2f. As the real distance between the grid lines was 1 mm, values measured after projection were a direct estimate of the magnification at any given point on the photograph. The range of magnifications found over the horizontal and vertical planes then served as an estimate of distortion. In Table 4.8 the range, mean and standard deviation of the magnifications found over the horizontal and vertical planes of the grid, after projection, are shown.

MAGNIFICATION	Horizontal plane	Vertical plane
Observations (N)	100	100
Range	21.5 - 22.5 mm	21.5 - 22.5 mm
Mean	21.87 mm	22.03 mm
Standard deviation	0.39 mm	0.41 mm

Table 4.8   The range of magnifications found over the horizontal and vertical planes of the projected grid photograph (see appendix 2f).

As the difference between the average magnification values found over the horizontal and vertical planes was only 0.16 mm (i.e. well within the standard deviation values), the results were pooled to give a final estimate of 21.95 ± 0.40 mm for the magnification. The range of magnification values (distortion) found in both planes also never exceeded 1 mm which represented only 4.6% of the mean value and a scaled down distance of only 0.045 mm. Therefore, any distortion which could have led to this spread in the results was considered to be negligible.

(B) PURKINJE IMAGE I (CORNEAL SURFACE)

The height of Purkinje image I was measured from the projected ophthalmophakometric photographic negatives. Table 4.9 shows the precision of the results in terms of the range of standard deviations which occurred on all 34 eyes, from repeat readings taken on one occassion. The table only includes results from the first set of ophthalmophakometric measurements (as shown in appendix 2g). As explained in section 3.2.3B, the mean and standard deviation values were calculated from 9 estimates of the image height. Measurements were made with a steel ruler to the nearest 0.5 mm which, when scaled down by X 21.95, is equivalent to 0.02 mm actual size.

STANDARD DEVIATION	OPHTHALMOPHAKOMETRY (First readings only)	
	Unscaled	Scaled down (X 21.95)
Range	0.25 - 1.5 mm	0.011 - 0.068 mm
Mean	0.546 mm	0.025 mm

Table 4.9 The precision of photographic ophthalmophakometric measurements of Purkinje image I in terms of the range and mean of the standard deviations observed by taking nine repeat readings, on one occasion only, on 34 eyes (see appendix 2g).

Figure 4.9 shows a scatter plot of the first set of Purkinje I heights (see appendix 2g) and the corneal radii in the near vertical meridian, measured using the PEK (see appendix 2a). The corneal radii were not resolved to 90° since the axes of orientation of the near vertical meridians were always found to be very close to 90° and if the latter was not the case, the differences between the radii in the near vertical and near horizontal meridians were very small (see section 4.2.1A). It can be seen that the readings correlate very well considering the difficulties encountered in measuring the very bright Purkinje I image (see figure 4.8).

Figure 4.10 shows a scatter plot of the first set of Purkinje I heights compared with the second set (see appendix 2h). Repeat ophthalmophakometric measurements were only possible on 32 eyes due to the Purkinje images being too faint to measure in two of the subjects. A relatively low correlation was observed, although it was still highly significant, which was most likely to be due to the problems of measuring the very bright Purkinje I image.

It must also be remembered, however, that the readings in fig. 4.9 were taken on the same occasion whereas those of fig. 4.10 were taken on separate occasions (see section 3.4.2). It would seem that because the former graph showed a higher correlation compared with the latter, that the precision of the Purkinje I measurements was effected by observations taken on separate occasions. Previous repeat measurements of the curvature of the corneal surface (see section 4.2.1), however, imply that the various biological variations have little influence on the results. Therefore, it may be that errors arose from re-setting the ophthalmophakometer for taking repeat measurements. On the other hand, the small range of values observed for the Purkinje I image heights may have been causative (see section 4.2.3C).
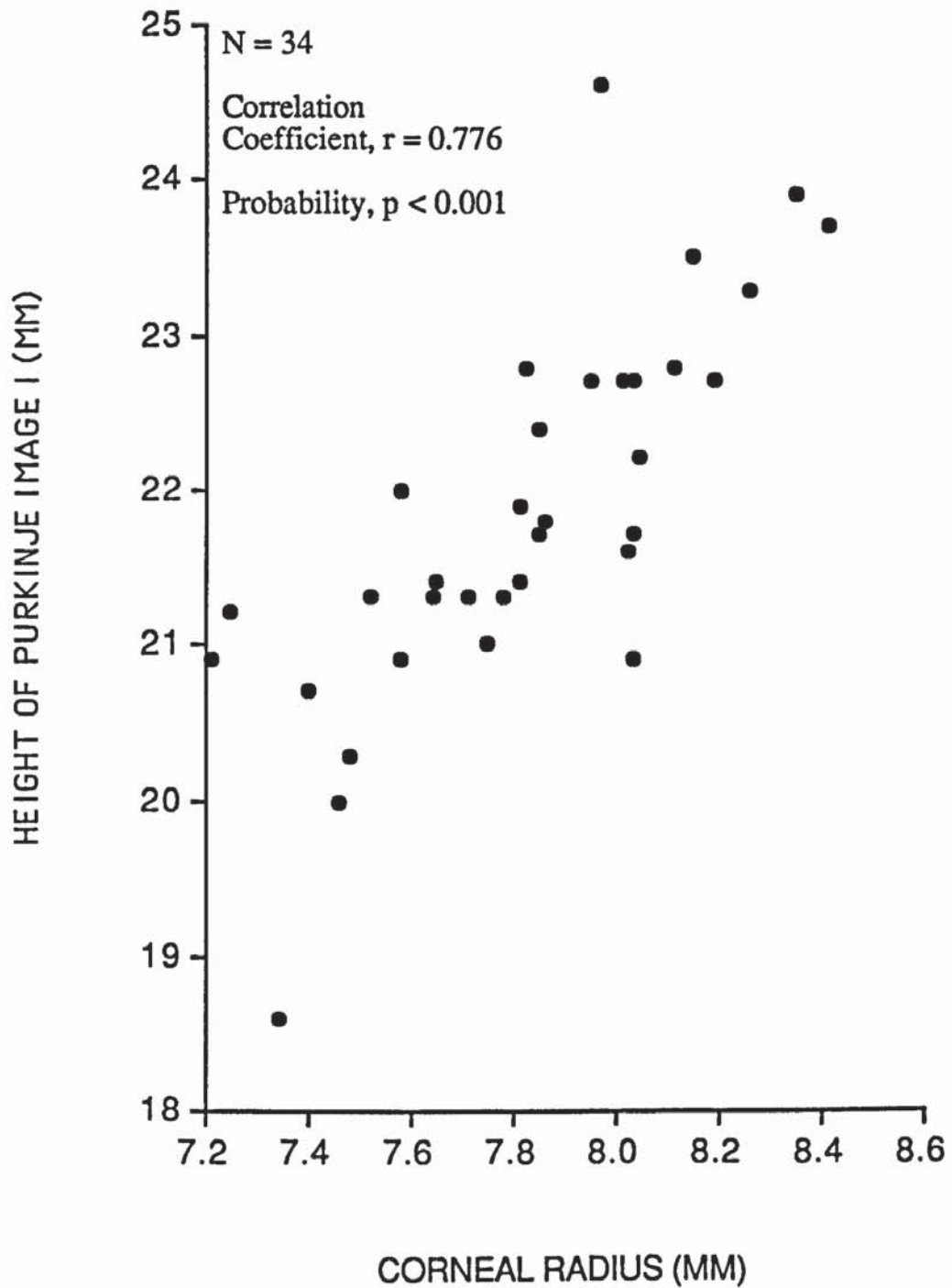
Fig. 4.9 Scatter plot of the corneal radius, in the near vertical meridian, as measured using the PEK (x) and the first set of measurements of the height of Purkinje image I (unscaled) as measured using the photographic ophthalmophakometer (y).
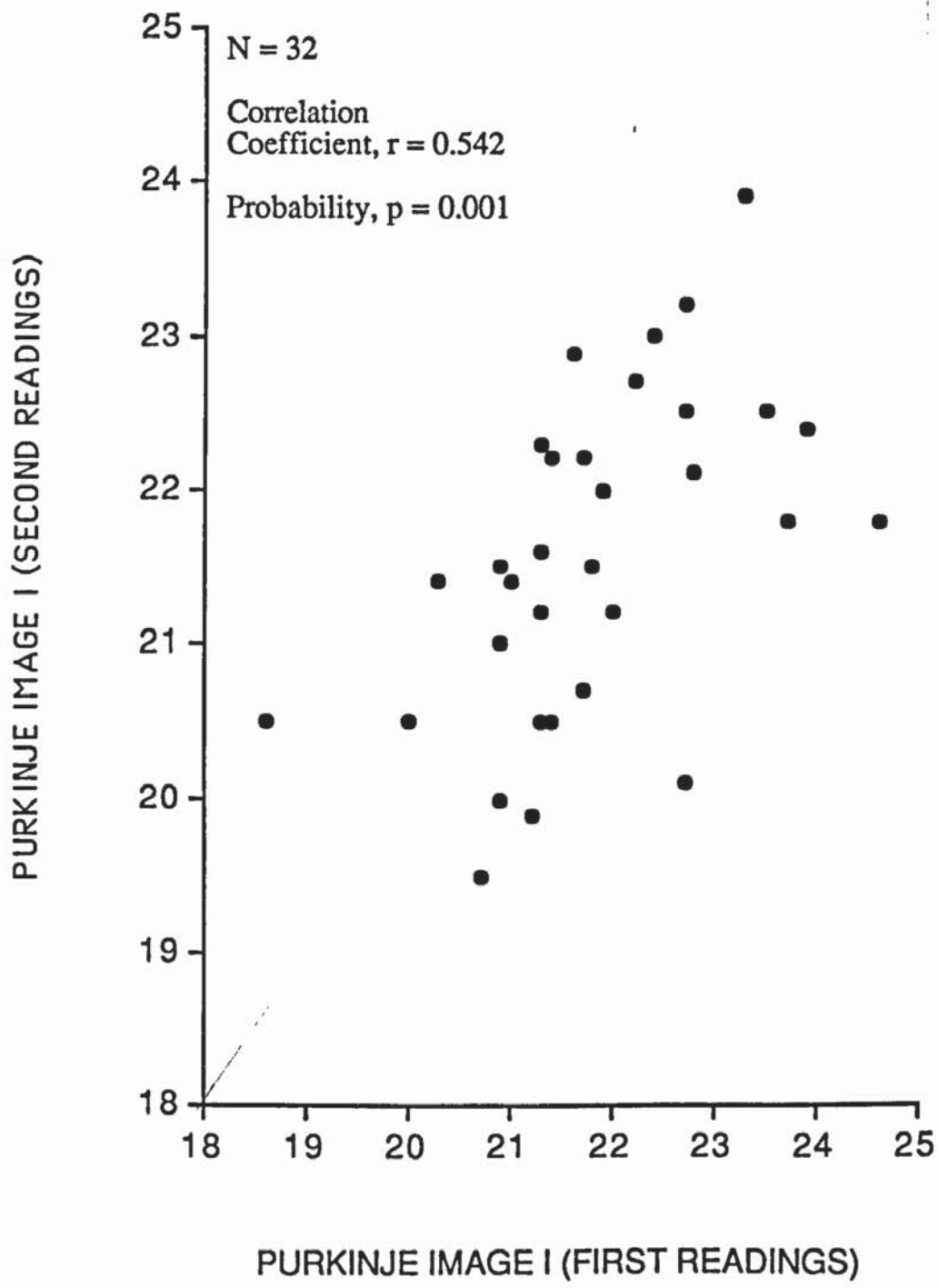
Fig. 4.10 Scatter plot of the first (x) and second (y) photographic ophthalmophakometric measurements (unscaled) of the Purkinje image I heights (mm).

(C) PURKINJE IMAGES III AND IV (LENTICULAR SURFACES)

Purkinje III and IV were measured using the photographs from the ophthalmophakometer, at the same time as measurements of Purkinje I. Table 4.10 shows the precision of the results in terms of the range of standard deviations which occurred, on all 34 eyes, from repeat readings taken on one occasion. Again, the table only includes the first set of readings as shown in appendix 2g. Mean and standard deviation values were calculated from nine estimates of the image height as measured with a steel ruler to the nearest 0.5 mm (equivalent to 0.02 mm actual size).

STANDARD DEVIATION	OPHTHALMOPHAKOMETRY (First readings only)	
	Unscaled	Scaled down (X 21.95)
PURKINJE III IMAGES:		
Range	0.29 - 2.10 mm	0.013 - 0.096 mm
Mean	0.930 mm	0.042 mm
PURKINJE IV IMAGES:		
Range	0 - 0.87 mm	0 - 0.040 mm
Mean	0.377 mm	0.017 mm

Table 4.10 The precision of photographic ophthalmophakometric measurements of Purkinje images III and IV in terms of the range and mean of the standard deviations observed by taking nine repeat readings, on one occasion only, on 34 eyes (see appendix 2g).

It is apparent that the magnitude of the measurement precision of Purkinje I (table 4.9), III and IV (table 4.10) follows the order of their relative sizes (see section 3.2.3A and fig. 4.8). The latter observations can be logically explained by the fact that measurements were made from centre to centre for each pair of images and estimates of the centre of an image become more difficult as the image size increases. According to Bennett and Rabbetts (1984) the calculated ratio between Purkinje images I : III : IV

160

is approximately 1 : 2 : 0.75 (see section 3.2.3A). The equivalent ratio of the relative precisions, found in the present study, is 1 : 1.70 : 0.69. The concordance between the latter two ratios would suggest that image size is the dominant factor effecting the precision of Purkinje image measurements, although other effects such as "shagreen" (see fig. 4.8) may also have some influence.

Figure 4.11 shows a scatter plot of the first (appendix 2g) and the second (appendix 2h) set of photographic ophthalmophakometric readings of Purkinje III, carried out on 32 eyes. Figure 4.12 shows a similar scatter plot for readings of Purkinje image IV. The high correlation shown in both graphs indicated that measurements of the lenticular Purkinje images could be made, on different occasions, to a higher degree of precision than those of the corneal Purkinje images. However, it must be noted that if the Purkinje images are arranged in order of the correlation coefficients (r) calculated for repeat measurements:

$$\text{III } (r = 0.942) \; > \; \text{IV } (r = 0.703) \; > \; \text{I } (r = 0.542),$$

the order found is very similar to that which arises when the interval between the smallest and largest Purkinje image heights (unscaled) is the criterion looked at:

$$\text{III } (29.4 \text{ mm}) > \text{IV } (6.1 \text{ mm}) > \text{I } (6.0 \text{ mm}).$$

Therefore, it appears that the high correlation observed for measurements of Purkinje III is the result of the wide range of values found for it. For Purkinje I and IV, the small range of values measured possibly makes the correlation between repeat readings more susceptible to measurement errors, hence giving rise to lower correlation coefficients. Bearing in mind the repeatability of Purkinje IV image heights, it seems unlikely that biological variations markedly influence the lenticular Purkinje image results.
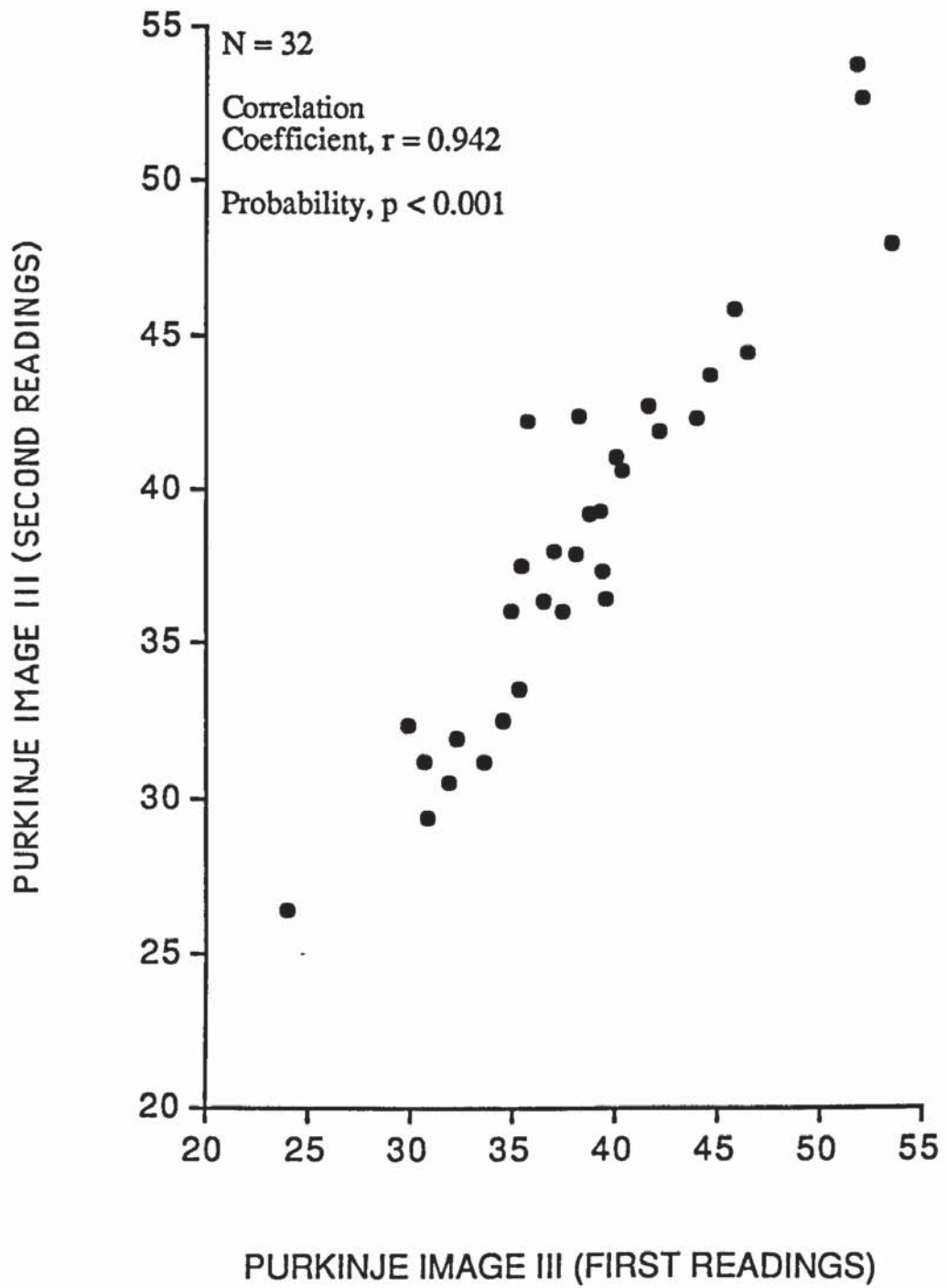
Fig. 4.11 Scatter plot of the first (x) and second (y) photographic ophthalmophakometric measurements (unscaled) of the Purkinje image III heights (mm).
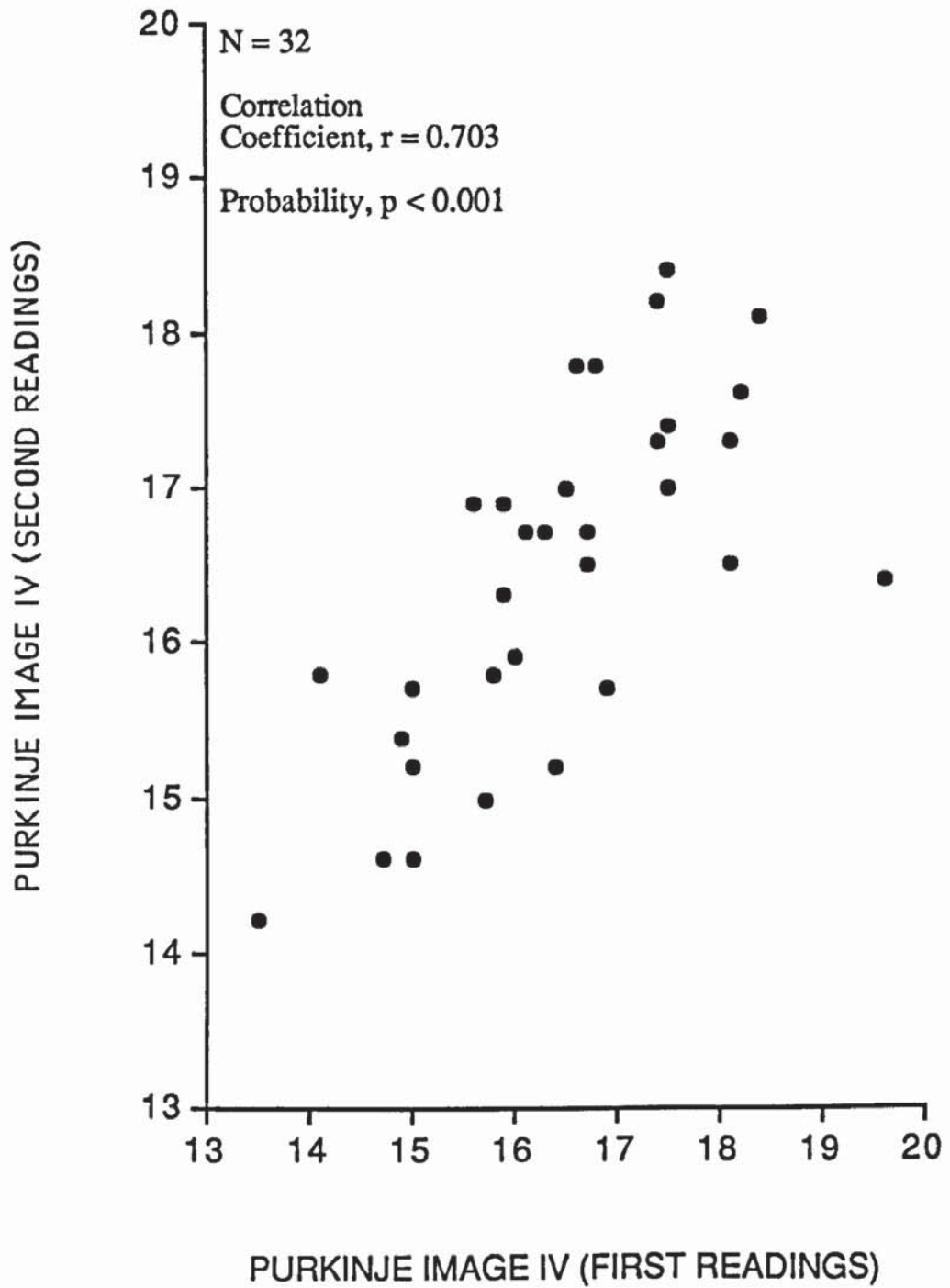
Fig. 4.12 Scatter plot of the first (x) and second (y) photographic ophthalmophakometric measurements (unscaled) of the Purkinje image IV heights (mm).

4.2.4 REFRACTIVE ERROR

(A) CENTRAL REFRACTION

Central and peripheral refractive measurements were made at the same time. Peripheral refractive results are usually described in terms of the variation of refractive error in the tangential and sagittal meridians (see chapter 2). Therefore, to avoid confusion, the central refractive results will also be referred to in the same manner. As measurements were made over the horizontal plane, the tangential refraction is that measured in the near horizontal meridian whilst the sagittal refraction refers to that measured in the near vertical meridian.

Measurements of the central refractive error and axis orientation of the tangential and sagittal meridians were measured using the Zeiss Jena Hartinger coincidence optometer (see section 3.2.4B) and the Canon Autoref R-1 automated infra-red optometer (see section 3.2.4C). Table 4.11 shows the precision of the results in terms of the range of standard deviations which occurred in all 34 eyes, from repeat readings taken on one occasion. Mean and standard deviation values were calculated from three repeat readings taken with the Hartinger optometer (see appendix 2i) and five repeat readings taken with the Canon Autoref R-1 (see appendix 2j). The Hartinger optometer gave refractive error and axis readings in 0.25 D and 1° intervals respectively. Refractive error and axis readings were given, by the Canon Autoref R-1, in 0.12 D and 1° steps respectively. As the Canon Autoref R-1 results were given in spherocylindrical form, only one axis value was indicated. For this reason, only the axis of orientation in the tangential meridian is shown in table 4.11.

STANDARD DEVIATION		MERIDIAN	
		Tangential	Sagittal

HARTINGER OPTOMETER:

		Tangential	Sagittal
Refractive Error	Range	0 - 0.5 D	0 - 0.63 D
	Mean	0.175 D	0.175 D
Axis	Range	0 - 23.6°	0 - 13.7°
	Mean	2.297°	1.613°

CANON AUTOREF R-1:

		Tangential	Sagittal
Refractive Error	Range	0 - 0.55 D	0.04 - 0.58 D
	Mean	0.127 D	0.139 D
Axis	Range	1 - 38°	-
	Mean	6.871°	-

Table 4.11   The precision of central refractive results in terms of the range and mean of the standard deviations observed by taking repeat readings, on one occasion only, on 34 eyes (see appendix 2i and appendix 2j).

The precision of the refractive error measurements using the Canon Autoref R-1 was slightly greater than that of the Hartinger optometer. This appeared to be attributable to the smaller intervals in which the refractive error readings were given by the Canon Autoref R-1. For axis values, however, the precision of Canon Autoref R-1 measurements were considerably worse than those obtained using the Hartinger optometer. Canon Autoref R-1 axis determinations (as mentioned in section 3.2.4C), become less reliable for subject's with less than 0.75 D of astigmatism. Indeed, 41% of the eyes, measured using the Canon Autoref R-1, possessed less than 0.75 D of astigmatism, which could explain the reduced precision. 85% of the eyes, measured using the Hartinger optometer possessed less than 0.75 D of astigmatism, which also indicated that the Canon Autoref R-1 produced larger values of astigmatism.
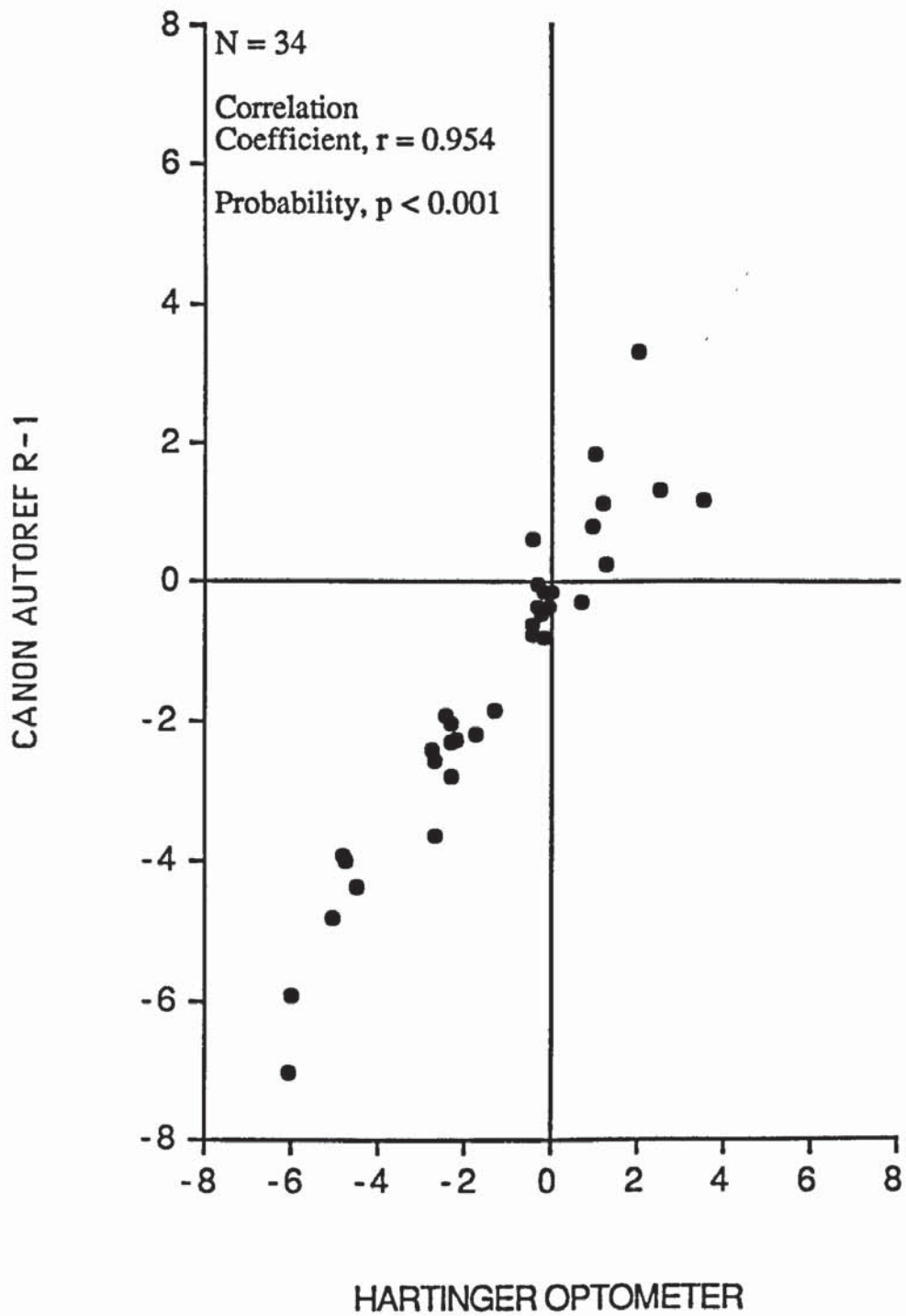
Fig. 4.13 Scatter plot of central refractive error (D) for the tangential meridian as measured using the Hartinger optometer (x) and the Canon Autoref R-1 optometer (y).
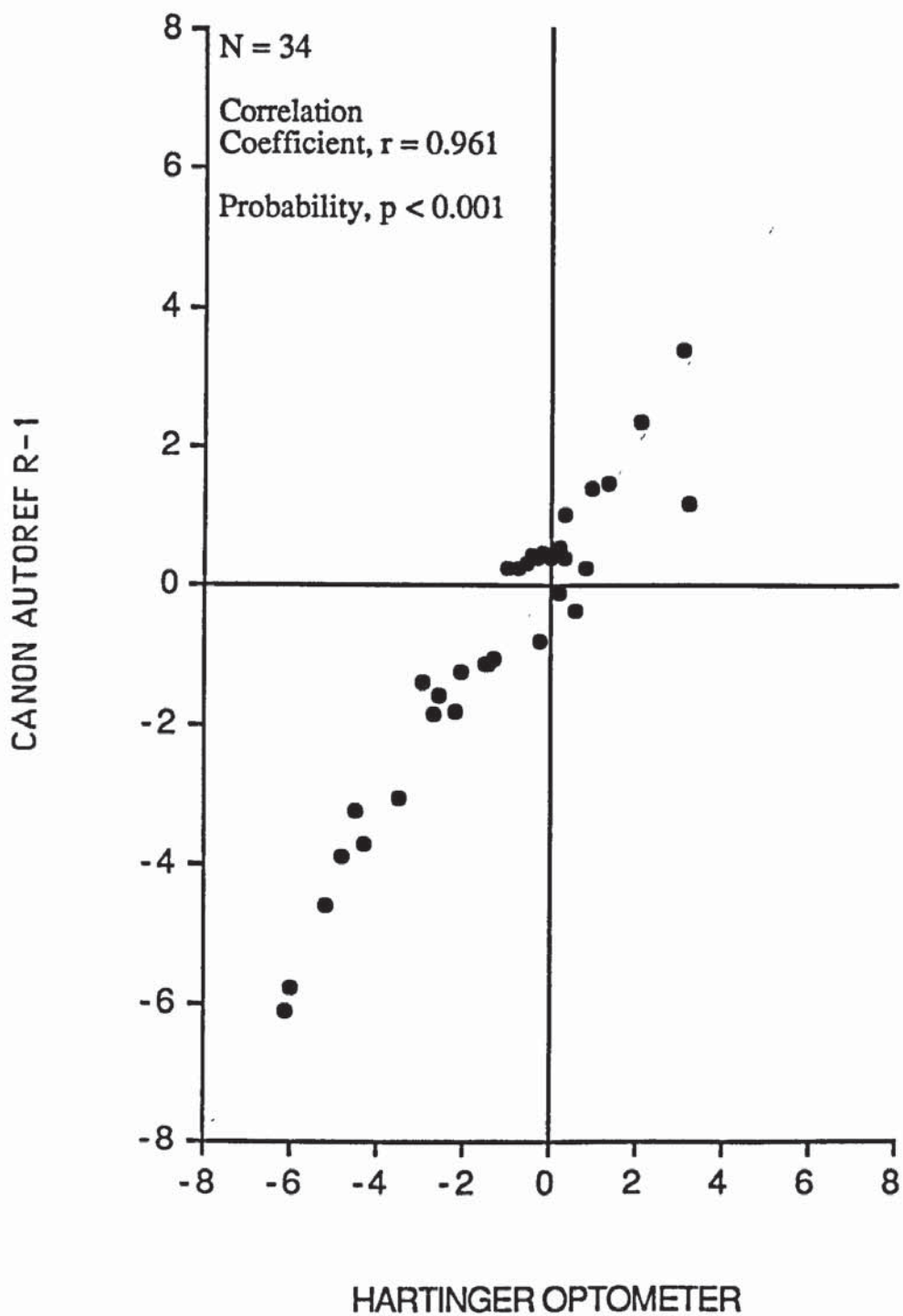
Fig. 4.14 Scatter plot of central refractive error (D) for the sagittal meridian as measured using the Hartinger optometer (x) and the Canon Autoref R-1 optometer (y).

Figure 4.13 shows a scatter plot of the central refractive error in the tangential meridian measured using the Hartinger optometer and the Canon Autoref R-1. A similar scatter plot is shown in fig. 4.14 for central refractive error measurements made in the sagittal meridian. It can be seen that the readings obtained from the different methods were highly correlated. This implied that the readings from both optometers were very accurate, assuming that they were not effected by the same systematic errors. As the data in both scatter plots was taken on separate occasions, the high correlations observed also implied that the various biological variations had little influence on the results. Furthermore, accommodation appeared to cause minimal fluctuations in the results.

A scatter plot of the axis orientation of the tangential meridian determined using the Hartinger optometer and the Canon Autoref R-1 is not shown. The reason for this was two fold. First, the axis values measured using the Canon Autoref R-1, as have already been mentioned, were very variable and would have reduced any correlation. Second, any correlation between these results would have been poor due to the low spread of the data caused by the axes in tangential meridian being close to 180° for most subjects as indicated by the values measured using the Hartinger optometer.

(B) PERIPHERAL REFRACTION

Originally, it was intended that peripheral refraction was to be measured out to field angles of 60° nasally and temporally. However, because it was not always possible to obtain readings at even 50° with the Hartinger optometer, as the instrument target (see section 3.2.4B) was either too dim or too distorted, values beyond 40° were not included in the final results (see appendix 2k). When using the Canon Autoref R-1, readings could not always be taken beyond 30°. This was possibly due to the width of

the obliquely viewed entrance pupil being narrower than that required by the Canon Autoref R-1 to take readings (see section 3.2.4C). Therefore, the final refractive results taken using the Canon Autoref R-1 did not include any measurements beyond 30° field angle (see appendix 2l).

A slight decrease in the precision of the refractive results was found with both instruments as the field angle increased. At field angles of 40° average standard deviation values of between 0.25 D and 0.43 D were recorded for the Hartinger optometer (see appendix 2k). Values of between 0.11 D and 0.37 D were recorded for the Canon Autoref R-1 at field angles of 30° (see appendix 2l). Comparing these values to those found for the central refractive readings (table 4.11) an approximately two fold decrease in the precision is evident. The precision of axis determinations as measured using the Hartinger optometer showed no change with increasing field angle. For axis measurements taken with the Canon Autoref R-1, however, a noticeable increase in precision occurred at larger field angles, possibly indicating the greater ease with which axis determinations could be made as the amount of astigmatism increased (fig. 4.17).

Figure 4.15 shows the variation with field angle of the sagittal refractive error values measured using the Hartinger optometer (appendix 2k) and the Canon Autoref R-1 (appendix 2l). Similar graphs are shown for the variation with field angle of the tangential refractive error (fig. 4.16) and astigmatism (fig. 4.17). In these graphs, each datum point represents the averaged results of all 34 eyes measured. As readings are only shown to 30° nasally and temporally, correlation coefficients were based on the seven datum points measured using both instruments. High correlations were found in each graph, which implied that the readings from both optometers were very accurate, assuming that they were not effected by the same systematic errors.

169
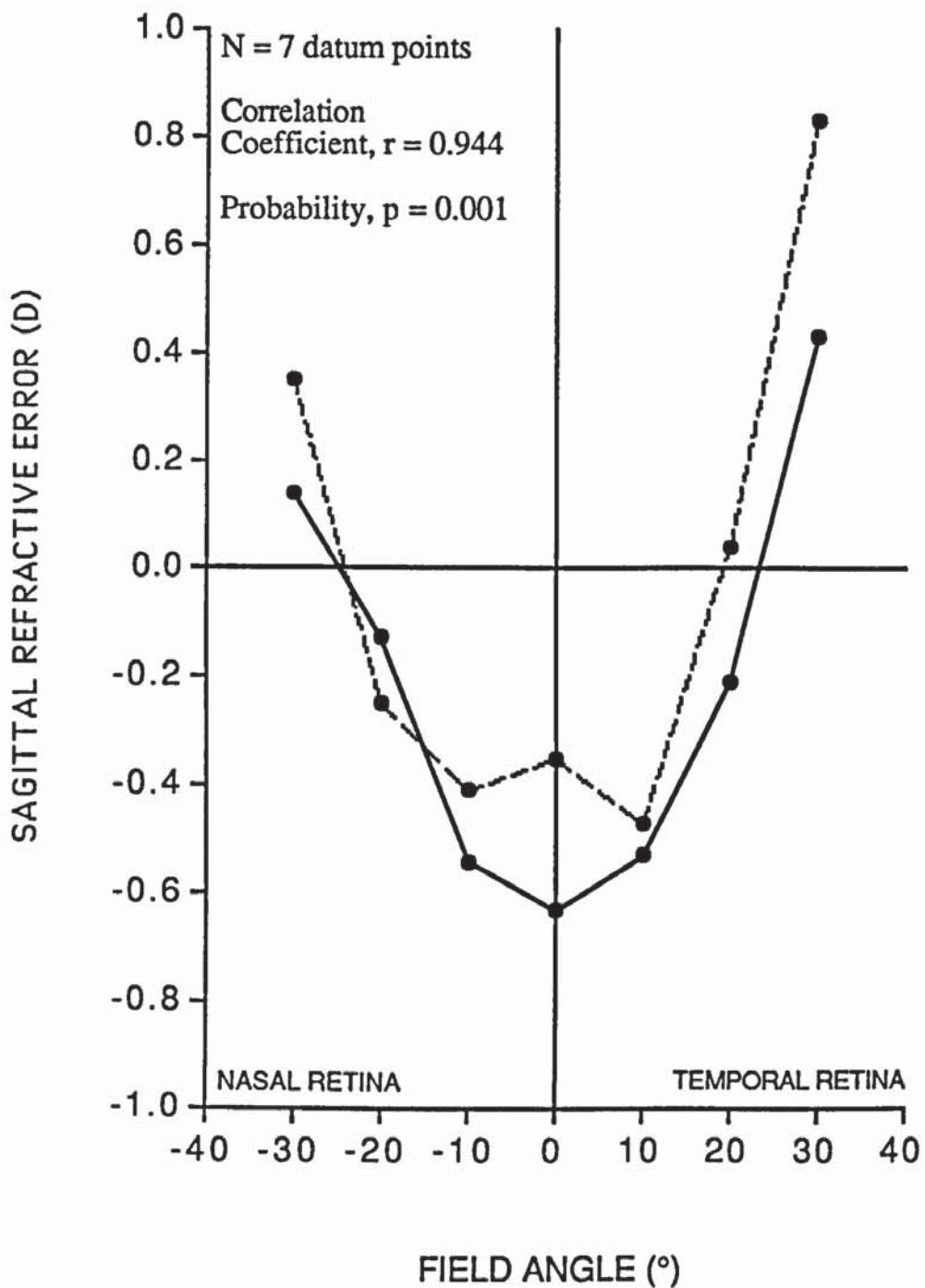
Fig. 4.15 Graph of the variation, with field angle, of sagittal refractive error (D) as measured using the Hartinger optometer (solid lines) and the Canon Autoref R-1 optometer (broken lines). Each datum point represents the averaged results of all 34 eyes measured. Correlation coefficients are based on the seven datum points measured using both instruments.
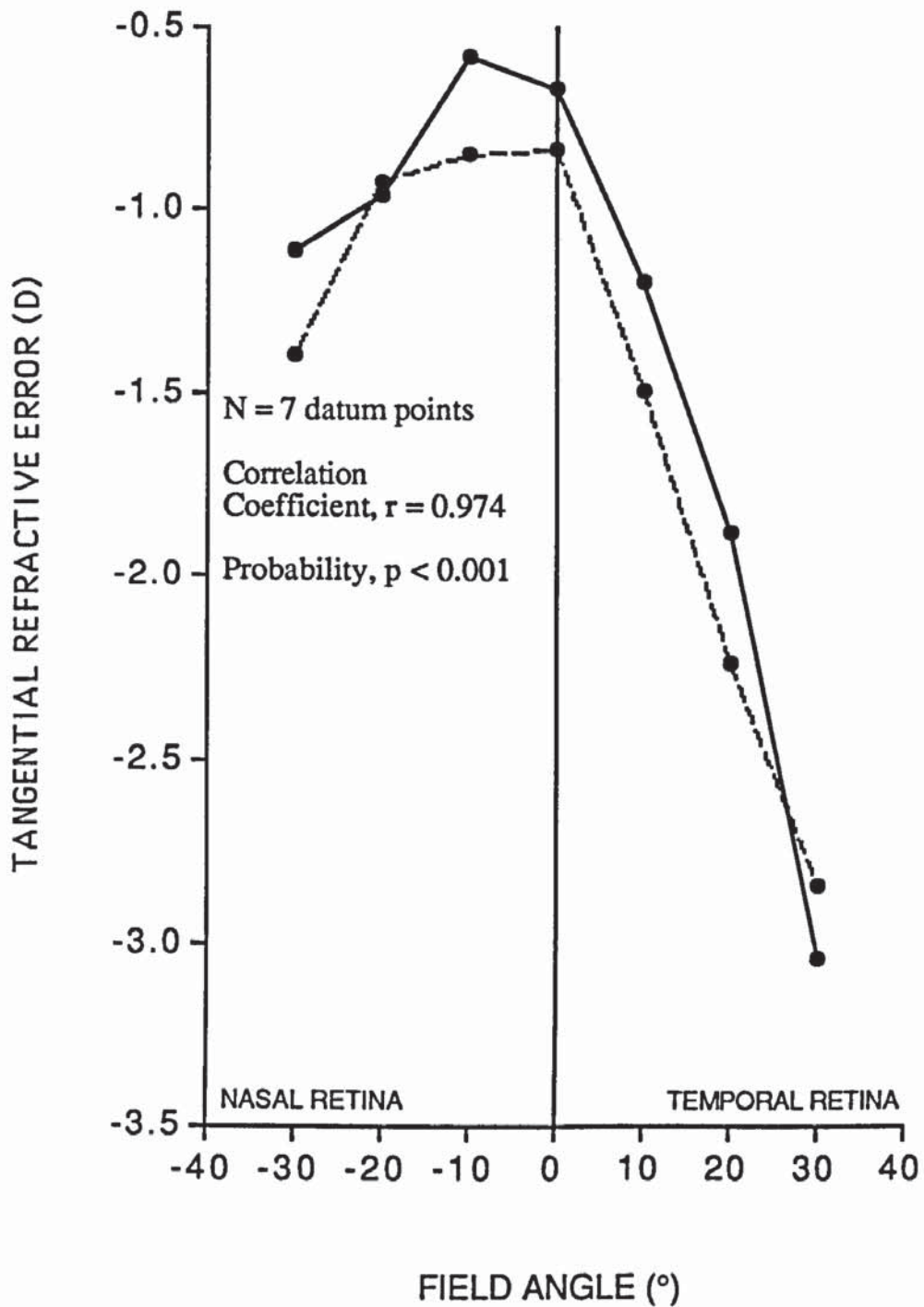
Fig. 4.16 Graph of the variation, with field angle, of tangential refractive error (D) as measured using the Hartinger optometer (solid lines) and the Canon Autoref R-1 optometer (broken lines). Each datum point represents the averaged results of all 34 eyes measured. Correlation coefficients are based on the seven datum points measured using both instruments.
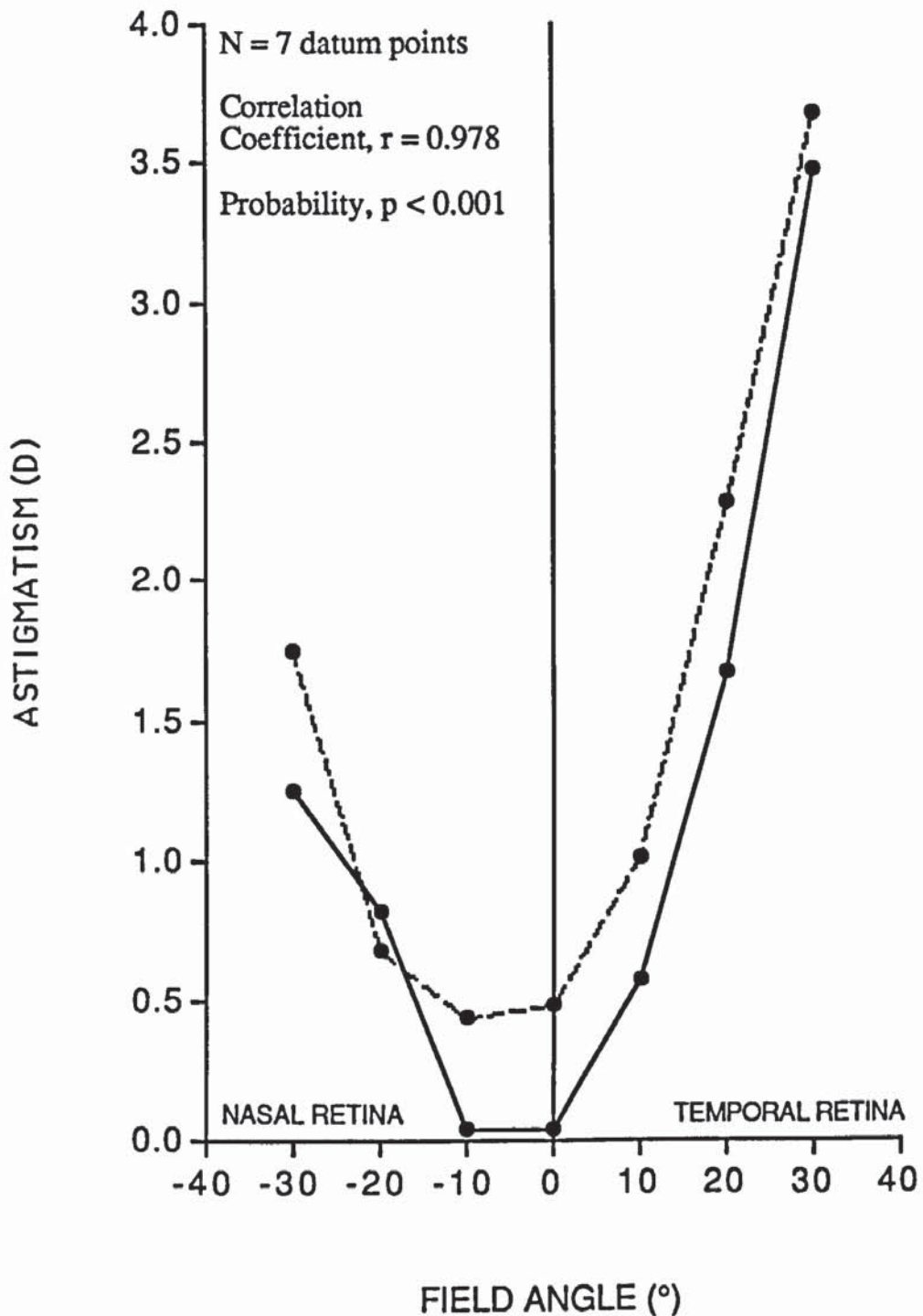
Fig. 4.17 Graph of the variation, with field angle, of astigmatism (D) as measured using the Hartinger optometer (solid lines) and the Canon Autoref R-1 optometer (broken lines). Each datum point represents the averaged results of all 34 eyes measured. Correlation coefficients are based on the seven datum points measured using both instruments.

As the data were taken on separate occasions, the high correlations observed also implied that the various biological variations had little influence on the data.

Although the readings from both instruments fell very close to each other and showed the same degrees of asymmetry, the Canon Autoref R-1 results tended to be more hyperopic in the sagittal meridian and more myopic in the tangential meridian giving rise to larger values of astigmatism (as already noted in section 4.2.4A).

A graph of the tangential axis measurements taken using both instruments is not shown for reasons explained in section 4.2.4A. However, measurements made with the Hartinger optometer indicated that the tangential axes remained very close to 180° for all field angles.

4.2.5 ENTRANCE PUPIL DIAMETER

The entrance pupil diameter was measured in the vertical plane only (see section 3.2.5B), from the projected ophthalmophakometric photographic negatives. Table 4.12 shows the precision of the results in terms of the range of standard deviations which occurred on all 34 eyes, from repeat readings taken on one occasion. The table only includes results from the first set of measurements (appendix 2m). As explained in section 3.2.5B, the mean and standard deviation values were calculated from nine estimates. Measurements were made with a steel ruler to the nearest 0.5 mm which, when scaled down by the magnification of the projected photograph of X 21.95 (see section 4.2.3A), is equivalent 0.02 mm actual size.

N = 30

Correlation
Coefficient, r = 0.628

Probability, p < 0.001
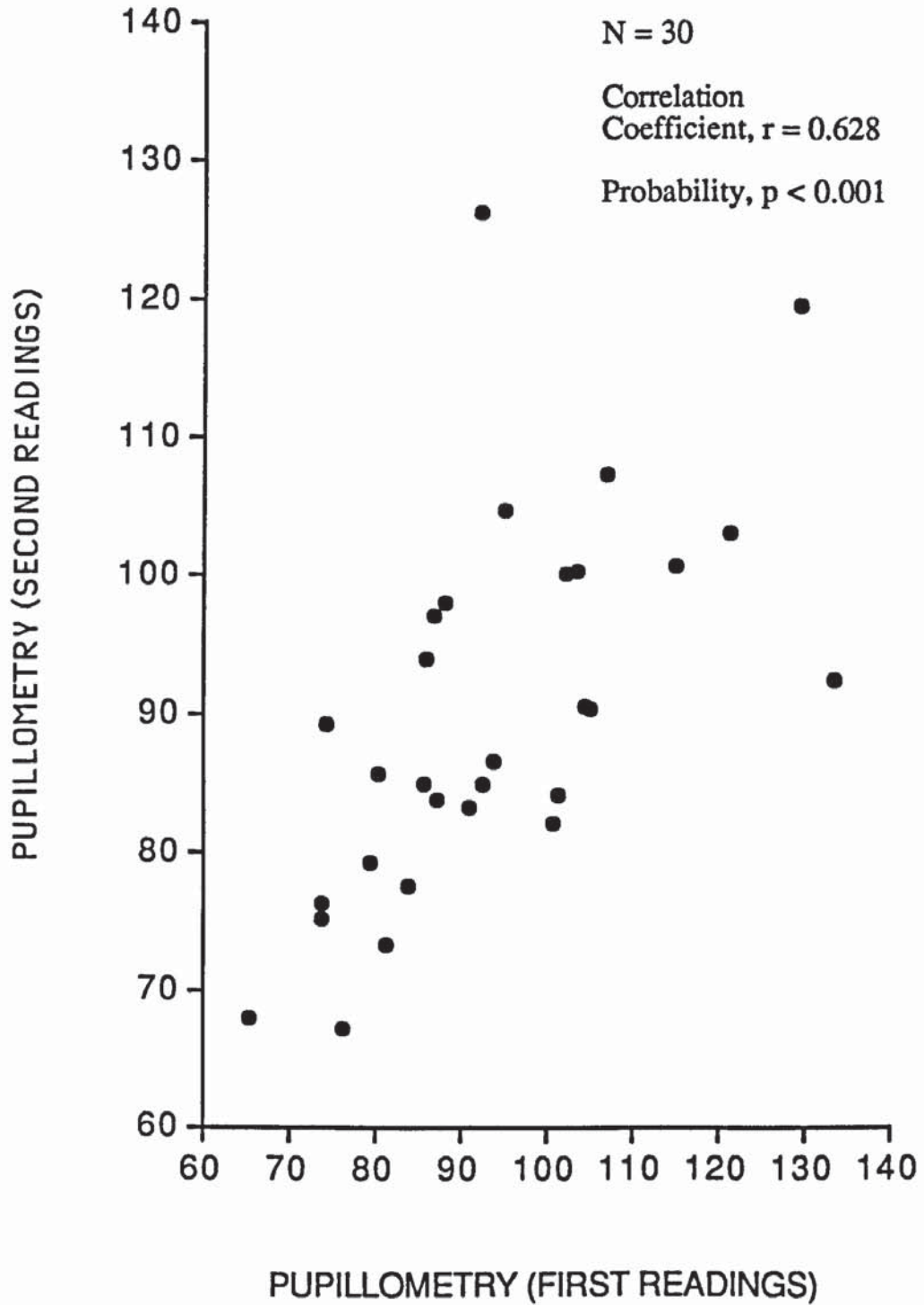
Fig. 4.18 Scatter plot of the first (x) and second (y) pupillometric measurements (unscaled) of entrance pupil diameter in the vertical plane (mm).

| STANDARD DEVIATION | PUPILLOMETRY (First readings only) | |
	Unscaled	Scaled down (X 21.95)
Range	0.5 - 8.0 mm	0.02 - 0.36 mm
Mean	3.14 mm	0.14 mm

Table 4.12 The precision of pupillometric measurements in terms of the range and mean of the standard deviations observed by taking nine repeat readings, on one occasion only, on 34 eyes (see appendix 2m).

Figure 4.18 shows a scatter plot of the first pupillometric measurements compared with the second (see appendix 2m). In some subjects the photographed pupil margins were not clear, making repeat measurements only possible on 30 eyes. A remarkably high correlation was observed considering the natural variability of the pupil size. This finding suggested that despite the possible influence of fluctuations of accommodation and the extraneous photographic ophthalmophakometric light sources, repeat measurements of the pupil size could be made on different occasions to a reasonably high degree of precision.

4.3 AVERAGED PERIPHERAL REFRACTIVE DATA

A graph of the averaged peripheral refractive data for near-emmetropic (triangles), myopic (squares) and hyperopic (circles) eyes is shown in fig. 4.19. The results plotted are those taken with the Hartinger optometer (appendix 2k) which allowed the refractive error to be measured out to field angles of 40°. Sagittal (broken lines) and tangential (solid lines) image shells are shown separately for clarity. Field angles are expressed with respect to the nasal and temporal retina rather than the visual field. As the optometer was aligned with respect to the subject's line of sight to take central refractive readings, zero degrees field angle coincides with the line of sight.
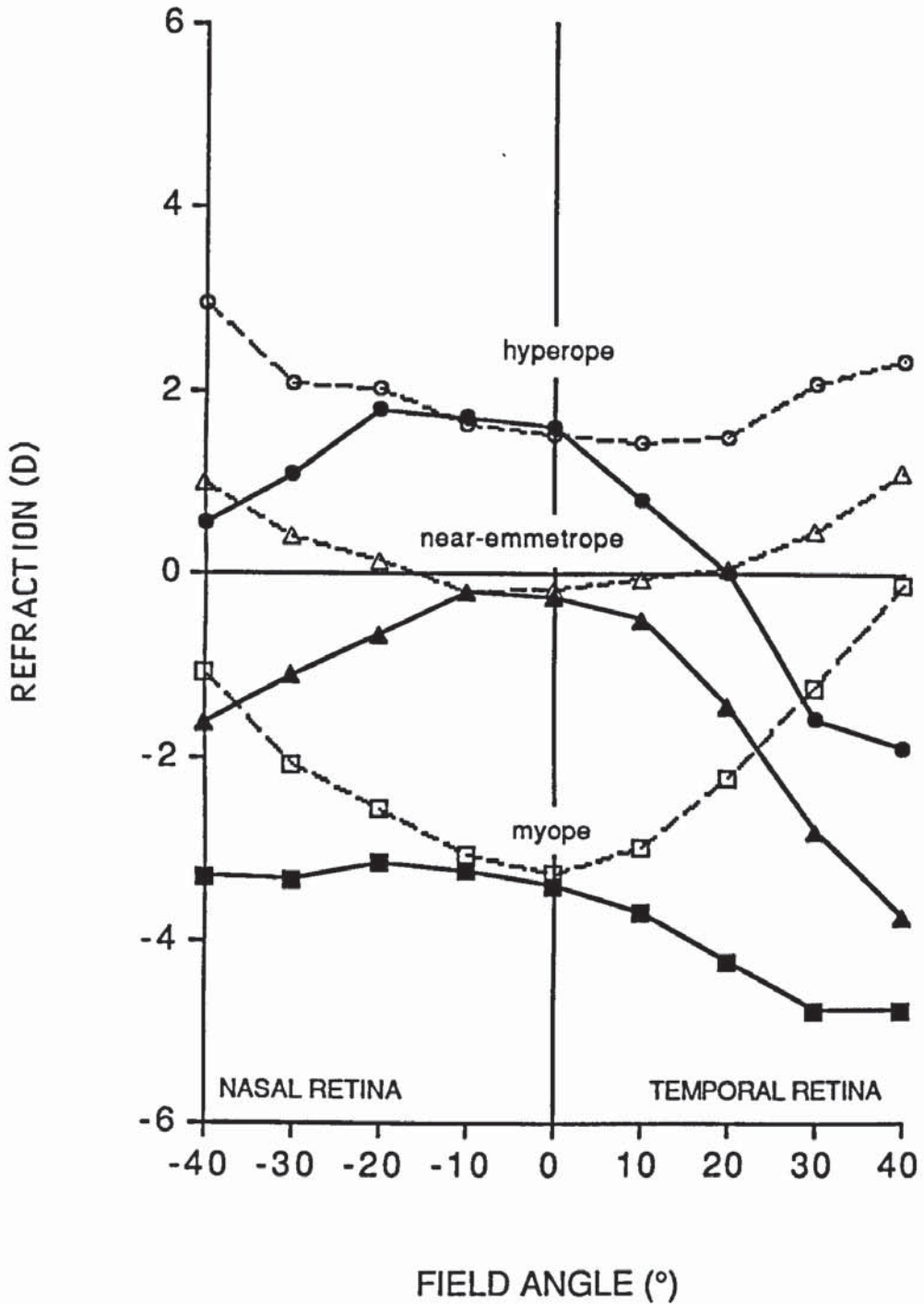
Fig. 4.19 Graph of averaged peripheral refraction, measured using the Hartinger optometer (appendix 2k), in near-emmetropes [N = 10] (triangles), myopes [N = 16] (squares) and hyperopes [N = 8] (triangles) and plotted as a function of field angle. Sagittal (broken lines) and tangential (solid lines) image shells are shown separately for clarity. Zero degrees field angle coincides with the line of sight.

Several aspects of these peripheral refractive findings were similar to those of Millodot (1981) (see fig. 2.4):

1. Each refractive group possessed the normal type IV peripheral refractive pattern (see chapter 2). That is to say, the refraction became more hyperopic in the sagittal meridian and more myopic in the tangential meridian as field angle increased. Consequently, the amount of astigmatism increased towards the periphery.

2. Small amounts of asymmetry were evident, with larger values of peripheral astigmatism found over the temporal retina than the nasal retina.

3. Near-emmetropes exhibited mixed astigmatism, myopes compound myopic astigmatism and hyperopes compound hyperopic astigmatism at nearly all field angles.

4. Although the central refractions differed markedly for the three groups, the sagittal and tangential image shells appeared to converge at higher field angles. This, however, was less apparent for hyperopes.

The peripheral refractive results of each group appeared to be decentred towards the nasal retina. Although the latter was not evident in Millodot's (1981) results, a similar decentration was noted by Jennings and Charman (1978, 1981) with regard to the deterioration of the optical imagery.

4.4 AVERAGED BIOMETRIC RESULTS

Table 4.13 shows the averaged biometric results for near-emmetropic, myopic and hyperopic eyes. Purkinje image and entrance pupil dimensions given in the table are

177

scaled down by X 21.95 (this figure is derived in section 4.2.3A) to show their actual sizes. The readings from which average values were calculated were the first ultrasonic results (for axial distances), the first ophthalmophakometric results (for Purkinje image heights and entrance pupil diameters), the PEK results (for corneal surface data) and the Hartinger optometer results (for central refractive errors).

PARAMETER	REFRACTIVE GROUP		
	Near-Emmetropes (N = 10)	Myopes (N = 16)	Hyperopes (N = 8)
CORNEAL DATA: HORIZONTAL			
Radius (mm)	7.98	7.91	7.78
Conic constant (P)	0.74	0.70	0.78
Axis (°)	179	181.6*	180
VERTICAL			
Radius (mm)	7.90	7.83	7.69
Conic constant (P)	0.81	0.73	0.86
AXIAL DISTANCES:			
Anterior chamber depth (mm)	3.87	3.93	3.49
Lens thickness (mm)	3.56	3.44	3.75
Vitreous length (mm)	16.52	17.74	15.33
Axial length (mm)	23.95	25.11	22.57
PURKINJE IMAGES: VERTICAL ONLY			
I (mm)	1.008	0.996	0.979
III (mm)	1.740	1.867	1.567
IV (mm)	0.775	0.754	0.716
ENTRANCE PUPIL:			
Vertical diameter (mm)	4.2	4.3	4.1
REFRACTIVE ERROR: HORIZONTAL			
Refraction (D)	-0.26	-3.38	1.63
Axis (°)	179.6	180.2*	177.7
VERTICAL			
Refraction (D)	-0.18	-3.26	1.54
Axis (°)	89.8	90.4	88.4

Table 4.13 Averaged biometric data. * The unconventional way in which some of the axes are shown arises from simplifying the process of averaging the data.

178

These ocular dimensions fall well within the ranges of the values found by other workers (see chapter 1). No corneal conic constant values were quoted in chapter 1 but those shown above accord well with the average value of 0.85 ± 0.15 found by Guillon et al. (1986). Also, the relative sizes of the measured Purkinje image heights, being approximately 1 : 2 : 0.75 (I : III : IV), are very close to the theoretical predictions of Bennett and Rabbetts (1984).

In agreement with previous research findings, the anterior chamber depth, vitreous length, axial length and pupil size increased while the crystalline lens thickness decreased as the refractive error progressed from hyperopia to myopia. However, the corneae in myopic and hyperopic eyes are both found to be steeper than in near-emmetropic eyes which is in conflict with the findings of some workers (see section 1.3.1) who have shown that hyperopic eyes tend to possess flatter corneae than emmetropic eyes.

From the radii and conic constant values shown in table 4.13, it can be seen that the corneae were flattest in the horizontal meridian giving rise to with-the-rule corneal astigmatism. Conversely, the central ocular astigmatism for each group, except for the hyperopes, was against-the-rule. The research evidence reviewed in chapter 1 (see sections 1.5 and 1.6) indicates that this is a common finding, the difference between corneal and ocular astigmatism being referred to as residual astigmatism. Indeed, the amount of residual astigmatism found in the averaged near-emmetropic, myopic and hyperopic eyes was 0.51 D, 0.55 D and 0.41 D respectively, which agrees well with the value of 0.50 D incorporated in Javal's formula (Javal, 1890) to account for the difference between corneal and ocular astigmatism.

4.5 CONSTRUCTION OF SCHEMATIC EYES

Schematic eyes were constructed from the biometric data shown in table 4.13 and using the computer program described in section 3.3B (see appendix 1). Table 4.14 shows schematic eye values calculated from the data collected in the vertical meridian.

PARAMETER	SCHEMATIC EYES (VERTICAL MERIDIAN)		
	Near-Emmetrope	Myope	Hyperope
ASSUMED REFRACTIVE INDICES:			
Aqueous	1.3374	1.3374	1.3374
Crystalline lens	1.42	1.42	1.42
Vitreous	1.336	1.336	1.336
AXIAL DISTANCES:			
Anterior chamber depth (mm)	3.87	3.93	3.49
Lens thickness (mm)	3.56	3.44	3.75
Vitreous length (mm)	16.52 (16.62)	17.74 (17.72)	15.33 (15.29)
Axial length (mm)	23.95 (24.05)	25.11 (25.09)	22.57 (22.53)
SURFACE RADII:			
Resolved cornea (mm)	7.90	7.83	7.69
Anterior crystalline lens (mm)	9.28	9.64	8.73
Posterior crystalline lens (mm)	-6.08 (-6.30)	-6.17 (-6.13)	-5.81 (-5.71)
SURFACE POWER:			
Resolved cornea (D)	42.71	43.09	43.88
Anterior crystalline lens (D)	8.90	8.57	9.46
Posterior crystalline lens (D)	13.82 (13.32)	13.61 (13.71)	14.46 (14.71)
Equivalent lens (D)	22.42 (21.93)	21.89 (21.99)	23.56 (23.80)
Total eye (D)	60.88 (60.50)	60.79 (60.87)	63.06 (63.25)
REFRACTIVE ERROR:			
Resolved refraction (D)	-0.18	-3.26	1.54

Table 4.14 Schematic eyes calculated in the vertical meridian. The figures calculated using routine 2 are shown in brackets next to those derived using routine 1 (see section 3.3B). Comparison of the latter values serves as an "internal validation check".

Results calculated using ultrasonically determined axial lengths (routine 1 in section 3.3B) are shown next to the figures in bracket/s which gave rise to calculated axial

lengths (routine 2 in section 3.3B). The accumulated experimental error was estimated by comparing the latter values which formed the basis of the "internal validation check". Differences between measured and calculated vitreous and axial lengths ranged from 0.02 mm to 0.10 mm while differences in the estimated powers of the posterior lens surface, equivalent lens and total eye ranged from 0.10 D to 0.50 D. These differences were remarkably small considering the experimental error that could have arisen from the numerous techniques used.

In addition to testing the compatibility of the various biometric measurements made, the "internal validation check" also tested the compatibility of the invariant schematic indices assumed. Ludlam (1967) calculated that an error of ±0.01 in the assumed refractive index of the aqueous resulted in a change in total refracting power of ±0.25 D whilst an error of ±0.004 for either the crystalline lens or the vitreous refractive index resulted in a change in the total refracting power of ±0.85 D and ±0.50 D respectively. Bearing these figures in mind, the accumulated errors observed were very small. It cannot be said, however, that the various sources of error were not acting in such a way as to cancel each other out.

It is important to note that the schematic eye parameters shown in table 4.14 were not those used for the modelling of peripheral refraction. The reason for this was that the presence of residual astigmatism posed a considerable mathematical problem with regard to reproducing the central astigmatism observed in fig. 4.19. Although the biometric values shown in table 4.13 still formed the basis of the schematic eyes used for mathematical modelling, values relating to the corneal curvature and the central refractive error had to be recalculated in a manner which is discussed in chapter 6.

181

4.6 SUMMARY

Ocular measurements were made to a high degree of precision in terms of the average standard deviations reported; averaged standard deviations of ultrasonically determined axial distances never exceeded ± 0.10 mm; averaged standard deviations of opthalmophakometric determinations of the Purkinje image heights never exceeded ± 0.05 mm; averaged standard deviations of refractive error measurements made with the Hartinger optometer never exceeded ± 0.2 D centrally and ± 0.5 D at field angles of 30°. Average differences found between repeat measurements of the corneal radii using the PEK, never exceeded ± 0.04 mm. The statistical probability of correlation coefficients calculated for repeat component measurements was never greater than 0.001, which further implied the high degree of precision with which estimates could be made. With regard to the construction of schematic eyes from the biometric data, the accumulated error did not exceed 0.10 mm for axial distance determinations and 0.50 D for power determinations. However, it is not known to what extent random errors cancelled themselves out.

A significant point in this chapter and indeed the whole thesis is that one aspect of the eye's optical performance, the variation of refraction over the central and peripheral retina (see fig. 4.19), has been measured along with the ocular component dimensions (see table 4.13) in individual eyes. As far as the present author is aware this has never been done before. In the following chapters, a scheme will be described in which such aspects as the translation and rotation of the ocular surfaces as well as the peripheral surface profiles are altered with the aim of matching modelled values of peripheral refraction with observed values.

CHAPTER FIVE

A SCHEME FOR MODELLING PERIPHERAL REFRACTION

IN SCHEMATIC EYES USING THE LINEAR ALGEBRAIC

RAY TRACING PROGRAM

5.1 INTRODUCTION

The oversimplification involved in the construction of schematic eyes is very well illustrated when one compares modelled peripheral refractive patterns with the patterns found in real eyes. Chapter 2 outlined several major differences between measured and modelled peripheral refractive results which are summarised below :

1. A certain amount of peripheral refractive asymmetry exists in real eyes which has not, so far, been modelled in schematic eyes. The reason for this is that to simplify the construction of schematic eyes, all optical surfaces are assumed to be centred upon a common optical axis. In real eyes, however, there is evidence to suggest that the whole eye is rotated away from the line of sight and that some asymmetry might arise from rotation and translation of the corneal and crystalline lens surfaces with respect to each other (see chapter 1).

2. Schematic eyes generally produce peripheral refractive patterns in which the tangential and sagittal image shells are positioned in front of and behind the retina respectively. Considerable variation in the position of these image shells exists in real eyes which is most likely to be due to subtle variations in the shape and position of the retinal surface.

3. The amount of peripheral astigmatism measured in real eyes is usually smaller than that predicted by schematic eyes. Possible reasons for this are that most schematic eyes assume that all surfaces are spherical, neglecting the aspheric nature of the optical surfaces in real eyes, and that these surfaces are separated by homogenous optical media, neglecting the gradient index optical structure of the crystalline lens. From the peripheral refractive results of various sophisticated schematic eyes which take into

account the aspheric nature of the refracting surfaces and the gradient index optical nature of the crystalline lens, it would appear that aspheric surfaces may play a relatively major role in the reduction of peripheral astigmatism in real eyes.

To model more realistic peripheral astigmatic patterns, this chapter describes a ray tracing method in which the degree of surface translation and rotation as well as the aspheric nature of the optical and retinal surfaces can be altered. This ray tracing method is tested on a schematic eye constructed from typical human ocular dimensions in order to develop a scheme which in chapter 6 will be used to model the measured peripheral refraction with the ocular biometric dimensions described in chapter 4.

5.2 THE LINEAR ALGEBRAIC RAY TRACING PROGRAM

For the purpose of modelling peripheral refraction in schematic eyes a linear algebraic ray tracing method was developed and incorporated in a BASIC program for use on the Apple Mackintosh 512K computer (see appendix 3a). This traced skew rays through aspheric surfaces which could be translated and rotated with respect to each other. Methods of tracing skew rays through aspheric optical surfaces have already been described in detail (Smith, 1966) but do not lend themselves to ray tracing through translated or rotated surfaces.

It is beyond the scope of this thesis to describe the theory underlying the ray tracing technique. The algebra used is covered in detail by Cohn (1961) and a clear introduction in the context of eye rotations is provided by Solomons (1977). A description of the ray tracing calculations can also be found in Clement et al. (1987) (see appendix 4). This section, however, concentrates on the operation of the program shown in appendix 3a.

5.2.1 INPUT OF SURFACE PARAMETERS

(A) SURFACE CURVATURE

In section 3.2.1C, a formula was described which specified any surface in terms of an apical radius, r, and a conic constant, P :

$$P x^2 - 2xr + y^2 = 0 \qquad (1)$$

The advantage of this formula is that the intersection coordinates x, measured along the optic axis, and y, measured perpendicularly to the optic axis, belong to a family of ellipses influenced purely by P which has no influence on the paraxial optical power determined by r. Therefore the peripheral curvature of a surface could be altered without effecting its central curvature.

This formula, however, specifies a two-dimensional conic curve whilst refracting surfaces in the linear algebraic ray tracing program are of a three-dimensional quadric form. Nevertheless, as long as the refractive surfaces are rotationally symmetrical, the cross-sections described by the conic and quadric equations are identical.

In the program, quadric surfaces were expressed in matrix notation by equations of the form :

$$X^T A X + B^T X + c = 0$$

where A is a 3 by 3 symmetric matrix, B^T is a row vector and c is a scalar constant. The simplest equation for an ellipsoid arises when it is centred at the origin of the system of coordinates and its axes are aligned with the axes of the system of coordinates. It is convenient to set up the equation for a given surface assuming that these conditions are satisfied, for then all the elements of the associated matrix A are

zero except for those along the leading diagonal, which are equal to the square of the reciprocal of the radius of curvature in the X , Y and Z directions (where the Z- axis is aligned with the optical axis of the eye). It also holds that if these conditions are met, then the vector B is zero and the scalar constant c = -1. Therefore :

$$A = \begin{matrix} X & 0 & 0 \\ 0 & Y & 0 \\ 0 & 0 & Z \end{matrix} \qquad B = \begin{matrix} 0 \\ 0 \\ 0 \end{matrix} \qquad c = -1$$

The parameters of a given surface are therefore input into the computer in terms of the radius of curvature in the X, Y and Z directions. To calculate these from known values of the apical radius, r , and the conic constant, P , then :

(i) Find Z - equation (1) represents an ellipse as shown in fig. 5.1 :
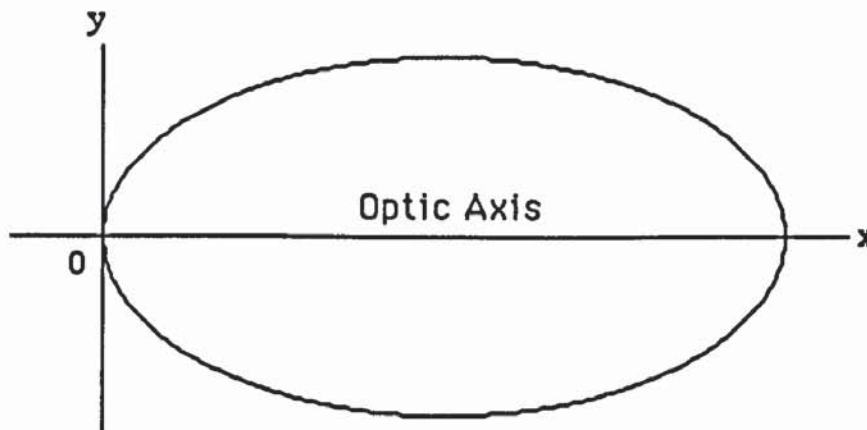
Fig. 5.1   Diagram of the relationship between the intersection coordinates, x (along the optical axis) and y (perpendicular to the optical axis), as specified by the conic equation: $Px^2 - 2xr + y^2 = 0$ where r is the apical radius and P is the conic constant for that surface.

When y = 0, the value of the intersection coordinate x gives the diameter of the surface along the optical axis. Rearranging equation (1) and substituting y = 0, the radius of curvature (Z) along the optic axis is :

$$Z = r + P \qquad (2)$$

<u>(ii) Find X and Y</u> - using equation (3) (Kooijman, 1983):

$$P = (b \div a)^2 \qquad (3)$$

where : a = Z, and b = X = Y.

Rearranging for X and Y :

$$X = Y = b = \sqrt{P} \times a^2 \qquad (4)$$

It is worth mentioning that the radius of curvature in the X direction only equals that in the Y direction when the surface is rotationally symmetrical. If the radii were different in these two directions, then a non-rotationally symmetrical (or astigmatic) surface would arise.

(B) SURFACE LOCATION

The location of a surface is expressed as the distance of its centre from the coordinate system centre. The system centre was taken as the anterior crystalline lens surface vertex. A surface centre positioned to the left of this point has a positive value whilst one to the right has a negative value.

A traced ray intersects an ellipsoid surface twice, once at its front surface and once at its rear surface. One of these has to be ignored and it is specified in the program as the portion parameter. If the front intersection is used, then a portion parameter of +1 is specified. If the back intersection is used, the portion parameter becomes -1. The portion parameter needs to be considered when typing the surface locations into the computer.

Location parameters, like surface parameters, are input into the computer in terms of distances in the $\bar{X}$, $\bar{Y}$ and $\bar{Z}$ direction. The value of $\bar{Z}$ represents the distance of the centre of the surface from the system centre along the optical axis. The radius of

188

curvature of a surface in the Z direction indicates the distance of a surface's apex to its centre and has to be taken into account when calculating the location $\overline{Z}$ parameter for that surface so that the apex of the surface is moved to the required position. $\overline{X}$ and $\overline{Y}$ are translations of the surface at right angles to the optic axis. Therefore, if both of these are zero, the surface is centred on the optical axis.

(C) CALCULATION OF SURFACE PARAMETERS FOR A SCHEMATIC EYE

Rays were traced through the schematic eye (consisting of two corneal surfaces, two lenticular surfaces and a retinal surface) of Le Grand and El Hage (1980) modified by Kooijman (1983) to incorporate elliptical corneal, hyperbolic anterior lens and parabolic posterior lens surfaces. Kooijman's calculated conic constants were based on the results of Mandell and St. Helen (1971) for the asphericity of the corneal surface (see also section 1.3.1) and Howcroft and Parker (1977), for the asphericity of the lenticular surfaces (see also section 1.3.4). Calculation of the surface curvature (see section 5.2.1A) and location (see section 5.2.1B) parameters is now discussed.

For the anterior corneal surface, r = 7.8 mm and P = 0.75 (a prolate ellipse). Therefore, in accordance with equation (2), the surface curvature parameters are:

$$Z = 7.8 + 0.75 = 10.4 \text{ mm}$$

and using equation (4):

$$X = Y = \sqrt{0.75} \times 10.4^2 = 9.01 \text{ mm}$$

The specified distance of the anterior corneal surface from the anterior surface of the crystalline lens (the system centre) is 3.6 mm. Since the first intersection of the traced rays with the ellipsoidal corneal surface is required (portion parameter = +1), the centre of the surface must move (10.4 - 3.6 =) 6.8 mm to the right of the lens vertex to

position the corneal apex 3.6 mm in front of the lens. The location parameters are thus:

$$\tilde{Z} = -6.8 \text{ mm}; \tilde{X} \text{ and } \tilde{Y} = 0 \text{ if centred upon optical axis.}$$

Likewise for the posterior corneal surface where r = 6.5 mm and P = 0.75 (a prolate ellipse), the surface curvature parameters are:

$$Z = 6.5 + 0.75 = 8.67 \text{ mm,}$$

$$X = Y = \sqrt{0.75} \times 8.67^2 = 7.51 \text{ mm.}$$

The specified distance of the posterior corneal surface from the anterior surface of the crystalline lens (the system centre) is 3.05 mm. Since the first intersection of traced rays with this surface is required (portion parameter = +1), the centre of the surface must move (8.67 - 3.05 =) 5.61 mm to the right of the lens vertex to position the posterior corneal surface apex 3.05 mm in front of the lens. The location parameters are thus:

$$\bar{Z} = -5.61 \text{mm}; \bar{X} \text{ and } \hat{Y} = 0 \text{ if centred upon optical axis.}$$

For the retinal surface Kooijman (1983) specified that r = -14.1mm and P = 1.346 (an oblate ellipse). However, the apical radius need not be given a negative value as the portion parameter may be chosen so that only the intercept between the traced rays and the second surface of retinal ellipse is computed (portion parameter = -1). The surface curvature parameters are:

$$Z = 14.1 + 1.346 = 10.48 \text{ mm,}$$

$$X = Y = \sqrt{1.346} \times 10.48^2 = 12.16 \text{mm.}$$

The specified distance of the retina from the anterior surface of the crystalline lens (the system centre) is 20.6 mm. Since the intersection of the traced rays with the second surface is that required (portion parameter = -1), the centre of the retina must move (20.06 - 10.48 =) 10.12 mm to the right of the lens vertex. The location parameters are

190

thus:

$$\overline{Z} = -10.12mm \; ; \; \widehat{X} \text{ and } \overline{Y} = 0 \text{ if centred upon optical axis.}$$

Special treatment is required for the anterior lens surface as Kooijman (1983) defined this surface as being a hyperbola. For the program the only suitable three-dimensional surface which can be used is a hyperboloid of two sheets (fig. 5.2).
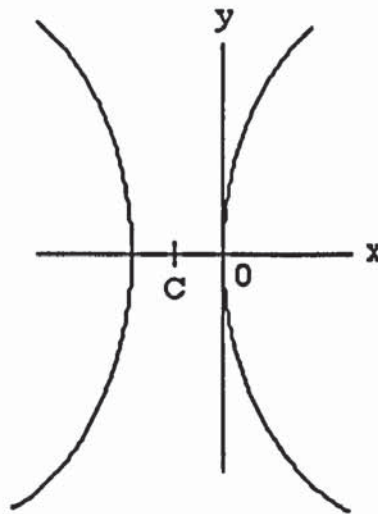
Fig. 5.2 Cross-section of a hyperboloid of two sheets showing the surface centre (C) and the intersection coordinate axes, x (along the optical axis) and y (perpendicular to the optical axis) placed in alignment with the the rear surface (as used in the computer program).

As a result of the shape of this surface, the computer program always requires a positive value for the surface curvature parameter Z and the portion parameter needs to be chosen so that only the intercept between the traced rays and the second surface is computed (portion parameter = -1). For the anterior lens surface, Kooijman (1983) specified that r = 10.2 mm and P = -2.06 (a hyperbola). The surface curvature parameters are therefore :

$$Z = 10.2 \div -2.06 = -4.95 \text{ mm} \quad \text{(but entered as +4.95)}$$

$$X = Y = \sqrt{-2.06} \times 4.95^{2} = -7.10 \text{ mm}$$

191

The apex of the anterior surface of the crystalline lens is taken to be the system centre. As the intersection of the traced rays with the second surface is that required (portion parameter = -1), the centre of lens surface must move 4.95 mm to the left so that its apex coincides with the system centre. The location parameters are thus :

$$\overset{\frown}{Z} = 4.95 \text{ mm} \; ; \overset{\frown}{X} \text{ and } \overset{\frown}{Y} = 0 \text{ if centred upon optical axis.}$$

Special treatment is also required for the posterior crystalline lens surface which Kooijman (1983) defined as a parabola. In the program the three-dimensional surface used is an elliptic paraboloid. As a parabola always has a conic constant of 0 (see section 3.2.1C), then application of equations (2) and (4) only leads to X, Y and Z surface curvature parameter values of zero. For computation, however, the computer defaults these parameters as :

$$Z = 0 \text{ and } X = Y = 1.$$

To alter this surface for different apical radii values vector B is given a value of (2 x r). It is also important to note that the scalar constant for this surface has a value of zero.

For the posterior lens surface, Kooijman (1983) stated that $r = -6$ mm and $P = 0$ (a parabola). As with the retina, the need for a negative apical radius value is removed if the portion parameter is chosen so that only the intercept between the traced rays and the second surface of elliptic paraboloid is computed (portion parameter = -1). The value of vector B is then (2 x 6 =) 12.

The specified distance between the posterior and the anterior crystalline lens surface (the system centre) is 4 mm. Since the portion parameter = -1, the centre of the former surface must move 4 mm to the right to place its apex in the correct position behind the anterior lens surface. The location parameters are thus :

$$\overset{\frown}{Z} = -4\text{mm} \; ; \overline{X} \text{ and } \overline{Y} = 0 \text{ if centred upon optical axis.}$$

The non-zero components of the matrix formulation of all of the above surfaces are given in table 5.1.

SURFACE	A(1,1)	A(2,2)	A(3,3)	B(3)	c	T(3)
FRONT CORNEA	0.012320	0.012320	0.009245	0	-1	-6.8
BACK CORNEA	0.017730	0.017730	0.013303	0	-1	-5.61
FRONT LENS	-0.019837	-0.019837	0.040812	0	-1	4.95
BACK LENS	1.000000	1.000000	0.000000	12	0	-4
RETINA	0.006763	0.006763	0.009105	0	-1	-10.12

Table 5.1　　　　　　　　Schematic eye parameters

In table 5.1 the first three terms in the table represent values of the leading diagonal in matrix A which are equal to the square of the reciprocal of the surface radii; the fourth term represents the values of vector B; the fifth term represents values of the scalar constant and the sixth term represents values of the surface location parameter $\overline{Z}$.

5.2.2 INPUT OF REFRACTIVE INDICES AND PUPIL SIZE

The computer program allows the refractive indices to be altered. The indices used, taken from Le Grand and El Hage (1980), were 1.3771 for the cornea, 1.3374 for the aqueous humour, 1.42 for the crystalline lens and 1.336 for the vitreous humour.

One limitation of the program is that it does not incorporate a layered crystalline lens. In the present context, this is of particular relevance with respect to reducing the modelled values of peripheral astigmatism to values found in real eyes. However, as discussed in chapter 2, it would appear that aspheric surfaces may play a relatively major role in the reduction of peripheral astigmatism compared to that of gradient index

optics. Therefore, the gradient index optical structure of the crystalline lens was not included to reduce the complexity of the computer program and to firmly establish the role of aspheric surfaces.

The physical pupil is described as a circle whose centre is coincident with the anterior surface vertex of the lens. Its diameter can be altered in the computer program.

5.2.3 ROTATION OF SURFACES

The program shown in appendix 3a allows the crystalline lens to be rotated about its anterior surface vertex in the meridian of oblique incidence only, by entering the angle of rotation required in degrees. For simplicity of explanation, if the cornea is considered to lie to the left of the crystalline lens a positive angle rotates the lens in a clockwise manner while a negative angle rotates the lens in an anti-clockwise manner. The system centre was taken to coincide with the anterior surface vertex of the crystalline lens to facilitate the process of rotation.

The program is limited in that rotations in more than one plane of individual surfaces are not readily performed. Although lenticular, corneal and total eye rotations about the vertical and horizontal planes are described in the following text, they required the alteration of some of the parameters in the program. For example, rotation of the cornea about its anterior point required the locations of all surfaces to be specified with respect to the corneal vertex and for rotation of the total eye, the locations of all surfaces were specified with respect to the centre of rotation of the eye.

5.2.4 RAY TRACING PROCEDURE

Principal rays are traced out of the eye, starting at the physical pupil centre, from 0° to an obliquity of 50° in 10° steps on both sides of the optical axis. The angle between the the optic axis and the principal rays, after emerging from the cornea into air, is taken to be the field angle. Each principal ray is traced back down its path and to completion accompanied by four parallel marginal rays, one on either side and one above and below.

The distance, in air, of the marginal rays is increased incrementally from 0 in 0.1 mm steps until they reach the physical pupil edge after refraction through the cornea. This means that the total distance of the marginal rays from each other, in both planes, represents the apparent diameters of the physical pupil as seen from outside the eye at different obliquities (i.e. the entrance pupil).

Because of the effects of relative obliquity, the marginal rays, particularly those in the plane of oblique incidence, do not intersect the principal ray in exactly the same position. Therefore three values for the tangential and sagittal image foci are computed: two representing the intersections of each marginal ray with the principal ray and one representing the intersection of the marginal rays with each other (see fig. 5.3). The former are taken to be the outermost limits of the comatically distorted image whose centre lies in the position of the latter. These values are expressed in dioptres and calculated using the formula of Lotmar and Lotmar (1974).

For simplicity the plane of oblique incidence, the tangential plane, was taken as horizontal with negative field angles corresponding to the nasal retina and positive ones to the temporal retina. Negative angles in the plane at right angles to that of

oblique incidence, the sagittal plane, were taken to correspond to the inferior retina and positive ones to the superior retina.

5.3 FACTORS EFFECTING THE MODELLED PERIPHERAL REFRACTION

5.3.1 TRANSLATION AND ROTATION OF OCULAR COMPONENTS

(A) COMATIC IMAGE LIMITS

In section 5.2.4 it was stated that the separation between the points at which opposite marginal rays intersected the principal ray represented the outermost limits of the comatically distorted image. As reference will be made to the latter throughout section 5.3.1, the following explanation serves to describe these image limits in more detail (Barnes et al., 1987 [see appendix 4]).

Figure 5.3 shows the paths of two marginal rays, M_1 and M_2, accompanying the principal ray, P, in the tangential plane through a centred optical system. Marginal rays intersect each other forming an image point, $M_1'M_2'$, which is displaced from the principal ray. This is due to the intersection of M_2 with the principal ray forming an image point, $M_2'P'$, in front of $M_1'P'$. As the optical system is centred, marginal and principal rays in the sagittal plane all coincide to produce a single image.

In figs. 5.4 to 5.13, bold lines indicate the more hyperopic sagittal and myopic tangential image shells constructed from image foci corresponding to $M_1'M_2'$ in fig. 5.3. Sagittal image limits derived from superior and inferior marginal rays are denoted by dotted and dashed lines respectively, as are the tangential image limits from

temporal and nasal marginal rays.
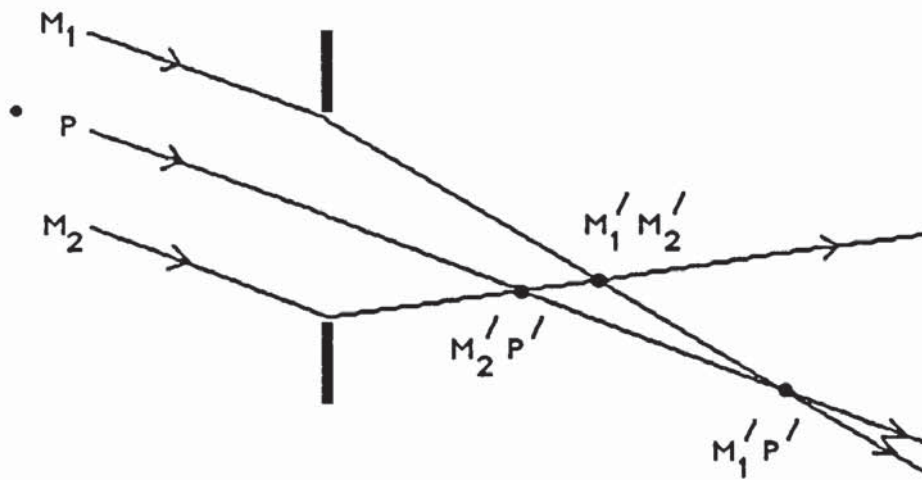
Fig. 5.3   Image foci produced by a principal ray, P, and two marginal rays,
           M_1 and M_2, in the tangential plane of a centred optical system. Marginal
           rays intersect each other forming an image point, $M_1'M_2'$, which is
           displaced from the principal ray. M_2 intersects the principal ray forming
           an image point, $M_2'P'$, in front of $M_1'P'$. Because the optical system
           is centred, marginal and principal rays in the sagittal plane all coincide
           to produce a single image.

(B) THE AXIALLY ALIGNED SCHEMATIC EYE: EFFECT OF PUPIL SIZE

Physical pupil diameters of 2.5 mm (fig. 5.4) and 5 mm (fig. 5.5) were investigated in

the axially aligned schematic eye (Barnes et al., 1987 [see appendix 4]). As the system

was optically centred in both figures, nasal marginal rays on the nasal retina resemble

M_2 in fig. 5.3, producing more myopic image values. The same rays on the temporal

retina resemble M_1 in fig. 5.3, producing more hyperopic image values. The dotted

line showing these image limits is therefore asymmetric. This situation is exactly

reversed for temporal marginal rays, shown by the dashed lines. Consequently the

overall comatic tangential image limits are maximal for large field angles and diminish

to zero centrally. Lotmar (1971) also found the comatic image curves to be asymmetric
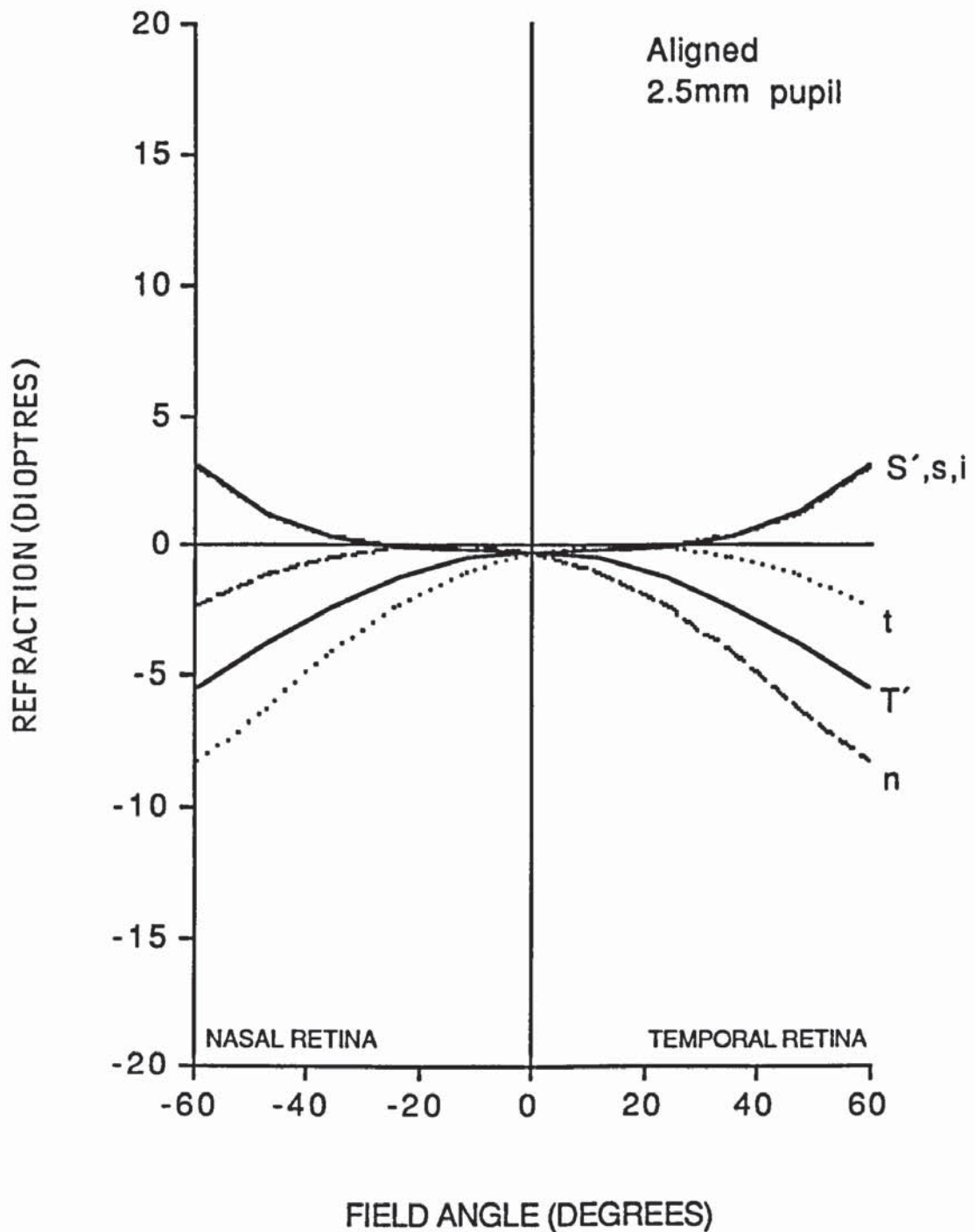
Fig. 5.4 Peripheral refraction for the axially aligned schematic eye with a physical pupil diameter of 2.5 mm. Bold lines in this and figs. 5.5 to 5.13 indicate the more hyperopic sagittal (S´) and myopic tangential (T´) image shells constructed from image foci corresponding to $M_1 M_2´$ in fig. 5.3.

Sagittal image limits derived from superior (s) and inferior (i) marginal rays are shown denoted by dotted and dashed lines, respectively, as are the tangential image limits from temporal (t) and nasal (n) marginal rays. Zero degrees field angle coincides with the optical axis.

198
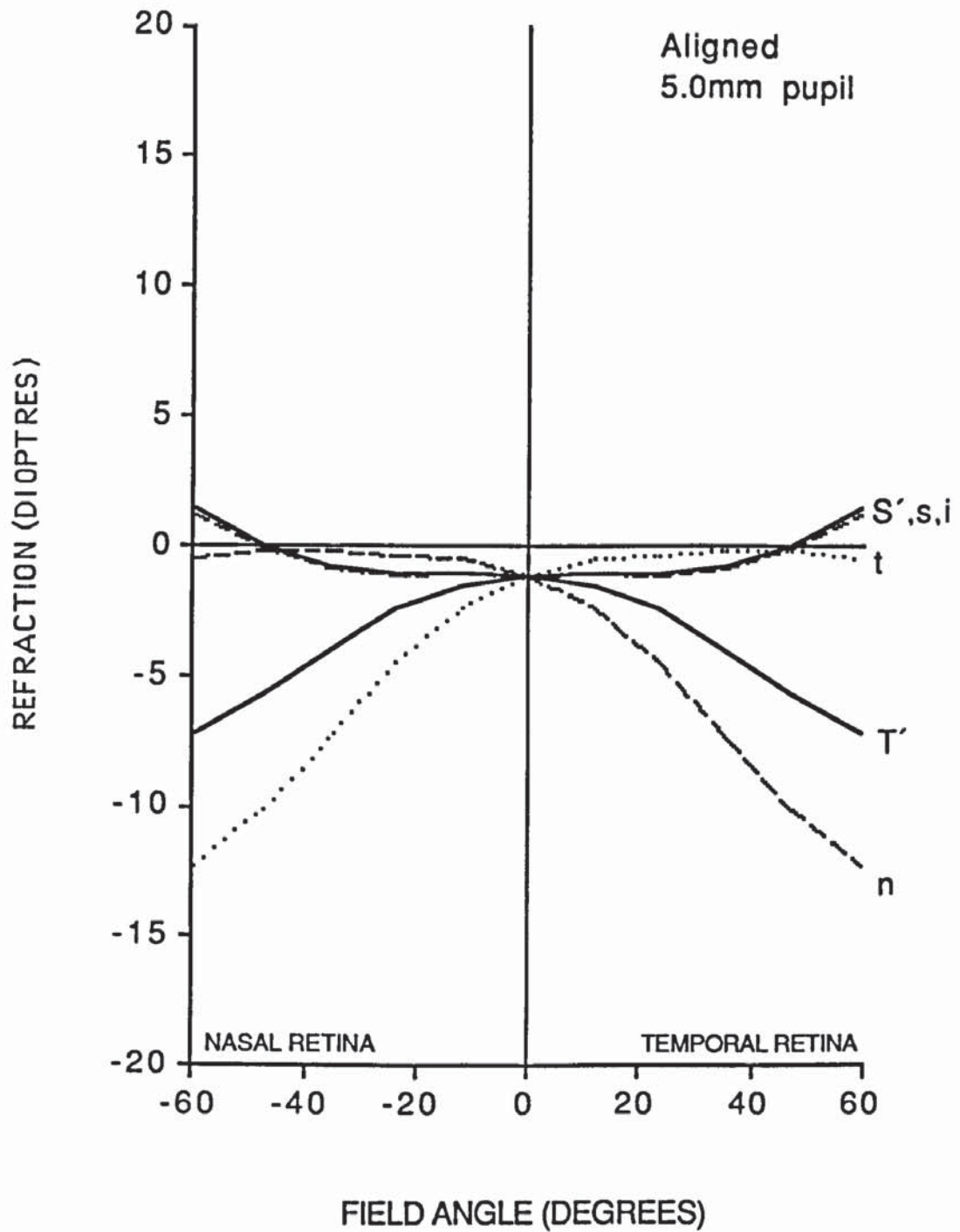
Fig. 5.5 Peripheral refraction for the axially aligned schematic eye with a physical pupil diameter of 5 mm. See fig. 5.4 for explanation of symbols. Zero degrees field angle coincides with the optical axis.

in a schematic eye with aspheric surfaces and considered that this was most probably due to the neglect of the shell structure of the crystalline lens.

Increasing pupil size (fig. 5.5) moves both astigmatic image shells towards myopia. This movement is greater for higher field angles, thus flattening the sagittal while steepening the tangential shell. The latter shows a slightly greater effect but gives rise to a practically negligible increase in the interval of Sturm. Conversely, temporal and nasal marginal ray foci move further away from each other, resulting in an increase of the overall tangential limits, which is approximately proportional to the increase in pupil size.

(C) THE SCHEMATIC EYE WITH NON-ALIGNED COMPONENTS

Various translations and rotations of the cornea and lens were performed with a fixed pupil of 2.5 mm (Barnes et al., 1987 [see appendix 4]). To demonstrate the various effects, translations of 1 mm and rotations of 5° are shown. Rotations of the cornea and lens were made about their anterior surface vertices such that the nasal or inferior portion moved towards the front of the eye. As explained in section 5.2.3, the program shown in appendix 3a needed to be altered in order to perform corneal rotations as well as rotations in two meridians.

Figure 5.6 demonstrates the effects of rotation and fig. 5.7 translation of the lens in the nasal direction. Both produce similar results involving an increase in the interval of Sturm temporally and a decrease nasally. This is accompanied by a movement of the astigmatic image shells towards hyperopia nasally and myopia temporally, this effect is greater for the tangential image shell. Each of these effects occur to a slightly greater extent for the 5° rotation (fig. 5.6) than for the 1mm translation (fig. 5.7).

200
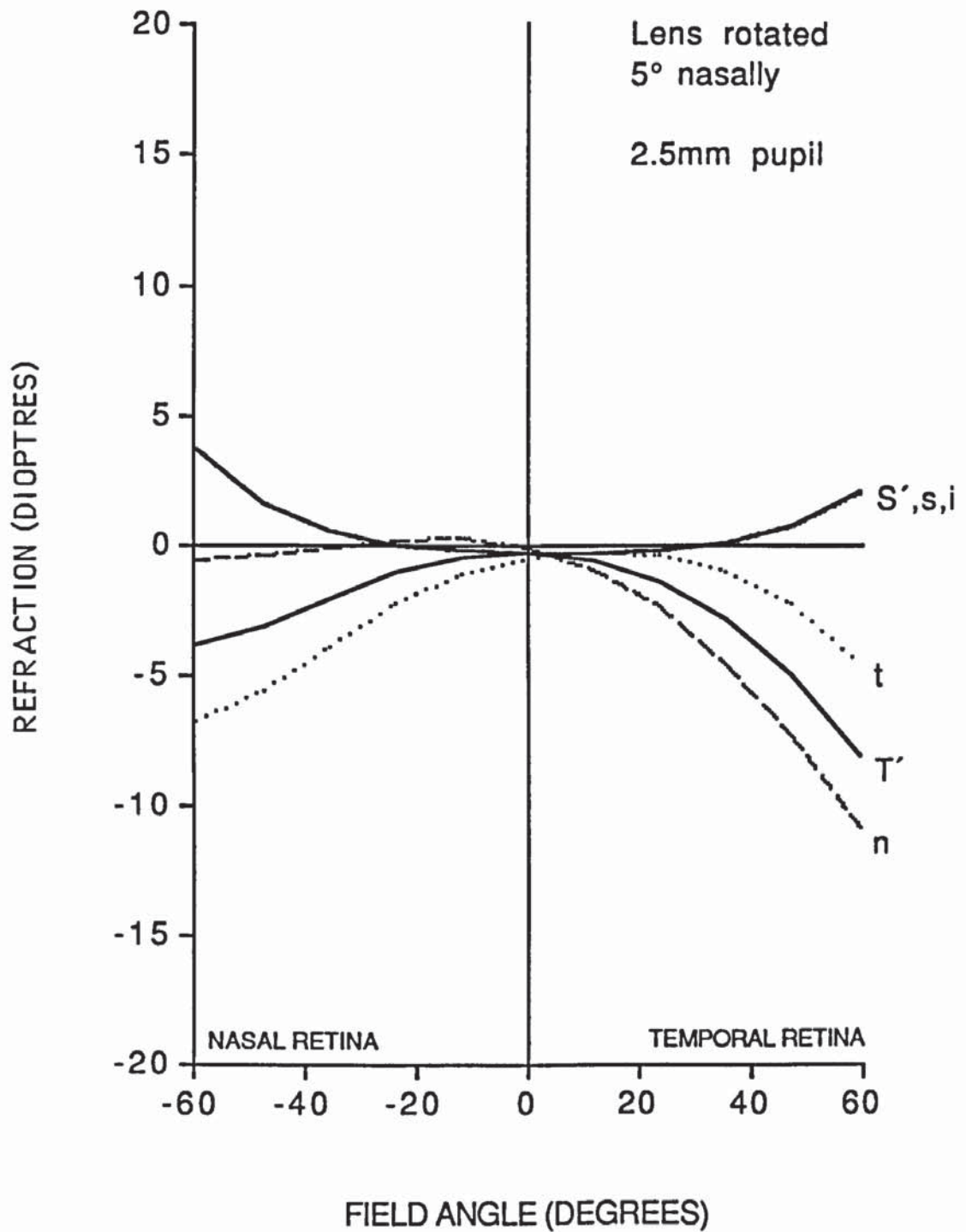
Fig. 5.6 Peripheral refraction for schematic eye with the crystalline lens rotated 5° in the nasal direction. 2.5 mm physical pupil. See fig. 5.4 for explanation of symbols. Zero degrees field angle coincides with the optical axis.
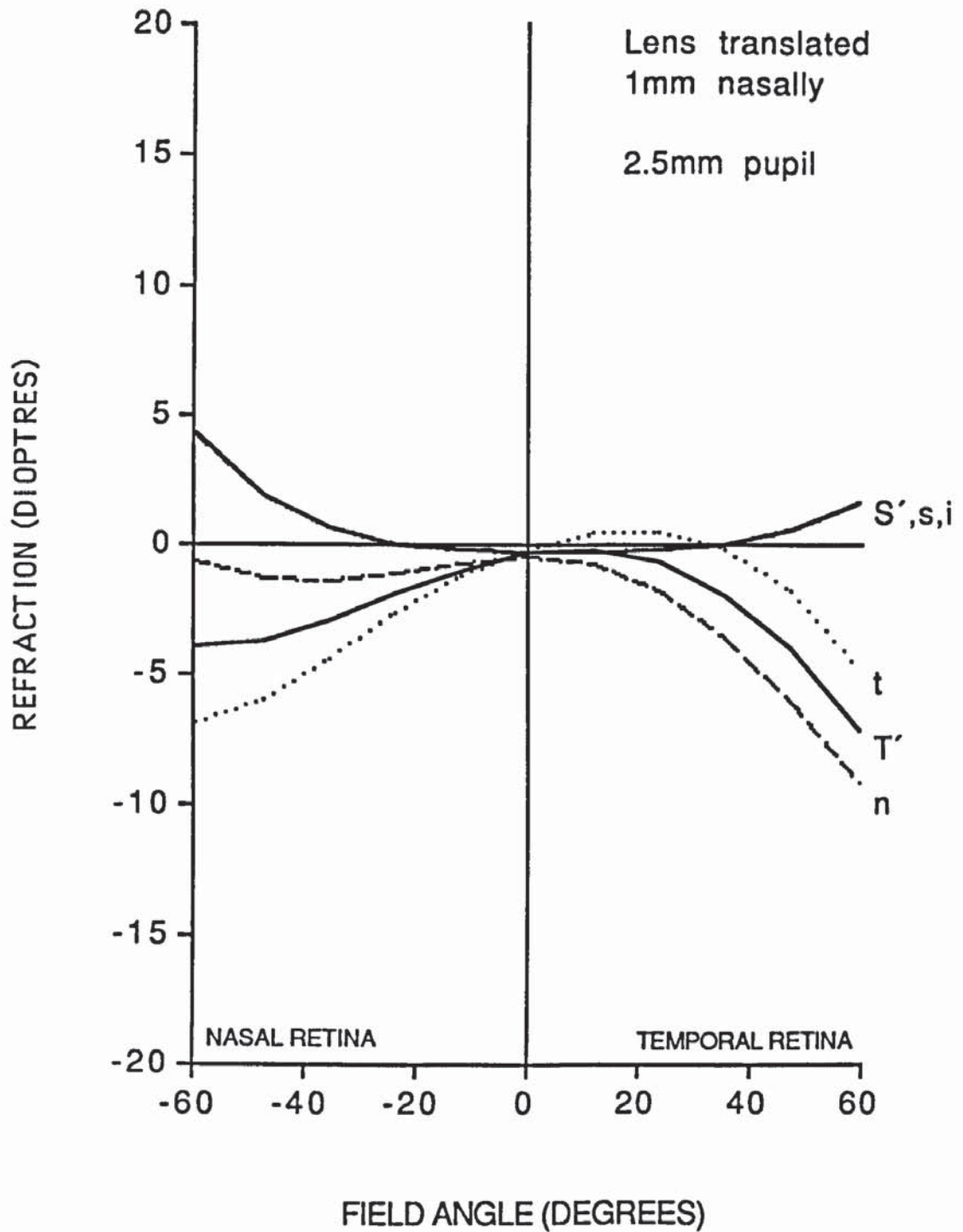
Fig. 5.7 Peripheral refraction for the schematic eye with the crystalline lens translated 1 mm in the nasal direction. 2.5 mm physical pupil. See fig. 5.4 for explanation of symbols. Zero degrees field angle coincides with the optical axis.

202

Subtle differences are evident. The astigmatic image shells do not coincide centrally with lens translation (fig. 5.7). They are also noticeably skewed so that at 10° temporally they cross over. Lens rotation has no such effect (fig. 5.6).

The interval between tangential marginal ray limits with rotation remains nearly the same for corresponding temporal and nasal field angles and is only a little greater than that found in the axially aligned schematic eye (fig. 5.4). For translation, the interval is slightly reduced temporally.

Figure 5.8 shows the effects of nasal rotation and fig. 5.9 nasal translation of the cornea. The effects are largely the same as for the lens, in that rotation and translation produce similar results; astigmatic image shells move towards hyperopia nasally and myopia temporally; the tangential image shell moves by a greater amount thereby increasing the interval of Sturm temporally whilst decreasing it nasally. The above effects are, however, more exaggerated than for the lens giving rise to compound hyperopic astigmatism nasally and compound myopic astigmatism temporally.

The astigmatic image shells for the specified rotation and translation of the cornea are both skewed to the nasal side. This effect is opposite to that for lens translation (fig. 5.7) and is due to the movement of the lens and cornea relative to the principal ray. Therefore, with corneal rotation the image shells cross over at 10° nasally (fig. 5.8). This occurs more extensively, from 0°-30° nasally, with corneal translation (fig. 5.9).
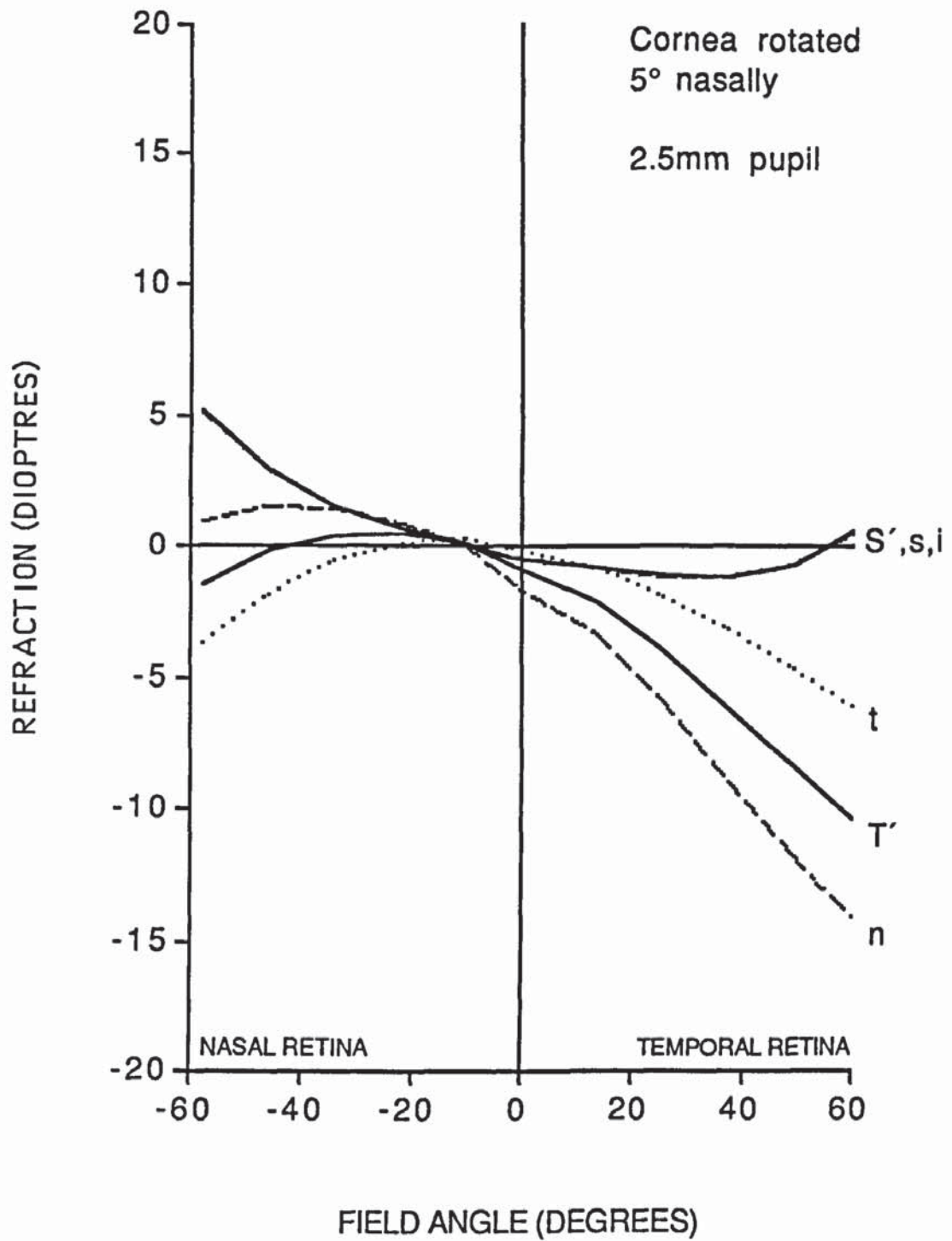
Fig. 5.8 Peripheral refraction for the schematic eye with the cornea rotated 5° in the nasal direction. 2.5 mm physical pupil. See fig. 5.4 for explanation of symbols. Zero degrees field angle coincides with the optical axis.
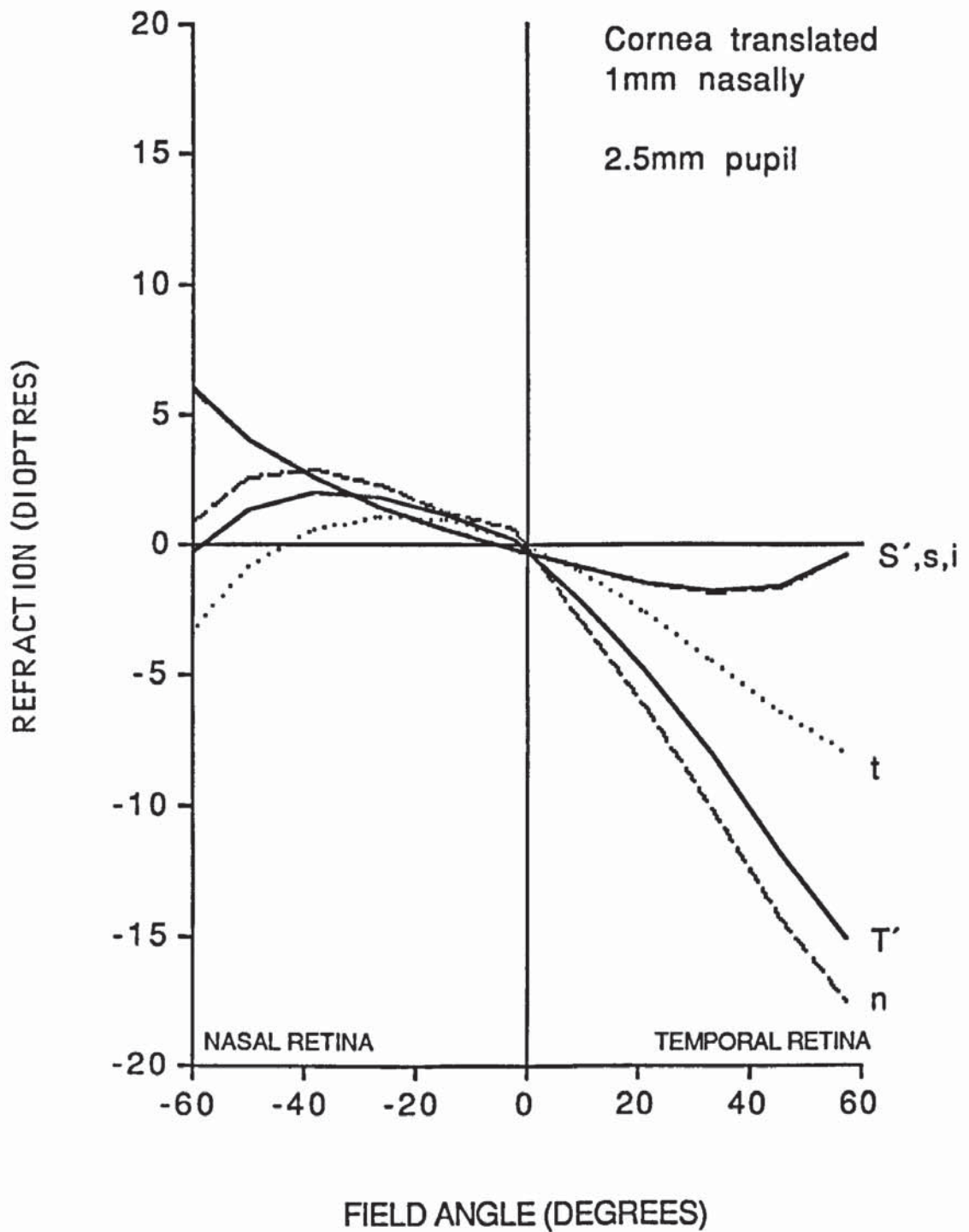
Fig. 5.9 Peripheral refraction for the schematic eye with the cornea translated 1 mm in the nasal direction. 2.5 mm physical pupil. See fig. 5.4 for explanation of symbols. Zero degrees field angle coincides with the optical axis.

205

Figure 5.10 demonstrates the effects of rotation and fig. 5.11 translation of the lens in the inferior direction. Again, similar results arise for both treatments. In contrast to decentrations in the nasal direction, there is no asymmetry over nasal and temporal field angles. A small reduction in the interval of Sturm occurs due to a myopic shift of the image shells at increasing field angles, the shift appearing greater for the sagittal shell.

Centrally there is no myopic shift but astigmatic image shells cross. This is of the same magnitude as the interval between the uncrossed image shells found with nasal decentration.

Sagittal marginal and principal rays no longer coincide. The superior rays form image foci which are more hyperopic with translation and more myopic with rotation than inferior ones. The interval between sagittal limits is greatest centrally and diminishes peripherally. Tangential marginal ray limits remain similar to those of the centred system (fig. 5.4).

Figure 5.12 shows rotation and fig. 5.13 translation of the cornea in the inferior direction. These yield similar results to those found with the lens. Tangential image shells and accompanying marginal ray limits remain in practically the same position as in figs. 5.10 and 5.11. Conversely, the sagittal image shell shifts towards myopia, thus bringing about a further decrease in the the interval of Sturm and an increased interval between the astigmatic image shells which cross over centrally. Sagittal marginal ray limits are also more effected, their separation (i.e. si) being increased but remaining relatively constant over all field angles. The interval between tangential marginal ray limits (i.e. tn) decreases nasally and increases temporally with translation and rotation compared with the centred system (fig. 5.4).
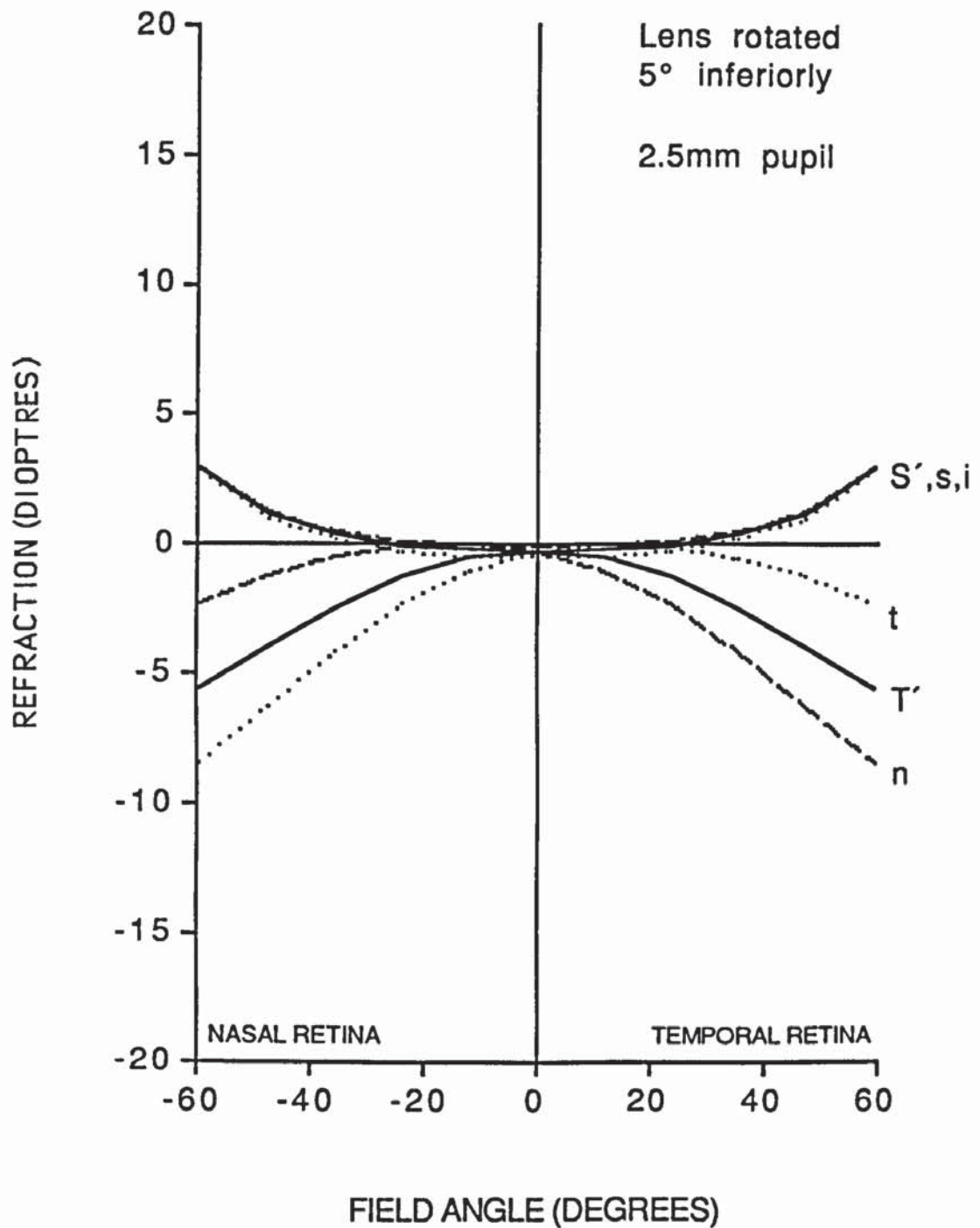
Fig. 5.10 Peripheral refraction for the schematic eye with the crystalline lens rotated 5° in the inferior direction. 2.5 mm physical pupil. See fig. 5.4 for explanation of symbols. Zero degrees field angle coincides with the optical axis.
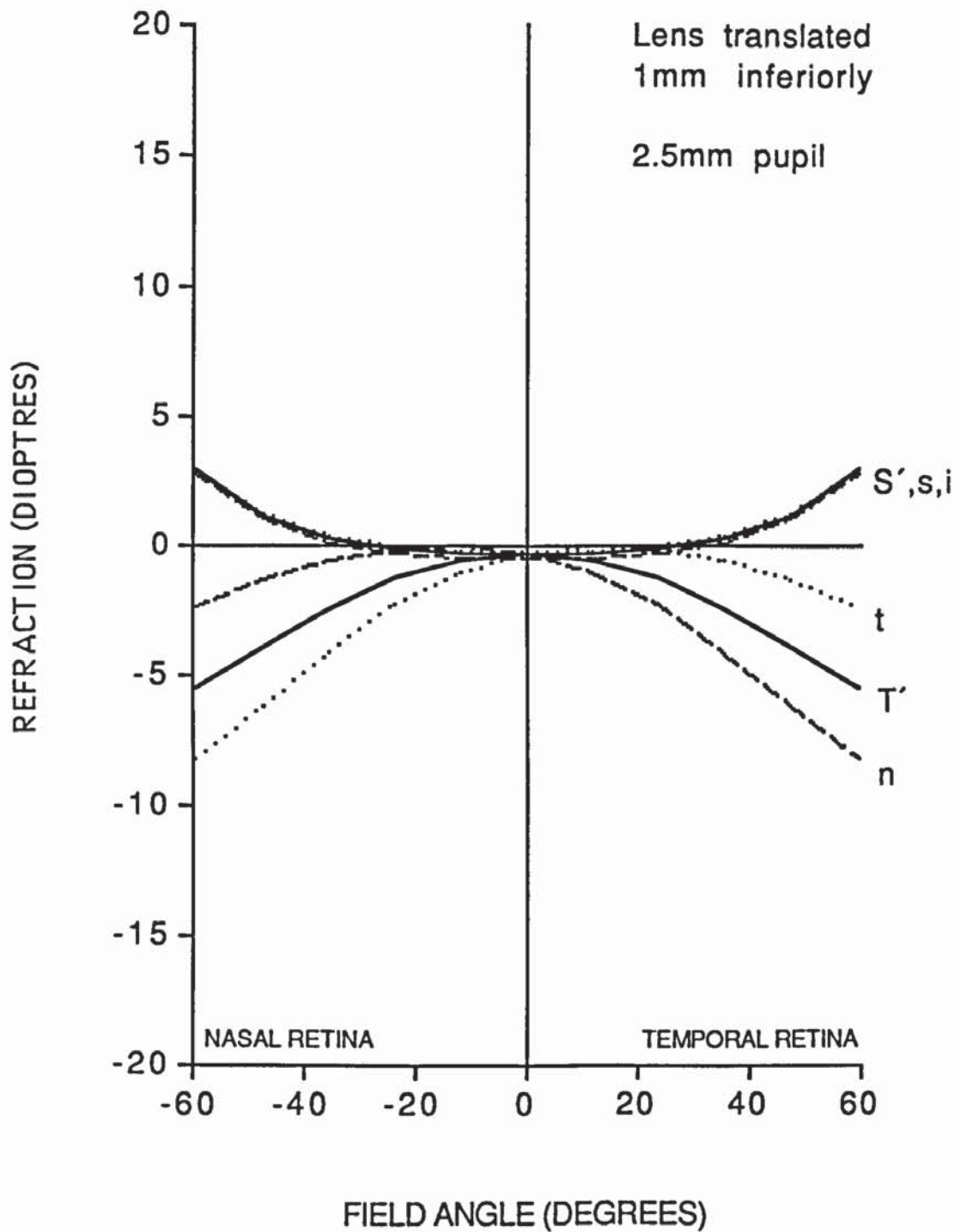
Fig. 5.11   Peripheral refraction for the schematic eye with the crystalline lens
translated 1 mm in the inferior direction. 2.5 mm physical pupil. See
fig. 5.4 for explanation of symbols. Zero degrees field angle coincides
with the optical axis.

208
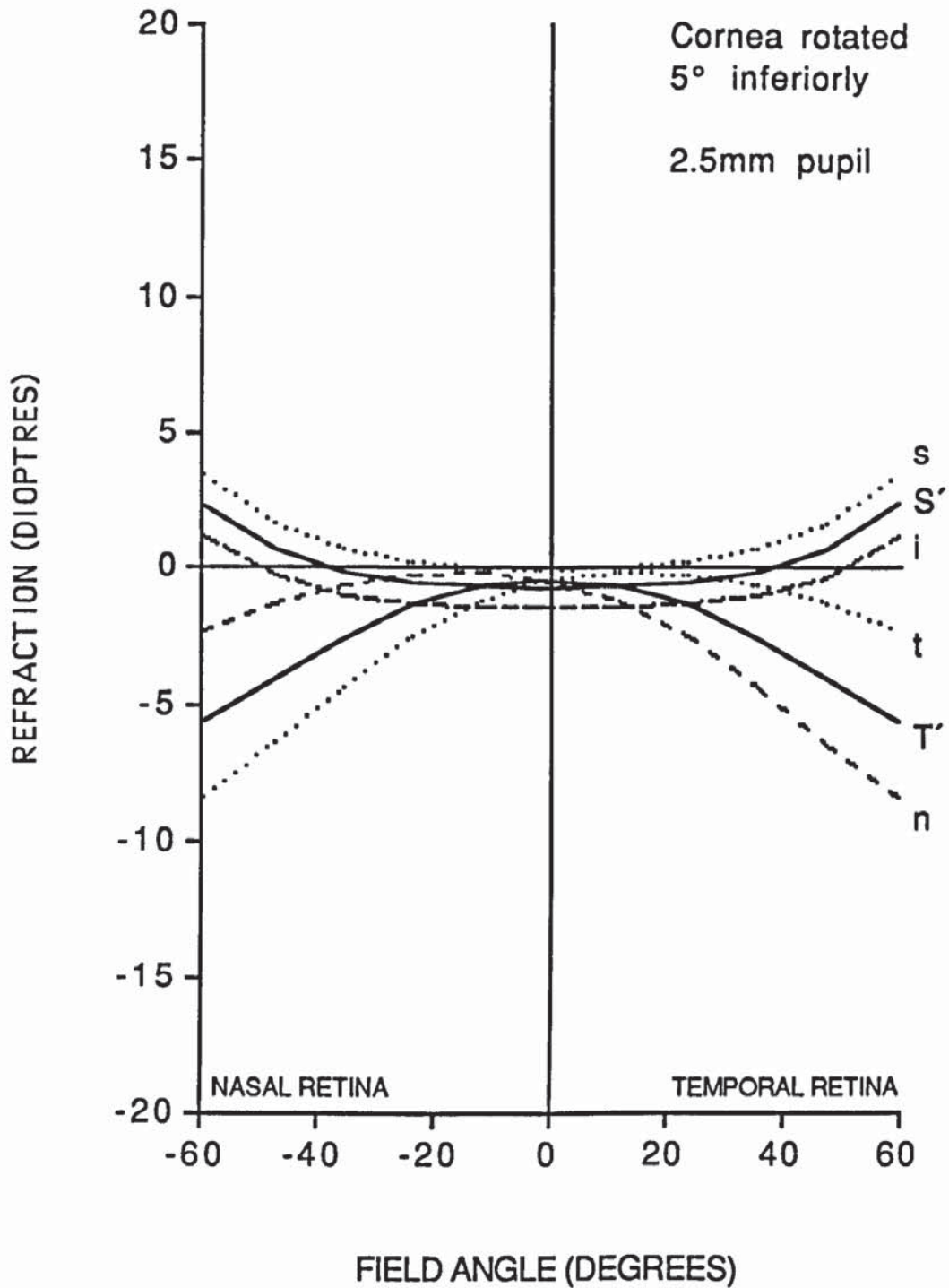
Fig. 5.12 Peripheral refraction for the schematic eye with the cornea rotated 5° in the inferior direction. 2.5 mm physical pupil. See fig. 5.4 for explanation of symbols. Zero degrees field angle coincides with the optical axis.
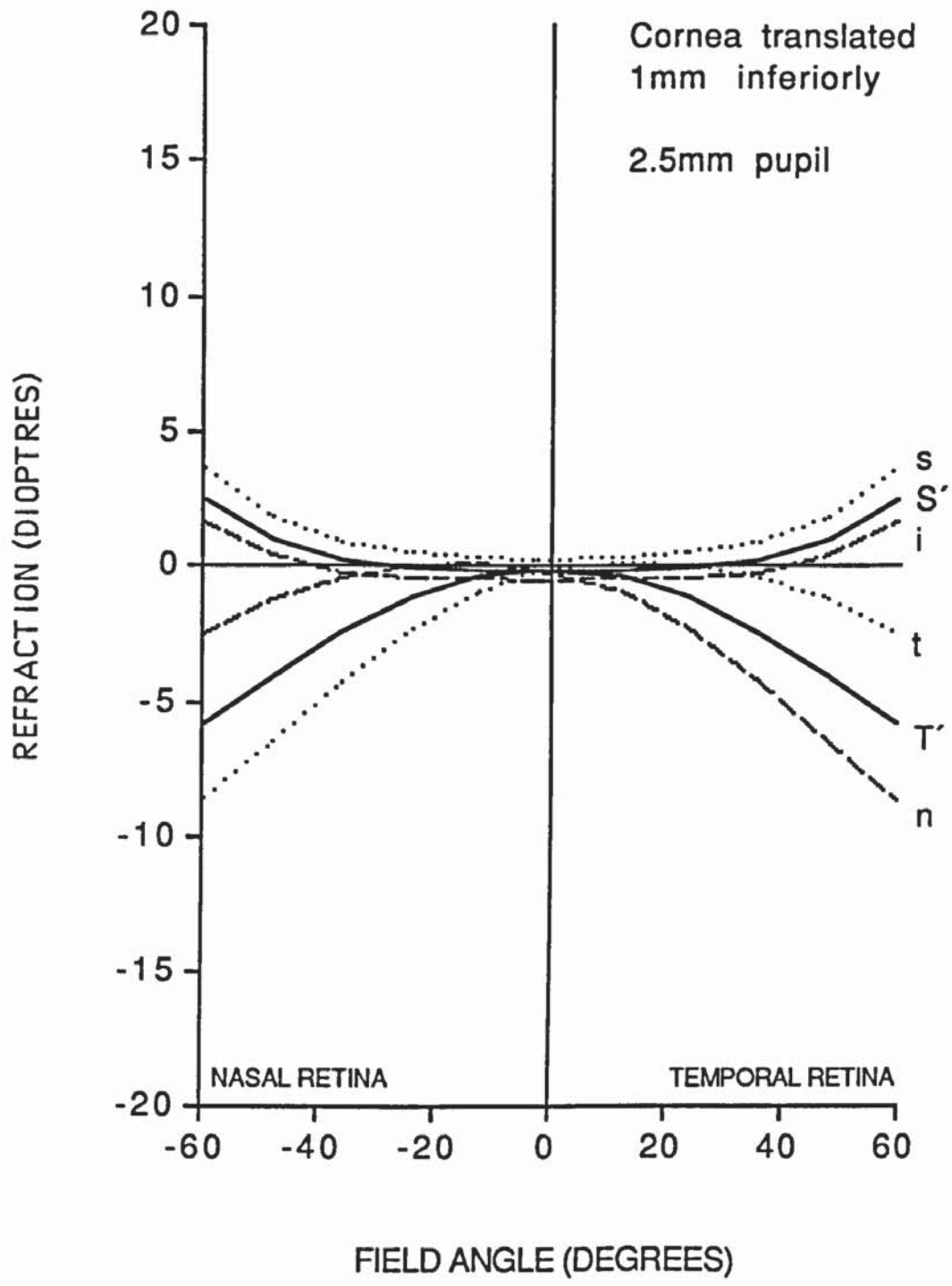
Fig. 5.13 Peripheral refraction for the schematic eye with the cornea translated 1 mm in the inferior direction. 2.5 mm physical pupil. See fig. 5.4 for explanation of symbols. Zero degrees field angle coincides with the optical axis.

(D) THE EFFECT OF A NON-ALIGNED CORNEA ON ENTRANCE PUPIL SIZE

The distance between the sagittal and tangential marginal rays, measured outside the eye, represents the diameters of the entrance pupil (see section 5.2.4). This section demonstrates the variation in entrance pupil size for different field angles and shows how translation and rotation effects this variation (Barnes et al., 1987 [see appendix 4]).
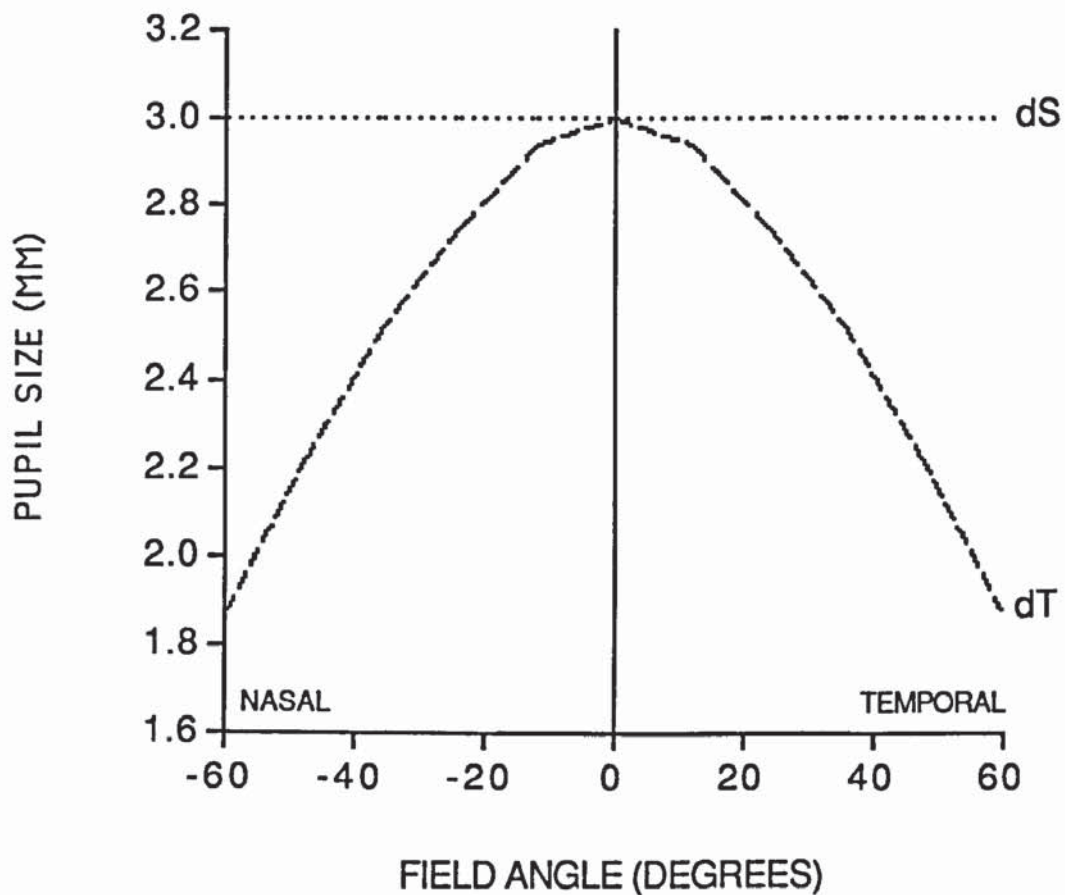
Fig. 5.14 Entrance pupil size as a function of field angle in the axially aligned schematic eye with a physical pupil of 2.5 mm. Sagittal (dS) and tangential (dT) pupil diameters are shown by dotted and dashed lines, respectively. Zero degrees field angle coincides with the optical axis.

Figure 5.14 shows the entrance pupil size at different field angles in the sagittal (dotted lines) and tangential (dashed lines) planes in the axially aligned schematic eye. The

physical pupil appears larger when observed from outside the eye. Since the sagittal entrance pupil size (dS) remains constant while its tangential dimension (dT) diminishes with increasing field angle, the entrance pupil becomes more elliptical with oblique gaze. Assuming an angle alpha of 5° to represent measurements made with respect to the line of sight rather than the optical axis (see section 1.5), the ratio of the horizontal to vertical entrance pupil diameters are 0.74 at approximately 55° temporal field angle. This compares well with the measurements of Spring and Stiles (1948) who reported a value of 0.73 at the same field angle in 13 subjects with an average tangential entrance pupil diameter of 2.66 mm viewed from straight ahead.
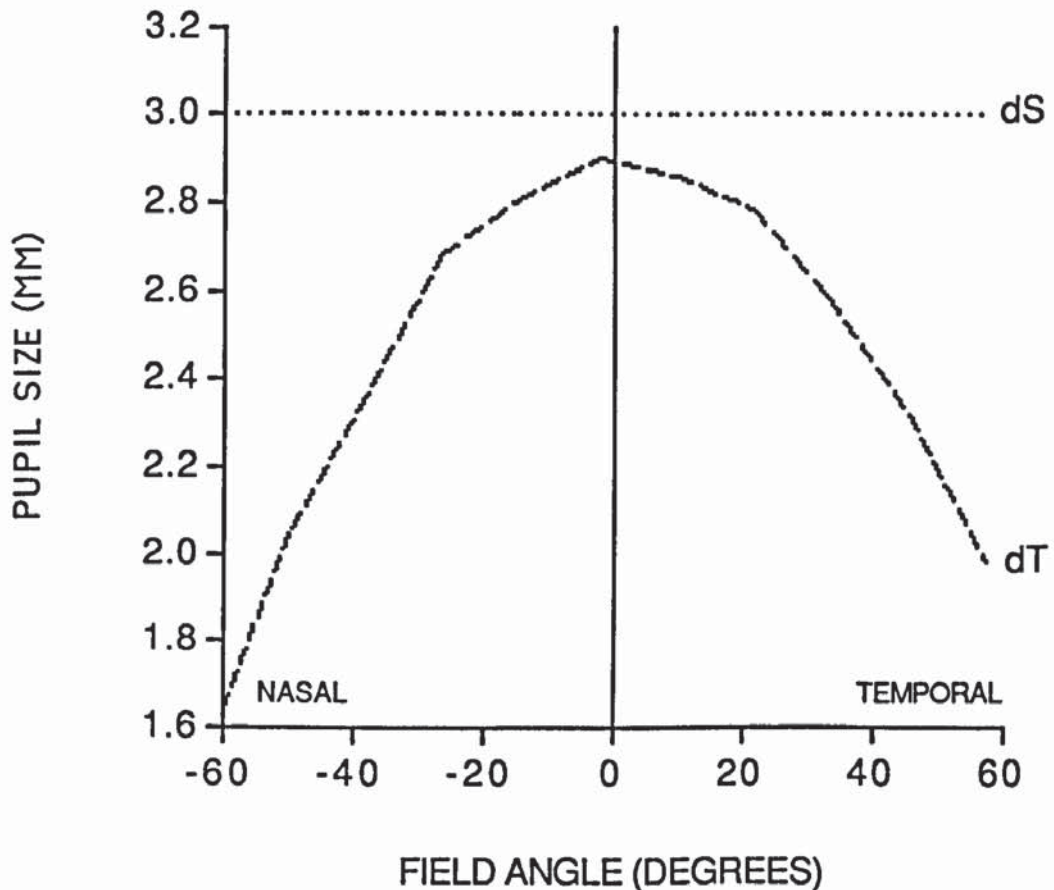
Fig. 5.15   Entrance pupil size as a function of field angle in the schematic eye with the cornea translated 1 mm in the nasal direction. 2.5 mm physical pupil. Sagittal (dS) and tangential (dT) pupil diameters are shown by dotted and dashed lines, respectively. Zero degrees field angle coincides with the optical axis.

Figure 5.15 shows the effects of corneal translation in the nasal direction on the entrance pupil shape. Translation causes the pupil to appear smaller nasally and larger temporally than seen in figure 5.14. The maximum size of the entrance pupil in the tangential plane also never reaches the sagittal pupil size. Rotation has a very small effect. As the graph produced is almost identical to figure 5.14, it is not shown.
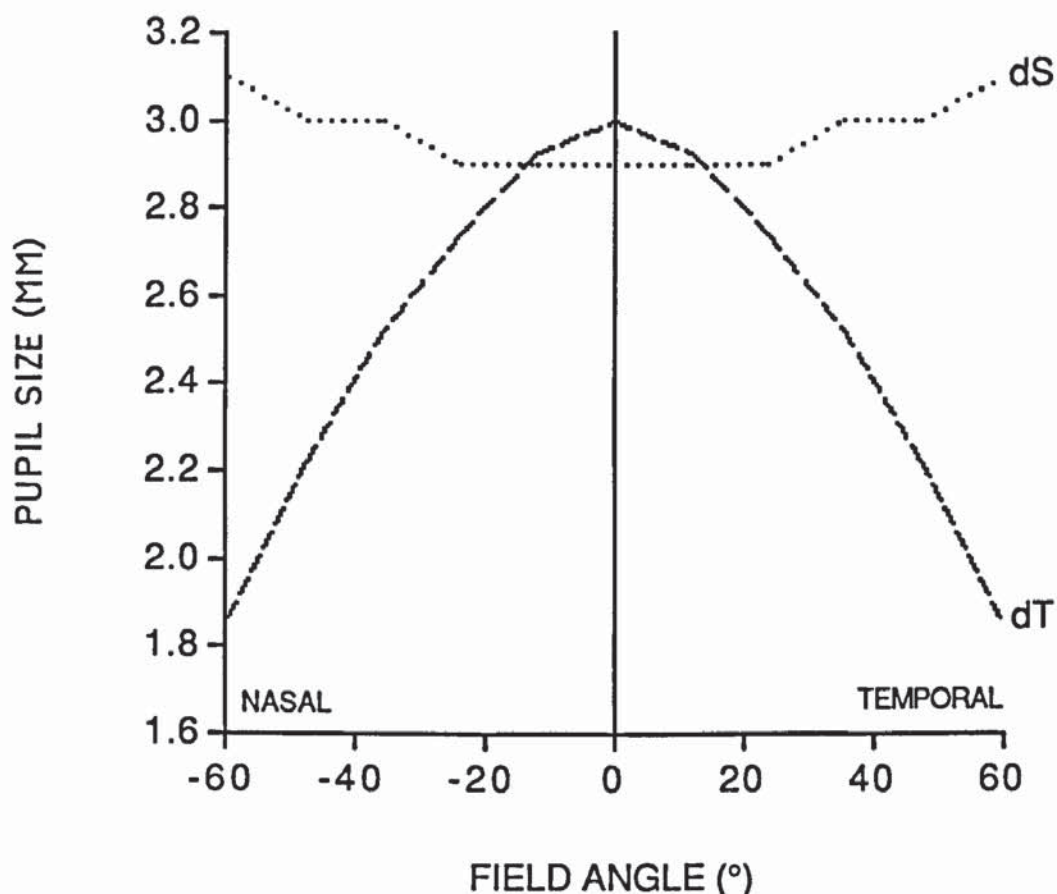
Fig. 5.16 Entrance pupil size as a function of field angle in the schematic eye with the cornea translated 1 mm in the inferior direction. 2.5 mm physical pupil. Sagittal (dS) and tangential (dT) pupil diameters are shown by dotted and dashed lines, respectively. Zero degrees field angle coincides with the optical axis.

Figure 5.16 shows the effects of corneal translation in the inferior direction. In the tangential plane the entrance pupil size (dT) remains the same as in figure 5.14. In the sagittal plane the entrance pupil size (dS) appears largest at large field angles and diminishes to a value smaller than the maximum tangential size when viewed from

straight on. Again, because there is no appreciable effect with rotation, this graph is not shown.

5.3.2 RETINAL SHAPE AND POSITION

In section 2.3, the peripheral refractive patterns found by Millodot (1981) (see fig. 2.4) in ametropic eyes were considered to be caused by differences in retinal shape and position (Charman and Jennings, 1982: Charman, 1983). It was pointed out that similar results would be expected if each of the ametropic eyes were of more or less the same dioptric power so that the ametropia was purely due to differences in axial length. Then, if the retinae of each eye occupied the same position in the region of the equator, the convergence of refractions at large field angles, evident in Millodot's (1981) results, would also occur. In this section, these retinal shape changes are modelled to demonstrate their effect on peripheral refraction (Dunne et al., 1987 [see appendix 4]).

A spherical retina of 12.05 mm radius was necessary to position the tangential and sagittal peripheral astigmatic image shells in front of and behind the retina respectively, as normally occurs in emmetropia (see section 2.3). About 4 dioptres of axial ametropia was modelled by changing the axial length by $\pm$ 2 mm while keeping the equatorial radius constant, the retina having an ellipsoidal surface made to conform with these parameters.

In terms of the input parameters described in section 5.2.1A, the X, Y and Z retinal surface curvature parameters were all given radius values of 12.05 mm (giving rise to a sphere) for the modelled emmetrope. To keep the equatorial radius constant in the modelled myopic and hyperopic eyes, X and Y were also given values of 12.05 mm.

The radius of curvature in the Z direction was then altered to (12.05 + 2 =) 14.05 mm (giving rise to a prolate ellipsoid) for the modelled myope and (12.05 - 2 =) 10.05 mm (giving rise to an oblate ellipsoid) for the modelled hyperope in order to produce the required axial length variations.

The surface location parameter $\bar{Z}$ was kept constant so that the equators of each of the modelled retinae coincided in position. $\bar{Z}$ was given a value of -8.45 mm so that the axial length of the emmetropic eye (24.2 mm) was equal to that specified by Le Grand and El Hage (1980).
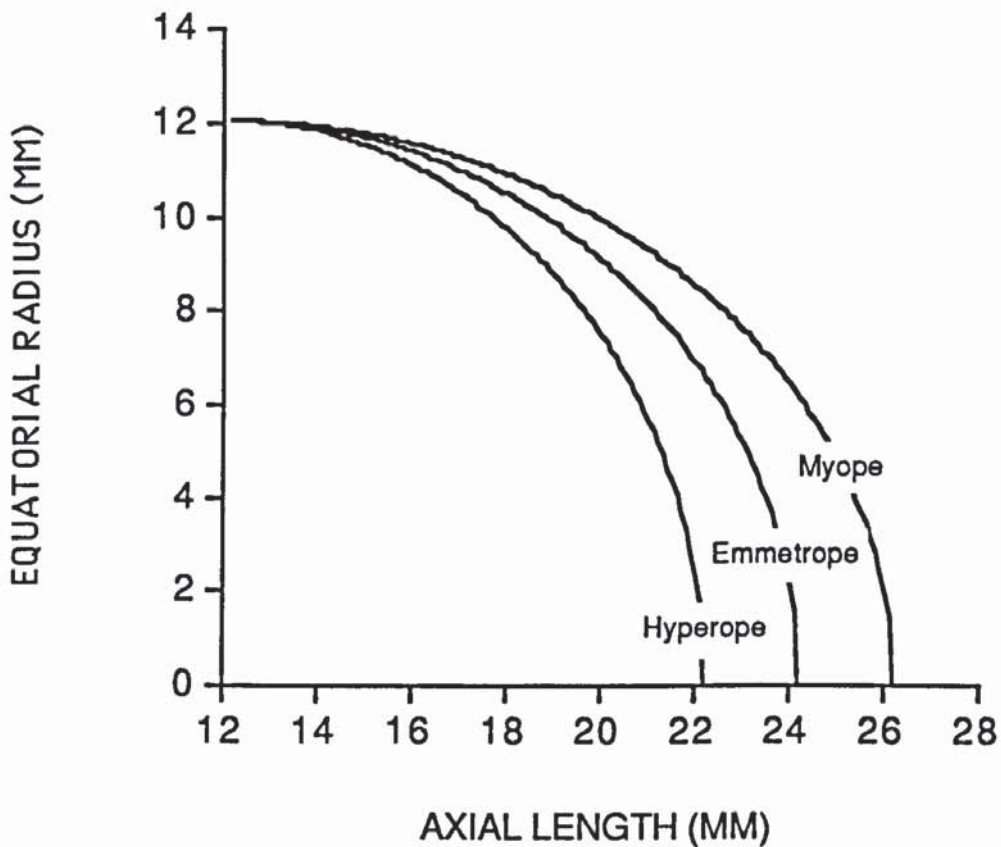
Fig. 5.17 Computer plot of cross sections of retinal shape in the modelled axially hyperopic, emmetropic and myopic eyes.

The non-zero components of the matrix formulation (see section 5.2.1C) for the modelled retinal surfaces are given in table 5.2. Figure 5.17 shows cross sections of the ellipsoidal retinal surfaces generated by the parameters shown in table 5.2.

SURFACE	A(1,1)	A(2,2)	A(3,3)	B(3)	c	T(3)
EMMETROPE	0.006886	0.006886	0.006886	0	-1	-8.45
MYOPE	0.006886	0.006886	0.005066	0	-1	-8.45
HYPEROPE	0.006886	0.006886	0.009901	0	-1	-8.45

Table 5.2 Retinal surface parameters (see 5.2.1C for explanation of symbols).

In fig. 5.18, modelled peripheral refractive patterns are shown for an axial length increase to produce myopia (squares); decrease to produce hyperopia (circles) and with no change to produce emmetropia (triangles). Sagittal (broken lines) and Tangential (solid lines) image shells are shown separately for clarity. The latter were constructed from image foci corresponding to $M_1 'M_2'$ in fig. 5.3. Sagittal and tangential comatic image limits, however, are not shown. A 2.5 mm physical pupil was used.

The results are in agreement with those of Millodot (1981) in that central refractions differ markedly for the three types of eye whilst both the tangential and sagittal image shells have nearly the same value at field angles of 60°. The effect is to produce steep sagittal and flat tangential image shells in the myope and vice versa in the hyperope, whereas the gradient of both image shells in the emmetrope are nearly equal.
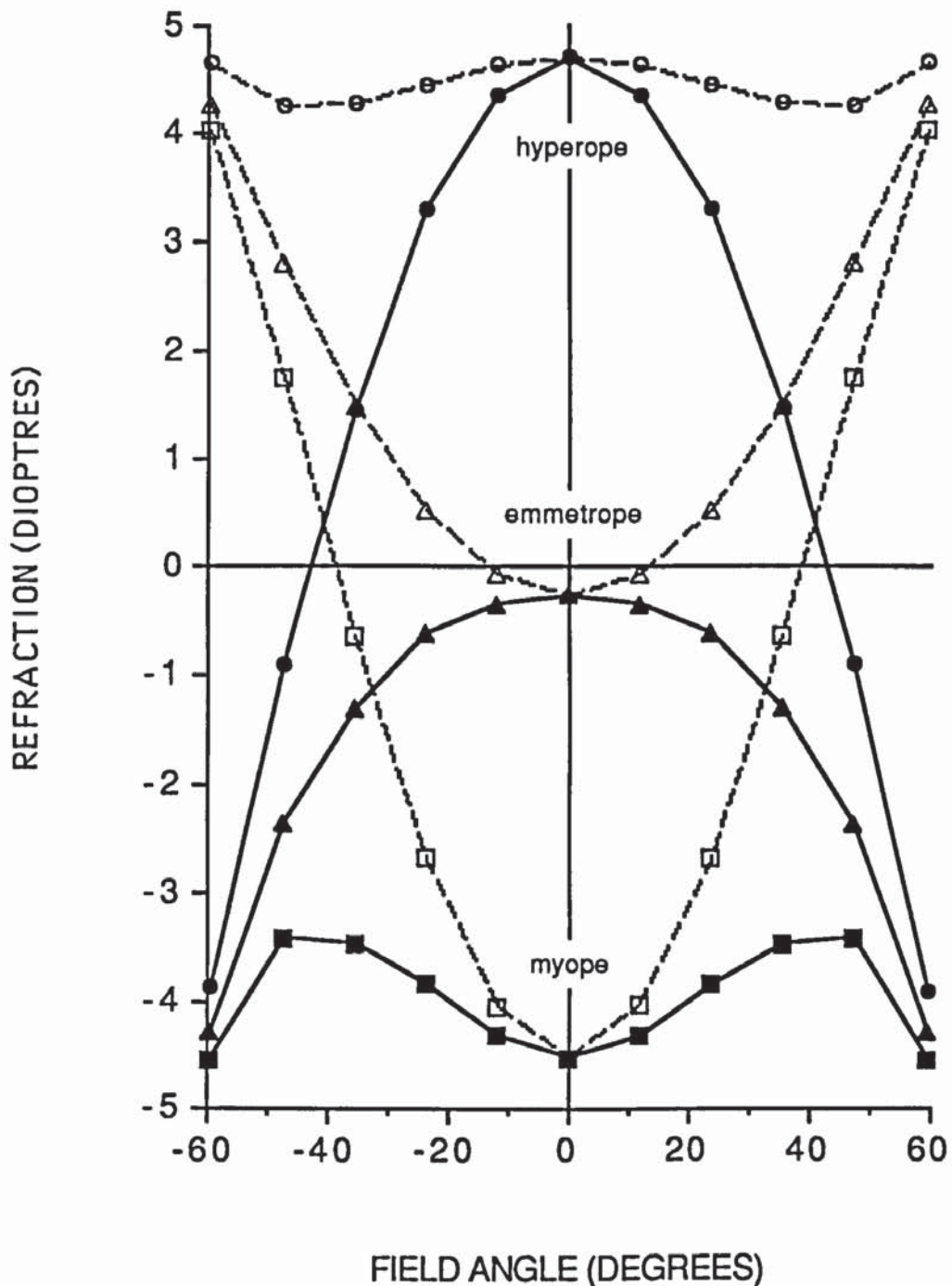
Fig. 5.18 Graph of the modelled peripheral refractive patterns for an axial length increase to produce myopia (squares); decrease to produce hyperopia (circles) and with no change to produce emmetropia (triangles). The equatorial radius is kept constant. Sagittal (broken lines) and Tangential (solid lines) image shells are shown separately for clarity. 2.5 mm physical pupil. Zero degrees field angle coincides with the optical axis.

217

5.3.3 ALTERATION OF THE CRYSTALLINE LENS PARAMETERS

In sections 5.3.1 and 5.3.2, the amount of modelled peripheral astigmatism was found to be approximately 8 D at 60° field angle. The latter is greater than values observed experimentally.

As described in section 2.3, there is a considerable variation in the amount of peripheral astigmatism found in the human population. At 60° field angle, Type IV eyes (see fig. 2.3) normally possess approximately 5 D of astigmatism whereas approximately 1.5 D of astigmatism is usually found in type I eyes. Lotmar (1971) considered these types of eye to be the limiting cases.

From the literature reviewed in section 2.4 it would appear that neither the inclusion of aspheric surfaces or a gradient index crystalline lens reduces the amount of peripheral astigmatism predicted in schematic eyes to values found in either type IV or type I eyes. The question therefore arises as to how much manipulation is necessary before a schematic eye produces realistic peripheral astigmatic results.

This question is considered in this section (Dunne and Barnes, 1987 [see appendix 4]). The schematic eye parameters used were the same as described in section 5.2.1C with the exception of the crystalline lens refractive index and the conic constant values for its anterior an posterior surfaces. These were manipulated to study their effect on peripheral astigmatism. A 4 mm physical pupil was also assumed. The corneal surfaces were not altered as Bennett and Rabbetts (1984) have already shown that even extreme flattening of the anterior corneal surface does not yield the low values of peripheral astigmatism found in type I eyes. On the other hand, the peripheral astigmatic effect of varying the profile of the anterior lens surface, as far as the present

author is aware, have never been studied before.

The peripheral astigmatic and central refractive results shown in this section refer to image foci corresponding to $M_1'M_2'$ in fig. 5.3. Sagittal and tangential comatic image limits, however, are not considered here.
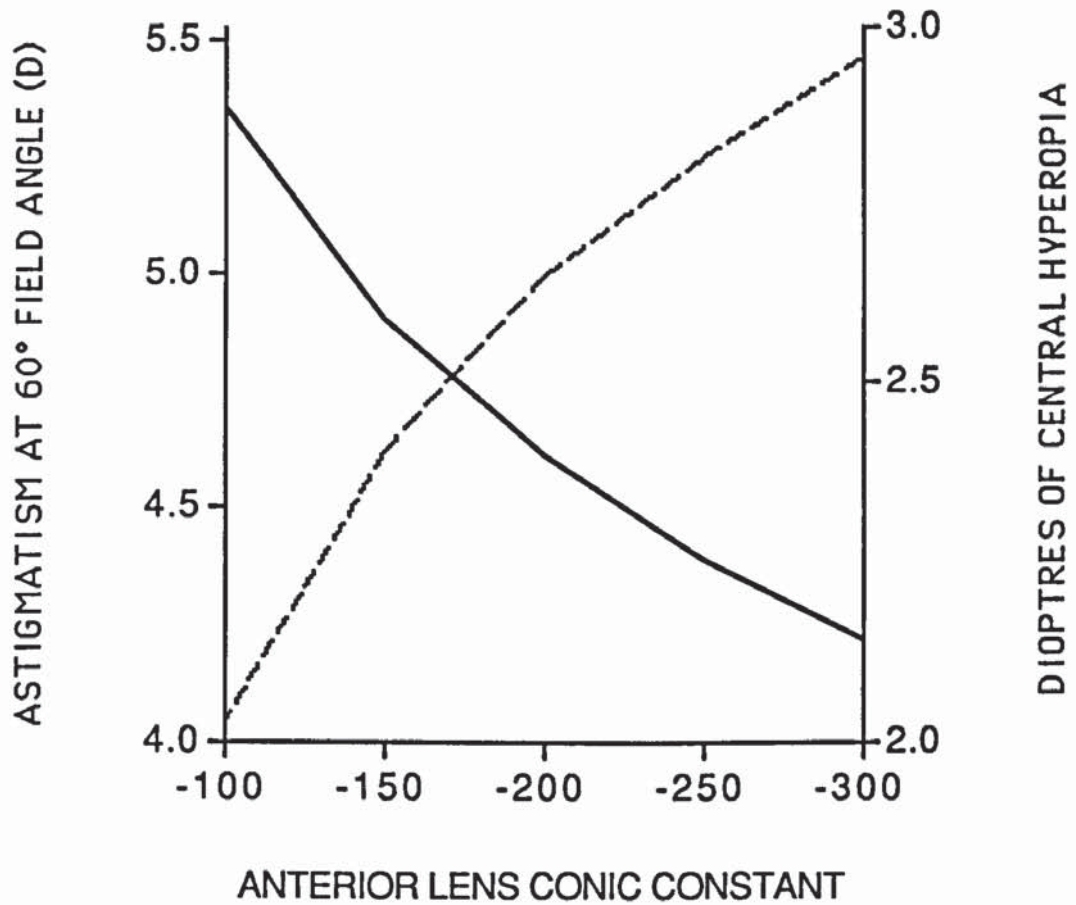
Fig. 5.19 The effect of varying the anterior crystalline lens surface conic constant upon peripheral astigmatism at 60° field angle (solid line) and central refraction (broken line).

Figure 5.19 shows that the amount of astigmatism at 60° field angle is reduced to more realistic values by flattening the anterior crystalline lens surface peripherally with a more negative (hyperbolic) conic constant. However, this yields a considerable amount of central hyperopia.

There is no significant reduction of peripheral astigmatism when the parabolic posterior crystalline lens surface (conic constant = 0) is either flattened peripherally by making it more hyperbolic or steepened by making it more ellipsoidal (fig. 5.20). Altering this surface in either direction leads to increased peripheral astigmatism. Flattening the posterior lens surface also shifts the central refraction in the hyperopic direction.
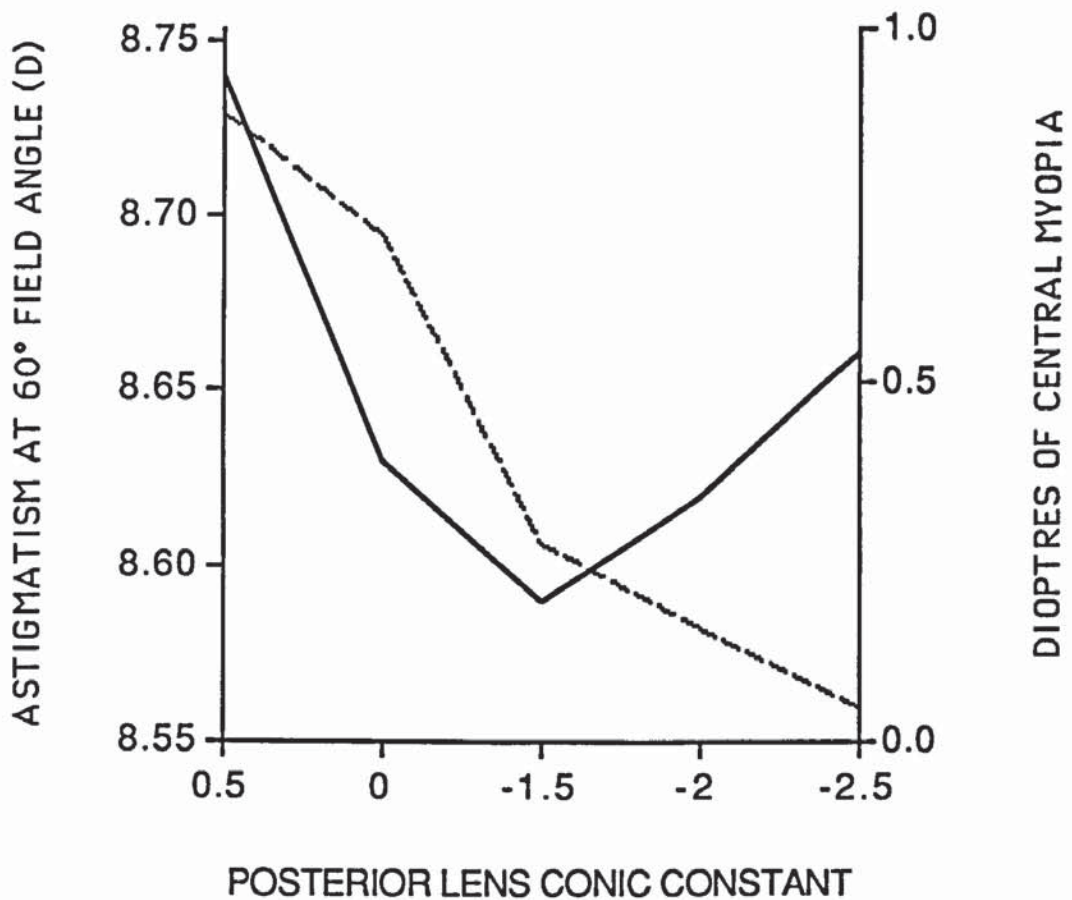
Fig. 5.20   The effect of varying the posterior crystalline lens surface conic constant upon peripheral astigmatism at 60° field angle (solid line) and central refraction (broken line).

Increasing the refractive index of the crystalline lens, as in fig. 5.21, reduces the peripheral astigmatism at 60° field angle and induces large amounts of central myopia. As this is the case, it is possible to adjust the peripheral astigmatism for the schematic eye to equal any particular value at 60° by using several different combinations of

220

anterior crystalline lens flattening and lenticular refractive index increase, each combination giving rise to a different central refraction.
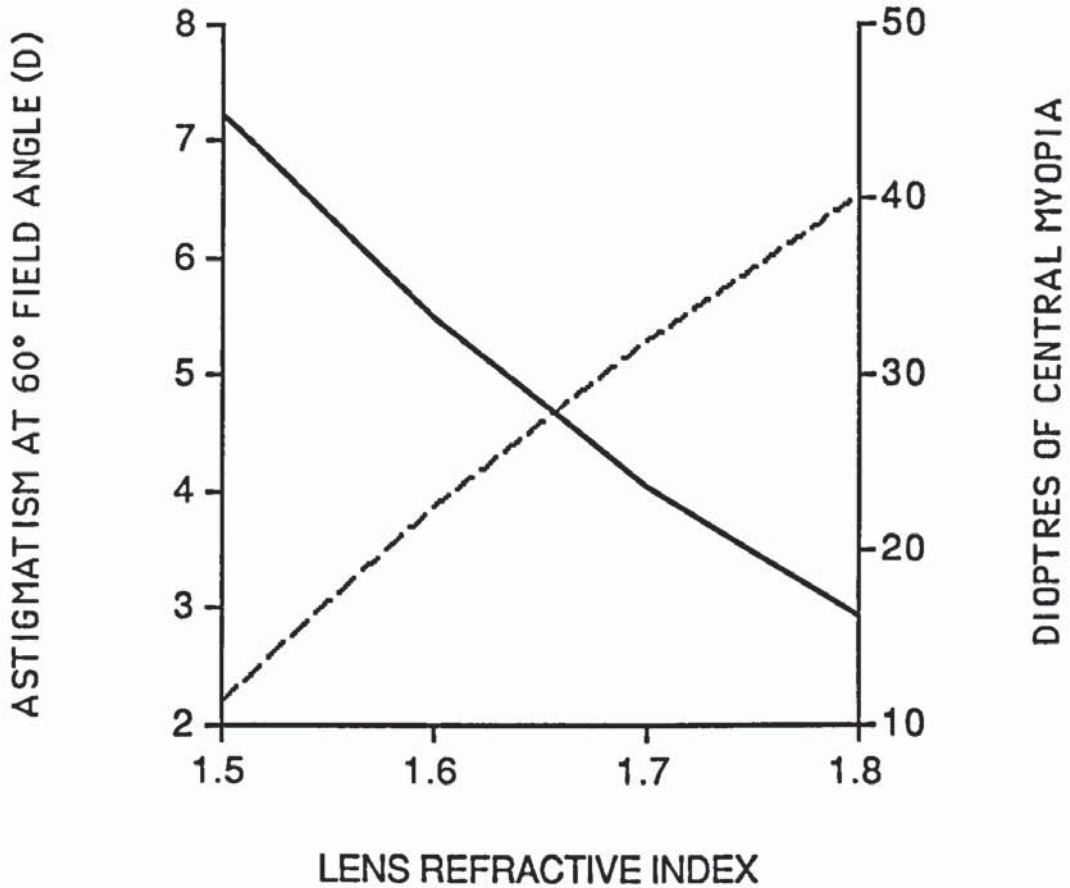
Fig. 5.21 The effect of varying the crystalline lens refractive index upon peripheral astigmatism at 60° field angle (solid line) and central refraction (broken line).

In fig. 5.22, the peripheral astigmatism at 60° field angle is reduced to a value typically found in type IV eyes (4.6 D) with different anterior lens conic constant/refractive index combinations. This value was calculated using the equation derived by Lotmar and Lotmar (1974) from the results of Rempt et al. (1971) (see section 2.4). By interpolation from fig. 5.22, an anterior lens conic constant of -106 (hyperbola) combined with a lenticular refractive index of 1.439 is found to produce emmetropia.
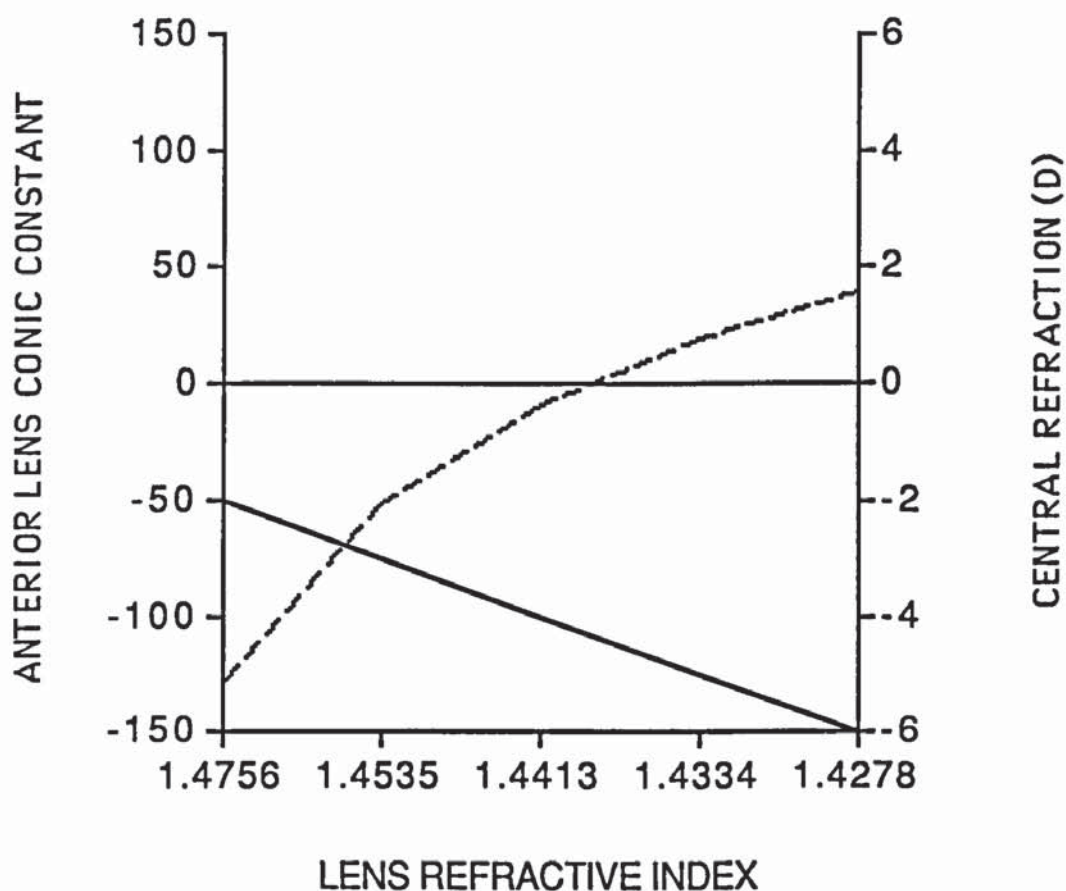
Fig. 5.22 Various combinations of anterior crystalline lens surface conic constant and lenticular refractive index required to reduce the peripheral astigmatism to a value (4.6 D) found typically in type IV eyes at 60° field angle (solid line). Each combination produces a different value for central refraction (broken line).

Figure 5.23 shows the reduction of peripheral astigmatism at 60° field angle to a value typically found in type I eyes (1.5 D). This value was taken from the study of Ferree et al. (1931) (see section 2.3). Here, an anterior crystalline lens conic constant of -1057 (hyperbola) is required in combination with a lenticular refractive index of 1.458 to produce emmetropia.
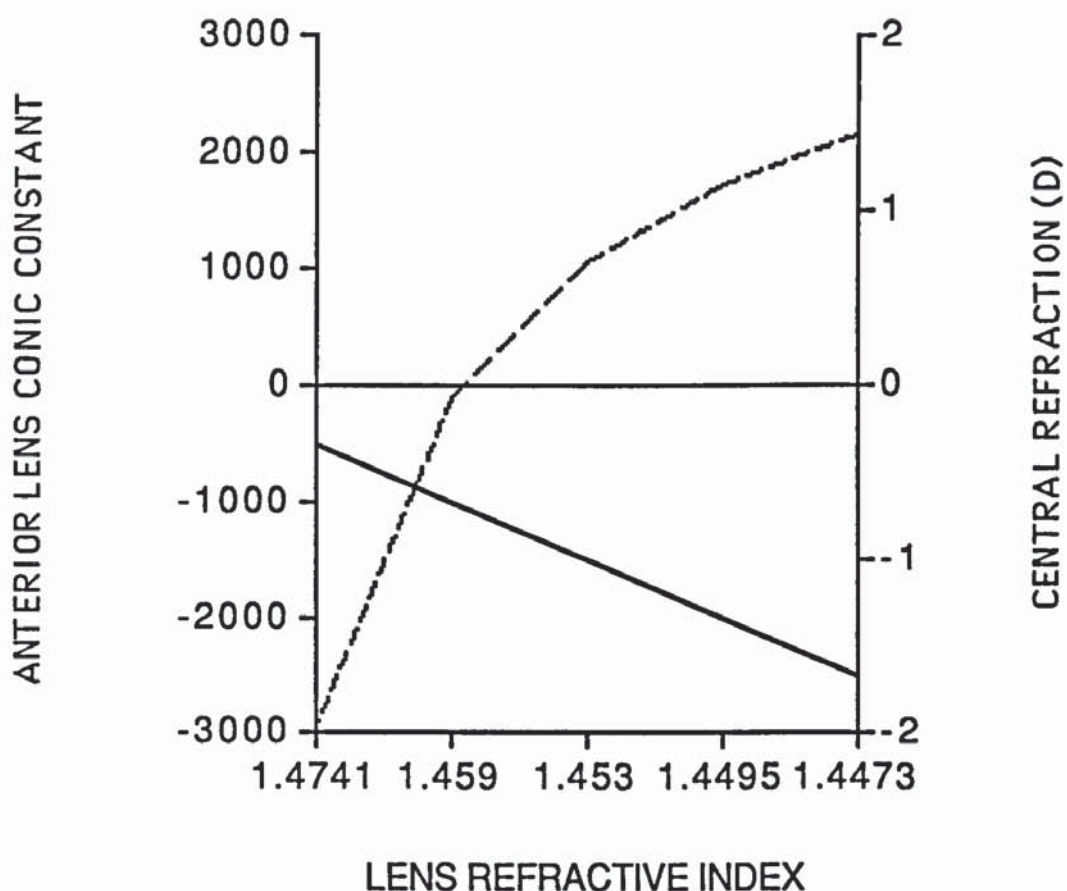
Fig. 5.23 Various combinations of anterior crystalline lens surface conic constant and lenticular refractive index required to reduce the peripheral astigmatism to a value (1.5 D) found typically in type I eyes at 60° field angle (solid line). Each combination produces a different value for central refraction (broken line).

The non-zero components of the matrix formulation (see section 5.2.1C) for the anterior crystalline lens surfaces for type IV and type I eyes are given in table 5.3.

FRONT LENS	A(1,1)	A(2,2)	A(3,3)	B(3)	c	T(3)
TYPE IV EYE	-1.018838	-1.018838	107.9979	0	-1	0.0962
TYPE I EYE	-10.15955	-10.15955	10738.54	0	-1	0.0096

Table 5.3 Anterior crystalline lens surface parameters for type IV and type I eyes (see 5.2.1C for explanation of symbols).
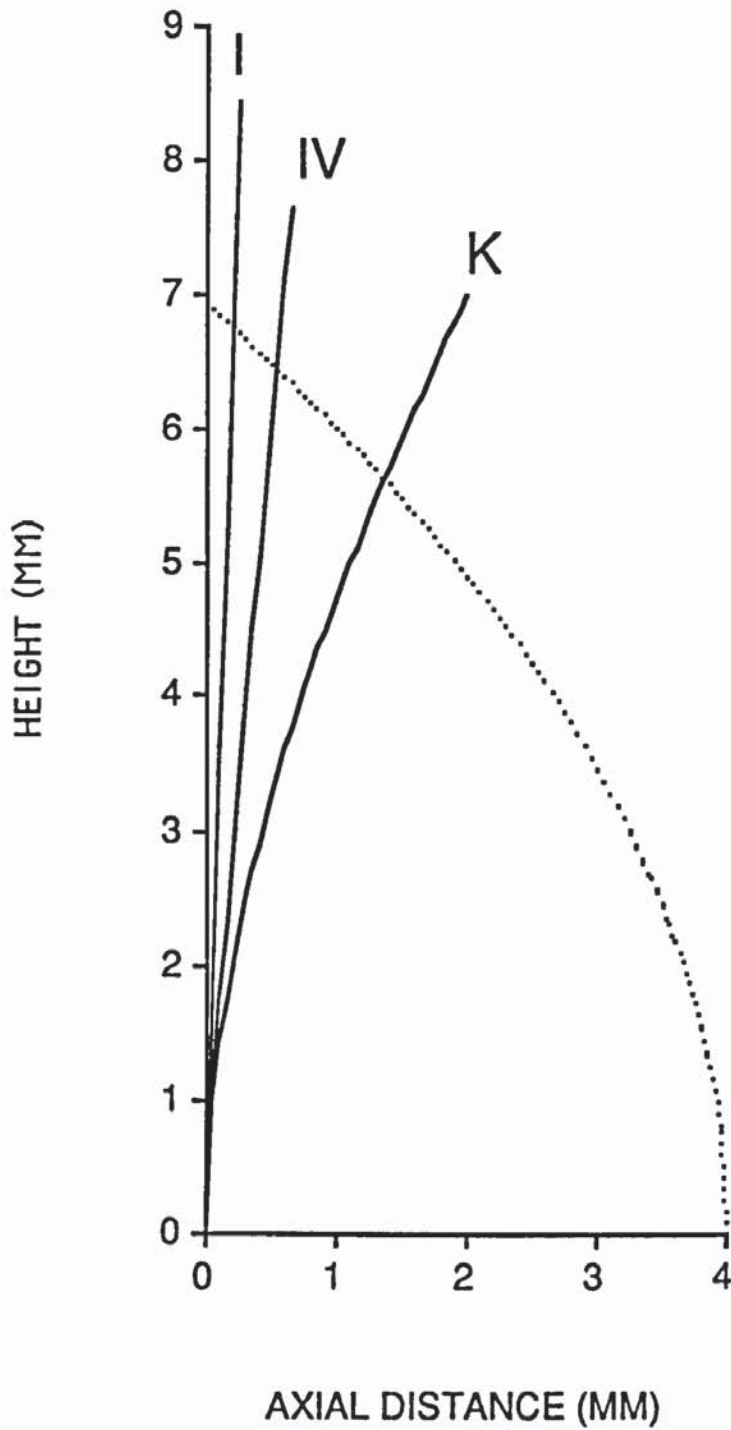
Fig. 5.24 A computer plot of the modelled crystalline lens surfaces. The anterior lens surfaces (solid lines) from the eye model of Kooijman (1983) (denoted K), the modelled type IV eye (denoted IV) and the modelled type I eye (denoted I) are shown. The parabolic posterior lens surfaces used in all three eye models is also shown (dotted lines).

Figure 5.24 illustrates that the anterior crystalline lens surface cross sections (generated by the parameters shown in table 5.3) for the type IV and type I eye models are considerably flatter than that used by Kooijman (1983) (generated by the parameters shown in table 5.1). The parabolic posterior lens surface used in all three eye models ~~are~~ is also shown.
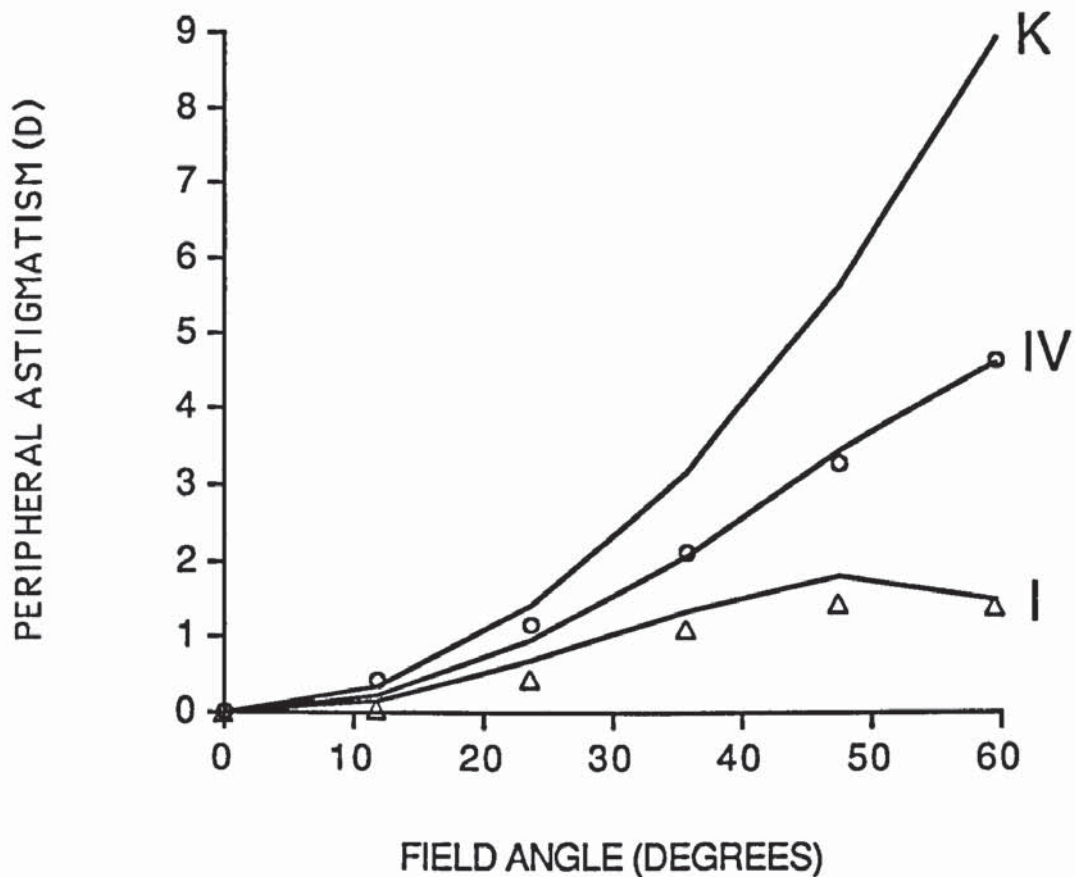
Fig. 5.25   Graph of peripheral astigmatism plotted as a function of field angle in the eye model of Kooijman (1983) (denoted K), the modelled type IV eye (denoted IV) and the modelled type I eye (denoted I). The averaged experimental results of Rempt et al. (1971) for type IV eyes (circles) and Ferree et al. (1931) for type I eyes (triangles) are shown for comparison. Zero degrees field angle coincides with the optical axis.

The amount of peripheral astigmatism found from 0° to 60° field angle in Kooijman's (1983) eye model and the present type I and type IV eyes are shown in fig. 5.25. There is good agreement with the experimental data of Rempt et al. (1971) for type IV

eyes and Ferree et al. (1931) for type I eyes. The graph also shows that when the modelled peripheral astigmatism is reduced to experimental values found at field angles of 60°, the modelled and experimental values are well matched at smaller field angles as well.
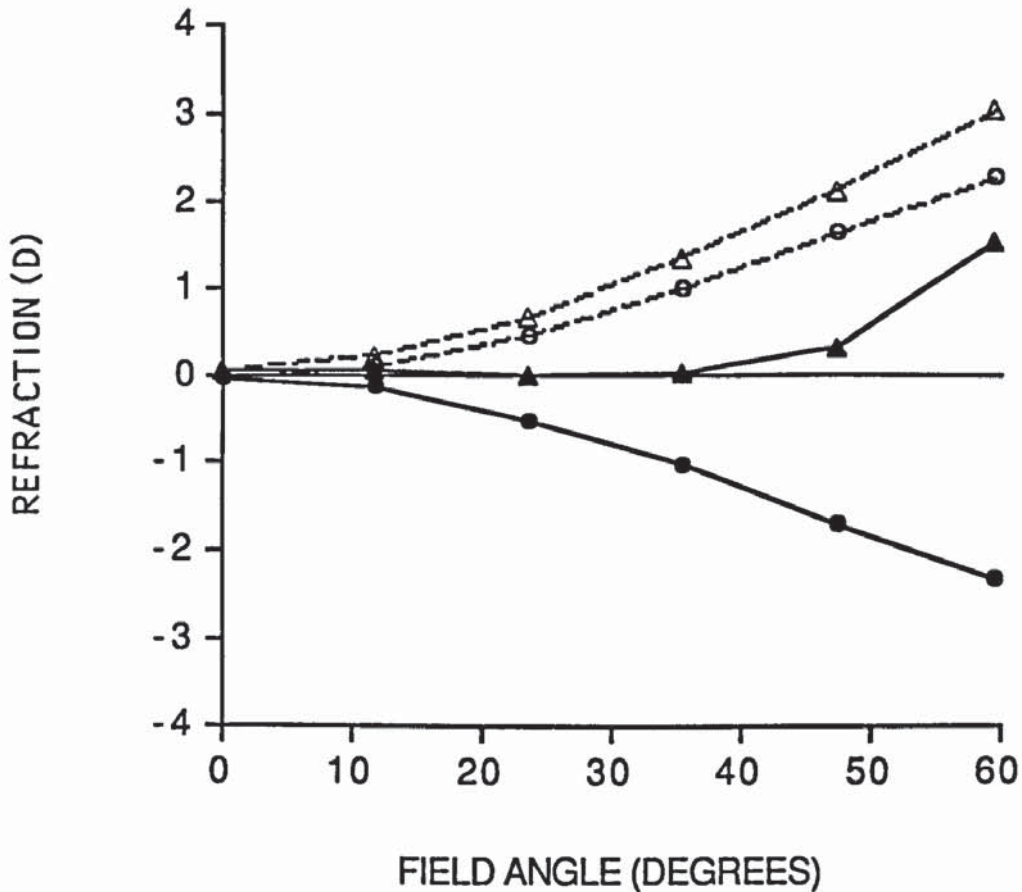
Fig. 5.26 Graph showing the sagittal (broken lines) and tangential (solid lines) peripheral refraction found in the type IV (circles) and type I (triangles) eye models. Both models possess a spherical retina of 13.18 mm. Zero degrees field angle coincides with the optical axis.

In fig. 5.26, the sagittal and tangential image shells are shown for the modelled type I and type IV eye models. A spherical retina of 13.18 mm radius is required so that it lies halfway between both image shells as normally occurs in the emmetropic type IV eye (see section 2.3). This is somewhat flatter than the retina required to do the same for the schematic eye of Kooijman (1983) (see section 5.3.2). This arises because the

method used to reduce the peripheral astigmatism (by altering the conic constant for the anterior crystalline lens surface whilst keeping its apical radius constant) which causes the tangential and sagittal image shells to move towards hyperopia peripherally, the former moving relatively more than the latter. Indeed, Bennett and Rabbetts (1984) found that this also occurs when the corneal surface is treated in the same way and described it as one of the properties of aspheric surfaces (see section 2.4). It is interesting to note that, as a result of this, the type I eye exhibits compound hyperopic peripheral astigmatism (fig. 5.26), as do real type I eyes (see fig. 2.3), when modelled with the same retina used for the type IV eye.

Having produced eye models which give rise to more realistic amounts of peripheral astigmatism, it was naturally of particular interest to find out whether other aspects of the ocular performance could be equally well modelled in the same schematic eyes. One aspect which has recieved some attention in section 2.4, is axial spherical aberration. This was estimated in the eye model of Kooijman (1983) and the present type IV eye, by calculating the difference between central refractive error values arising from a paraxial pupil of 0.1 mm and the values occurring with pupils of successively larger radii. If the refractive error became more myopic with increasing pupil size, the spherical aberration was described as being under-corrected. If it became more hyperopic, the spherical aberration was described as being over-corrected.

Modelled values of the axial spherical aberration were compared with a curve devised by Van Meeteren (1974) to represent typical experimental values. The curve was defined by the equation:

$$\Delta P = 4Ar^2$$

Where ΔP gives the amount of under-corrected axial spherical aberration for a pupillary zone of radius r and the constant $A = 4 \times 10^{-3}$.
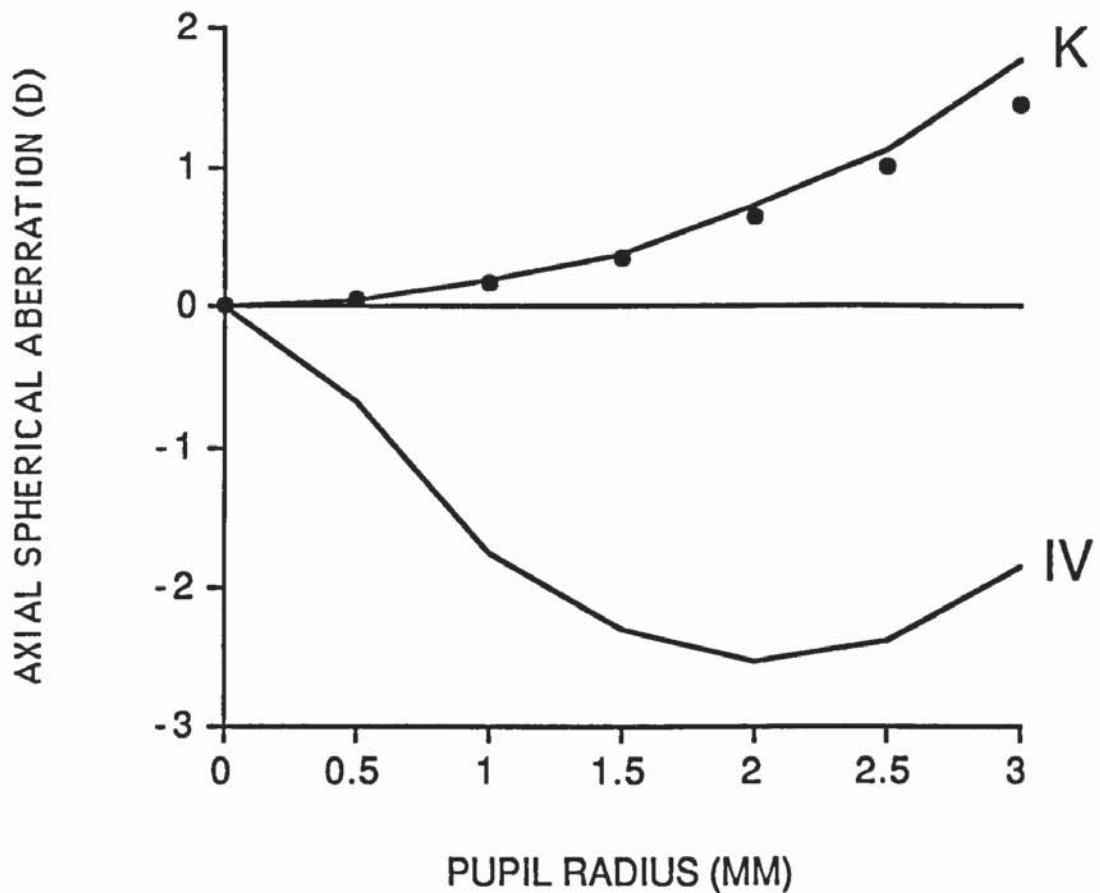
Fig. 5.27 Graph showing the axial spherical aberration for the eye model of Kooijman (1983) (denoted K) and the type IV eye model (denoted IV). Points representing average experimental values (circles) according to the curve of Van Meeteren (1974) are plotted for comparison. Positive and negative values represent undercorrected and overcorrected axial spherical aberration, respectively.

Figure 5.27 shows the spherical aberration found in the schematic eye model of Kooijman (1983) to be of the order found experimentally, represented by the average values of Van Meeteren (1974). The present type IV model, however, yields increasing amounts of over-corrected (negative) spherical aberration up to a pupil diameter of 4 mm, at which point it begins to decrease.

The schematic eyes described in section 2.4 gave rise to the correct amounts of axial spherical aberration but too much peripheral astigmatism. This also happens with Kooijman's (1983) eye model. When the peripheral astigmatism is reduced to more realistic values, as in the present study, over-corrected spherical aberration occurs. Therefore, with the schematic eyes presently available, correction of either aberration occurs at the expense of the other. The inability of these schematic eyes to model both peripheral astigmatism and spherical aberration at the same time limits their capacity to provide a comprehensive evaluation of the optical performance of real eyes.

However, Kooijman's (1983) eye model produces peripheral astigmatic values which are within ± 0.5 D of those measured by Rempt et al. (1971) up to field angles of approximately 30° (see fig. 5.25). This difference is very small when one considers that Rempt et al. (1971) reported differences of between 0.25 D and 0.5 D for estimates of even the central refractive error, measured by different observers, using their retinoscopic method. Therefore, as Kooijman's (1983) eye model also yields the correct spherical aberration (see fig. 5.27), it can be said that it is a useful model for the prediction of optical performance over the central 60° of the visual field.

5.4 OCULAR SURFACE ALIGNMENT AND PURKINJE IMAGE POSITION

(A) THEORY

In section 5.3.1C, various translations and rotations of the cornea and crystalline lens were modelled to demonstrate their effects on peripheral refractive asymmetry. No attempt, however, was made to determine which of these were likely to cause the types of peripheral refractive asymmetry found in real eyes. The reason for this was that corneal and crystalline lens non-alignment produced very much the same results apart

from the fact that more asymmetry occurred the former than the latter. Therefore, without corroborative evidence, it would not have been possible to suggest the relative importance of either in real eyes. Corroborative evidence is, however, provided by Tscherning's (1904) classical observations of the non-alignment of the Purkinje images in real eyes.

Tscherning (1904), using his ophthalmophakometer (see section 3.2.3A), observed that when looking down the subject's line of sight the Purkinje images arising from the anterior (image III) and posterior (image IV) crystalline lens surfaces were displaced nasally and temporally respectively, relative to the Purkinje images arising from the anterior corneal surface (image I) (fig. 5.28).
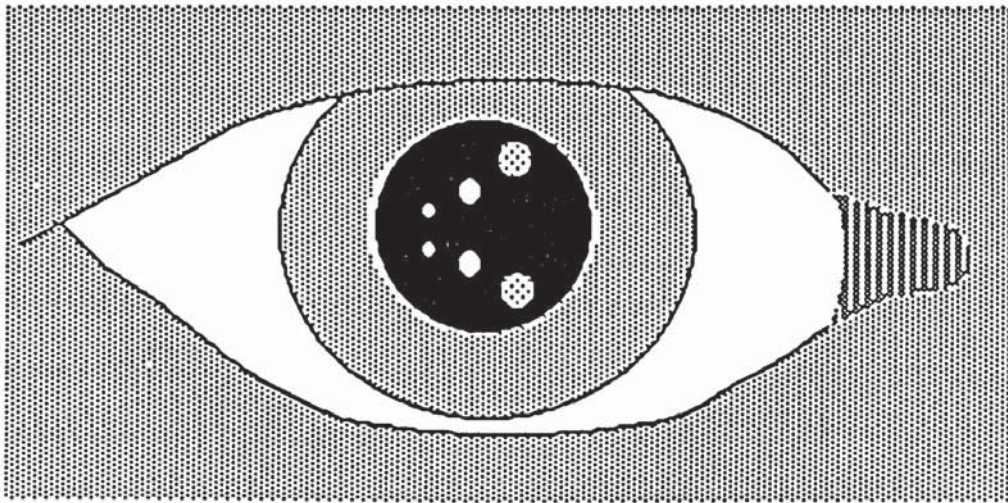
Fig. 5.28   Diagrammatic representation of the position of the Purkinje images as observed down the line of sight by Tscherning (1904). The smallest pair of images are those arising from the posterior crystalline lens surface (IV). The largest pair of images are those arising from the anterior lens surface (III). Between the two of these are the anterior corneal images (I). Purkinje images III and IV lie nasally and temporally with respect to I.

He stated that this non-alignment clearly indicated that the corneal and lenticular surfaces were not centred with respect to the line of sight. In most cases, between 4°

230

and 7° of eye rotation in the nasal direction was required to bring the Purkinje images into alignment (thereby establishing the position of the optical axis in the horizontal plane). The latter angle therefore corresponded with the horizontal component of angle alpha (see section 1.5).

Although, to the present author, the above findings indicate that angla alpha arises due to rotation of the eye temporally with respect to the line of sight, various other workers (e.g. Bennett, 1984; Shipley and Rawlings, 1970) believe that it arises due to approximately 5° rotation of the crystalline lens such that its nasal portion moves closer to the cornea. In this section, the linear algebraic ray tracing program is altered to predict the non-alignment of the Purkinje images that occurs with rotation of the whole eye as well as rotation and translation of the cornea and crystalline lens (Clement et al., 1987 [see appendix 4]).

(B) MODIFICATION OF THE LINEAR ALGEBRAIC RAY TRACING PROGRAM

The program described in section 5.2 (see appendix 3a) was modified in order to calculate the Purkinje image positions.

Ray tracing calculations were based on an observer located 1 m along the direction of the line of sight of the subject's eye, with two lights located 20 cm above and below this line. Image locations were calculated by an iterative procedure in which a ray was traced from the light to the reflecting surface and back towards the observer. The direction of the ray was adjusted in 0.0003° steps until it intersected the vertical plane (representing the observer) located at 1 m from the subject's eye. The apparent location of the image was obtained from the intersection of the returning ray with the front surface of the cornea.

231

The modified program, listed in appendix 3b, is defaulted to the same schematic eye parameters as described in section 5.2.1 except that the surface location parameters are all specified with respect to a system centre positioned at 13.6 mm behind the corneal vertex. The system was centred in the latter position to allow the whole eye to be rotated about its centre of rotation (as defined by Carpenter, 1977), in the horizontal plane only, by entering the angle of rotation required (in degrees). As described in section 5.2.3, if the eye is considered to be pointing to the left a positive angle rotates the eye in an clockwise manner whilst a negative angle rotates it in an anti-clockwise manner. Further alteration of the program was required to perform the corneal and crystalline lens rotations about thair anterior surface vertices.

(C) MODELLED PURKINJE IMAGE POSITIONS
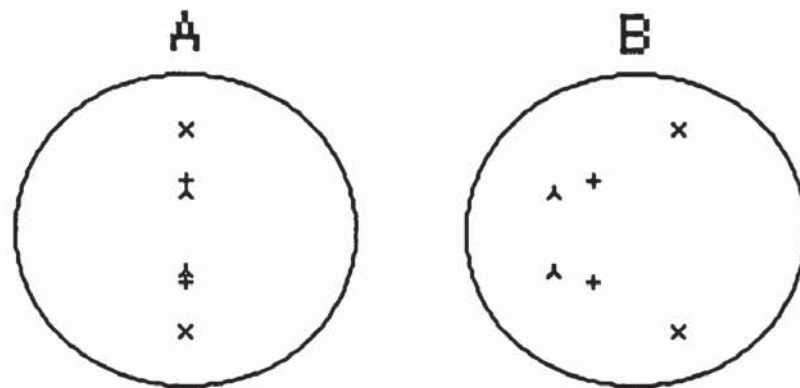
Fig. 5.29   Computer generated diagrams depicting the modelled Purkinje image positions. A - shows the locations of the images with the eye in the straight ahead position. B - shows the locations of the images with the whole eye rotated 5° temporally. Purkinje I images are denoted by "+", Purkinje III images by an "x" and the Purkinje IV images by an inverted "y". The circle corresponds to a pupil size of 5 mm. For the present purposes, the right hand side of each diagram is nasal and the left hand side is temporal (as in fig. 5.28).

The calculated positions of the Purkinje images, with the eye looking straight ahead, are shown in fig. 5.29A. The position of image I is marked with a "+" sign, the position of image III by an "x" and the position of image IV by an inverted "y". The circle around the images corresponds to a pupil size of 5 mm. This circle is only an approximation of the apparent (entrance) pupil in the cases where either the whole eye is rotated or the cornea is rotated or translated.

In fig. 5.29B, the positions of the images after a 5° rotation of the eye temporally are shown. The third images (III) are located nasally and the fourth images (IV) temporally to the first images (I), which is the form of non-alignment that was described by Tscherning (1904) (fig. 5.28).
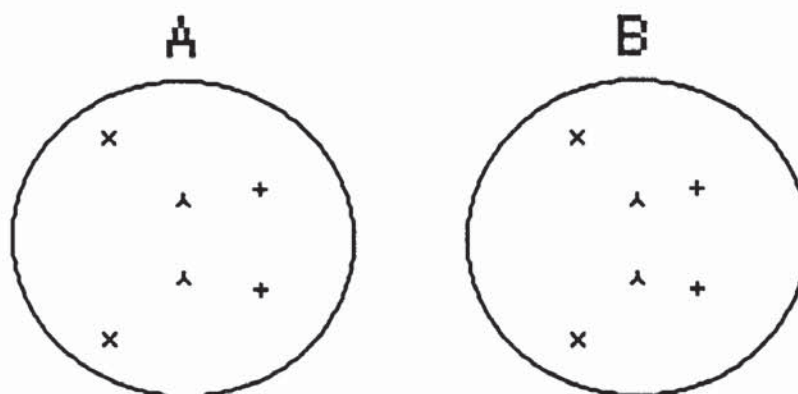
Fig. 5.30   Computer generated diagrams depicting the modelled Purkinje image positions. A - shows the effect of a 1 mm translation of the cornea nasally. B - shows the effect of a 5° rotation of the cornea about its anterior surface vertex so that its nasal side moves forwards. Purkinje I images are denoted by "+", Purkinje III images by an "x" and the Purkinje IV images by an inverted "y". The circle corresponds to a pupil size of 5 mm. For the present purposes, the right hand side of each diagram is nasal and the left hand side is temporal (as in fig. 5.28).

A different form of non-alignment is predicted with translation and rotation of the cornea. Figure 5.30A shows the positions of the images after the cornea has been translated 1 mm nasally and fig. 5.30 B shows the positions of the images after the

233

cornea has been rotated by 5° rotation about its anterior surface vertex so that its nasal side moves forwards. Treating the corneal surface in either way leads to the third (III) and fourth (IV) images being displaced temporally with respect to the first images (I). These do not conform to the types of non-alignment illustrated in fig. 5.28.

The crystalline lens was treated in exactly the same way as the cornea. Figure 5.31A shows the effect of translation and fig. 5.31B the effect of rotation. Whereas translation displaces the third (III) and fourth (IV) images to the nasal side of the first images (I), rotation of the crystalline lens produces the same Purkinje image shifts as shown in fig. 5.28. It must be added, however, that as the lens was rotated about its anterior surface vertex, the rotation of its posterior surface also includes a component of translation, and this has cancelled out some of the effect of the rotation.
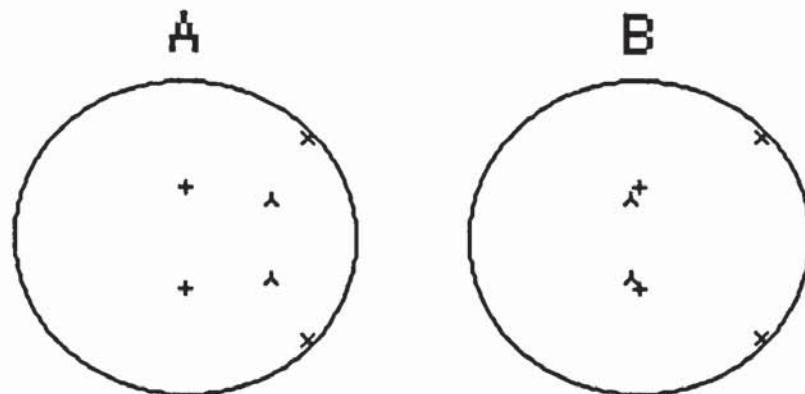
Fig. 5.31   Computer generated diagrams depicting the modelled Purkinje image positions. A - shows the effect of a 1 mm translation of the crystalline lens nasally. B - shows the effect of a 5° rotation of the crystalline lens about its anterior surface vertex so that its nasal side moves forwards. Purkinje I images are denoted by "+", Purkinje III images by an "x" and the Purkinje IV images by an inverted "y". The circle corresponds to a pupil size of 5 mm. For the present purposes, the right hand side of each diagram is nasal and the left hand side is temporal (as in fig. 5.28).

It appears that 5° temporal rotation of the whole eye or 5° nasal rotation of the crystalline lens brings about a similar pattern of Purkinje image displacement to that observed by Tscherning (1904).

In terms of peripheral astigmatic asymmetry, determining the effect of 5° temporal eye rotation only requires the modelled results of a schematic eye with aligned ocular surfaces (figs. 5.4 and 5.5, for example) to be displaced by 5° towards the nasal retina. In this context, Lotmar and Lotmar (1974) found that a symmetric curve, based on the data of Rempt et al. (1971), needed to be displaced by 4° from the line of sight to reproduce the peripheral astigmatic asymmetries found in the experimental data (see section 2.4). Therefore it would appear that eye rotation can explain the existence of angle alpha and hence the non-alignment of the Purkinje images as well as the peripheral astigmatic asymmetry which is observed when taking measurements with respect to the line of sight. Furthermore, the observed decentrations of the corneal apex (see section 1.3.1) and the pupil (see section 1.3.3) are also consistent with the presence of eye rotation.

On the other hand, 5° nasal rotation of the crystalline lens (fig. 5.6) appears to produce peripheral astigmatic asymmetry of the same order as that found in real eyes. Angle alpha also dissappears in aphakic eyes (see section 1.5), suggesting that the crystalline lens is its source. As well as this, crystalline lens rotation produces the types of Purkinje image non-alignment observed by Tscherning (1904). However, Tscherning (1904) suggested that the amount of lens decentration with respect to the cornea was normally negligible. Nevertheless, one cannot be sure as to whether rotation of the whole eye or the crystalline lens is responsible for the optical asymmetries found in the human eye. Indeed both may occur to some extent.

Therefore, although the corroborative evidence provided by observing Purkinje image non-alignment and peripheral astigmatic asymmetry for the causes of optical asymmetry in the human eye indicates that corneal decentration or translation of the various ocular surfaces play a relatively minor role, the relative influences of rotation of the total eye or the crystalline lens cannot be clearly determined.

With regard to the Purkinje images it is interesting to note that the ratios between the heights of Purkinje images, as predicted for the present schematic eye (see fig. 5.29A), are 1 : 2.04 : 0.79 (I : III : IV). The exact ratio reported by Bennett and Rabbetts (1984) for the same schematic eye used in the present study but without aspheric surfaces was 1 : 1.97 : 0.82. The differences between the present values and those predicted by Bennett and Rabbetts (1984) are no greater than 4% and are therefore considered to be negligible. This finding is of great interest as it implies that the determination of apical radii in real eyes by comparison phakometry is little effected when schematic eyes with spherical surfaces are used to perform the ophthalmophakometric calculations (see section 3.2.3).

Bennett and Rabbetts (1984) also pointed out that the technique of comparison phakometry depends upon the Purkinje image light sources being relatively distant. In the case of the ophthalmophakometer described in section 3.2.3B, the light sources were positioned 20 mm away from the test eye which clearly does not satisfy the above condition. Although the light entering the fibre optic cable was collimated, it is unlikely that the same could be said for light emerging from it. For this reason, the Purkinje image heights were modelled for the schematic eye in the straight ahead position (as shown in fig. 5.29A) but with the light sources positioned 6 mm apart and 20 mm in front of the eye. The ratios found were 1 : 2.06 : 0.81, the values of which differed by no greater than 3% of those previously quoted for Purkinje image light

sources positioned 1 m away. This difference was thus considered to be negligible.

5.5 SUMMARY

From the literature reviewed in chapter 2, it was proposed that the main factors effecting peripheral refraction are the asphericity of the components of the refracting system, the symmetry of action of the refracting system as well as the shape and position of the retina. The best way to discuss the modelled results, presented in this chapter, would be to compare the relative influences of each of these factors in the five patterns of peripheral refraction described by Rempt et al. (1971) (see fig. 2.3).

The type IV peripheral refractive pattern represents the normal condition (see section 2.3). It has been found that a schematic eye constructed from typical ocular components, including representative aspheric surfaces, produces the type IV pattern. Such a model also produces peripheral astigmatic values which are of the order found experimentally within the central 60° of the visual field. Realistic peripheral astigmatic values have been modelled at larger field angles (fig. 5.25) by introducing considerable amounts of peripheral flattening to the anterior crystalline lens surface. This, however, gives rise to over-corrected spherical aberration (fig. 5.27).

Large amounts of aspheric flattening of the anterior crystalline lens surface are able to produce the low values of peripheral astigmatism and the peripheral hyperopic shifts of the sagittal and tangential image shells which characterise the type I eye (fig. 5.26). Although the required lens surface changes appear to be somewhat unrealistic (fig. 5.24), the results at least show the kind of subtle optical surface changes that are required to produce this kind of peripheral refractive pattern.

It would appear that differences in retinal shape and position are largely responsible for the type II and type V peripheral refraction forms (fig. 5.18). The results indicate that type II eyes may be produced by a prolate ellipsoidal retinal surface whilst an oblate ellipsoidal retina might give rise to an eye of the type V form. A spherical retina lies approximately half way between the sagittal and tangential image shells as in the type IV eye.

The corroborative evidence provided by modelling the types of Purkinje image non-alignment which occur with various translations and rotations of the cornea and crystalline lens suggests that small amounts of peripheral refractive asymmetry, normally present in human eyes, arise due to either temporal rotation of the whole eye or rotation of the crystalline lens such that its nasal side moves forward (fig. 5.6).

The type III eye, which exhibits more extreme amounts of peripheral refractive asymmetry, may be the result of combined rotation of the whole eye and the crystalline lens or where the rotation of either one is more exaggerated. However, 1 mm nasal translation (fig. 5.9) or 5° rotation (fig. 5.8) of the cornea gives rise to the very large amounts of peripheral refractive asymmetry indicating that a non-aligned cornea may be responsible. The Purkinje image displacement that occurs with this (fig. 5.30) is quite characteristic and, therefore, could possibly be used to determine whether the cornea is actually involved.

The limitations of the present linear algebraic ray tracing program (appendix 3a) are that it only considers aspheric surfaces of the quadric form. It also does not include the gradient index optical nature the crystalline lens and performs a limited number of rotations (though it is capable of an infinite variety of surface translations). Nevertheless, the flexibility of the linear algebraic ray tracing program is illustrated by

its ability to generate every form of peripheral refractive pattern that has been measured in real eyes. This flexibility can be extended to the modelling of peripheral refraction in real eyes whose biometric components are known by following the scheme outlined below:

(1) Input surface curvatures, surface locations, and pupil size in accordance with the values measured. Manipulation of the surface curvature parameters can give rise to an astigmatic surface if required (see section 5.2.1A).

(2) Input required refractive indices.

(3) Model correct amount of peripheral astigmatism and central refraction by altering crystalline lens anterior surface curvature and refractive index values using the procedure described in section 5.3.3.

(4) Model correct disposition of sagittal and tangential image shells by altering retinal curvature as described in section 5.3.2.

(5) Model correct amount of peripheral astigmatic asymmetry by using either one or a combination of the following:
(i) rotating crystalline lens (see section 5.2.3);
(ii) simulating total eye rotation by adding a correction factor to the field angle values given in the peripheral refractive results [The latter technique was used by Le Grand (1967) and Lotmar and Lotmar (1974) (see section 2.4)];
(iii) translating any of the ocular surfaces.

In chapter 6 the above scheme is applied to the real eye data described in chapter 4.

CHAPTER SIX

APPLICATION OF THE COMPUTING SCHEME

FOR MODELLING PERIPHERAL REFRACTION

IN REAL EYES

6.1 INTRODUCTION

In this chapter, the computing scheme outlined in section 5.5 is applied to the real eye data described in chapter 4.

Before applying this scheme, however, it is necessary to consider the problems which arise concerning the need for an optical system which is centred upon an optical axis, to facilitate schematic eye construction, and the conflicting requirement for ocular measurements to be made with respect to the line of sight (see section 3.5).

One problem is that the peripheral refractive results exhibit a certain degree of asymmetry (see section 4.3). This is overcome by constructing symmetrical curves from the measured data to provide a basis for schematic modelling (adopting approximately the same approach as described by Lotmar and Lotmar, 1974 [see section 2.4]).

Next is the problem of residual astigmatism (see section 4.4). Although the differences between corneal and ocular astigmatism may be due to the posterior corneal surface (see section 1.3.1) or either of the crystalline lens surfaces (see section 1.3.4), the influence of these is assumed to be negligible. In any case, the schematic eye used in this study neglects the posterior corneal surface (see section 3.3B). The anterior corneal surface is therefore manipulated to account for the observed residual astigmatism.

Finally, schematic eyes were constructed in the vertical plane whilst peripheral refractive readings were obtained in the horizontal plane (see section 3.5). However, as the lenticular refracting surfaces were assumed to possess no astigmatism, their

curvatures in the horizontal and vertical planes are equal. As the curvature of the anterior corneal surface was measured in both planes, the schematic eyes could be specified with respect to the horizontal plane.

By applying the proposed computing scheme an attempt is made to assess the usefulness of peripheral refractive measurements, made in conjunction with measurements of the ocular dimensions, for yielding extra information regarding ocular surface asphericities, retinal contour and the amount of non-alignment of the whole eye and its components. Indeed, the comment made by Ferree and Rand (1933) still holds today, that some of this information is obtainable by no other in vivo technique presently known.

6.2 INITIAL TREATMENT OF THE DATA MEASURED IN REAL EYES

6.2.1 SPECIFICATION OF DATA WITH RESPECT TO THE PUPILLARY AXIS

(A) THEORY

A considerable mathematical problem occurs due to the presence of residual astigmatism as the astigmatism arising from the corneal surface does not correspond with the central refractive values (see section 4.4). The research evidence previously discussed, however, provides a convenient and valid way of reconciling the data.

There is considerable evidence to suggest that the eye is approximately centred about the pupillary axis, which is considered to be acceptable as a "working optical axis", and is rotated by approximately 5° temporally with respect to the line of sight. As all ocular measurements were made with respect to the line of sight, it follows that

242

asymmetry and nasal decentration of peripheral refractive data is to be expected. The effectively rotated aspheric corneal surface would also give rise to residual astigmatism (see sections 1.5 and 1.6). Therefore, one simply needs to re-specify the ocular measurements with respect to the pupillary axis. The latter would give rise to new values for the central refraction and corneal curvature.

Although the above treatment assumes, as a first approximation, that the observed asymmetry is entirely due to eye rotation, the effects of rotation of either the whole eye or the crystalline lens or a combination of both are investigated in a later stage of the computing scheme. The present section considers the initial treatment of the central and peripheral refractive data as well as the corneal curvature.

(B) CONSTRUCTING SYMMETRICAL PERIPHERAL REFRACTIVE CURVES

Lotmar and Lotmar (1974) averaged the peripheral refractive data of Rempt et al. (1971) over corresponding nasal and temporal field angles and fitted a symmetrical curve to the results. Approximately the same approach was adopted in the present study. The peripheral refraction at 10°, 20°, 30° and 40° over the nasal and temporal retina were averaged. Fourth-order polynomial curves were found to produce the best fit to the averaged data. Values predicted by these curves for zero degrees field angle were taken to be the new central refractive error values as specified with respect to the pupillary axis.

For near-emmetropic eyes (see section 4.3), polynomial curves fitted to the averaged sagittal refractive data, S(e), tangential refractive data, T(e), and astigmatic data, Δ(e), for field angles, A, of between 0° and 40° are :

$$S(e) = -0.1856 + (6.130303 \times 10^{-4}. A^2) + (1.055 \times 10^{-7}. A^4)$$

$$T(e) = -0.0892 + (-2.6671212 \times 10^{-3}. A^2) + (6.548 \times 10^{-7}. A^4)$$

$$\Delta(e) = -0.0964 + (3.2801515 \times 10^{-3}. A^2) + (-5.494 \times 10^{-7}. A^4)$$

The first term in each of the above equations represents the new central refractive values. Expressing these results to two decimal places shows that the central refraction in the sagittal plane is -0.19 D whilst that in the tangential plane is -0.09 D. Therefore (0.19 - 0.09 =) 0.1 D of with-the-rule astigmatism exists, which is in very good agreement with the central astigmatism predicted by the polynomial curve for $\Delta(e)$. This value is negative which indicates with-the-rule astigmatism. Against-the-rule astigmatism is indicated by a positive value.

		RETINAL FIELD ANGLE (A)			
REFRACTION	0°	10°	20°	30°	40°
SAGITTAL (D)					
Averaged value	-	-0.14	0.11	0.43	1.07
S(e)	-0.19	-0.12	0.08	0.45	1.07
TANGENTIAL (D)					
Averaged value	-	-0.35	-1.05	-1.96	-2.68
T(e)	-0.09	-0.35	-1.05	-1.96	-2.68
ASTIGMATISM (D)					
Averaged value	-	0.21	1.16	2.39	3.75
$\Delta(e)$	-0.10	0.23	1.13	2.41	3.75

Table 6.1   Comparison between the sagittal, S(e), tangential, T(e), and astigmatic, $\Delta(e)$, values produced by the symmetrical polynomial curves fitted to the data collected from near-emmetropic eyes (see section 4.3) and averaged over corresponding nasal and temporal retinal field angles (A).

That the central results of each independently fitted polynomial curve agree so well gives some indication as to the accuracy of this technique. As a further estimate of its validity, table 6.1 compares the values produced by the polynomial curves with those

244

obtained from the experimental data for near-emmetropic eyes.

Applying the same procedure to the results obtained from the myopic eyes (see section 4.3), polynomial curves fitted to the averaged sagittal refractive data, S(m), tangential refractive data, T(m), and astigmatic data, Δ(m), for field angles, A, of between 0° and 40° are:

$$S(m) = -3.1584 + (1.8801515 \times 10^{-3}.A^2) + (-1.827 \times 10^{-7}.A^4)$$

$$T(m) = -3.3312 + (-1.11466667 \times 10^{-3}.A^2) + (4.533 \times 10^{-7}.A^4)$$

$$\Delta(m) = 0.1728 + (3.0268182 \times 10^{-3}.A^2) + (-6.361 \times 10^{-7}.A^4)$$

Table 6.2 compares the values produced by these polynomial curves with those obtained from the experimental data for myopic eyes.

		RETINAL FIELD ANGLE (A)			
REFRACTION	0°	10°	20°	30°	40°
SAGITTAL (D)					
Averaged value	-	-3.00	-2.38	-1.65	-0.61
S(m)	-3.16	-2.97	-2.44	-1.61	-0.62
TANGENTIAL (D)					
Averaged value	-	-3.46	-3.68	-4.02	-4.00
T(m)	-3.33	-3.44	-3.72	-4.00	-4.01
ASTIGMATISM (D)					
Averaged value	-	0.46	1.30	2.37	3.39
Δ(m)	0.17	0.47	1.28	2.38	3.39

Table 6.2   Comparison between the sagittal, S(m), tangential, T(m), and astigmatic, Δ(m), values produced by the symmetrical polynomial curves fitted to the data collected from myopic eyes (see section 4.3) and averaged over corresponding nasal and temporal retinal field angles (A).

Finally, with regard to the results collected from the hyperopic eyes (see section 4.3), polynomial curves fitted to the averaged sagittal refractive data, S(h), tangential refractive data, T(h), and astigmatic data, Δ(h), for field angles, A, of between 0° and 40° are :

$$S(h) = 1.4788 + (6.169697 \times 10^{-4}. A^2) + (7.45 \times 10^{-8}. A^4)$$

$$T(h) = 1.5968 + (-2.5224242 \times 10^{-3}. A^2) + (6.836 \times 10^{-7}. A^4)$$

$$\Delta(h) = -0.118 + (3.1393939 \times 10^{-3}. A^2) + (-6.091 \times 10^{-7}. A^4)$$

Table 6.3 compares the values produced by the above polynomial curves to those obtained from the experimental data for hyperopic eyes.

	RETINAL FIELD ANGLE (A)				
REFRACTION	0°	10°	20°	30°	40°
SAGITTAL (D)					
Averaged value	-	1.53	1.76	2.08	2.66
S(h)	1.48	1.54	1.74	2.09	2.66
TANGENTIAL (D)					
Averaged value	-	1.25	0.90	-0.25	-0.66
T(h)	1.60	1.35	0.70	-0.12	-0.69
ASTIGMATISM (D)					
Averaged value	-	0.28	0.86	2.33	3.32
Δ(h)	-0.12	0.19	1.04	2.21	3.35

Table 6.3   Comparison between the sagittal, S(h), tangential, T(h), and astigmatic, Δ(h), values produced by the symmetrical polynomial curves fitted to the data collected from hyperopic eyes (see section 4.3) and averaged over corresponding nasal and temporal retinal field angles (A).

Construction of symmetrical peripheral refractive curves facilitates the modelling of correct amounts of peripheral astigmatism and image shell dispositions. It also enables an accurate estimate to be made of the refractive findings at any specified field angle.

246

This is particularly useful as the computer printout does not necessarily specify the modelled results with respect to the same field angles at which the original refractive data were taken. The new central refractive values are another outcome of the symmetrical curves and, because they are assumed to represent the refractive findings which occur along the pupillary axis, they provide the basis upon which the corneal surfaces are altered.

(C) ALTERATION OF THE ANTERIOR CORNEAL CURVATURE

As already explained, the corneal surfaces need to be re-specified with respect to the pupillary axis which, by definition, coincides with their apices. The astigmatism arising from the corneal surface should then equal the ocular astigmatism found along the same axis. Although it is not possible to work back to the true apical radii, given the information that is available, an approximation can be made if one carefully considers the information that is at hand in the light of previous research evidence.

The difference between the horizontal and vertical central corneal radii for the averaged near-emmetropic, myopic and hyperopic eyes were 0.08 mm (0.43 D), 0.08 mm (0.43 D) and 0.09 mm (0.51 D) respectively (see section 4.4) (calculations of corneal power were made assuming a corneal refractive index of 1.3374). As the corneae were all flattest in the horizontal plane, the above values represent with-the-rule astigmatism. A comparison between these values and the ocular astigmatism calculated in section 6.2.1B for near-emmetropic eyes (0.10 D with-the-rule), myopic eyes (0.17 D against-the-rule) and hyperopic eyes (0.12 D with-the-rule) indicates that the corneal surfaces give rise to too much astigmatism and, in the case of the averaged myopic eye, the incorrect axis of astigmatism.

These results are in good accord with the comments of Ludlam and Wittenberg (1966a, b) who believed that measurements made with respect to the line of sight could lead to over-estimated corneal astigmatism (see section 1.3.1). Indeed, experimental evidence for this was provided by Ludlam et al. (1967) and Mandell and St. Helen (1969). Mandell and St Helen (1969) also found that the corneal curvature was steeper at the apex than at the line of sight and that the most marked differences occured in the horizontal plane.

It seemed justifiable, therefore, as an approximation at least, to average the horizontal and vertical corneal radii values and then to alter the mean value by an equal amount in each meridian, in order to account for the calculated ocular astigmatism. This would reduce the corneal astigmatism and steepen the horizontal corneal curvature in keeping with the research evidence. On the other hand, the vertical corneal curvature would become flatter which is not in agreement with previous research findings. Horizontal and vertical corneal conic constant values were also averaged but addition of the required amount of astigmatism, using the procedure described above, was not easily performed. Instead, astigmatism was accounted for by alterating the conic constant values by the same proportional amount as the radii values.

The new corneal curvature values, calculated using the above procedure, are shown in table 6.4 and are taken to represent the corneal curvature along the pupillary axis. The corneal radius and conic constant values shown in table 6.4 are resolved to the vertical and horizontal meridians (in the manner described by Bennett and Rabbetts, 1984) and are specified to six decimal places (as recommended by Smith, 1966, for ray tracing purposes).

REFRACTIVE	RADIUS (mm)		CONIC CONSTANT (P)	
GROUP	Horizontal	Vertical	Horizontal	Vertical
NEAR-EMMETROPE:				
Line of sight	7.979976	7.900024	0.740021	0.809979
Pupillary axis	7.949354	7.930668	0.774735	0.775265
MYOPE:				
Line of sight	7.909938	7.830062	0.700023	0.729977
Pupillary axis	7.854427	7.885634	0.715565	0.714435
HYPEROPE:				
Line of sight	7.780000	7.690000	0.780000	0.860000
Pupillary axis	7.745654	7.724375	0.819752	0.820248

Table 6.4   Comparison between the original horizontal and vertical corneal radius and conic constant values, specified with respect to the line of sight, and the new values calculated to represent the corneal curvature along the pupillary axis.

In table 6.4, the required alteration to the corneal radii values never exceeded 0.06 mm (0.30 D). Calculations of corneal power were made assuming a corneal refractive index of 1.3374. Mandell and St Helen (1969) reported curvature differences comparing measurements taken down the line of sight and the pupillary axis (corneal apex) of 0.36 D horizontally and 0.13 D vertically. Therefore, the changes made in the present study fall within those found by Mandell and St Helen (1969).

6.2.2 RE-CALCULATION OF BASIC SCHEMATIC EYES

Having altered the corneal curvature and central refractive data to produce values which were at least representative of those occurring along the pupillary axis, it became possible to recalculate the crystalline lens surface radii with respect to the same axis. For this purpose, the axial distances and Purkinje image heights used were the same as shown in table 4.13.

The question arises as to whether the axial distance and Purkinje image data should have been altered to represent values taken down the pupillary axis. However, as the present author was unable to determine exactly whether the ultrasonic transducer was aligned to the line of sight or the pupillary axis, the assumption was made that axial distance measurements taken down either would show no significant difference (see section 3.2.2B). Also, because the Purkinje image heights were not measured along any specific axis (see section 3.2.3B), there would have been no basis upon which any alteration to their values could have been made.

| PARAMETER | SCHEMATIC EYES (VERTICAL MERIDIAN) | | |
	Near-Emmetrope	Myope	Hyperope
ASSUMED REFRACTIVE INDICES:			
Aqueous	1.3374	1.3374	1.3374
Crystalline lens	1.42	1.42	1.42
Vitreous	1.336	1.336	1.336
AXIAL DISTANCES:			
Anterior chamber depth (mm)	3.87	3.93	3.49
Lens thickness (mm)	3.56	3.44	3.75
Vitreous length (mm)	16.52 (16.71)	17.74 (17.86)	15.33 (15.40)
Axial length (mm)	23.95 (24.15)	25.11 (25.23)	22.57 (22.64)
SURFACE RADII:			
Resolved cornea (mm)	7.93	7.89	7.72
Anterior crystalline lens (mm)	9.32	9.73	8.78
Posterior crystalline lens (mm)	-5.92 (-6.35)	-5.97 (-6.20)	-5.6 (-5.75)
SURFACE POWER:			
Resolved cornea (D)	42.54	42.79	43.67
Anterior crystalline lens (D)	8.86	8.49	9.41
Posterior crystalline lens (D)	14.19 (13.23)	14.05 (13.54)	15 (14.59)
Equivalent lens (D)	22.74 (21.80)	22.26 (21.76)	24.04 (23.64)
Total eye (D)	60.97 (60.25)	60.79 (60.40)	63.25 (62.94)
REFRACTIVE ERROR:			
Resolved refraction (D)	-0.19	-3.16	1.48

Table 6.5   Schematic eyes re-calculated in the vertical meridian with the altered corneal and central refractive data. The figures calculated using routine 2 are shown in brackets next to those derived using routine 1 (see section 3.3B for explanation of routines). Comparison of the latter values serves as an "internal validation check".

Table 6.5 shows the re-constructed schematic eyes calculated using the computer program described in section 3.3B. These values can be compared with those calculated in table 4.14. As mentioned in section 4.5, the "internal validation check" compares the results calculated using ultrasonically determined axial lengths (routine 1) with those which give rise to calculated axial lengths (routine 2) to assess the accumulated error. In table 6.5, differences between measured and calculated axial lengths ranged from 0.07 to 0.20 mm while differences in the estimated powers of the posterior lens surface, equivalent lens and total eye ranged from 0.31 D to 0.96 D. Although the above differences are approximately twice the value of those found in section 4.5, they are still very small considering the many assumptions made to derive the altered corneal and central refractive values.

The difference between the re-calculated crystalline lens surface radii (table 6.5) and the values given in table 4.14 ranged from 0.04 mm to 0.21 mm. Differences that occurred for the powers of the crystalline lens surfaces, the equivalent lens and the total eye ranged from 0 D to 0.54 D. It is perhaps worth noting that these differences were of the same order as the accumulated errors demonstrated using the "internal validation check". Therefore, even if the procedure adopted for re-specifying the ocular components with respect to the pupillary axis is open to question, the effective change to the ocular components does not even exceed the range of experimental uncertainty.

6.3 APPLICATION OF THE LINEAR ALGEBRAIC COMPUTING SCHEME

The schematic eye components shown in table 6.5 (derived using an ultrasonically determined axial length) formed the basis upon which more sophisticated eye models were constructed using the computing scheme proposed in section 5.5. In this section

the computing scheme is applied.

6.3.1 INPUT OF SURFACE PARAMETERS AND PUPIL SIZE

This section represents the first step in the computing scheme. Conversion of the surface apical radii, conic constant values and axial separations to the notation required for the linear algebraic ray tracing program (see section 5.2) is fully described in section 5.2.1.

(A) INPUT OF ASTIGMATIC CORNEAL SURFACES

As explained in section 5.2.1A, surface curvatures were defined in terms of three radius values; one in the Z direction (measured along the optical axis) and one in the X and Y directions (measured perpendicularly to the optical axis). For simplicity, if the radius of curvature in the X direction defines the horizontal value and Y the vertical value, it follows that when the latter are equal then the surface is rotationally symmetrical and possesses no astigmatism. Conversely, the values of X and Y are unequal for an astigmatic surface.

Although the above method of defining an astigmatic surface provided no difficulty, a problem occurred with respect to the corneal surfaces as their horizontal and vertical cross-sections (see section 6.2.1C) were defined in terms of separate apical radii and conic constant values. These not only gave rise to unequal radii in the X and Y directions but also yielded two values for the radius in the Z direction. As only one value for Z can be specified for a single surface, the latter produced an impossible situation.

To rectify the problem, surface curvature parameters Z and X, as defined by the horizontal corneal apical radius and conic constant values, were left unchanged. In the vertical plane, however, new curves were calculated which shared the same Z surface curvature parameters as specified in the horizontal plane and produced almost identical profiles to those defined by the original vertical corneal surface radius and conic constant values. The method employed to calculate the new curves was very cumbersome and is therefore only demonstrated on the corneal results for the averaged near-emmetropic eyes.

In the horizontal plane, the corneal apical radius r = 7.949354 mm and the conic constant P = 0.774735. The surface curvature parameters arising from these values were Z = 10.260739 mm and X = 9.031403 mm. In the vertical plane, r = 7.930668 mm and P = 0.775265 which gave rise to surface curvature parameters of Z = 10.229622 mm and Y = 9.007094 mm. As can be seen, two different values for Z occurred. Because the horizontal corneal values were to remain unchanged, a new vertical curve was required which matched the curve profile of the original vertical corneal parameters and for which Z = 10.260739 mm.

Experimental attempts to fit new curves to the vertical corneal data showed that more accurate results were produced if the corneal area matched was as small as possible. In keeping with this, an area of no larger than the measured entrance pupil was considered as the edges of the latter marked the most extreme positions of the marginal rays during ray tracing. As the diameter of the entrance pupil was 4.2 mm (see section 4.4) the new curve was matched out to a distance of (4.2 + 2 =) 2.1 mm.

By rearranging equation (1) in section 5.2.1A, the following expression was derived:

$$y = \sqrt{2xr} - P x^2 \qquad (5)$$

253

where x and y are intersection coordinates measured along and perpendicular to the optical axis respectively. Using this expression, it was found that the original vertical corneal apical radius, r, and conic constant, P, predicted a corneal surface height of nearly 2.1 mm (y = 2.165335 mm) at a distance, x, of 0.3 mm behind the corneal vertex. The new ellipsoidal surface was calculated by finding a value for the surface curvature parameter Y which, in conjunction with Z = 10.260739 mm, produced a surface of the same height at the same distance along the optical axis.

In order to carry out the above calculations, different values of Y were tested. For each Y value, a new conic constant, P, was determined using equation (3) as described in section 5.2.1A:

$$P = (Y + Z)^2.$$

A new value for the apical radius, r, was then calculated using the following equation derived by rearranging equation (1) shown in section 5.2.1A:

$$r = (Y^2 + P\ Z^2) \div 2Z \qquad (6),$$

where intersection coordinates x and y are replaced by surface curvature parameters Z and Y respectively. Finally, using the new values of r and P, the height, y, of the surface produced was calculated for a distance of x = 0.3 mm along the optical axis by applying equation (5) previously described.

To avoid the need for unnecessary calculations, a linear expression was derived from test values of Y = 8 mm, 9 mm and 10 mm and the corresponding y intersection coordinates produced by them for x = 0.3 mm:

$$Y = 4.166y.$$

As the required value of y was 2.165335 mm, this equation predicted a new surface curvature parameter Y = 9.020786 mm.

254

As an estimate of the closeness of fit (Vo - Vn) of the new vertical corneal curve (Vn) to the original (Vo), table 6.6 shows values of the y intersection coordinates calculated for a set of x intersection coordinate values ranging from 0.05 mm to 0.3 mm in 0.05 mm steps. Intersection coordinate y values are also shown for the horizontal corneal curve (H) to indicate the closeness of the horizontal and vertical corneal intersection coordinates (H - Vo) in this region. The values shown in table 6.6 were calculated using equation (5).

DISTANCE ALONG OPTIC AXIS (x / mm)	DISTANCE PERPENDICULAR TO OPTIC AXIS (y / mm)				
	H	Vo	Vn	(H - Vo)	(Vo - Vn)
0.05	0.890507	0.889454	0.889458	0.001053	0.000004
0.10	1.257828	1.256336	1.256346	0.001492	0.000010
0.15	1.538631	1.536801	1.536819	0.001830	0.000018
0.20	1.774477	1.772359	1.772387	0.002118	0.000028
0.25	1.981483	1.979111	1.979149	0.002372	0.000038
0.30	2.167928	2.165335	2.165381	0.002539	0.000046

Table 6.6 Values of the x intersection coordinates (measured along the optic axis) and the y intersection coordinates (measured perpendicular to the optic axis) calculated, using equation (5), for the horizontal corneal curve (H), the original vertical corneal curve (Vo) and the new vertical corneal curve (Vn). Differences between the new and old vertical curves (Vo - Vn) are shown along with differences between the original horizontal and vertical values (H - Vo).

It can be seen, from table 6.6, that the new vertical corneal curve (Vn) matches the original curve (Vo) to at least four decimal places giving rise to a difference (Vo - Vn) of no greater than 0.00005 mm. The latter shows that this manner of curve fitting produces excellent results. It is worth mentioning, however, that the differences between the horizontal and vertical corneal readings (H - Vo) range between 0.001 mm and 0.003 mm.

This procedure was repeated for the myopic and hyperopic corneae (see table 6.4), the results of which are summarised in table 6.7 in terms of the required X, Y and Z surface curvature parameters. Also shown, in table 6.7, are the corneal surface location $\overline{Z}$ parameters which are specified with respect to the anterior crystalline lens surface (see section 5.2.1B).

CORNEAL SURFACE PARAMETERS	REFRACTIVE GROUP		
	Near-emmetrope	Myope	Hyperope
CURVATURE (mm):			
X	9.031403	9.285172	8.554938
Y	9.020786	9.304597	8.542412
Z	10.260739	10.976539	9.448777
LOCATION (mm):			
$\overline{Z}$	-6.390739	-7.046539	-5.958777

Table 6.7   Near-emmetropic, myopic and hyperopic astigmatic corneal surface parameters specified in terms of their curvatures in the X, Y and Z directions. Z is measured along the optical axis whilst X and Y are measured perpendicularly to the optical axis in the horizontal and vertical planes respectively. Also shown are the corneal surface location $\overline{Z}$ parameters which are specified with respect to the anterior crystalline lens surface (see section 5.2.1B).

(B) INPUT OF CRYSTALLINE LENS SURFACES

In the absence of any data regarding the crystalline lens surface asphericities, the conic constant values used by Kooijman (1983) (see section 5.2.1C), giving rise to hyperbolic anterior and parabolic posterior lens surfaces, were adopted. These were combined with the anterior and posterior crystalline lens apical radii derived using an ultrasonically determined axial length, shown in table 6.5. Conversion of the values to X, Y and Z surface curvature parameters and $\overline{Z}$ surface location parameters (specified with respect to the anterior crystalline lens surface vertex) was carried out using the

same procedure described in section 5.2.1C. Special considerations required for the calculation of these surface parameters, inluding the use of vector B for the posterior surfaces, are also described in section 5.2.1C. The calculated surface parameters are shown in table 6.8. As the crystalline lens surfaces were assumed to possess no astigmatism (see section 6.1), the X and Y surface curvature parameters are equal.

CRYSTALLINE LENS SURFACE PARAMETERS	REFRACTIVE GROUP		
	Near-emmetrope	Myope	Hyperope
ANTERIOR SURFACE CURVATURE (mm):			
X	-6.479617	-6.758310	-6.131251
Y	-6.479617	-6.758310	-6.131251
Z	4.514563	4.708738	4.271845
LOCATION (mm):			
$\bar{Z}$	4.514563	4.708738	4.271845
POSTERIOR SURFACE CURVATURE (mm):			
X	1	1	1
Y	1	1	1
Z	0	0	0
Vector B	11.8	12	11.2
LOCATION (mm):			
$\bar{Z}$	-3.56	-3.44	-3.75

Table 6.8   Near-emmetropic, myopic and hyperopic anterior (hyperbolic) and posterior (parabolic) crystalline lens surface parameters specified in terms of their curvatures in the X, Y and Z directions. Z is measured along the optical axis whilst X and Y are measured perpendicularly to the optical axis in the horizontal and vertical planes respectively. The special considerations required for the calculation of these surface parameters, including the use of vector B for the posterior surfaces, are described in section 5.2.1C. Also shown are the crystalline lens surface location $\bar{Z}$ parameters which are specified with respect to the anterior crystalline lens surface.

(C) INPUT OF RETINAL SURFACE PARAMETERS

At this stage, the retina in each of the eyes was assumed to be spherical and of 12 mm radius. Table 6.9 shows the inital X, Y and Z retinal surface curvature parameters along with the surface location $\overline{Z}$ parameters which were calculated (see section 5.2.1C) to take into account the axial length variations measured in the near-emmetropic, myopic and hyperopic eyes (see table 6.5) when specified with respect to the anterior crystalline lens surface.

RETINAL SURFACE PARAMETERS	REFRACTIVE GROUP		
	Near-emmetrope	Myope	Hyperope
CURVATURE (mm):			
X	12	12	12
Y	12	12	12
Z	12	12	12
LOCATION (mm):			
$\overline{Z}$	-8.08	-9.18	-7.08

Table 6.9 Near-emmetropic, myopic and hyperopic retinal surface parameters specified in terms of their curvatures in the X, Y and Z directions. Z is measured along the optical axis whilst X and Y are measured perpendicularly to the optical axis in the horizontal and vertical planes respectively. Also shown are the retinal surface location $\overline{Z}$ parameters which are specified with respect to the anterior crystalline lens surface.

(D) MATRIX FORMULATION FOR INITIAL OCULAR PARAMETERS

The non-zero components of the matrix formulation (see section 5.2.1C) for the initial ocular surface parameters, calculated in sections 6.3.1A, B and C for near-emmetropic, myopic and hyperopic eyes, are given in table 6.10.

SURFACE	A(1,1)	A(2,2)	A(3,3)	B(3)	c	T(3)
NEAR-EMMETROPES:						
CORNEA	0.012260	0.012289	0.009498	0	-1	-6.390739
FRONT LENS	-0.023818	-0.023818	0.049065	0	-1	4.514563
BACK LENS	1.000000	1.000000	0.000000	11.8	0	-3.56
RETINA	0.006944	0.006944	0.006944	0	-1	-8.08
MYOPES:						
CORNEA	0.011599	0.011551	0.008300	0	-1	-7.046539
FRONT LENS	-0.021894	-0.021894	0.045101	0	-1	4.708738
BACK LENS	1.000000	1.000000	0.000000	12	0	-3.44
RETINA	0.006944	0.006944	0.006944	0	-1	-9.18
HYPEROPES:						
CORNEA	0.013664	0.013704	0.011201	0	-1	-5.958777
FRONT LENS	-0.026601	-0.026601	0.054799	0	-1	4.271845
BACK LENS	1.000000	1.000000	0.000000	11.2	0	-3.75
RETINA	0.006944	0.006944	0.006944	0	-1	-7.08

Table 6.10   Initial schematic eye parameters for near-emmetropes, myopes and hyperopes (see section 5.2.1C for explanation of symbols).

(E) INPUT OF PHYSICAL PUPIL SIZE

Although the linear algebraic ray tracing program required a value for the physical pupil diameter (see section 5.2.2), it was only possible to measure the vertical entrance pupil diameter in real eyes (see section 3.2.5B). Nevertheless, the required physical pupil size could be derived, using the computer program, if the entrance pupil size was known. Indeed, in section 5.2.4 it was explained that the computer program

incrementally (0.1 mm steps) increases the separation, in air, of a set of marginal rays until they reach the physical pupil edge after refraction through the cornea. Therefore, the separation of these marginal rays, in the vertical and horizontal planes, represent the diameters of the entrance pupil. As this was the case, the required physical pupil diameter was determined for each schematic eye by ray tracing through a range of physical pupil sizes until the corresponding entrance pupil produced was equal in size to that measured.

As each schematic eye possessed astigmatic corneal surfaces, which would naturally lead to small differences in the horizontal and vertical entrance pupil size, it was considered necessary to match the measured vertical entrance pupil diameters with the vertical values generated by the computer program. In actual fact, the small amounts of corneal astigmatism present appeared to have no effect on the modelled horizontal and vertical entrance pupil diameters. To some extent, however, this may have been due to the distance between the marginal rays being altered in steps of 0.1 mm thereby obscuring any difference between the horizontal and vertical entrance pupil diameters of less than this value.

To avoid unnecessary calculations, only three trial physical pupil diameters (3, 3.5 and 4 mm) were used. A second order polynomial curve was then fitted to the vertical entrance pupil values predicted by each physical pupil size for each schematic eye. From these curves, the required physical pupil diameters were determined. It is important to understand that although the entrance pupil diameters were matched in the vertical meridian, the derived physical pupil diameters served for both the horizontal and vertical meridians as the computer program assumed the physical pupil to be circular.

In table 6.11, the measured vertical entrance pupil diameters, the second order polynomial curves and the calculated physical pupil diameters are shown for the near-emmetropic, myopic and hyperopic schematic eyes.

PUPIL DIAMETERS (mm)

REFRACTIVE GROUP	Measured vertical entrance pupil (E)	Fitted second order polynomial curve	Calculated physical pupil (P)
NEAR-EMMETROPE	4.2	$P = -7.5 + 4.416E + 0.416E^2$	3.7
MYOPE	4.3	$P = -7.5 + 4.416E + 0.416E^2$	3.8
HYPEROPE	4.1	$P = 0.16 + 0.83 E + 0.001E^2$	3.6

Table 6.11   The measured vertical entrance pupil diameters (E), second order polynomial curves and the calculated physical pupil diameters (P) for the near-emmetropic, myopic and hyperopic schematic eyes.

6.3.2 INPUT OF REQUIRED REFRACTIVE INDICES

This section represents the second step in the computing scheme proposed in section 5.5. The refractive indices for each schematic eye remained the same as the values previously used for the basic three surfaced eye model (see table 6.5). Refractive indices of 1.3374 for the aqueous humour, 1.42 for the crystalline lens and 1.336 for the vitreous humour were assumed.

The chosen crystalline lens refractive index, however, was only provisional as this needed to be altered, as described in the following section, when applying the procedure devised to model the correct amounts of central refraction and peripheral astigmatism (see section 5.3.3) in each schematic eye.

6.3.3 ALTERATION OF CRYSTALLINE LENS PARAMETERS

This section represents the third step in the computing scheme proposed in section 5.5. Here, the correct amounts of central refraction and peripheral astigmatism were modelled by applying the procedure devised in section 5.3.3 involving the alteration of the crystalline lens parameters. Before doing so, however, it was necessary to analyse the performance of the initial model.

(A) INITIAL ANALYSIS OF MODEL PERFORMANCE

Linear algebraic ray tracing calculations were carried out, as described in section 5.2.4, on the near-emmetropic, myopic and hyperopic schematic eyes constructed in sections 6.3.1 and 6.3.2. The initial performance of each eye model was then tested by comparing the central and peripheral refractive results with those of the symmetrical curves constructed in section 6.2.1B.

For the central results, values of the spherical equivalent refraction and astigmatism were considered while peripheral results were assessed in terms of the astigmatism produced at 35.5° field angle (table 6.12). This value was chosen as peripheral astigmatic readings were only taken out to 40° field angle (see section 4.2.4B) and the closest corresponding field angle generated by the program was 35.5° (±0.5° accounting for the corneal curvature variations which occur between the three eye models). As mentioned in section 6.2.1B, the use of a polynomial curve to describe the measured peripheral astigmatic results was of great advantage as it enabled an accurate estimate to be made of the astigmatism that occurred at the field angle of 35.5°.

262

REFRACTIVE GROUP	Central spherical equivalent refraction (D)	Central astigmatism (D)	Peripheral atigmatism at 35.5° field angle (D)
NEAR EMMETROPE:			
Modelled	-0.75	-0.09	2.75
Symmetrical curve	-0.14	-0.10	3.13
MYOPE:			
Modelled	-3.34	0.15	2.91
Symmetrical curve	-3.24	0.17	2.94
HYPEROPE:			
Modelled	0.62	-0.11	3.16
Symmetrical curve	1.54	-0.12	2.89

Table 6.12 Comparison between the modelled results of the initial near-emmetropic, myopic and hyperopic eye models and their corresponding symmetrical curves.

The results shown in table 6.12 indicate that there was excellent agreement between modelled central astigmatic values and those produced by the symmetrical curves. This is attributable to the treatment of the corneal surfaces described in sections 6.2.1C and 6.3.1A. As described in section 6.2.1B, negative astigmatic values indicate the presence of with-the-rule astigmatism whilst positive values occur when the astigmatism is against-the-rule.

The modelled eyes produced consistently more myopic spherical equivalent central refractive values than those present in the symmetrical curves. This was considered to be the result of the spherical aberration produced by ray tracing through finite aperture pupils thus bringing about more central myopia. Indeed, the differences found, which ranged between 0.1 D and 1.0 D, would have been greater had aspheric optical surfaces not been used in each eye model.

With regard to the peripheral astigmatism, modelled near-emmetropic and myopic values were smaller than those which occurred for the symmetrical curves. Values produced by the hyperopic model eye, however, were a little larger. As the observed differences ranged from 0.03 D to 0.38 D and were within the range of standard deviations given in section 4.2.4B for peripheral refractive estimates made using the Hartinger out to 40° (0.25 D to 0.43D), they were considered to be negligible. It is interesting to note that the agreement between the measured and modelled results were somewhat better than that observed at 35.5° field angle (approximately 1.0 D) between Kooijman's (1983) eye model and the symmetrical curve derived by Lotmar and Lotmar (1974) from the experimental results of Rempt et al (1971). This perhaps illustrates the usefulness of modelling the measured peripheral refraction in eyes whose optical dimensions are known.

In the light of the above results, no attempt was made to alter the modelled peripheral refractive results to the symmetrical curve values. It was, however, considered necessary to impliment some change to the crystalline lens parameters which would bring about the correct amounts of central refraction.

(B) MODELLING THE CORRECT AMOUNTS OF CENTRAL REFRACTION

The results described in section 5.3.3 (see fig. 5.21) indicate that reduction of the crystalline lens refractive index brings about large amounts of central hyperopia and small increases in peripheral astigmatism. This method presented the most convenient way of reducing the excess central myopia evident in the modelled results compared to the corresponding symmetrical curves. It was assumed that any increase in the peripheral astigmatism, resulting from the use of this method, would be very small. In any case, such a change would produce better agreement between the modelled

264

peripheral astigmatic results for the near-emmetropic and myopic eye and their associated symmetrical curves, although the agreement between the measured and modelled hyperopic results would suffer.

Table 6.13 shows the new values for the crystalline lens refractive indices for the near-emmetropic, myopic and hyperopic eye models. Also shown are the modelled spherical equivalent central refractive values for comparison with those required according to the respective symmetrical curves (see table 6.12).

REFRACTIVE GROUP	New crystalline lens refractive index	Modelled spherical equivalent central refraction (D)
NEAR EMMETROPE	1.4160	-0.15
MYOPE:	1.4193	-3.24
HYPEROPE:	1.4142	1.54

Table 6.13   New crystalline lens refractive indices for the near-emmetropic, myopic and hyperopic eye models. Modelled spherical equivalent central refractive values are shown for comparison with those required according to the respective symmetrical curves (see table 6.12).

Differences between the new crystalline lens refractive indices and the value originally assumed (1.42) ranged between 0.0007 and 0.006 units. These changes fall well within the range of lens refractive index values assumed for schematic eyes used by other workers. The increase in peripheral astigmatism (at 35.5°) which occurred as a result of these changes was no greater than 0.03 D and was therefore, as previously suspected, negligible.

In figs. 6.1 to 6.3, peripheral astigmatism is plotted as a function of field angle. Solid lines show modelled values and the closed circles represent those of the symmetrical

curve. As the data is symmetrical, only half of the retinal field is shown.
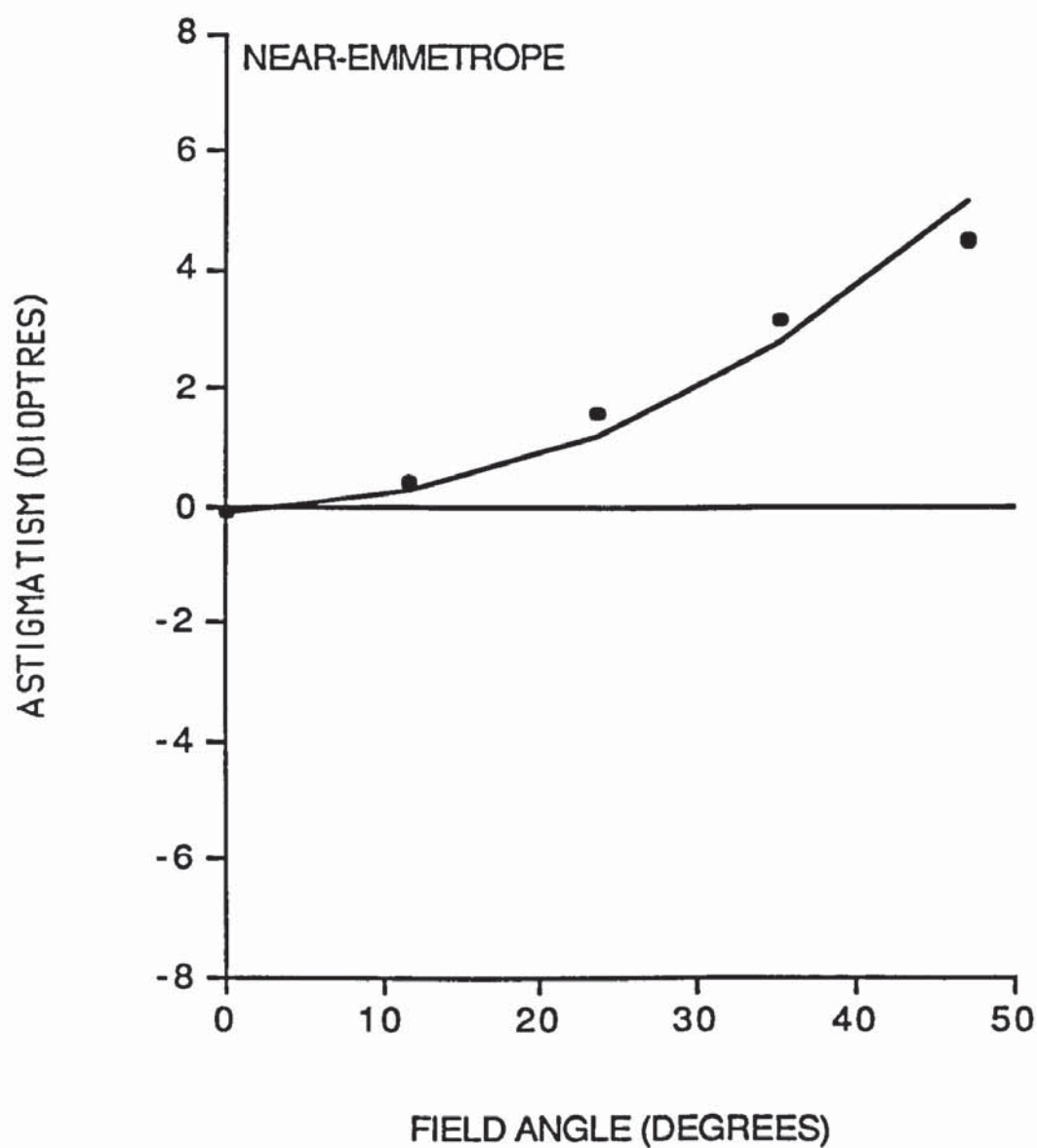
Fig. 6.1 Graph of the peripheral astigmatism in near-emmetropes. Solid lines show modelled values and closed circles represent those of the symmetrical curve.

Excellent agreement was found between the peripheral astigmatic results of the modelled near-emmetropic (fig. 6.1), myopic (fig. 6.2) and hyperopic (fig. 6.3) eyes and their respective symmetrical curves.
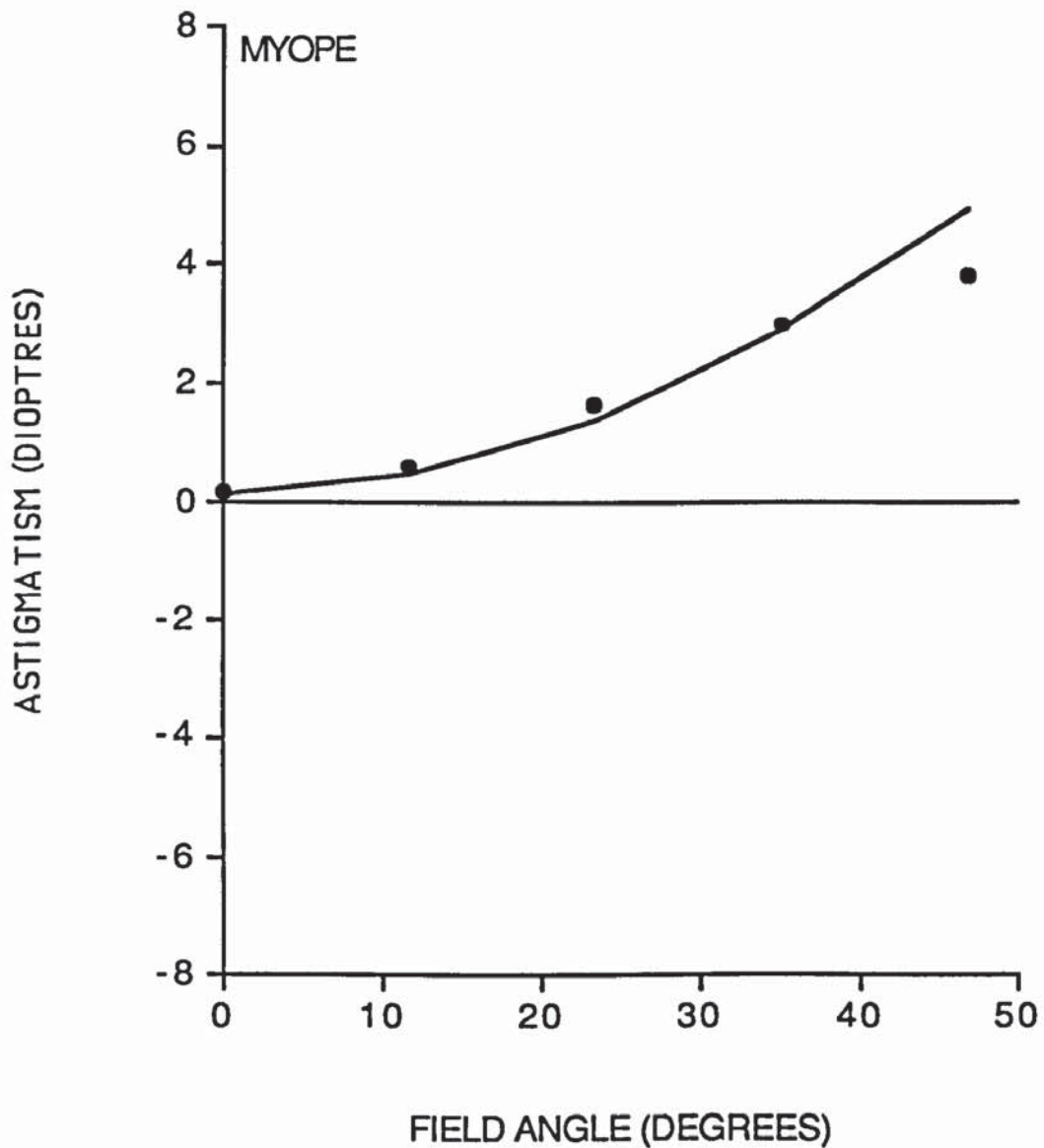
Fig. 6.2   Graph of the peripheral astigmatism in myopes. Solid lines show modelled values and closed circles represent those of the symmetrical curve.

At field angles of close to 50°, however, the modelled astigmatism appeared to be larger than that of the symmetrical curves. It is important to note that the data was matched at field angles of approximately 0°, 11.5°, 23.5°, 35.5° and 47° (±0.5° accounting for the corneal curvature variations which occur between each of the eye

models) for the reasons already explained in section 6.3.3A. As symmetrical curves were based on measurements made in real eyes from field angles of 0° to 40° (see section 6.2.1B), it follows that at field angles of 47° the symmetrical curve values do not strictly represent those found in the real eyes.
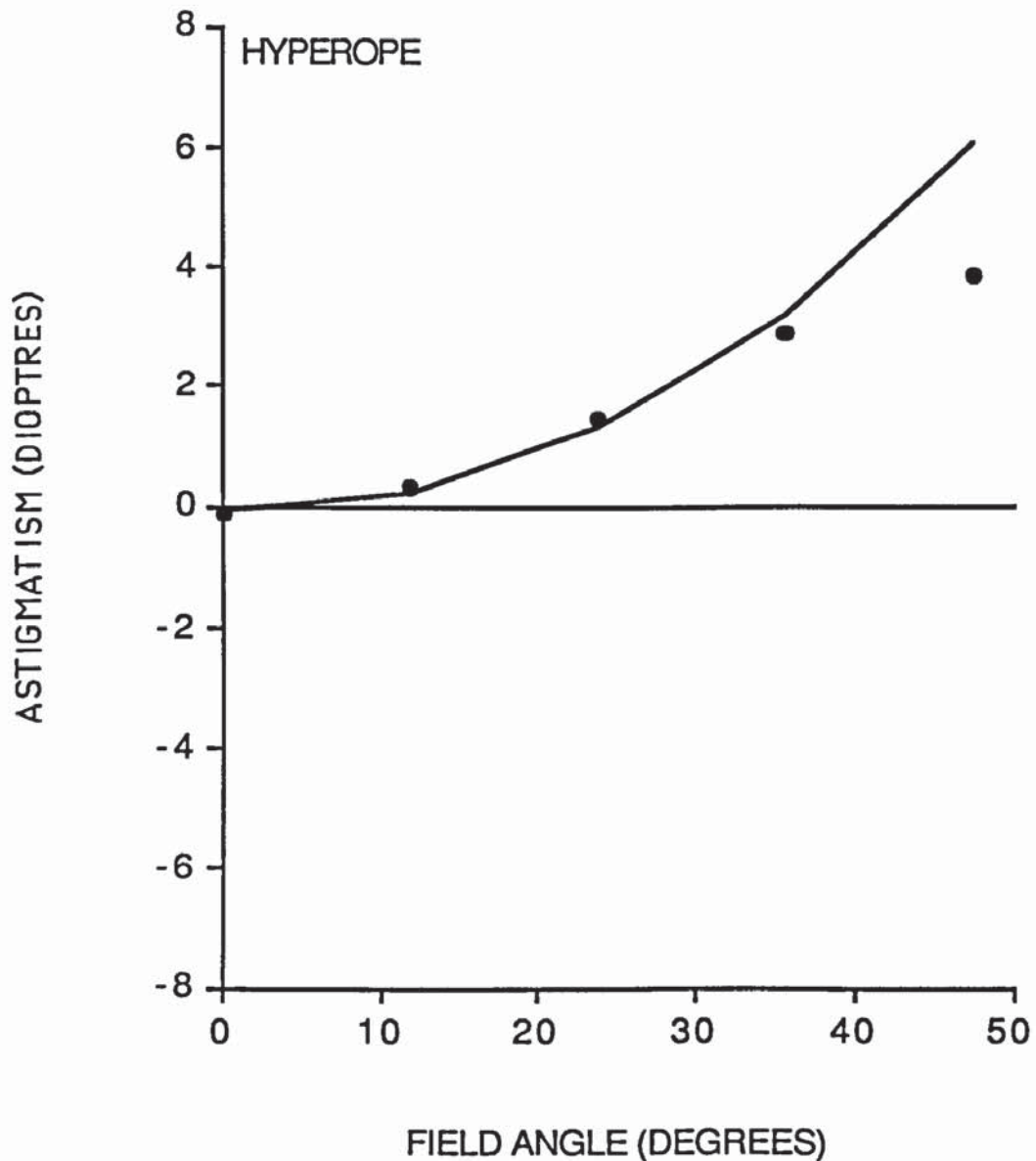
Fig. 6.3 Graph of the peripheral astigmatism in hyperopes. Solid lines show modelled values and closed circles represent those of the symmetrical curve.
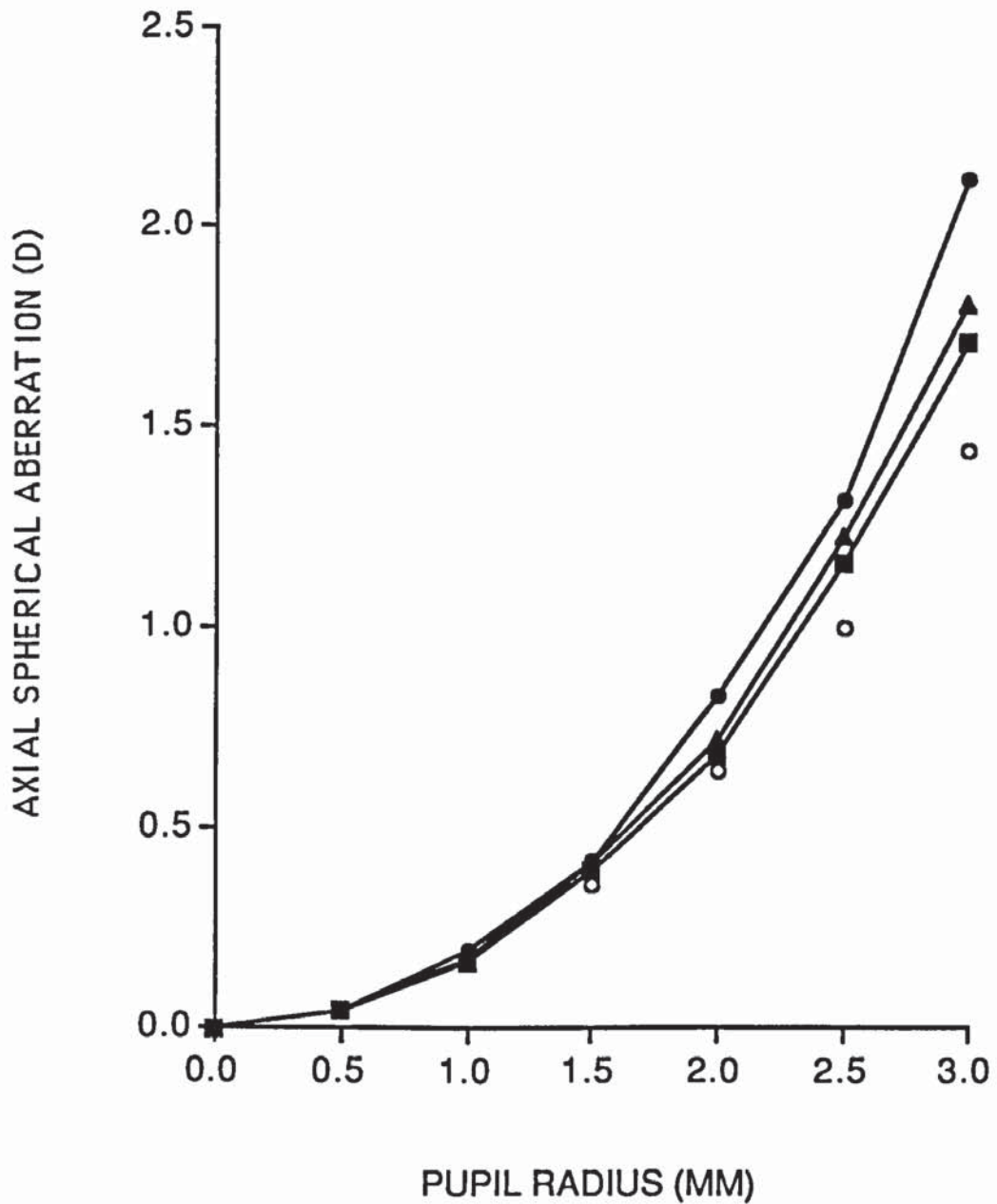
Fig. 6.4 Graph of the axial spherical aberration modelled in near-emmetropes (solid triangles), myopes (solid squares) and hyperopes (solid circles). Typical values found in real eyes (open circles) are represented by the curve of Van Meeteren (1974).

Figure 6.4 shows the axial spherical aberration produced by the near-emmetropic (solid triangles), myopic (solid squares) and hyperopic (solid circles) eye models. Modelled values of axial spherical aberration were calculated and compared to the

curve of Van Meeteren (1974) (open circles) in the same manner as described in section 5.3.3. The modelled results agreed well with the curve of Van Meeteren (1974) up to physical pupil diameters of 3 mm. At larger pupil sizes, each eye model produced more undercorrected axial spherical aberration than found typically in real eyes. This difference, however, never exceeded 0.75 D, even for pupils of 6 mm diameter.

6.3.4 ALTERATION OF RETINAL CONTOUR

This section represents the fourth step in the computing scheme proposed in section 5.5. Here, the correct dispositions of the sagittal and tangential image shells were modelled by altering the retinal shape. From the schematic eye components shown in section 6.2.2 (see table 6.5), it is evident that the near-emmetropic and myopic schematic eyes have similar refractive components hence giving rise to approximately equal ocular powers. However, the axial length in the myopic eye is considerably longer than that of the near-emmetrope indicating that its ametropia is almost entirely axial in origin (as was assumed to be the case for the myopic eye modelled in section 5.3.2). On the other hand, the hyperopic eye is considerably shorter and possesses more ocular power, compared to the near-emmetrope, thereby exhibiting ametropia of both axial and refractive origin.

The above observations offered a clue to the best method for fitting the appropriate retina to each of these models. Spherical retinae we̶re used to model the correct positions of the sagittal and tangential image shells in the near-emmetropic and hyperopic schematic eyes. However, as the ametropia exhibited by the myopic schematic eye appeared to be axial in origin, its retina was defined by an ellipsoidal surface whose equatorial position and radius was equal to that of the near-emmetrope,

270

thereby adopting a similar form to the myopic retina modelled in section 5.3.2. Although the present author admits that the spherical near-emmetropic and hyperopic retinae, required to position the sagittal and tangential image shells correctly, were found by trial and error, the procedure adopted to model the myopic retina was precisely the same as that described in section 5.3.2.

In terms of the input parameters described in section 5.2.1, the X, Y and Z retinal surface curvature parameters were all given equal radius values of 12.84 mm and 11.68 mm for the modelled spherical near-emmetropic and hyperopic retinae respectively. In the modelled myopic eye, the equatorial retinal radius was made to equal that of the near-emmetrope by giving X and Y values of 12.84 mm. Z, however was increase by the difference between the near-emmetropic and myopic axial lengths, giving a value of (12.84 + 1.1 =) 13.94 mm (a prolate ellipsoid). Values of -7.24 mm and -7.40 mm were specified for the near-emmetropic and hyperopic retinal surface location $\overline{Z}$ parameters. In the myope, the $\overline{Z}$ surface location parameter was equal to that of the near-emmetrope so that the equators of each of the modelled retinae coincided in position.

SURFACE	A(1,1)	A(2,2)	A(3,3)	B(3)	c	T(3)
EMMETROPE	0.006066	0.006066	0.006066	0	-1	-7.24
MYOPE	0.006066	0.006066	0.005146	0	-1	-7.24
HYPEROPE	0.007330	0.007330	0.007330	0	-1	-7.40

Table 6.14 New retinal surface parameters (see 5.2.1C for explanation of symbols).

Table 6.14 gives the non-zero components of matrix formulation (see section 5.2.1C) for the above retinal surfaces. Figure 6.5 shows cross sections of the retinal surfaces generated by the parameters shown in table 6.14.
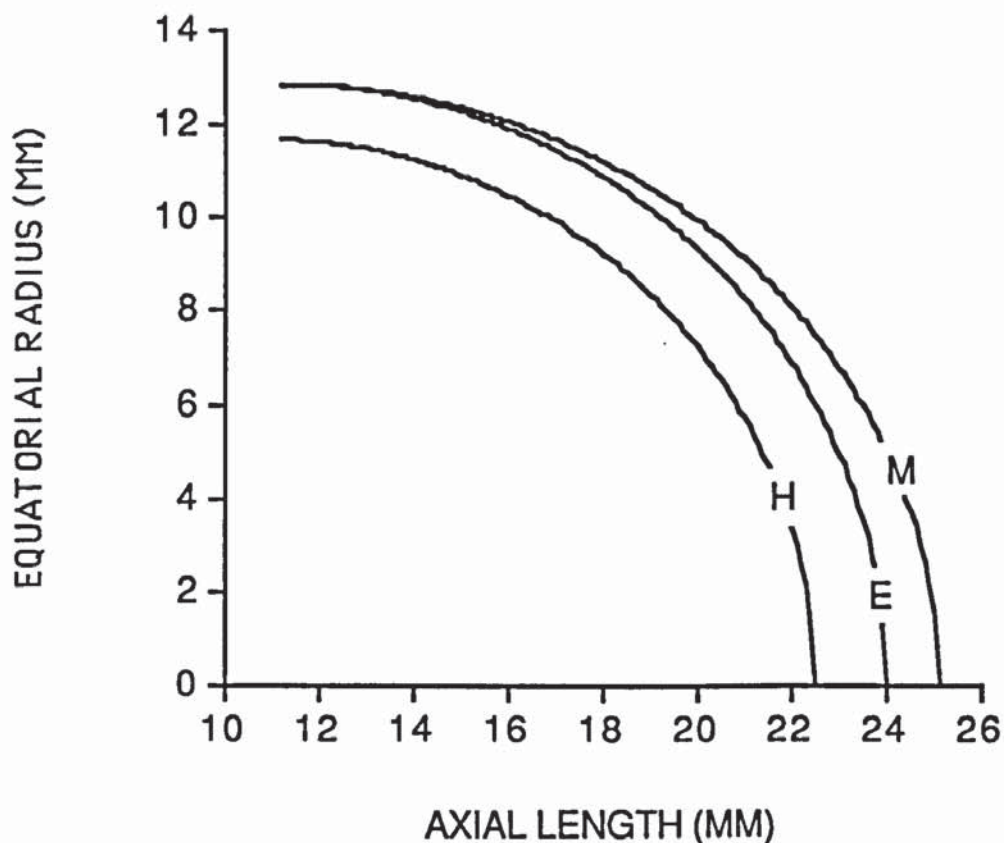
Fig. 6.5 Computer plot of cross sections of retinal shape in the modelled near-emmetropic (E), myopic (M) and hyperopic (H) eyes.

Figure 6.6 illustrates that these retinal surfaces produce excellent agreement between the sagittal and tangential image shell dispositions of the modelled eyes and their respective symmetrical curves. In this graph, the modelled sagittal image shells for the near-emmetropic (Es), myopic (Ms) and hyperopic (Hs) eyes are shown as broken lines whilst the tangential image shells (Et, Mt, and Ht) are shown as solid lines. Open (sagittal) and closed (tangential) symbols denote the symmetrical curve values for the near-emmetropes (triangles), myopes (squares) and hyperopes (circles). As the data is symmetrical, only half of the retinal field is shown. A departure of the results occurred at field angles of nearly 50°. However, this was partly due to the fact that this field angle fell outside the range of the measured data (see section 6.3.3B).
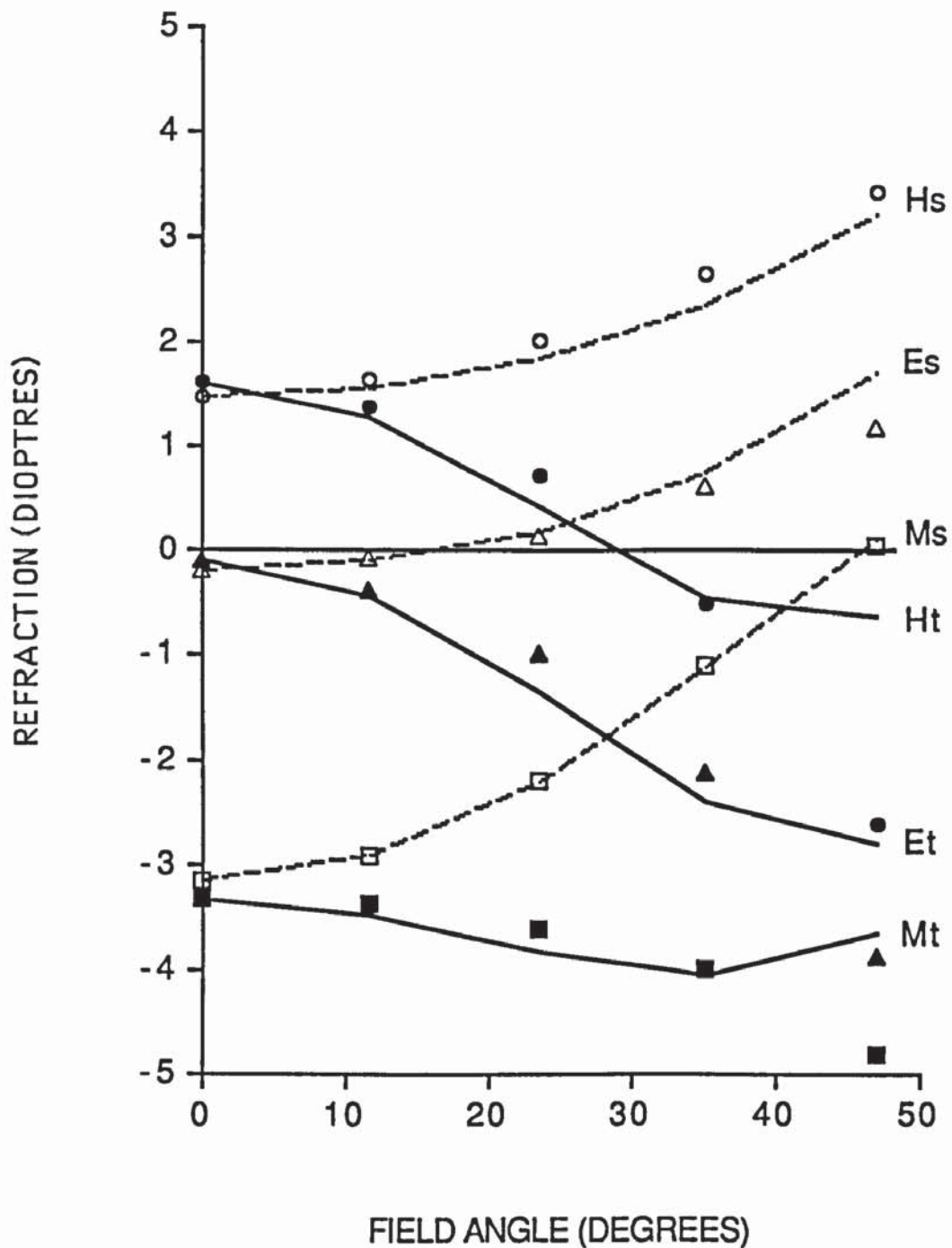
Fig. 6.6 Peripheral refraction plotted as a function of field angle. Broken lines represent modelled sagittal image shells for the near-emmetropic (Es), myopic (Ms) and hyperopic (Hs) eyes whilst solid lines represent modelled tangential image shells (Et, Mt, and Ht). Open (sagittal) and closed (tangential) symbols denote the symmetrical curve values for the near-emmetropes (triangles), myopes (squares) and hyperopes (circles). As the data is symmetrical, only half of the retinal field is shown.

The retinal cross sections, shown in fig. 6.5, indicate that the hyperopic eye is smaller both equatorially and axially than the near-emmetrope. Therefore, for hyperopic eyes measured in this study, it is tempting to speculate that the growth of the eyeball, which occurred during development, was less than that required to produce emmetropia. Whether this was due to genetic influences, environmental influences or both (see section 1.4), however, cannot be estimated. On the other hand, it appears that the eyes in the myopic group grew by the "correct" amount equatorially but some additional factor caused their excess elongation in the antero-posterior direction. It is of interest that this type of axial elongation is similar to that which occurs according to the theory proposed by Greene (1980) in which the extraocular muscles involved with convergence are able to increase the vitreous pressure. This, in addition to the weakpoint at the back of the eye caused by the penetration of the optic nerve, then gives rise to elongation in the antero-posterior direction (see section 1.4).

6.3.5 MODELLING OCULAR ASYMMETRY

This section represents the fifth and final step in the computing scheme proposed in section 5.5. From the evidence provided by assessing the various effects of ocular surface translation and rotation on peripheral refraction (see section 5.3.1C) and Purkinje image non-alignment (see section 5.4C), it would appear that either 5° rotation of the whole eye in the temporal direction or of the crystalline lens such that its nasal side moves towards the cornea or otherwise a combination of both, could represent the type of ocular asymmetries found in human eyes.

Therefore, attempts were made to incorporate each of these, in turn, into the axially aligned schematic eyes developed in the previous sections. The symmetrical curves (see section 6.2.1B) were obsolete and the modelled peripheral refractive results were

compared, instead, directly to the measured peripheral refractive data shown in fig. 4.19 (see appendix 2k).

To model 5° temporal rotation of the whole eye a correction was made to the computed field angles (see section 5.5) such that 0° became -5° (i.e. shifted to 5° on the nasal retina). Although this produced the nasalward decentration observed in the measured results (see fig. 4.19), only approximately half of the measured peripheral astigmatic asymmetry was accounted for.

With 5° nasal rotation of the crystalline lens about its anterior surface vertex (see section 5.2.3), no noticeable nasalward decentration occurred (see also fig. 5.6). However, the astigmatic image shells moved towards hyperopia over the nasal retina and myopia over the temporal retina, which was particularly noticeable with the tangential image shells in the measured data (fig. 4.19). Nevertheless, as with eye rotation, only approximately half of the measured peripheral astigmatic asymmetry was accounted for.

As a result of these findings the measured peripheral astigmatic asymmetry was modelled by combining 5° of crystalline lens rotation with 5° of eye rotation. Whereas the former produced the observed nasalward decentration, the latter produced the nasal hyperopic and temporal myopic shifts of the image shells.

However, the observed asymmetry for the averaged hyperopic eyes was still not entirely accounted for. The measured image shells were still more hyperopic over the nasal retina and myopic over the temporal retina than the modelled values. As the correct amounts of peripheral astigmatic asymmetry had been modelled in this eye (indicating that the amounts of eye/crystalline lens rotation were approximately

correct), it was considered that this may be the result of the retinal surface being steeper nasally and flatter temporally. Indeed, a 0.25 mm translation of the retinal surface in the temporal direction (so that surface location parameter $\overline{X} = 0.25$ [see section 5.2.1B]) produced this effect approximately and greatly improved the results.

Figure 6.7 shows the final modelled peripheral refractive results. Broken lines represent the sagittal image shells for the near-emmetropic (Es), myopic (Ms) and hyperopic (Hs) eyes and solid lines represent the tangential image shells (Et, Mt, and Ht). As 5° temporal eye rotation was involved in modelling this graph, it follows that the pupillary axis (the "working optical axis" [see section 1.5]) coincides with a field angle of 5° over the nasal retina. Zero degrees field angle then coincides with the line of sight.

To enhance the accuracy of the central portion of fig. 6.7, a modification was made to the linear algebraic ray tracing program shown in appendix 3a. The line reading:

$$ooo = (iooo - 6) / 5.73 + 0.0001$$

which instructs the computer to trace 11 sets of principal and marginal rays (see section 5.2.4) in steps of 10°, was changed to:

$$ooo = ((iooo - 6) / 5.73 + 0.0001) / 10$$

in order to allow 11 sets of rays to be traced at 1° intervals. This method also allowed the modelled sagittal and tangential refractive error to be estimated down the line of sight for direct comparison with values measured in real eyes, as shown in table 6.15.
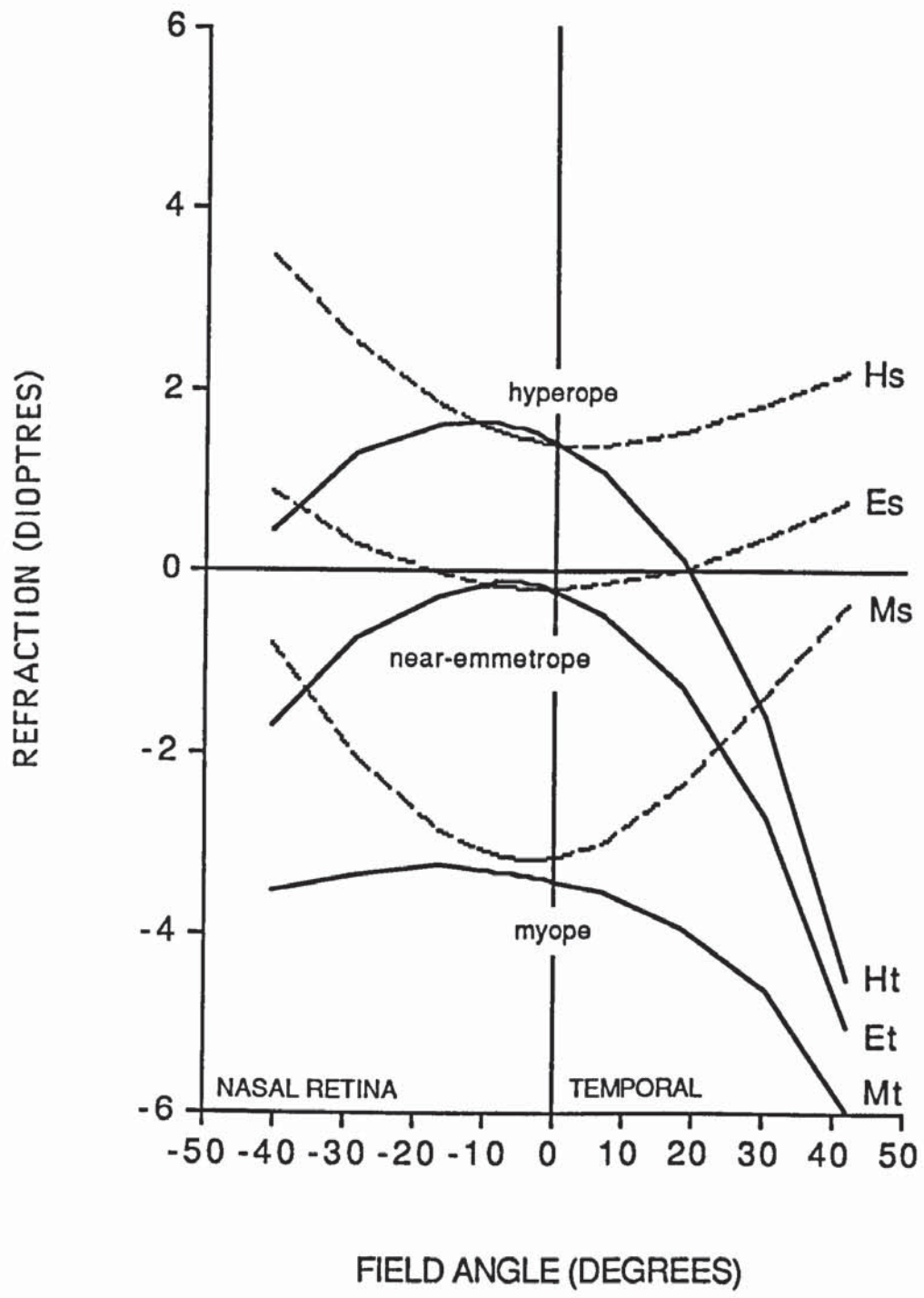
Fig. 6.7 Modelled peripheral refraction plotted as a function of field angle. Broken lines represent the sagittal image shells for the near-emmetropic (Es), myopic (Ms) and hyperopic (Hs) eyes whilst solid lines represent the tangential image shells (Et, Mt, and Ht). Zero degrees field angle coincides with the line of sight.

REFRACTION ALONG LINE OF SIGHT	REFRACTIVE GROUP		
	Near-emmetrope	Myope	Hyperope
Sagittal refraction (D)			
Measured	-0.18	-3,26	1.54
Modelled	-0.21	-3.15	1.40
Tangential refraction (D)			
Measured	-0.26	-3.38	1.63
Modelled	-0.26	-3.42	1.42
Astigmatism (D)			
Measured	0.08"against"	0.12"against"	0.09"with"
Modelled	0.05"against"	0.27"against"	0.02"with"

Table 6.15   Comparison between the measured and modelled tangential and sagittal refractive results, for near-emmetropic, myopic and hyperopic eyes, as found along the line of sight (0° field angle). The term "with" refers to with-the-rule astigmatism and "against" refers to against-the-rule astigmatism.

Table 6.15 illustrates that the present models produce very good agreement with the central refractive findings measured down the line of sight in real eyes. This offers some validation of the treatment of the central refractive and corneal curvature results described in section 6.2.1. In doing so, it also shows that eye rotation can offer a feasible explanation for the presence of residual astigmatism.

As, in previous sections, the modelled peripheral results were compared to those of the symmetrical curve at 35.5° field angle, the same was done for the results shown in fig. 6.7. Rather conveniently, arising from the field angle corrections made to simulate eye rotation, the above field angle now represented 40.5° on the nasal retina and 30.5° on the temporal retina. These corrected field angles were so close to those employed for making measurements in real eyes (40° nasally and 30° temporally [see section 4.2.4B]) that it was possible to make direct comparison between the measured and modelled values. This was carried out as shown in table 6.16.

278

| | REFRACTIVE GROUP | | |
FIELD ANGLE	Near-emmetrope	Myope	Hyperope
40° NASAL RETINA:			
Sagittal refraction (D)			
Measured	1.01	-1.10	2.97
Modelled	0.87	-0.86	3.46
Tangential refraction (D)			
Measured	-1.63	-3.28	0.55
Modelled	-1.70	-3.56	0.43
30° TEMPORAL RETINA:			
Sagittal refraction (D)			
Measured	0.46	-1.24	2.08
Modelled	0.37	-1.42	1.84
Tangential refraction (D)			
Measured	-2.80	-4.73	-1.60
Modelled	-2.70	-4.65	-1.61

Table 6.16   Comparison between the measured and modelled tangential and sagittal peripheral refractive results for near-emmetropic, myopic and hyperopic eyes. Values were compared at retinal field angles of 40° nasally and 30° temporally.

Generally, the differences between the measured and modelled results, shown in table 6.16, fell well within the range of standard deviations given in section 4.2.4B for peripheral refractive estimates made using the Hartinger optometer out to 40° field angle (0.25 D to 0.43D). In only one instance, that in which the hyperopic sagittal refractions at 40° nasal retinal field angle were compared, was the difference (0.49 D) greater than the above range.

279

6.4 SUMMARY

The computing scheme outlined in section 5.5 was applied to the real eye data in order to model the measured peripheral refraction. It was, however, necessary to re-specify the measured optical component and peripheral refractive data with respect to the pupillary axis rather than the line of sight, down which measurements were initially made (see chapter 4). It was also assumed that the central ocular astigmatism was entirely due to the cornea. This not only solved the problem of residual astigmatism but also facilitated the modelling of peripheral refraction over the horizontal plane (see section 6.1).

Excellent agreement was found (see fig. 6.7 and table 6.16) between the measured and modelled peripheral refractive values over at least 70° of the retinal field (from 40° nasally to 30° temporally). Furthermore, the modelled central refractive values, specified with respect to the line of sight, matched the measured values very closely (table 6.16). These findings at least imply that the biometric features incorporated in each eye model, in addition to the measured components, are representative of those which exist in the measured eyes.

One of the additional biometric features studied was the asphericity of the anterior and posterior crystalline lens surfaces. Conic constant values assumed for the latter were the same as derived by Kooijman (1983) and produced very good agreement between the measured and modelled peripheral astigmatism (see table 6.12). It is worth noting that this agreement was considerably better than that found between the peripheral astigmatic results of the schematic eye used by Kooijman (1983) and those measured by Rempt et al. (1971). This perhaps illustrates the need for modelling the peripheral refractive findings measured in real eyes whose optical dimensions are known.

Small changes were made to the crystalline lens refractive index to reproduce the measured central refractive findings. These changes, however, fell well within the variety of values assumed for different schematic eyes by different workers.

Another additional biometric feature studied was retinal shape and position. The measured data indicated that the myopic eyes exhibited purely axial ametropia while the hyperopic eyes exhibited axial and refractive ametropia. The retinae required in each eye to produce the correct sagittal and tangential image shell dispositions, indicated that the hyperopic eyeball was smaller both equatorially and axially than that of the near-emmetrope. The myopic eye, on the other hand, shared the same equatorial radius as that of the near-emmetrope but was somewhat elongated in the antero-posterior direction. It was therefore speculated that the axial component of the ametropia in the hyperopic eye was due to some factor effecting its overall growth whilst that of the myope was due to some factor which stretched the eyeball.

Possibly the most interesting additional biometric feature studied was rotation of the whole eye and the crystalline lens. Approximately the same amounts of peripheral refractive asymmetry were found in each of the averaged eyes. This was modelled by incorporating 5° of temporal eye rotation and 5° of crystalline lens rotation, such that its nasal side moved toward the cornea, in the corresponding schematic eye models. That the above treatment was necessary is in keeping with Gullstrand's (1924) belief that the eye possessed no true optical axis (see section 1.5). Tilt and decentration of the corneal surface would also be the natural consequence of eye rotation thus accounting for the occurrence of corneal surface asymmetry and apical decentration reported in the literature (see section 1.3.1). Furthermore, the effect of a tilted corneal surface would appear to account for residual astigmatism (see also section 1.5).

Although the crystalline lens was rotated about its anterior surface vertex, it is possible that rotation about other points could give rise to a greater amount of nasalward decentration than found in section 6.3.5 (see also fig. 5.6). If this were so, the presence of crystalline lens rotation could contribute to angle alpha by effectively displacing the principal ray representing the line of sight from the optical axis. This would then explain, in part, the disappearance of angle alpha in aphakics (see section 1.5).

Ferree et el. (1931) were of the opinion that some very interesting biometric inferences could be made from the observed peripheral refraction (see section 2.3). Lotmar and Lotmar (1974) considered that peripheral refractive measurements could provide a more sensitive indication of the asymmetries in the eye than the study of Purkinje image non-alignment (see section 5.4). In agreement with the above authors, this chapter has illustrated that variation of refraction in the periphery offers a very useful optical method for studying human ocular component dimensions.

CHAPTER SEVEN

SUMMARY AND DISCUSSION

7.1 REVIEW OF PREVIOUS CHAPTERS

In chapter one, the current knowledge regarding human ocular component dimensions was discussed. An attempt was made to assess the way in which ocular components combined to produce emmetropia and to give some indication of the variations found with age and sex.

Research evidence has shown that ocular components are normally distributed. This is not reflected in the distribution of refractive errors and leads to the conclusion that growth of the eye is a coordinated process aimed at producing emmetropia. Genetic and environmental factors appear to be involved. Interruption of this process gives rise to ametropia.

The eye is highly adaptable to a variety of visual environments which is attributable to its accommodative facility as well as having a variable pupillary aperture. Aspheric optical surfaces and the gradient index optical nature of the crystalline lens may contribute to optimising the system by reducing the spherical aberration which results from large pupils.

Most eyes possess some asymmetry. The position of the corneal apex and the asymmetry of its surface profile are consistent with the decentration of the pupil suggesting that the eye is rotated away from the line of sight and may be regarded as approximately symmetrical about the pupillary axis. This may explain why residual astigmatism and asymmetry in the degradation of the peripheral optical imagery have been observed when measurements are taken with respect to the line of sight and not the pupillary axis. Not all asymmetry is due to eye rotation as there is evidence to

suggest that some asymmetry arises from the crystalline lens.

It is evident that most studies in this area have concentrated on the ocular components which occur in eyes exhibiting differing amounts of central refractive error. For the present study, however, it was proposed that an investigation into the refraction in the periphery of the human eye could yield more information regarding the nature of the optical surfaces and their asymmetries and could even provide further insight into the way in which they combine.

A review of the previous studies on peripheral refraction was carried out in chapter two. Peripheral refraction has either been measured in real eyes, usually in the horizontal plane, or has otherwise been modelled in schematic eyes of varying levels of sophistication.

The most striking difference between the modelled and measured results is that the amount of peripheral astigmatism predicted by the former is usually larger than the latter. This is often blamed on the neglect of aspheric optical surfaces and the gradient index optical nature of the crystalline lens in most schematic eyes. In the present author's opinion, however, the evidence provided by schematic eyes which incorporate either of the above suggests that the aspheric nature of particularly the anterior crystalline lens surface might play a relatively major role, compared to that of gradient index optics, in the reduction of astigmatism in the periphery.

The sagittal and tangential image shells in real eyes show considerable variation which is not evident in schematic eyes. The research indicates that this may be due to the fact that schematic eyes are usually constructed with spherical retinae of about 12 mm

radius. In real eyes, subtle differences in the retinal shape are likely to have a major effect on the image shell dispositions.

Real eyes exhibit varying degrees of peripheral refractive asymmetry. In most eyes this is only small but in some rare cases there is considerable asymmetry. Although the effect of total eye rotation has been simulated in schematic eyes, the effects of various ocular surface translations and rotations have never been carried as traditional ray tracing procedures do not readily lend themselves to such procedures.

As some very useful information could be derived by observing peripheral refraction in various eyes, a study was proposed in which the ocular components and the peripheral refraction were measured in the same eyes. By constructing schematic eyes from the biometric data such effects as ocular surface asphericity, retinal contour and various ocular asymmetries could be investigated. The manipulation required to model the measured peripheral refraction would then represent the conditions found in the real eyes. Such an optical method for studying human ocular dimensions has never been conducted before.

Chapter three was concerned with the design of a procedure to measure the ocular component dimensions and peripheral refraction in real eyes.

To measure the ocular components, a method was employed which essentially combined ultrasonic and phakometric techniques. This maximised the number of independent measurements made. Where possible, different techniques were used for measuring the same parameter on two separate occasions. Therefore the anterior corneal radius was determined using keratometric and keratoscopic techniques, the

anterior chamber depth was determined using A-scan ultrasonic and pachometric techniques and the central and peripheral refractive error, over the horizontal plane, were determined using a coincidence optometer and an automated infra-red optometer. If alternative techniques were not available, repeat measurements were made using the same technique on different occasions. The latter was necessary for A-scan ultrasonographic determinations of the lens thickness, vitreous length and axial length as well as photographic opthalmophakometric determinations of the Purkinje image heights.

A computer program was written to calculate the anterior and posterior crystalline lens surface radii and to construct basic spherical surfaced schematic eyes from the independently measured data. An "internal validation check" was also provided by the computer program as a further test of the reliability of the results.

In addition to the biometric measurements made to construct the basic schematic eyes, the corneal contours were measured by keratoscopy and the entrance pupil diameter measured from the opthalmophakometric photographs.

All biometric and peripheral refractive measurements were made with respect to the line of sight as this was the only logical means of identifying a common axis. An illuminated target was constructed to control fixation and accommodation.

For the subject group chosen in this investigation a large sample of eyes was screened with the result that each eye possessed small amounts of peripheral refractive asymmetry and normal amounts of peripheral astigmatism. It was therefore decided that a group of eyes, possessing as wide a range of refractive errors as possible, were

to be measured. The final sample consisted of 10 near-emmetropes, 16 myopes and 8 hyperopes thereby exhibiting a range of central refractive errors of from +3.34 D to -6.07 D (spherical equivalent). Right eyes were measured in all but 4 of the subjects. The age of the subjects, of which 24 were male and 10 were female, ranged between 19 and 30 years.

The biometric and peripheral refractive results were discussed in chapter four. Although, to model the observed peripheral refractive patterns, it would have been desirable to construct schematic eyes from each of the 34 eyes measured, the time required to do so would have made such an approach impractical. Therefore, the data was averaged to produce three sets of results; relating to one near-emmetropic, one myopic and one hyperopic eye.

Measurements were made to a high degree of precision (expressed in terms of the average standard deviations found); averaged standard deviations of ultrasonically determined axial distances never exceeded ±0.10 mm; averaged standard deviations of opthalmophakometric determinations of Purkinje image heights never exceeded ±0.05 mm; averaged standard deviations of refractive error measurements made with the Hartinger optometer never exceeded ±0.2 D centrally and ±0.5 D at field angles of 30°. Average differences found between repeat measurements of the corneal radii using the keratoscope never exceeded ±0.04 mm. The statistical probability of correlation coefficients calculated for repeat component measurements was never greater than 0.001 which further implied the high degree of precision with which estimates could be made.

For the construction of schematic eyes from the biometric data the accumulated error (as estimated using the "internal validation check") did not exceed 0.10 mm for axial distance determinations and 0.50 D for power determinations.

Using the coincidence optometer peripheral refractive measurements could be made out to field angles of 40° nasally and temporally. The averaged peripheral refractive results for the near-emmetropes, myopes and hyperopes showed a remarkable similarity to those of Millodot (1981).

In order to model the peripheral refractive findings using more sophisticated eye models derived from the previously constructed basic schematic eyes, a linear algebraic ray tracing program was written and investigated in chapter five. This method allowed rays to be traced through aspheric surfaces which were translated or rotated with respect to each other. To simplify the program, however, the gradient index optical nature of the crystalline lens was ignored. To test the linear algebraic ray tracing technique, a schematic eye was used which was constructed from typical ocular components, including representative aspheric surfaces.

It was found that the peripheral astigmatism produced by the above schematic eye was of the order found experimentally (type IV eyes) within the central 60° of the visual field. The model also produced approximately the same amount of axial spherical aberration as reported in the literature for real eyes. Realistic peripheral astigmatic values were modelled over the central 120° of the visual field by introducing considerable amounts of peripheral flattening to the anterior crystalline lens surface. This, however, gave rise to grossly over-corrected spherical aberration. Further aspheric flattening of the anterior crystalline lens surface also produced the very low

amounts of peripheral astigmatism and the peripheral hyperopic shifts of the sagittal and tangential image shells which are sometimes present in (type I) eyes. Although the crystalline lens surface changes appeared to be somewhat unrealistic, the results at least indicated the kind of optical surface changes that are required to produce the normal variation in peripheral astigmatism.

Alterations in the retinal shape and position were found to give rise to considerable amounts of movement of the sagittal and tangential image shells. It was considered that eyes exhibiting flat tangential and steep sagittal image shells (type II) could result from prolate ellipsoidal retinal surfaces. On the other hand, eyes exhibiting steep tangential and flat sagittal image shells (type V) could arise from oblate ellipsoidal retinal surfaces. A spherical retina was found to lie approximately half way between the sagittal and tangential image shells (as in the type IV eyes).

Another version of the linear algebraic ray tracing program was constructed in order to model the types of Purkinje image non-alignment which occur with various ocular surface translations and rotations. The corroborative evidence provided by this program suggested that the small amounts of peripheral refractive asymmetry normally present in human eyes, arise due to either temporal rotation of the whole eye or rotation of the crystalline lens such that its nasal side moves towards the cornea. Eyes which exhibit more extreme amounts of peripheral refractive asymmetry (type III) may be the result of combined rotation of the whole eye and the crystalline lens or where the rotation of either one is more exaggerated. However, 1 mm nasal translation or 5° rotation of the cornea gave rise to large amounts of peripheral refractive asymmetry indicating that a non-aligned cornea may also be responsible. The Purkinje image displacement that occured was quite characteristic and therefore could possibly be used

to determine whether the cornea is actually involved.

The flexibility of the linear algebraic ray tracing program was illustrated by its ability to generate every form of peripheral refractive pattern that has been measured in real eyes. This flexibility was extended to the development of a computing scheme for modelling the peripheral refractive measurements made in the present study. This computing scheme consisted of:

(1) Specifying the surface curvatures, surface locations, and pupil size in accordance with the values measured. As the surfaces used in the program were three dimensional, manipulation of the surface curvature parameters could give rise to astigmatic surfaces if required.

(2) Specifying the required refractive indices.

(3) Modelling the correct amount of peripheral astigmatism and central refraction by altering crystalline lens anterior surface curvature and refractive index values.

(4) Modelling the correct dispositions of the sagittal and tangential image shells by altering the retinal contour.

(5) Modelling the correct amount of peripheral refractive asymmetry by rotating the crystalline lens, simulating total eye rotation or translating any of the ocular surfaces.

In chapter six, some initial treatment of the real eye data was required before applying the above computing scheme. A discrepancy was found between the measured corneal and ocular astigmatism (residual astigmatism) which was assumed to be due to measurements being made along the line of sight. Therefore, the biometric and peripheral refractive data were effectively re-specified with respect to the pupillary axis, along which it was assumed the corneal and ocular astigmatism would be equal. It was also assumed that the crystalline lens surfaces possessed no astigmatism.

Another problem was caused as the schematic eyes were calculated in the vertical meridian, due to limitations arising from the photographic ophthalmophakometer, while the peripheral refractive readings were taken about the horizontal meridian. However, because the horizontal and vertical crystalline lens radii were assumed to be equal, the only difference between the schematic eye components in either plane amounted to the known differences between the horizontal and vertical cornea radii.

In accordance with the computing scheme, the asphericity of the anterior and posterior crystalline lens surfaces was considered. Representative aspheric values were assumed and produced very good agreement between the measured and modelled peripheral astigmatism. Small changes were also made to the crystalline lens refractive index to reproduce the measured central refractive findings. These changes, however, fell well within the variety of values assumed for different schematic eyes by different workers.

Alterations were made to the shape of the retinae. The measured data indicated that the myopic eyes exhibited purely axial ametropia whilst the hyperopic eyes exhibited axial and refractive ametropia. The retina required in each eye, to produce the correct sagittal and tangential image shell dispositions, indicated that the hyperopic eyeball was smaller both equatorially and axially than that of the near-emmetrope. The myopic eye, on the other hand, shared the same equatorial radius as the near-emmetrope but was somewhat elongated in the antero-posterior direction. It was speculated that the axial component of the ametropia in the hyperopic eye was due to some factor effecting its overall growth whilst that of the myope was due to some factor which stretched the eyeball.

Rotations of the whole eye and the crystalline lens were performed. Approximately the same amounts of peripheral refractive asymmetry were found in each of the averaged eyes. This was modelled by incorporating 5° of temporal eye rotation and 5° of crystalline lens rotation, such that its nasal side moved toward the cornea, in the corresponding schematic eye models. That the above treatment was necessary is in keeping with Gullstrand's (1924) belief that the eye possesses no true optical axis. Tilt and decentration of the corneal surface would also be the natural consequence of eye rotation thus accounting for the occurrence of the corneal surface asymmetry and apical decentration reported in the literature. Furthermore, the effect of a tilted corneal surface would appear to account for residual astigmatism. In the hyperopic schematic eye, some retinal translation was also necessary to account for all of the measured peripheral refractive asymmetry.

Excellent agreement was found between the final modelled and measured peripheral refractive values over at least 70° of the retinal field (from 40° nasally to 30° temporally). Furthermore, the modelled central refractive values found down the line of sight matched the measured values very closely. These findings at least implied that the additional biometric features incorporated in each eye model were representative of those which were present in the measured eyes. As some of these features are not otherwise obtainable using in vivo techniques, this thesis has illustrated that the variation of refraction in the periphery offers a very useful optical method for studying human ocular component dimensions.

7.2 SUGGESTIONS FOR FURTHER WORK

Most of the present measurements were confined to a single meridian. The measurement of peripheral refraction in horizontal, vertical or even oblique meridians would be of great interest particularly for observing variations in ocular asymmetry and retinal contour. Multimeridional ophthalmophakometric measurements might offer some corroborative evidence regarding ocular asymmetries if one studied the alignment of the Purkinje images. Variations in the Purkinje image heights measured in different meridians could also indicate the contribution of each optical surface to the central ocular astigmatism.

Measurement of surface profiles might be improved or, in the case of the posterior corneal surface, made possible by making use of Scheimphflug photography (Brown, 1973), provided that the distortion due to the various refractive media is accounted for. By using infra-red light, measurements could also be obtained without the need for mydriasis. Alternatively the phakometric method could be enhanced by improving the quality of the Purkinje images by using infra-red illumination (Wulfeck, 1955; Otsuku et.al., 1965; Kabe, 1968) and by improving the technique used to measure the image separations. It is, however, possible that future improvements in the resolution of B-scan ultrasonography could eventually make either of the above methods obselete.

The linear algebraic ray tracing program is limited in that it assumes that all ocular surfaces are of the quadric form. Higher order polynomial surfaces may well provide a significant improvement in the amounts of peripheral astigmatism and spherical aberration modelled. For instance, the anterior lens surface asphericity, used in the present study, produces realistic amounts of peripheral astigmatism and spherical

aberration over the central 60° of the visual field. If the asphericity is altered to produce realistic values over the central 120° grossly overcorrected spherical aberration occurs. However, if the anterior lens surface was contoured so that it effectively bulged centrally and flattened peripherally, as could be modelled with higher order polynomial surfaces, then it is possible that realistic values would occur for both spherical aberration and peripheral astigmatism at large field angles.

Two other ways in which the linear algebraic ray tracing program might be improved would be to include gradient index optics and to expand the facility to rotate the ocular surfaces. Although an infinite number of individual ocular surface translations are possible, rotation is restricted to the entire crystalline lens about its anterior surface vertex. It would be very useful to be able to rotate a combination of individual surfaces simultaneously and, if rotating the entire cornea or crystalline lens, to be able to alter the point about which rotation occurs.

A number of possibilities exist for further research. The nature of the optical systems in those eyes which exhibit low amounts of peripheral astigmatism (type I) still remains a mystery. The pursuit of this might be of great importance as Hoogerheide et al. (1971) believed that these were prone to late myopic progression. Indeed, the onset of myopia after the age of approximately 15 years has been used by some workers as a criterion to define a separate refractive class called "late onset myopes" (Goldschmidt, 1968; McBrien and Millodot, 1986a,b; Rosenfield and Gilmartin, 1987).

None of the eyes measured in the present study exhibited considerable amounts of peripheral refractive asymmetry (type III eyes). Nevertheless, it would be of great interest to study the optical components in individual eyes which do so.

The present study has not attempted to investigate peripheral refraction under different levels of accommodation or in aphakic and pseudophakic eyes. The latter is of particular interest as the gradient index optical structure of the human crystalline lens presents a stumbling block for the design of schematic eyes. Therefore the study of eyes without a crystalline lens (as conducted by Millodot, 1984) and eyes which possess an intra-ocular lens inplant of known thickness, curvature and refractive index would provide very useful information.

In the light of these points, the present author sincerely hopes that this thesis marks the beginning of some very productive and interesting research.

APPENDICES

APPENDIX 1: ULTRASONIC OPHTHALMOPHAKOMETRY PROGRAM (FOR THE COMMODORE CBM 3032 C0MPUTER)

```
10 PRINT "CLEAR SCREEN" : PRINT : PRINT
20 PRINT " PROG : U-OPK (2) : PRINT : PRINT
30 PRINT "ULTRASONIC OPHTHALMOPHAKOMETRY"
40 PRINT "_____" : PRINT
50 PRINT " INCLUDING COMPARISON OF"
60 PRINT "_____" : PRINT
70 PRINT " A MEASURED AND CALCULATED"
80 PRINT "_____" : PRINT
90 PRINT " AXIAL LENGTH"
100 PRINT "_____" : PRINT
110 PRINT "[AFTER LEARY AND YOUNG(1968)]" : PRINT : PRINT
120 PRINT "BY M. DUNNE"
124 FOR I = 1 TO 4000 STEP 1
125 NEXT I
130 PRINT "CLEAR SCREEN"
140 PRINT "ASSUMED SCHEMATIC REFRACTIVE INDICES"
150 PRINT "_____" : PRINT
160 PRINT "(N1)AIR _____ 1.0000" : N1 = 1 : PRINT
170 PRINT "(N2)AQUEOUS ____ 1.3374" : N2 = 1.3374 : PRINT
180 PRINT "(N3) LENS _____ 1.42" : N3 = 1.42 : PRINT
190 PRINT "(N4) VITREOUS ____ 1.336" : N4 = 1.336 : PRINT : PRINT
200 PRINT " NB:- CORNEAL THICKNESS"
220 PRINT "         NEGLIGIBLE SO NO"
230 PRINT "         REFRACTIVE INDEX"
240 FOR I = 1 TO 5000 STEP 1 : STEP 1 : NEXT I : PRINT "CLEAR SCREEN"
250 PRINT "SUBJECT DATA :-"
260 PRINT "_____" : PRINT
270 INPUT " NAME/NUMBER : " ; N$
280 INPUT " EYE (R/L) : " ; E$
290 INPUT " COMMENTS : " ; C$ : PRINT "CLEAR SCREEN"
300 PRINT "PURKINJE IMAGE DATA :-"
310 PRINT "_____" : PRINT
320 INPUT " HEIGHT OF IMAGE I : " ; H1 : PRINT
330 INPUT " HEIGHT OF IMAGE III : " ; H3 : PRINT
340 INPUT " HEIGHT OF IMAGE IV : " ; H4 : PRINT: PRINT : PRINT : H4 = -H4
350 PRINT " NB:- SINGLE SURFACED CORNEA"
360 PRINT "   SO IMAGE II NOT USED" : FOR I =1 TO 2000 STEP 1 : NEXT I : PRINT "CLEAR SCREEN"
380 PRINT "ULTRASOUND DATA :-" : PRINT "_____" : PRINT
390 INPUT " ANTERIOR CHAMBER DEPTH : " ; D1 : PRINT
400 INPUT " LENS THICKNESS : " ; D2 : PRINT
410 INPUT " VITREOUS CHAMBER DEPTH : " ; D3 : PRINT
420 INPUT " AXIAL LENGTH : " ; D4 : PRINT : PRINT "CLEAR SCREEN"
430 PRINT "OCULAR REFRACTION :-" : PRINT "_____" : PRINT
440 INPUT " SPHERE/D : " ; S : PRINT
445 INPUT " CYLINDER/D : " ; C : PRINT
450 INPUT " SINE OF AXIS : " ; X : PRINT
460 FA=C*X^2 : K=S+FA : PRINT "CLEAR SCREEN"
470 PRINT "CORNEAL READINGS :-" : PRINT "_____" : PRINT
480 PRINT : PRINT "CONVERT INTO SPHEROCYLINDRICAL FORM" : PRINT
490 INPUT " SPHERE RADIUS/MM : " ; KS : PRINT
500 INPUT " CYLINDER RADIUS/MM : " ; KC : PRINT
510 INPUT " SINE OF AXIS : " ; KX : PRINT
520 FK=KC*KX^2 : R1=KS+FK : F1=((N2-N1)*1000)/R1 : PRINT "CLEAR SCREEN"
550 PRINT : PRINT : PRINT
560 PRINT : PRINT : PRINT : PRINT
570 PRINT "PROCESSING DATA"
600 REM - CALCULATION OF DATA USING H1, H3
610 RB=(H3*R1)/H1
620 DA=(1000*N1)/((((1000*N2)/D1)-F1)
630 R2=((1000*N2)/(((1000*N1)/(RB+DA))+F1)-D1)
640 F2=((N3-N2)*1000)/R2
650 REM - SPLIT UP EQUATION FOR L3
660 W=((1000*N2)/(K+F1))-D1
665 WW=(((1000*N2)/W)+F2)
670 L3=(1000*N3)/(((1000*N3)/WW)-D2)
680 F3=((1000*N4)/(D4-(D1+D2)))-L3
690 R3=((N4-N3)*1000)/F3
800 REM -1 - CALCULATION OF DATA USING H1, H2 AND H3
810 REM -2 - RB, DA, R2 AND F2 ALREADY KNOWN
820 RC=(H4*R1)/H1
830 DB=(1000*N2)/(((1000*N3)/D2)-F2)
840 PA=DB+D1
850 PB=(1000*N1)/(((1000*N2)/PA)-F1)
860 Q=PB+RC
870 REM - RAY TRACING FOR POSTERIOR LENS
880 T1=(1000*N1)/Q
890 T2=T1+F1
```

```
900 T3=1000/((1000/T2)-(D1/N2))
910 T4=T3+F2
920 T5=(1000*N3)/T4
930 ER=-D2+T5
940 EF=(1000*(N4-N3))/ER
950 REM - RAY TRACING FOR AXIAL LENGTH
960 A6=L3+EF
980 EV=(N4*1000)/A6
990 EA=D1+D2+EV
1000 PRINT "CLEAR SCREEN"
1100 REM - CALCULATE EQUIVALENT LENS POWER (FE) - (ULTRA)
1110 REM - E2, E3, E4 ARE INTERMEDIATE TERMS
1120 E2=((1000*N3)/F3)-D2
1130 E3=((1000*N2)/(((1000*N3)/E2)+F2))-D1
1140 E4 = (1000*N1)/(((1000*N2)/E3)+F1)
1150 REM - GA IS INTERMEDIATE FOR FE
1160 GA=(1000*N2)/(((1000*N3)/E2)+F2)
1170 FE=(1000*N2*E2)/ (((1000*N3)/F3)*GA)
1180 REM - TOTAL POWER OF EYE (FT) - (ULTRA)
1190 FT=(FE+E3)/(N2*E4)
1200 REM - CALCULATE EQUIVALENT LENS POWER (VE) - (CALC)
1210 REM - Z2, Z3, Z4 ARE INTERMEDIATE TERMS
1220 Z2=((1000*N3)/EF)-D2
1230 Z3=((1000*N2)/(((1000*N3)/Z2)+F2))-D1
1240 Z4 = (1000*N1)/(((1000*N2)/Z3)+F1)
1250 REM - G9 IS INTERMEDIATE FOR VE
1260 G9=(1000*N2)/(((1000*N3)/Z2)+F2)
1270 VE=(1000*N2*Z2)/ (((1000*N3)/EF)*G9)
1280 REM - TOTAL POWER OF EYE (YT) - (CALC)
1290 YT=(VE+Z3)/(N2*Z4)
1500 REM - CARDINAL POINT SYSTEM (ULTRA-ONLY)
1510 REM - VERTEX POWERS AND DISTANCES OF LENS
1512 FL=((1000*N3)/(((1000*N3)/F3)-D2))+F2
1520 VL =-((1000*N2)/FL)
1525 FB=((1000*N3)/(((1000*N3)/F2)-D2))+F3
1530 VB=(1000*N4)/FB
1535 REM - VERTEX POWERS AND DISTANCES OF TOTAL EYE SYSTEM
1540 F1=((1000*N2)/(((1000*N2)/FL)-D1))+F1
1545 VI=-((1000*N1)/F1)
1550 J9=((1000*N2)/(((1000*N2)/F1)-D1))+F2
1551 FJ=((1000*N3)/(((1000*N3)/J9)-D2))+F3
1555 VJ=(1000*N4)/FJ
1560 REM - EQUIVALENT FOCAL DISTANCES OF LENS
1565 IA=-((1000*N2)/FE)
1570 IB=(1000*N4)/FE
1575 REM - EQUIVALENT FOCAL DISTANCES OF TOTAL EYE
1580 JA=-((1000*N1)/FT)
1585 JB=(1000*N4)/FT
1590 REM - POSITIONS OF PRINCIPAL POINTS OF LENS
1591 LF=VL-IA
1592 LB=VB-IB
1593 C1=D1+LF
1594 C2=D1+D2+LB
1615 REM - POSITIONS OF PRINCIPAL POINTS FOR TOTAL EYE SYSTEM
1620 P1=VI+JA
1625 EX=-(N4*(C1/N2)*(FL/FT))
1630 P2=D1+D2+VJ-JB
1635 REM - POSITION OF NODAL POINTS IN TOTAL EYE OPTICAL SYSTEM
1640 NA=JB+VI
1650 NB=D1+D2+VJ+JA
1655 REM - ENTRANCE AND EXIT PUPILS
1660 Y1=(1000*N1)/(((1000*N2)/D1)-F1)
1665 Y2=(D1+D2)*((1000*N2)/(((1000*N3)/D2)-FE))
1910 PRINT "CLEAR SCREEN" : PRINT : PRINT : PRINT : PRINT : PRINT : PRINT : PRINT
1920 INPUT "PRINTOUT (PRESS 1) OR SCREEN (PRESS 2)" ; QW
1930 IF QW=1 GOTO 2000
1940 IF QW=2 GOTO 2020
2000 REM - PRINTOUT
2001 PRINT : PRINT : PRINT : PRINT : PRINT : PRINT
2002 PRINT : PRINT : PRINT : PRINT : PRINT : PRINT
2003 PRINT " PRINTOUT"
2010 OPEN 4,4 : CMD 4
2020 PRINT " RESULTS" : PRINT" _____ "
2021 PRINT " SUBJECT : " ; N$
2022 PRINT " EYE : " ; E$
2023 PRINT " COMMENTS : " ; C$ : PRINT
2030 PRINT " INITIAL DATA:-" : PRINT" _____ "
2034 IF QW=1 GOTO 2040
```

299

```
2035 INPUT "TO GO ON PRESS Q" ; Q$
2040 PRINT "(A) PURKINJE IMAGE DATA" : PRINT "_____"
2050 PRINT "IMAGE I : " ; H1
2055 PRINT "IMAGE III : " ; H3
2060 PRINT "IMAGE IV : " ; H4
2064 IF QW=1 GOTO 2070
2065 INPUT "TO GO ON PRESS Q" ; Q$
2070 PRINT "(B) ULTRASOUND DATA" : PRINT "_____"
2080 PRINT "ANTERIOR CHAMBER DEPTH : " ; D1
2090 PRINT "LENS THICKNESS : " ; D2
2100 PRINT "VITREOUS CHAMBER DEPTH : " ; D3
2110 PRINT "AXIAL LENGTH : " ; D4 : PRINT
2114 IF QW=1 GOTO 2120
2115 INPUT "TO GO ON PRESS Q" ; Q$
2120 PRINT "(C) CORNEAL DATA" : PRINT "_____"
2130 PRINT "RESOLVED RADIUS : " ; R1 : PRINT
2140 PRINT "(D) REFRACTIVE ERROR" : PRINT "_____"
2150 PRINT "RESOLVED POWER : " ; K : PRINT
2151 IF QW=1 GOTO 2160
2155 INPUT "TO GO ON PRESS Q" ; Q$
2160 PRINT "CALCULATED DATA:-" : PRINT "_____"
2170 PRINT "(A) SURFACE RADII" : PRINT "_____"
2180 PRINT "CORNEAL : " ; R1
2190 PRINT "ANTERIOR LENS : " ; R2
2200 PRINT "POSTERIOR LENS (ULTRA) : " ; R3
2200 PRINT "                   (CALC) : " ; ER : PRINT
2214 IF QW=1 GOTO 2220
2215 INPUT "TO GO ON PRESS Q" ; Q$
2220 PRINT "(B) AXIAL DISTANCES" : PRINT "_____"
2230 PRINT "ANTERIOR CHAMBER DEPTH : " ; D1
2240 PRINT "LENS THICKNESS : " ; D2
2250 PRINT "VITREOUS CHAMBER DEPTH (ULTRA) : " ; D3
2260 PRINT "                   (CALC) : " ; EV
2270 PRINT "AXIAL LENGTH (ULTRA) : " ; D4
2280 PRINT "                   (ULTRA) : " ; EA : PRINT
2284 IF QW=1 GOTO 2290
2285 INPUT "TO GO ON PRESS Q" ; Q$
2290 PRINT "(C) SURFACE POWERS" : PRINT "_____"
2300 PRINT "CORNEAL : " ; F1
2310 PRINT "ANTERIOR LENS : " ; F2
2320 PRINT "POSTERIOR LENS (ULTRA) : " ; F3
2330 PRINT "                   (CALC) : " ; EF
2340 PRINT "EQUIVALENT LENS POWER (ULTRA) : " ; FE
2410 PRINT "                   (CALC) : " ; VE
2350 PRINT "TOTAL POWER OF EYE (ULTRA) : " ; FT
2351 PRINT "                   (CALC) : " ; YT : PRINT
2359 IF QW=1 GOTO 2361
2360 INPUT "TO GO ON PRESS Q" ; Q$
2361 PRINT : PRINT "CARDINAL POINTS"
2362 PRINT "_____" : PRINT
2363 PRINT "(A) LENTICULAR VERTEX POWERS/DISTANCES"
2364 PRINT "_____" : PRINT
2400 PRINT "FRONT VERTEX POWER : " ; FL : PRINT
2410 PRINT "FRONT VERTEX DISTANCE : " ; VL : PRINT
2420 PRINT "BACK VERTEX POWER : " ; FB : PRINT
2430 PRINT "BACK VERTEX DISTANCE : " ; VB : PRINT
2434 IF QW=1 GOTO 2440
2435 INPUT "TO GO ON PRESS Q" ; Q$
2440 PRINT "(B) TOTAL EYE VERTEX POWERS/DISTANCES"
2450 PRINT "_____" : PRINT
2460 PRINT "FRONT VERTEX POWER : " ; FI : PRINT
2470 PRINT "FRONT VERTEX DISTANCE : " ; VI : PRINT
2480 PRINT "BACK VERTEX POWER : " ; FJ : PRINT
2490 PRINT "BACK VERTEX DISTANCE : " ; VJ : PRINT
2494 IF QW=1 GOTO 2500
2495 INPUT "TO GO ON PRESS Q" ; Q$
2500 PRINT "(C) LENTICULAR EQUIVALENT FOCAL DISTANCE"
2505 PRINT "_____" : PRINT
2510 PRINT "ANTERIOR : " ; IA : PRINT
2515 PRINT "POSTERIOR : " ; IB : PRINT
2520 PRINT "(D) TOTAL EYE EQUIVALENT FOCAL DISTANCE"
2521 PRINT "_____" : PRINT
2525 PRINT "ANTERIOR : " ; JA : PRINT
2530 PRINT "POSTERIOR : " ; JB : PRINT
2533 IF QW=1 GOTO 2535
2534 INPUT "TO GO ON PRESS Q" ; Q$
```

APPENDIX 1 (CONTINUED)

```
2535 PRINT "(E) LENTICULAR PRINCIPAL POINTS"
2536 PRINT "_____" : PRINT
2540 PRINT "PP1 FROM ANT. SURFACE : " ; LF : PRINT
2545 PRINT "PP2 FROM POST. SURFACE : " ; LB : PRINT
2550 PRINT "PP1 FROM ANT. CORNEA : " ; C1 : PRINT
2554 PRINT "PP2 FROM ANT, CORNEA : " ; C2 : PRINT
2555 IF QW=1 GOTO 2560
2556 INPUT "TO GO ON PRESS Q" ; Q$
2560 PRINT "(F) TOTAL EYE PRINCIPAL POINTS"
2561 PRINT "_____" : PRINT
2565 PRINT "PP1 FROM CORNEA : " ; P1 : PRINT
2570 PRINT "PP2 FROM CORNEA : " ; P2 : PRINT
2580 PRINT "(G) TOTAL EYE NODAL POINTS"
2581 PRINT "_____" : PRINT
2585 PRINT "N1 FROM CORNEA : " ; NA : PRINT
2590 PRINT "N2 FROM CORNEA : " ; NB : PRINT
2595 PRINT "(H) TOTAL EYE ENTRANCE/EXIT PUPILS"
2596 PRINT "_____" : PRINT
2600 PRINT "ENTRANCE PUPIL : " ; Y1 : PRINT
2700 PRINT "EXIT PUPIL : " ; Y2
2900 IF QW=2 GOTO 3010
3005 PRINT #4
3006 CLOSE 4,4
3010 END
```

SAMPLE PRINTOUT:

RESULTS

SUBJECT : NEAR-EMMETROPE
EYE : RIGHT
COMMENTS : AVERAGED RESULTS

INITIAL DATA:-

(A) PURKINJE IMAGE DATA

IMAGE I :	22.12
IMAGE III :	38.2
IMAGE IV :	-17.02

(B) ULTRASOUND DATA

ANTERIOR CHAMBER DEPTH :	3.87
LENS THICKNESS :	3.56
VITREOUS CHAMBER DEPTH :	16.52
AXIAL LENGTH :	23.95

(C) CORNEAL DATA

RESOLVED RADIUS : 7.900024

(D) REFRACTIVE ERROR

RESOLVED POWER : -0.180004

CALCULATED DATA:-

(A) SURFACE RADII

CORNEAL :	7.900024
ANTERIOR LENS :	9.27727184
POSTERIOR LENS (ULTRA) :	-6.07705646
(CALC) :	-6.30358588

(B) AXIAL DISTANCES

ANTERIOR CHAMBER DEPTH :	3.87
LENS THICKNESS :	3.56
VITREOUS CHAMBER DEPTH (ULTRA) :	16.52
(CALC) :	16.6220969
AXIAL LENGTH (ULTRA) :	23.95
(CALC) :	24.0520969

APPENDIX 1 (CONTINUED)

(C) SURFACE POWERS

```
CORNEAL :                              42.7087311
ANTERIOR LENS :                         8.90347953
POSTERIOR LENS (ULTRA) :               13.8224818
              (CALC) :    .            13.3257484
EQUIVALENT LENS POWER (ULTRA) : 22.4174238
                    (CALC) : 21.9317786
TOTAL EYE POWER (ULTRA) :              60.875685
              (CALC) :                 60.5032449
```

CARDINAL POINTS

(A) LENTICULAR VERTEX POWERS/DISTANCES

FRONT VERTEX POWER :   23.2221537

FRONT VERTEX DISTANCE :   -57.5915574

BACK VERTEX POWER :   22.9292364

BACK VERTEX DISTANCE :   58.2662229

(B) TOTAL EYE VERTEX POWERS/DISTANCES

FRONT VERTEX POWER :   67.6037651

FRONT VERTEX DISTANCE :   -14.7920755

BACK VERTEX POWER :   81.1914564

BACK VERTEX DISTANCE :   16.4549333

(C) LENTICULAR EQUIVALENT FOCAL DISTANCE

ANTERIOR :   -59.6589516

POSTERIOR :   59.5965002

(D) TOTAL EYE EQUIVALENT FOCAL DISTANCE

ANTERIOR :   -16.4269199

POSTERIOR :   21.946365

(E) LENTICULAR PRINCIPAL POINTS

PP1 FROM ANT. SURFACE :   2.06739417

PP2 FROM POST. SURFACE :   -1.33027729

PP1 FROM ANT. CORNEA :   5.93739417

PP2 FROM ANT. CORNEA :   6.09972271

(F) TOTAL EYE PRINCIPAL POINTS

PP1 FROM CORNEA :   1.63484433

PP2 FROM CORNEA :   1.93856835

(G) TOTAL EYE NODAL POINTS

N1 FROM CORNEA :   7.1542894

N2 FROM CORNEA :   7.45801343

(H) TOTAL EYE ENTRANCE/EXIT PUPILS

ENTRANCE PUPIL :   3.30171758

EXIT PUPIL :   26.3956567

302

APPENDIX 2a : P.E.K. RESULTS

* † denotes a female subject.
* Refractive groups: E = near-emmetrope, M = myope, H = hyperope.
* Conic constant, P = 1- Wesley-Jessen "shape factor".
* The unconventional manner in which the axes are shown serves to simplify statistical calculations.
* Apex position with respect to the line of sight (resolved as described by Tomlinson and Schwartz, 1979)

      Horizontal : -ve = nasal, +ve = temporal.
      Vertical : -ve = inferior, +ve = superior.

Subject	Refractive Group	Radius (mm)		Conic Constant (P)		Axis of flat Meridian (°)	Apex position (mm)	
		Horizontal	Vertical	Horizontal	Vertical		Horizontal	Vertical
PCR	E	7.53	7.48	0.58	0.6	180	0	0
SB	E	8.05	8.11	0.78	0.98	90	0	0
JR	E	8.06	8.01	0.78	0.96	180	-0.35	1.97
TB	E	7.84	7.58	0.88	0.68	180	-2	0
ND	E	8.09	8.04	0.85	0.87	175	-1	1.73
SG†	E	7.96	7.85	0.73	0.84	180	-0.5	0.87
ST†	E	7.87	7.71	0.73	0.74	180	-0.87	0.5
SC†	E	8.12	7.95	0.59	0.52	180	-0.17	-0.98
RD	E	7.82	7.86	0.72	0.9	85	0	0
BF	E	8.46	8.41	0.75	1.02	180	0	0
DM	M	8.02	8.03	0.79	0.94	90	-0.17	-0.98
RP	M	7.62	7.46	0.67	0.53	175	0	0
MG†	M	8.1	8.19	0.87	0.86	90	0	-3
MES	M	7.75	7.81	0.63	0.89	95	0	0
CS†	M	7.66	7.58	0.72	0.76	185	-0.87	0.5
GP	M	7.88	7.82	0.68	0.88	180	0.17	-0.98
MEN	M	7.99	7.78	0.48	0.66	185	0.09	-1
SL†	M	7.85	7.75	0.88	0.8	185	-0.42	0.91
PCE	M	8.18	8.15	0.73	0.84	180	0	0
AL	M	7.33	7.21	0.69	0.71	175	0	0
MM	M	7.61	7.52	0.66	0.77	180	0	0
RC	M	8.04	8.03	0.59	0.59	185	0	0
RLA	M	8.06	7.85	0.65	0.41	185	0	0
TM	M	8.03	8.02	0.88	0.67	180	0.94	0.34
RT	M	8.43	8.35	0.68	0.71	175	-0.82	-0.57
MH	M	7.96	7.81	0.67	0.58	190	0	0
SH	H	8.13	8.26	0.93	0.89	85	-0.52	1.93
EH	H	7.59	7.34	0.42	1.09	180	-1	0
DC	H	8.19	8.03	0.81	0.77	185	0.26	0.96
AS	H	7.42	7.4	0.73	1.06	185	1	0
AH†	H	7.74	7.64	0.78	0.8	175	0	0
CM†	H	8.13	7.97	0.7	0.8	185	0.09	-1
RL†	H	7.27	7.25	1.03	0.76	175	1	0
HM†	H	7.77	7.65	0.71	0.7	180	0.64	-0.77

REPEAT P.E.K. READINGS TAKEN ON SIX SUBJECTS

* Interval denotes period of time which elapsed between first and second readings

Subject	Interval (months)	Radius (mm)				Axis of Flat Meridian (°)	
		Horizontal		Vertical			
		1st Reads	2nd Reads	1st Reads	2nd Reads	1st Reads	2nd Reads
MG†	4	8.09	8.1	8.2	8.19	95	90
MES	2.5	7.74	7.75	7.72	7.81	180	95
AL	6	7.35	7.33	7.25	7.21	185	175
MH	5	7.95	7.96	7.87	7.81	180	190
RD	5	7.83	7.82	7.82	7.86	180	85
DC	4.5	8.15	8.19	8.03	8.03	175	185

Subject	Conic constant (P)				Apex Position (mm)			
	Horizontal		Vertical		Horizontal		Vertical	
	1st Reads	2nd Reads	1st Reads	2nd Reads	1st Reads	2nd Reads	1st Reads	2nd Reads
MG†	0.77	0.86	0.68	0.87	-1.64	0	1.15	-3
MES	0.83	0.63	0.97	0.89	0	0	0	0
AL	0.7	0.69	0.58	0.71	0	0	0	0
MH	0.57	0.67	0.7	0.58	0.17	0	2	0
RD	0.75	0.72	0.82	0.9	0	0	0	0
DC	0.85	0.81	0.91	0.77	-0.57	0.26	-0.82	0.96

303

* † denotes a female subject.
* Refractive groups: E = near-emmetropes; M = myopes, H = hyperopes.
* The mean and standard deviation (SD) values are based on three repeat readings taken on one occasion only.
* The unconventional manner in which the horizontal axes are shown serves to simplify statistical calculations.

.

Subject	Refractive Group	Radius (mm)				Axis (°)			
		Horizontal		Vertical		Horizontal		Vertical	
		Mean	SD	Mean	SD	Mean	SD	Mean	SD
PCR	E	7.53	0.006	7.51	0.02	180.3	0.6	90	0
SB	E	8.07	0	8.11	0.02	211.7	10.5	103.7	9.1
JR	E	8.01	0	8.01	0	180	0	90	0
TB	E	7.77	0.01	7.55	0.005	180	0	90	0
ND	E	8.09	0.006	8.08	0.02	186	5.6	120.3	19.6
SG†	E	7.98	0.02	7.85	0.01	174.3	5.1	91	4.6
ST†	E	7.93	0.01	7.7	0.01	179	2	87.7	8.2
SC†	E	8.11	0.01	7.88	0.01	176	4	85.3	1.5
RD	E	7.84	0.006	7.81	0.006	180.3	0.58	87	3
BF	E	8.49	0.006	8.36	0.01	180	0	90	0
DM	M	8.05	0.02	8.05	0.02	178.3	2.1	86	4.6
RP	M	7.62	0.01	7.43	0.06	173.7	0.58	86	1
MG†	M	8.07	0.01	8.09	0.03	185.3	8.4	91	2.6
MES	M	7.77	0.01	7.74	0.03	180	0	90	0
CS†	M	7.72	0.006	7.59	0.01	181.3	0.58	92.3	2.5
GP	M	7.91	0.02	7.78	0.02	171.7	1.5	83.3	2.08
MEN	M	7.99	0.006	7.78	0.01	180	1	90	0
SL†	M	7.8	0.006	7.79	0.006	180	0	90	0
PCE	M	8.22	0.01	8.14	0.02	142.7	5.7	69.3	7.2
AL	M	7.38	0.01	7.2	0.01	165.7	2.1	84.7	1.5
MM	M	7.64	0.02	7.56	0.02	180	0	90	0
RC	M	8.11	0.01	8.02	0.02	178.3	1.5	89	2.6
RLA	M	8.07	0.025	7.83	0.01	180.3	1.15	91.7	1.5
TM	M	8.07	0.01	8.06	0.006	181	0	90.3	1.15
RT	M	8.48	0.01	8.39	0.01	179.7	0.58	90	0
MH	M	8.02	0.03	7.83	0.01	168.7	5.7	78.7	4
SH	H	8.09	0.006	8.31	0.01	183	5.2	90.7	1.1
EH	H	7.7	0	7.35	0.01	181.7	1.5	95.7	4.2
DC	H	8.21	0.02	8.06	0.006	181	1.7	92	1.7
AS	H	7.48	0.05	7.4	0.006	191	10.5	109	2
AH†	H	7.78	0.01	7.63	0.01	190.7	1.52	102.3	7.4
CM†	H	8.2	0.1	7.89	0.05	185.7	5.1	99	1
RL†	H	7.21	0.01	7.19	0.006	181.3	0.58	90.3	0.58
HM†	H	7.86	0.01	7.7	0.01	174.3	12.7	81.3	1.5

APPENDIX 2c : ANTERIOR CHAMBER DEPTH MEASUREMENTS

* † denotes a female subject.
* Refractive groups; E = near-emmetrope, M = myope, H = hyperope.
* N denotes number of ultrasonic observations from which mean and standard deviation values (SD) were calculated.
* The pachometric mean and standard deviation (SD) values were based on three repeat readings taken on one session only.
* Anterior chamber depth includes corneal thickness.

Subject	Refractive Group	Pachometry		Ultrasonography - First Readings			Ultrasonography - Second Readings		
		Mean	SD	N	Mean	SD	N	Mean	SD
PCR	E	3.64	0.03	10	3.67	0.04	11	3.69	0.05
SB	E	3.89	0.05	13	4	0.08	8	4.01	0.06
JR	E	4.18	0.09	17	4.08	0.08	16	4.1	0.06
TB	E	3.79	0.02	21	4	0.03	13	3.98	0.02
ND	E	3.9	0.05	9	3.83	0.31	-	-	-
SG†	E	3.49	0.05	18	3.72	0.1	-	-	-
ST†	E	3.66	0.06	14	3.85	0.04	15	3.55	0.07
SC†	E	3.56	0.04	23	3.71	0.02	12	3.65	0.06
RD	E	3.8	0.02	15	3.83	0.1	23	3.7	0.1
BF	E	3.87	0.02	41	4	0.07	15	4	0.08
DM	M	4.03	0.06	24	4.08	0.04	11	4.07	0.02
RP	M	3.68	0.03	29	3.85	0.02	14	3.67	0.05
MG†	M	3.67	0.04	11	3.54	0.08	22	3.37	0.08
MES	M	4.13	0.16	15	4.07	0.06	25	3.68	0.12
CS†	M	3.53	0	11	3.79	0.01	15	3.59	0.05
GP	M	3.81	0.03	9	4.02	0.02	10	3.85	0.07
MEN	M	3.98	0.05	8	4.14	0.02	17	4.13	0.09
SL†	M	3.79	0.04	7	3.95	0.17	18	3.61	0.08
PCE	M	3.79	0.04	15	3.77	0.05	14	3.74	0.06
AL	M	4.12	0	12	4.27	0.04	17	4.01	0.1
MM	M	3.8	0	10	3.93	0.07	10	3.83	0.08
RC	M	3.93	0.06	10	4.1	0.12	15	4.09	0.02
RLA	M	3.75	0.03	10	3.72	0.09	-	-	-
TM	M	4.02	0.07	15	4.27	0.04	15	4	0.2
RT	M	3.69	0.05	15	3.56	0.05	15	3.84	0.03
MH	M	3.77	0.04	9	3.81	0.07	6	3.97	0.08
SH	H	3.83	0.02	11	3.98	0.02	-	-	-
EH	H	2.89	0.06	13	3.01	0.12	13	3.12	0.05
DC	H	3.48	0.11	20	3.59	0.02	-	-	-
AS	H	3.15	0.04	12	3.3	0.08	10	3.24	0.05
AH†	H	3.55	0	13	3.63	0.05	-	-	-
CM†	H	3.75	0.04	15	3.92	0.03	7	3.75	0.08
RL†	H	3.04	0.04	12	3.09	0.07	14	3.2	0.04
HM†	H	3.65	0.09	8	3.43	0.08	12	3.58	0.06

APPENDIX 2d : ULTRASOUND RESULTS (FIRST READINGS)

* † denotes a female subject.
* Refractive groups; E = near-emmetrope, M = myope, H = hyperope.
* N denotes number of ultrasonic observations from which mean and standard deviation values (SD) were calculated.
* See appendix 2c for anterior chamber depth

Subject	Refractive Group	N	Lens Thickness (mm) Mean	SD	Vitreous Length (mm) Mean	SD	Axial length (mm) Mean	SD
PCR	E	10	3.46	0.03	15.98	0.08	23.12	0.11
SB	E	13	3.54	0.07	16.76	0.13	24.3	0.12
JR	E	17	3.81	0.01	16.43	0.09	24.33	0.07
TB	E	21	3.53	0.02	15.92	0.1	23.44	0.09
ND	E	9	3.73	0.05	16.66	0.04	24.23	0.32
SG†	E	18	3.79	0.09	15.89	0.17	23.4	0.18
ST†	E	14	3.58	0.05	15.96	0.04	23.39	0.05
SC†	E	23	3.4	0.02	17.05	0.04	24.16	0.04
RD	E	15	3.47	0.12	16.72	0.12	24.03	0.11
BF	E	41	3.32	0.08	17.82	0.06	25.14	0.11
DM	M	24	3.62	0.08	17.94	0.04	25.63	0.07
RP	M	29	3.87	0.04	16.74	0.06	24.46	0.06
MG†	M	11	3.6	0.01	18.18	0.04	25.32	0.08
MES	M	15	3.24	0.02	18.48	0.02	25.8	0.07
CS†	M	11	3.47	0.01	17.41	0.02	24.67	0.01
GP	M	9	3.32	0.02	18.85	0.05	26.2	0.05
MEN	M	8	3.48	0.19	17.87	0.18	25.5	0.04
SL†	M	7	3.25	0.02	17.31	0.09	24.51	0.15
PCE	M	15	3.74	0.03	17.18	0.07	24.69	0.11
AL	M	12	3.01	0.02	16.62	0.07	23.9	0.07
MM	M	10	3.36	0.08	16.63	0.04	23.92	0.06
RC	M	10	3.37	0.05	17.98	0.47	25.45	0.39
RLA	M	10	3.5	0.03	17.66	0.05	24.89	0.09
TM	M	15	3.38	0.04	19.1	0.03	26.75	0.03
RT	M	15	3.55	0.02	18.25	0.01	25.36	0.06
MH	M	9	3.24	0.03	17.71	0.09	24.77	0.07
SH	H	11	3.65	0.01	16.11	0.02	23.74	0.02
EH	H	13	4.07	0.03	14.8	0.04	21.88	0.11
DC	H	20	3.94	0.02	15.86	0.12	23.39	0.12
AS	H	12	3.92	0.14	15.62	0.16	22.85	0.04
AH†	H	13	3.91	0.06	15	0.06	22.54	0.06
CM†	H	15	3.17	0.03	16.73	0.05	23.83	0.06
RL†	H	12	3.87	0.05	13.75	0.04	20.71	0.09
HM†	H	8	3.49	0.08	14.76	0.12	21.69	0.12

306

APPENDIX 2e : ULTRASOUND RESULTS (SECOND READINGS)

* † denotes a female subject.
* Refractive groups; E = near-emmetrope, M = myope, H = hyperope.
* N denotes number of ultrasonic observations from which mean and standard deviation values (SD) were calculated.
* See appendix 2c for anterior chamber depth.

Subject	Refractive Group	N	Lens Thickness (mm) Mean	SD	Vitreous Length (mm) Mean	SD	Axial length (mm) Mean	SD
PCR	E	11	3.29	0.01	16.21	0.07	23.18	0.09
SB	E	8	3.52	0.08	16.78	0.1	24.31	0.13
JR	E	16	3.82	0.01	16.34	0.04	24.26	0.05
TB	E	13	3.51	0.02	15.9	0.06	23.39	0.06
ND	E	-	-	-	-	-	-	-
SG†	E	-	-	-	-	-	-	-
ST†	E	15	3.56	0.02	15.97	0.03	23.09	0.06
SC†	E	12	3.41	0.01	17.11	0.11	24.16	0.11
RD	E	23	3.31	0.12	16.86	0.07	23.88	0.16
BF	E	15	3.28	0.03	17.9	0.04	25.18	0.07
DM	M	11	3.63	0.01	17.9	0.03	25.61	0.04
RP	M	14	3.87	0.02	16.83	0.01	24.37	0.06
MG†	M	22	3.56	0.02	18.08	0.03	25.01	0.1
MES	M	25	3.26	0.01	18.44	0.03	25.39	0.11
CS†	M	15	3.52	0.02	17.37	0.08	24.48	0.12
GP	M	10	3.21	0.04	19.22	0.07	26.28	0.08
MEN	M	17	3.52	0.18	18.05	0.17	25.7	0.07
SL†	M	18	3.22	0.02	17.29	0.05	24.11	0.13
PCE	M	14	3.8	0.03	17.09	0.06	24.63	0.15
AL	M	17	3.03	0.07	16.63	0.12	23.67	0.15
MM	M	10	3.35	0.02	16.53	0.01	23.71	0.05
RC	M	15	3.41	0.01	17.88	0.08	25.39	0.07
RLA	M	-	-	-	-	-	-	-
TM	M	15	3.43	0.02	19.11	0.15	26.53	0.31
RT	M	15	3.48	0.16	18.24	0.12	25.57	0.02
MH	M	6	3.22	0.07	17.63	0.17	24.79	0.14
SH	H	-	-	-	-	-	-	-
EH	H	13	3.9	0.05	14.98	0.08	21.99	0.08
DC	H	-	-	-	-	-	-	-
AS	H	10	3.58	0.09	15.94	0.06	22.75	0.06
AH†	H	-	-	-	-	-	-	-
CM†	H	7	3.21	0.03	16.67	0.08	23.65	0.18
RL†	H	14	3.94	0.05	13.77	0.02	20.91	0.02
HM†	H	12	3.43	0.07	15.13	0.08	22.13	0.08

APPENDIX 2f: ASSESSMENT OF DISTORTION OF OPHTHALMOPHAKOMETRIC PHOTOGRAPHS

* Figures shown in table refer to distances measured between grid lines as seen after projection.
* The columns of figures show repeat readings taken from 10 grid photographs.
* As the real distance between grid lines was known to be 1 mm, distances shown in table represent
  the magnification of the grid at any given point on the photograph.
* Distances were measured, with a standard ruler, to the nearest 0.5 mm.

HORIZONTAL PLANE

LEFT 5	4	3	2	1	1	2	3	4	RIGHT 5
			Distance of grid line from centre of photograph (mm)						
21.5	22	21.5	22	21.5	21.5	22.5	21.5	21.5	22.5
21.5	22	22	21.5	22	21.5	21.5	22	22	22.5
21.5	21.5	22	21.5	22.5	21.5	22	22	22	22
21.5	21.5	22	21.5	22.5	21.5	22	21.5	21.5	22.5
22.5	21.5	22.5	21.5	21.5	21.5	22	22	22.5	22.5
21.5	21.5	22.5	21.5	22	22	21.5	22.5	22.5	21.5
22.5	22	22	22.5	21.5	22.5	21.5	21.5	22	21.5
21.5	21.5	22	22	22.5	21.5	22	22.5	22	22.5
22	22	22	21.5	21.5	21.5	21.5	21.5	22	21.5
22.5	21.5	22	21.5	21.5	22.5	21.5	21.5	22	21.5

AVERAGES AND STANDARD DEVIATIONS

21.85	21.7	22.05	21.7	21.9	21.75	21.8	21.85	22	22.05
0.45	0.24	0.27	0.33	0.44	0.40	0.33	0.39	0.32	0.47

VERTICAL PLANE

TOP 5	4	3	2	1	1	2	3	4	BOTTOM 5
			Distance of grid line from centre of photograph (mm)						
21.5	22.5	22	22.5	22	22	21.5	22.5	22.5	22.5
22.5	22	22.5	22	21.5	22.5	22	22	22.5	21.5
21.5	22.5	22	22	21.5	21.5	22	22	22	22
22.5	22.5	22	22.5	21.5	22	21.5	22	22	21.5
21.5	22.5	22	22	22.5	21.5	21.5	22.5	21.5	22.5
22.5	22.5	21.5	22.5	22.5	21.5	22	22	21.5	22.5
22.5	22	21.5	21.5	22.5	22.5	22	22	22	22
22.5	21.5	22.5	21.5	21.5	21.5	22	21.5	22	21.5
21.5	22.5	21.5	22.5	22.5	22	21.5	22.5	22.5	22.5
21.5	22.5	22	22	22	21.5	22	22.5	22	22.5

AVERAGES AND STANDARD DEVIATIONS

22	22.3	21.95	22.1	22	21.85	21.8	22.15	22.05	22.1
0.5	0.33	0.35	0.37	0.45	0.39	0.24	0.32	0.35	0.44

	HORIZONTAL	VERTICAL	TOTAL
AVERAGE	21.865	22.03	21.95
STANDARD DEVIATION	0.39	0.41	0.40

* † denotes a female subject.
* Refractive groups; E = near-emmetrope, M = myope, H = hyperope.
* Mean and standard deviation (SD) values were based on nine repeat readings taken on one session only.
* Figures in the table refer to unscaled Purkinje image heights i.e. as measured after projection.
* See appendix 2e for magnification of projected photographs.

Subject	Refractive Group	Purkinje Image Heights (mm)					
		Image I		Image III		Image IV	
		Mean	SD	Mean	SD	Mean	SD
PCR	E	20.3	0.67	35.4	0.74	15.9	0.33
SB	E	22.8	0.5	36.5	0.75	15	0.25
JR	E	22.7	0.83	39.6	0.82	18.7	0.36
TB	E	22	0.46	38	0.56	17.5	0.46
ND	E	22.2	0.66	42.1	0.99	16.3	0.57
SG†	E	21.7	0.29	34.5	0.5	15.7	0.29
ST†	E	21.3	0.52	34.9	0.66	17.4	0.2
SC†	E	22.7	0.56	39.5	0.58	18.1	0.33
RD	E	21.8	0.26	37.4	0.84	17.5	0.39
BF	E	23.7	0.41	44	0.71	18.1	0.2
DM	M	22.7	0.25	41.6	0.93	17.5	0.17
RP	M	20	0.3	35.3	0.62	15.8	0.35
MG†	M	22.7	0.41	37	1.9	16.7	0.26
MES	M	21.4	0.38	44.6	0.58	16.8	0.41
CS†	M	20.9	0.33	32.3	1.41	14.9	0.33
GP	M	22.8	0.82	38.6	0.86	16.3	0.68
MEN	M	21.3	0.26	40	0.89	17.4	0.3
SL†	M	21	0.5	40.2	0.79	16.5	0.3
PCE	M	23.5	0.35	33.5	0.61	16.4	0.33
AL	M	20.9	0.52	52	1.14	18.4	0.39
MM	M	21.3	0.51	45.8	1.3	15	0
RC	M	21.7	0.68	39.2	1.4	15.6	0.2
RLA	M	22.4	1.5	51.7	2.1	15.9	0.86
TM	M	21.6	0.48	38.1	0.55	16.6	0.33
RT	M	23.9	0.73	39.4	0.58	16.9	0.2
MH	M	21.9	0.39	46.4	0.8	18.2	0.26
SH	H	23.3	0.61	35.7	1.5	16.1	0.39
EH	H	18.6	0.8	24	0.77	14.1	0.49
DC	H	20.9	0.46	30.6	0.74	13.5	0.25
AS	H	20.7	0.66	38.7	0.69	16.7	0.62
AH†	H	21.3	0.9	31.8	0.79	14.7	0.44
CM†	H	24.6	0.58	53.4	1.85	19.6	0.66
RL†	H	21.2	0.29	30.8	0.29	16	0.87
HM†	H	21.4	0.68	29.9	1.38	15	0.35

APPENDIX 2h : PHOTOGRAPHIC OPHTHALMOPHAKOMETRY RESULTS (SECOND READINGS)

* † denotes a female subject.
* Refractive groups; E = near-emmetrope, M = myope, H = hyperope.
* Mean and standard deviation (SD) values were based on nine repeat readings taken on one session only.
* Figures in the table refer to unscaled Purkinje image heights i.e. as measured after projection.
* See appendix 2e for magnification of projected photographs.

| Subject | Refractive Group | Purkinje Image Heights (mm) | | | | | |
| | | Image I | | Image III | | Image IV | |
		Mean	SD	Mean	SD	Mean	SD
PCR	E	21.4	0.38	37.5	1.75	16.9	0.49
SB	E	22.1	0.48	36.3	0.9	14.6	0.33
JR	E	-	-	-	-	-	-
TB	E	21.2	0.27	37.9	2.15	17	0.32
ND	E	22.7	0.26	41.9	1.31	16.7	0.73
SG†	E	20.7	0.5	32.5	1.36	15	0.5
ST†	E	22.3	0.36	36	0.71	18.2	0.26
SC†	E	20.1	0.38	36.4	0.8	16.5	0.77
RD	E	21.5	0.35	36	1.07	17.4	0.39
BF	E	21.8	0.29	42.3	0.29	17.3	0.29
DM	M	23.2	0.36	42.7	0.87	18.4	0.17
RP	M	20.5	0.39	33.5	0.83	15.8	0.36
MG†	M	22.5	0.66	38	1.12	16.7	0.56
MES	M	22.2	0.69	43.7	0.69	17.8	0.6
CS†	M	21	0.71	32	1.88	15.4	0.39
GP	M	-	-	-	-	-	-
MEN	M	21.2	0.5	41	0.66	17.3	0.43
SL†	M	21.4	0.42	40.6	0.6	17	0.43
PCE	M	22.5	0.25	31.2	0.36	15.2	0.26
AL	M	20	0.32	52.8	0.75	18.1	0.2
MM	M	21.6	0.48	45.9	1.21	15.7	0.73
RC	M	22.2	0.83	39.3	1	16.9	0.17
RLA	M	23	0.79	53.8	1.1	16.3	0.73
TM	M	22.9	0.63	42.4	0.65	17.8	0.56
RT	M	22.4	0.49	37.3	0.98	15.7	0.26
MH	M	22	0.56	44.5	1	17.6	0.22
SH	H	23.9	0.38	42.2	0.68	16.7	0.52
EH	H	20.5	0.5	26.4	1.92	15.8	0.17
DC	H	21.5	0.71	31.2	1.22	14.2	0.5
AS	H	19.5	0.3	39.2	0.88	16.5	0.43
AH†	H	20.5	0.5	30.5	0.71	14.6	0.33
CM†	H	21.8	1.32	48	2.05	16.4	1.11
RL†	H	19.9	0.58	29.4	0.66	15.9	0.38
HM†	H	20.5	0.39	32.3	1.92	15.2	0.56

APPENDIX 2i : CENTRAL REFRACTIVE ERROR MEASUREMENTS (HARTINGER OPTOMETER)

* † denotes a female subject.
* Refractive groups; E = near-emmetrope, M = myope, H = hyperope.
* The mean and standard deviation (SD) values were based on three repeat readings taken on one session only.
* The unconventional manner in which the tangential axes are shown served to simplify statistical calculations.

Subject	Refractive Group	Tangential Meridian				Sagittal Meridian			
		Refraction (D)		Axis (°)		Refraction (D)		Axis (°)	
		Mean	SD	Mean	SD	Mean	SD	Mean	SD
PCR	E	-0.17	0.14	176.3	1.5	0.17	0.14	88.3	1.1
SB	E	-0.42	0.14	180	0	0.16	0.14	90	0
JR	E	-0.42	0.14	180	0	0	0	90	0
TB	E	-0.25	0	180	0	-0.58	0.14	90	0
ND	E	-0.42	0.14	180	0	-0.25	0.25	90	0
SG†	E	-0.08	0.38	180	0	0.33	0.29	90	0
ST†	E	-0.33	0.38	180	0	-0.33	0.14	90	0
SC†	E	-0.17	0.14	180	0	-0.75	0.25	90	0
RD	E	-0.33	0.14	180	0	-0.17	0.38	90	0
BF	E	0	0	180	0	-0.42	0.14	90	0
DM	M	-2.33	0.29	174.7	5	-1.42	0.14	83.3	3
RP	M	-2.67	0.29	180	0	-3.5	0	90	0
MG†	M	-4.78	0.41	185.3	5	-4.53	0.06	91.7	2.9
MES	M	-4.5	0	180.3	0.58	-4.33	0.14	90.3	0.58
CS†	M	-6.08	0.14	180	0	-6	0	90	0
GP	M	-6.03	0.06	180	0	-6.1	0.3	90	0
MEN	M	-4.83	0.14	179	1.7	-5.17	0.63	94.7	7.2
SL†	M	-1.33	0.14	180	0	-1.33	0.14	90	0
PCE	M	-2.33	0.29	186.3	5.5	-1.5	0	98.7	8.1
AL	M	-2.42	0.14	180	0	-2.58	0.14	90	0
MM	M	-2.67	0.29	180	0	-2.91	0.29	90	0
RC	M	-2.17	0.14	180	0	-2.17	0.14	90	0
RLA	M	-2.75	0.25	180	0	-2.67	0.14	90	0
TM	M	-5.08	0.14	180	0	-4.83	0.38	90	0
RT	M	-1.75	0.25	173.7	7.7	-1	0	88	3.6
MH	M	-2.33	0.29	184	6.9	-2.08	0.14	89.7	0.58
SH	H	0.7	0.09	179	1.73	1.3	0.09	90	0
EH	H	1.25	0.25	189.3	8.6	0.33	0.29	97.3	7.5
DC	H	1.16	0.14	171.3	10.3	0.58	0.29	82.3	6.6
AS	H	0.92	0.14	180	0	0.92	0.14	90	0
AH†	H	1	0	180	0	0.83	0.14	90	0
CM†	H	2	0	161.7	23.6	2.08	0.14	78	13.7
RL†	H	2.5	0.5	180	0	3.08	0.14	90	0
HM†	H	3.5	0	180	0	3.17	0.14	90	0

* † denotes a female subject.
* Refractive groups; E = near-emmetrope, M = myope, H = hyperope.
* The mean and standard deviation (SD) values were based on five repeat readings taken on one session only.
* The unconventional manner in which the tangential axes are shown served to simplify statistical calculations.
* Sagittal axis not shown since Canon R-1 only gives one axis reading.

| Subject | Refractive Group | Tangential Meridian | | | | Sagittal Meridian | |
| | | Refraction (D) | | Axis (°) | | Refraction (D) | |
		Mean	SD	Mean	SD	Mean	SD
PCR	E	-0.79	0.1	194	6.4	-0.1	0.1
SB	E	-0.77	0.55	186.2	12.9	0.52	0.3
JR	E	-0.65	0.1	165.2	1.6	0.4	0.06
TB	E	-0.5	0.08	145.8	2.9	0.32	0.11
ND	E	0.62	0.14	223	1.4	-0.81	0.07
SG†	E	-0.37	0.01	152	10.9	0.37	0.1
ST†	E	-0.38	0.09	159.6	1.8	0.37	0.09
SC†	E	-0.17	0.07	160.4	4.3	0.22	0.06
RD	E	-0.03	0.07	197.8	5.9	0.45	0.07
BF	E	-0.16	0.07	156.7	2.1	0.42	0.14
DM	M	-2.75	0.05	182.8	4.5	-1.17	0.06
RP	M	-3.62	0.17	201.2	4.3	-3.05	0.06
MG†	M	-4	0.29	144.8	5.4	-3.22	0.1
MES	M	-4.37	0.08	166.8	14	-3.7	0.24
CS†	M	-7.05	0.11	140.6	0.89	-5.77	0.1
GP	M	-5.93	0.07	184.3	4.5	-6.12	0.1
MEN	M	-3.92	0.16	221.8	3.3	-4.57	0.12
SL†	M	-1.85	0.05	154.8	3.8	-1.07	0.11
PCE	M	-2.05	0.07	179.2	2.3	-1.15	0.1
AL	M	-1.92	0.07	199	2.2	-1.62	0.15
MM	M	-2.56	0.07	155.5	7.2	-1.43	0.29
RC	M	-2.27	0.1	138.4	31.3	-1.8	0.11
RLA	M	-2.41	0.06	136.6	5.3	-1.86	0.04
TM	M	-4.79	0.07	187.4	9.4	-3.9	0.13
RT	M	-2.2	0.11	171	2.3	0.22	0.1
MH	M	-2.32	0.11	171.2	3.6	-1.27	0.05
SH	H	-0.32	0.24	184	2.2	1.48	0.58
EH	H	0.25	0.37	140.2	38	1.03	0.3
DC	H	1.12	0	166.4	4.6	-0.37	0.16
AS	H	0.8	0.17	156.6	3.8	1.37	0.22
AH†	H	1.84	0.2	212	1	0.25	0.1
CM†	H	3.31	0.12	211.5	25	2.34	0.16
RL†	H	1.3	0.14	208	0.71	3.37	0.09
HM†	H	1.16	0.17	160.2	3.8	1.16	0.17

APPENDIX 2k : AVERAGED PERIPHERAL REFRACTIVE MEASUREMENTS (HARTINGER OPTOMETER)

* The mean and standard deviation (SD) values shown were calculated by averaging the individual mean and standard deviation (STD) values collected from all subjects in each refractive group.
* Key : SAG. RX. = sagittal refraction (D); SAG. AXIS = sagittal axis (°);
   TAN. RX. = tangential refraction (D); TAN. AXIS = tangential axis (°).
* The unconventional manner in which the tangential axes are shown served to simplify statistical calculations.
* Readings could only be taken to 40° field angle.
* See appendix 2i for central refractive results.
* For total averaged data, the astigmatism was calculated from the total averaged sagittal and tangential refractive error values.

		Temporal Retina 40	30	20	Field Angle (°) 10	10	20	30	Nasal Retina 40
Near-Emmetropes (N = 10)									
SAG. RX.	Mean	1.13	0.46	0.06	-0.07	-0.21	0.16	0.4	1.01
	SD	1.16	0.83	0.56	0.53	0.35	0.79	0.84	1.11
STD	Mean	0.31	0.25	0.3	0.22	0.14	0.25	0.2	0.29
	SD	0.29	0.16	0.16	0.09	0.09	0.22	0.13	0.14
SAG.AXIS	Mean	89	87.6	90.8	93.6	91.1	93.9	92.9	92.6
	SD	6.03	8.58	7.44	10.21	3.74	7.85	6.12	10.34
STD	Mean	2.12	2.04	1.19	1.49	1.63	3.66	4.6	4.93
	SD	2.87	2.37	1.87	2.09	4.57	57	4.34	4.55
TAN. RX.	Mean	-3.73	-2.8	-1.43	-0.5	-0.2	-0.68	-1.12	-1.63
	SD	1.24	0.87	0.71	0.39	0.23	0.8	0.93	1.3
STD	Mean	0.32	0.35	0.28	0.16	0.13	0.25	0.32	0.43
	SD	0.17	0.21	0.27	0.08	0.1	0.14	0.19	0.42
TAN. AXIS	Mean	179.6	178	180.8	183.2	180.3	180.6	182.1	181.2
	SD	7.47	7.84	9.19	9.2	1.46	5.88	6.02	5.63
STD	Mean	1.73	2.09	3.35	1.83	0.82	2.25	2.72	2.93
	SD	2.06	2.01	3.37	2.63	1.65	3.53	3.22	3.7
Myopes (N = 16)									
SAG. RX.	Mean	-0.12	-1.24	-2.2	-2.96	-3.05	-2.57	-2.06	-1.1
	SD	1.8	1.59	1.7	1.73	1.78	1.7	1.89	1.96
STD	Mean	0.25	0.33	0.33	0.24	0.28	0.31	0.3	0.35
	SD	0.18	0.25	0.18	0.17	0.19	0.19	0.17	0.26
SAG.AXIS	Mean	89.6	89.9	91.7	91.5	90.7	88.6	91.4	89.5
	SD	4.12	7.62	5.23	13.21	10.14	9.11	7.7	12.45
STD	Mean	2.1	2.22	2.7	4.79	2.49	3.88	3.23	2.32
	SD	3.05	2.76	3.04	6.4	3.37	5.63	3.95	3.08
TAN. RX.	Mean	-4.73	-4.73	-4.22	-3.69	-3.24	-3.14	-3.32	-3.28
	SD	1.32	1.36	1.37	1.49	1.51	1.99	1.8	2.05
STD	Mean	0.31	0.3	0.28	0.24	0.27	0.42	0.43	0.34
	SD	0.14	0.21	0.1	0.12	0.14	0.3	0.29	0.29
TAN. AXIS	Mean	179.9	180.4	179.9	181.3	178.4	175	179.8	177.3
	SD	4.22	6.21	4.8	11.03	6.53	11.71	5.25	9.86
STD	Mean	1.21	2.28	3.02	3.31	1.57	2.64	1.96	2.05
	SD	1.75	2.96	3.69	4.29	2.38	3.33	2.92	2.37
Hyperopes (N = 8)									
SAG. RX.	Mean	2.36	2.08	1.51	1.43	1.64	2.02	2.09	2.97
	SD	1.44	1.95	1.62	1.02	0.96	1	1.11	1.05
STD	Mean	0.29	0.31	0.24	21	0.37	0.29	0.25	0.41
	SD	0.18	0.27	0.11	0.11	0.25	0.15	0.18	0.22
SAG.AXIS	Mean	91.2	92.7	94	100	94.8	88.9	88.7	85.8
	SD	5.87	6.65	5.78	14.6	17.08	2.9	12.81	9.48
STD	Mean	2.92	4.62	1.7	4.95	3.84	2.9	2.49	3.29
	SD	3.83	4.95	1.77	4.61	8.83	4.63	3.48	4.03
TAN. RX.	Mean	-1.87	-1.6	0.01	0.81	1.7	1.8	1.1	0.55
	SD	1.97	2.27	1.06	0.72	0.92	1.22	1.52	1.66
STD	Mean	0.34	0.39	0.27	0.19	0.29	0.21	0.28	0.39
	SD	0.09	0.24	0.21	0.12	0.09	0.12	0.21	0.29
TAN. AXIS	Mean	180.7	181.5	184.1	185.9	184.2	178.3	179.2	177.8
	SD	3.59	6.89	6.65	15.97	16.54	3.01	21.15	5.93
STD	Mean	2.49	3.48	2.66	2.63	6.07	3.69	3.02	1.53
	SD	2.92	4.24	3.15	3.04	9.68	6.32	4.62	2.93
Total averaged data (N = 34)									
SAG.	RX.	1.12	0.43	-0.21	-0.53	-0.54	-0.13	0.14	0.96
	AXIS	89.9	90.1	92.2	95	92.2	90.5	91	89.3
TAN.	RX.	-3.44	-3.04	-1.88	-1.12	-0.58	-0.96	-1.11	-1.45
	AXIS	180.1	180	181.6	183.5	181	178	180.4	178.8
ASTIGMATISM		4.56	3.47	1.67	0.59	0.04	0.83	1.25	2.41

313

APPENDIX 2l : AVERAGED PERIPHERAL REFRACTIVE MEASUREMENTS (CANON AUTOREF R-1 INFRA-RED OPTOMETER)

* The mean and standard deviation (SD) values shown were calculated by averaging the individual mean and
  standard deviation (STD) values collected from all subjects in each refractive group.
* Key : SAG. RX. = sagittal refraction (D); TAN. RX. = tangential refraction (D); TAN. AXIS = tangential axis (°).
* Sagittal axis not shown since Canon Autoref R-1 only gives one axis reading.
* The unconventional manner in which the tangential axes are shown served to simplify statistical calculations.
* Readings could only be taken to 30° field angle.
* See appendix 2j for central refractive results.
* For total averaged data, the astigmatism was calculated from the total averaged sagittal and tangential refractive error values.

| | | Temporal Retina | | Field Angle (°) | | | Nasal Retina |
		30	20	10	10	20	30
Near-Emmetropes (N = 10)							
SAG. RX.	Mean	1.13	0.41	0.26	0.13	0.25	0.78
	SD	0.57	0.3	0.26	0.39	0.48	0.61
STD	Mean	0.22	0.15	0.17	0.15	0.13	0.11
	SD	0.14	0.11	0.23	0.07	0.09	0.06
TAN. RX.	Mean	-2.5	-1.76	-1.06	-0.57	-0.81	-1.33
	SD	0.77	0.36	0.3	0.5	0.87	1.07
STD	Mean	0.27	0.16	0.15	0.12	0.15	0.15
	SD	0.1	0.09	0.1	0.08	0.1	0.13
TAN. AXIS	Mean	167.1	160	150.2	189.2	191.5	196.4
	SD	6.94	6.06	8.2	28.5	14.19	9.7
STD	Mean	3.81	2.14	3.9	8.14	6.39	3.74
	SD	2.66	1.94	3.41	8.71	6.49	4.6
Myopes (N = 16)							
SAG. RX.	Mean	-0.71	-1.86	-2.58	-2.72	-2.59	-1.75
	SD	1.52	1.7	1.83	1.77	1.97	1.96
STD	Mean	0.34	0.16	0.13	0.18	0.15	0.14
	SD	0.39	0.14	0.08	0.14	0.1	0.06
TAN. RX.	Mean	-4.12	-4.03	-3.62	-3.34	-3.22	-3.27
	SD	1.34	1.37	1.56	1.64	1.85	1.88
STD	Mean	0.37	0.14	0.16	0.14	0.15	0.16
	SD	0.53	0.1	0.08	0.08	0.1	0.08
TAN. AXIS	Mean	172.4	169.5	162.3	184.8	174.7	199.5
	SD	6.85	9.93	11.33	22.85	22.99	12.43
STD	Mean	2.97	5.13	3.63	10.31	4.87	3.08
	SD	3.22	10.05	5.04	11.27	5.51	2.31
Hyperopes (N = 8)							
SAG. RX.	Mean	2.08	1.56	0.91	1.37	1.6	2.03
	SD	1.54	1.14	1.53	1.13	1.21	0.85
STD	Mean	0.33	0.21	0.22	0.13	0.17	0.34
	SD	0.18	0.13	0.19	0.07	0.09	0.26
TAN. RX.	Mean	-1.91	-0.92	0.22	1.36	1.25	0.4
	SD	1.75	1.51	1.02	1.32	1.8	1.86
STD	Mean	0.34	0.27	0.3	0.14	0.12	0.35
	SD	0.15	0.26	0.17	0.06	0.05	0.27
TAN. AXIS	Mean	181.2	181.4	183.3	182.4	194.9	176.7
	SD	16.64	25.52	28.76	31.73	30.55	28.78
STD	Mean	1.55	2.68	5.31	8.28	5.43	5.41
	SD	1.24	1.8	5.27	6.74	6.49	4.18
Total averaged data (N = 34)							
SAG.	RX.	0.83	0.04	-0.47	-0.41	-0.25	0.35
TAN.	RX.	-2.84	-2.24	-1.49	-0.85	-0.93	-1.4
	AXIS	173.6	170.3	165.3	185.5	187	190.9
ASTIGMATISM		3.67	2.28	1.02	0.44	0.68	1.75

APPENDIX 2m : MEASUREMENTS OF THE VERTICAL DIAMETER OF ENTRANCE PUPIL

* † denotes a female subject.
* Refractive groups; E = near-emmetrope, M = myope, H = hyperope.
* Mean and standard deviation (SD) values were based on nine repeat readings taken on one session only.
* Figures in the table refer to unscaled vertical pupil diameters i.e. as measured after projection.
* See appendix 2e for magnification of projected photographs.

Subject	Refractive Group	Vertical entrance pupil diameter (mm)			
		First Readings		Second Readings	
		Mean	SD	Mean	SD
PCR	E	73.7	0.7	76.3	1.6
SB	E	74.4	4.3	89.2	2.5
JR	E	93.7	2.1	-	-
TB	E	101.3	3	84.2	5
ND	E	105.1	2.3	90.3	1
SG†	E	91	1	83.3	1.8
ST†	E	103.3	0.5	100.4	2.4
SC†	E	107	3.6	107.3	2.8
RD	E	80.2	2.9	85.8	2.5
BF	E	93.7	0.5	86.7	1.2
DM	M	88.2	3.4	97.8	1.6
RP	M	81.3	1.1	73.3	2.8
MG†	M	129.5	7.7	119.5	2.6
MES	M	100.7	6.4	82.3	5
CS†	M	115.1	3.6	100.7	0.8
GP	M	94	3.5	-	-
MEN	M	104.3	4	90.5	1.8
SL†	M	87.3	1.7	83.9	1.5
PCE	M	121.2	5.1	103	1
AL	M	102.1	8	100.2	0.9
MM	M	83.8	3.4	77.7	3.4
RC	M	76.3	3.3	67.4	4.1
RLA	M	75.2	2.6	-	-
TM	M	85.7	4	85	0.8
RT	M	79.3	4.5	79.3	4.9
MH	M	102.3	6.2	-	-
SH	H	95	3.5	104.8	1.7
EH	H	65.3	1.2	68	2.9
DC	H	86.8	3.3	96.9	0.9
AS	H	85.9	2.5	93.9	2.8
AH†	H	92.6	2.1	85	2.1
CM†	H	133.5	2.7	92.4	4
RL†	H	73.7	0.6	75.2	0.4
HM†	H	92.3	1.6	126.1	3.7

```
REM
REM Set up surface labels
REM
surf$(1)="Front Spectacle"
surf$(2)="Back Spectacle"
surf$(3)="Front Cornea"
surf$(4)="Back Cornea"
surf$(5)="Front Lens"
surf$(6)="Back Lens"
surf$(7)="Retina"

REM
REM Set up index labels
REM
ind$(1)="Spectacle"
ind$(2)="Cornea"
ind$(3)="Aqueous"
ind$(4)="Lens"
ind$(5)="Vitreous"

REM
REM Set up parameters of schematic eye
REM
DIM  ep(7),eq(7),es(7,7),et(3,7)
DIM  xp(7),xq(7),xs(7,7),xt(3,7)
DIM  a(3,3),b(3),x(3),y(3),t(3),n(3)
DIM  p(3),tt(3),xta(3)
DIM  r(3,3),ss(3,3),qq(3,3)
DIM  x1(3),y1(3),x2(3),y2(3),r1(3),r2(3)

REM
REM Specify portion of surface to be used.Anterior (+) or Posterior (-)
REM
eq(1)=1
eq(2)=-1
eq(3)=1
eq(4)=1
eq(5)=-1
eq(6)=-1
eq(7)=-1

REM
REM Specify the bilinear,linear and constant parameters
REM
es(1,1)=10
es(2,1)=10
es(3,1)=10
es(4,1)=0
es(5,1)=0
es(6,1)=0
es(7,1)=-1
es(1,2)=10
es(2,2)=10
es(3,2)=10
es(4,2)=0
es(5,2)=0
es(6,2)=0
es(7,2)=-1
es(1,3)=9.01#
es(2,3)=9.01#
es(3,3)=10.4#
es(4,3)=0
es(5,3)=0
es(6,3)=0
```

316

```
es(7,3)=-1
es(1,4)=7.51
es(2,4)=7.51
es(3,4)=8.67
es(4,4)=0          .
es(5,4)=0
es(6,4)=0
es(7,4)=-1
es(1,5)=-7.1#
es(2,5)=-7.1#
es(3,5)=4.95
es(4,5)=0
es(5,5)=0
es(6,5)=0
es(7,5)=-1
es(1,6)=1
es(2,6)=1
es(3,6)=0
es(4,6)=0
es(5,6)=0
es(6,6)=12#
es(7,6)=0
es(1,7)=12.16
es(2,7)=12.16
es(3,7)=10.48
es(4,7)=0
es(5,7)=0
es(6,7)=0
es(7,7)=-1

REM
REM Specify locations
REM
et(1,1)=0
et(2,1)=0
et(3,1)=20
et(1,2)=0
et(2,2)=0
et(3,2)=30
et(1,3)=0
et(2,3)=0
et(3,3)=-6.8#
et(1,4)=0
et(2,4)=0
et(3,4)=-5.61
et(1,5)=0
et(2,5)=0
et(3,5)=4.95
et(1,6)=0
et(2,6)=0
et(3,6)=-4
et(1,7)=0
et(2,7)=0
et(3,7)=-10.12

REM
REM Specify refractive indices
REM
ep(1)=1
ep(2)=1
ep(3)=1
ep(4)=1.3371
ep(5)=1.3374
ep(6)=1.42
ep(7)=1.336
```

317

```
REM
REM Set up working variables
REM
FOR i=1 TO 7
xp(i)=ep(i)
xq(i)=eq(i)          .
FOR j=1 TO 3
xs(j,i)=es(j,i)
xt(j,i)=et(j,i)
NEXT j
FOR j=4 TO 7
xs(j,i)=es(j,i)
NEXT j
NEXT i
pupil=2.5
lentilt=0

REM
REM Setup menus
REM
MENU 5,0,0,""

REM
REM Specify surfaces menu
REM
MENU 1,0,1,"SURFACES"
MENU  1,1,1,surf$(1)
MENU  1,2,1,surf$(2)
MENU  1,3,1,surf$(3)
MENU  1,4,1,surf$(4)
MENU  1,5,1,surf$(5)
MENU  1,6,1,surf$(6)
MENU  1,7,1,surf$(7)

REM
REM Specify locations menu
REM
MENU 2,0,1,"LOCATIONS"
MENU  2,1,1,surf$(1)
MENU  2,2,1,surf$(2)
MENU  2,3,1,surf$(3)
MENU  2,4,1,surf$(4)
MENU  2,5,1,surf$(5)
MENU  2,6,1,surf$(6)
MENU  2,7,1,surf$(7)

REM
REM Specify refractive indices menu
REM
MENU 3,0,1,"INDICES"
MENU  3,1,1,ind$(1)
MENU  3,2,1,ind$(2)
MENU  3,3,1,ind$(3)
MENU  3,4,1,ind$(4)
MENU  3,5,1,ind$(5)

REM
REM Specify ray bundle menu
REM
MENU 4,0,1,"TRACE"
MENU  4,1,1,"Lens tilt"
MENU  4,2,1,"Pupil size"
```

```
REM
REM Handle menu selections
REM
handle:
menuno=MENU(0)
IF menuno=0 THEN GOTO handle
IF menuno=1 THEN GOTO surfmenu
IF menuno=2 THEN GOTO locmenu
IF menuno=3 THEN GOTO indexmenu
IF menuno=4 THEN GOTO tracemenu
GOTO handle

REM
REM Handle surfaces menu
REM
surfmenu:
selectno=MENU(1)
IF selectno < 1 THEN GOTO handle
IF selectno > 7 THEN GOTO handle
x$(1)=STR$(xs(1,selectno))
x$(2)=STR$(xs(2,selectno))
x$(3)=STR$(xs(3,selectno))
GOSUB choice3
xs(1,selectno)=VAL(x$(1))
xs(2,selectno)=VAL(x$(2))
xs(3,selectno)=VAL(x$(3))
GOTO handle

REM
REM Handle locations menu
REM

locmenu:
selectno=MENU(1)
IF selectno < 1 THEN GOTO handle
IF selectno > 7 THEN GOTO handle
x$(1)=STR$(xt(1,selectno))
x$(2)=STR$(xt(2,selectno))
x$(3)=STR$(xt(3,selectno))
GOSUB choice3
xt(1,selectno)=VAL(x$(1))
xt(2,selectno)=VAL(x$(2))
xt(3,selectno)=VAL(x$(3))
GOTO handle

REM
REM Handle index menu
REM
indexmenu:
selectno=MENU(1)
IF selectno < 1 THEN GOTO handle
IF selectno > 5 THEN GOTO handle
selectno=selectno+1
IF selectno > 2 THEN  selectno=selectno+1
x$(1)=STR$(xp(selectno))
GOSUB choice1
xp(selectno)=VAL(x$(1))
GOTO handle

REM
REM Handle trace menu
REM
tracemenu:
selectno=MENU(1)
IF selectno <1 THEN GOTO handle
IF selectno>2 THEN GOTO handle
IF selectno=2 THEN GOTO traceskip
x$(1)=STR$(lentilt)
GOSUB choice1
lentilt=VAL(x$(1))/57.3
```

319

```
GOTO handle
traceskip:
x$(1)=STR$(pupil)
GOSUB choice1
pupil=VAL(x$(1))

REM
REM Print out altered values
REM
LPRINT
LPRINT "ALTERED PARAMETERS:-"
LPRINT
FOR i=1 TO 7
flag$="off"
FOR j=1 TO 3
IF ABS(xs(j,i)-es(j,i)) > .0001 THEN flag$="on"
NEXT j
IF flag$="on" THEN LPRINT surf$(i);" shape",xs(1,i),xs(2,i),xs(3,i)
NEXT i
LPRINT
FOR i=1 TO 7
flag$="off"
FOR j=1 TO 3
IF ABS(xt(j,i)-et(j,i)) > .0001 THEN flag$="on"
NEXT j
IF flag$="on" THEN LPRINT surf$(i);" location",xt(1,i),xt(2,i),xt(3,i)
NEXT i
LPRINT
IF ABS(xp(2)-ep(2)) > 0 THEN LPRINT ind$(1);" index",xp(2)
IF ABS(xp(4)-ep(4)) > 0 THEN LPRINT ind$(2);" index",xp(4)
IF ABS(xp(5)-ep(5)) > 0 THEN LPRINT ind$(3);" index",xp(5)
IF ABS(xp(6)-ep(6)) > 0 THEN LPRINT ind$(4);" index",xp(6)
IF ABS(xp(7)-ep(7)) > 0 THEN LPRINT ind$(5);" index",xp(7)
LPRINT
LPRINT "Pupil",pupil
LPRINT "Lens tilt",lentilt*57.3
LPRINT

REM
REM Copy current parameters
REM
FOR i=1 TO 7
ep(i)=xp(i)
eq(i)=xq(i)
FOR j=1 TO 3
IF ABS(xs(j,i))<.00001 THEN es(j,i)=0
IF ABS(xs(j,i))<.00001 THEN GOTO avoid
es(j,i)=1/(xs(j,i)^2)
IF xs(j,i)<0 THEN es(j,i)=-es(j,i)
avoid:
et(j,i)=xt(j,i)
NEXT j
FOR j=4 TO 7
es(j,i)=xs(j,i)
NEXT j
NEXT i
pupil=pupil/2

REM
REM Carry out trace
REM
GOSUB rotmat
GOSUB ultra
FOR iooo=1 TO 11
ooo=(iooo-6)/5.73+.0001
```

320

```
      GOSUB back
      zzx(1)=x(1)
      zzx(2)=x(2)
      zzx(3)=x(3)
      pxp=y(3)
      GOSUB acos
      fangle=pxp*57.3
      REM
      REM Calculate direction of principal ray
      REM
      GOSUB back
      lensnum=7
      GOSUB path
      fdist=SQR((zzx(1)-x(1))^2+(zzx(2)-x(2))^2+(zzx(3)-x(3))^2)
      x1(1)=x(1)
      x1(2)=x(2)
      x1(3)=x(3)
      y1(1)=y(1)
      y1(2)=y(2)
      y1(3)=y(3)
      REM
      REM Calculate +  pupil tangential ray
      REM
      GOSUB back
      GOSUB tangential1
      tpupil1=mmm*ABS(y(3))*.1
      GOSUB path
      xaax(1)=x(1)
      xaax(2)=x(2)
      xaax(3)=x(3)
      yaay(1)=y(1)
      yaay(2)=y(2)
      yaay(3)=y(3)
      x2(1)=x(1)
      x2(2)=x(2)
      x2(3)=x(3)
      y2(1)=y(1)
      y2(2)=y(2)
      y2(3)=y(3)
      GOSUB inter
      tdist1=SQR((zzx(1)-r1(1))^2+(zzx(2)-r1(2))^2+(zzx(3)-r1(3))^2)
      REM
      REM Calculate - pupil tangential ray
      REM
      GOSUB back
      GOSUB tangential2
      tpupil2=-mmm*ABS(y(3))*.1
      tpupil=ABS(tpupil1)+ABS(tpupil2)
      GOSUB path
      x2(1)=x(1)
      x2(2)=x(2)
      x2(3)=x(3)
      y2(1)=y(1)
      y2(2)=y(2)
      y2(3)=y(3)
      GOSUB inter
      tdist2=SQR((zzx(1)-r1(1))^2+(zzx(2)-r1(2))^2+(zzx(3)-r1(3))^2)
      REM
      REM Calculate pupil extremes rays
      REM
      x1(1)=xaax(1)
      x1(2)=xaax(2)
      x1(3)=xaax(3)
      y1(1)=yaay(1)
      y1(2)=yaay(2)
      y1(3)=yaay(3)
      GOSUB inter
```

321

```
trange=SQR((r1(1)-r2(1))^2+(r1(2)-r2(2))^2+(r1(3)-r2(3))^2)
r1(1)=(r1(1)+r2(1))/2
r1(2)=(r1(2)+r2(2))/2
r1(3)=(r1(3)+r2(3))/2
tdist3=SQR((zzx(1)-r1(1))^2+(zzx(2)-r1(2))^2+(zzx(3)-r1(3))^2)
REM
REM Print results
REM
LPRINT
tooo=(iooo-6)*10
LPRINT "Peripheral angle = ";tooo
LPRINT "Field angle = ";fangle
LPRINT "Positive tangential pupil size = ";tpupil1
LPRINT "Negative tangential pupil size = ";tpupil2
LPRINT "Total tangential pupil size = ";tpupil
fdiop=1000*ep(7)/fdist
tdiop1=fdiop-1000*ep(7)/tdist1
tdiop2=fdiop-1000*ep(7)/tdist2
tdiop3=fdiop-1000*ep(7)/tdist3
LPRINT "Positive pupil tangential dioptric power = ";tdiop1
LPRINT "Negative pupil tangential dioptric power = ";tdiop2
LPRINT "Pupil extremes tangential dioptric power = ";tdiop3
LPRINT "Pupil extremes perpendicular distance = ";trange
REM
REM Calculate + pupil sagittal ray
REM
GOSUB back
GOSUB path
x1(1)=x(1)
x1(2)=x(2)
x1(3)=x(3)
y1(1)=y(1)
y1(2)=y(2)
y1(3)=y(3)
GOSUB back
GOSUB sagittal1
spupil1=mmm*.1
GOSUB path
xaax(1)=x(1)
xaax(2)=x(2)
xaax(3)=x(3)
yaay(1)=y(1)
yaay(2)=y(2)
yaay(3)=y(3)
x2(1)=x(1)
x2(2)=x(2)
x2(3)=x(3)
y2(1)=y(1)
y2(2)=y(2)
y2(3)=y(3)
GOSUB inter
sdist1=SQR((zzx(1)-r1(1))^2+(zzx(2)-r1(2))^2+(zzx(3)-r1(3))^2)
REM
REM Calculate - pupil sagittal ray
REM
GOSUB back
GOSUB sagittal2
spupil2=mmm*.1

spupil=ABS(spupil1)+ABS(spupil2)
GOSUB path
x2(1)=x(1)
x2(2)=x(2)
x2(3)=x(3)
y2(1)=y(1)
y2(2)=y(2)
y2(3)=y(3)
GOSUB inter
sdist2=SQR((zzx(1)-r1(1))^2+(zzx(2)-r1(2))^2+(zzx(3)-r1(3))^2)
```

322

```
REM
REM Calculate pupil extremes rays
REM
x1(1)=xaax(1)
x1(2)=xaax(2)
x1(3)=xaax(3)
y1(1)=yaay(1)
y1(2)=yaay(2)
y1(3)=yaay(3)
GOSUB inter
srange=SQR((r1(1)-r2(1))^2+(r1(2)-r2(2))^2+(r1(3)-r2(3))^2)
r1(1)=(r1(1)+r2(1))/2
r1(2)=(r1(2)+r2(2))/2
r1(3)=(r1(3)+r2(3))/2
sdist3=SQR((zzx(1)-r1(1))^2+(zzx(2)-r1(2))^2+(zzx(3)-r1(3))^2)
REM
REM Print results
REM
LPRINT "Positive sagittal pupil size = ";spupil1
LPRINT "Negative sagittal pupil size = ";spupil2
LPRINT "Total sagittalal pupil size = ";spupil
sdiop1=fdiop-1000*ep(7)/sdist1
sdiop2=fdiop-1000*ep(7)/sdist2
sdiop3=fdiop-1000*ep(7)/sdist3
LPRINT "Positive pupil sagittal dioptric power = ";sdiop1
LPRINT "Negative pupil sagittal dioptric power = ";sdiop2
LPRINT "Pupil extremes sagittal dioptric power = ";sdiop3
LPRINT "Pupil extremes perpendicular distance = ";srange
sturm=-1000*(ep(7)/sdist3-ep(7)/tdist3)
LPRINT "Interval of Sturm = ",sturm
PRINT tooo,sturm
NEXT looo
REM
REM End of main program
REM
GOTO finish

REM
REM Subroutine to calculate sagittal positive pupil size
REM
sagittal1:
mmm=1
tx(1)=x(1)
tx(2)=x(2)
tx(3)=x(3)
ty(1)=y(1)
ty(2)=y(2)
ty(3)=y(3)
sagloop1:
x(1)=tx(1)
x(2)=tx(2)+mmm*.1
x(3)=tx(3)
y(1)=ty(1)
y(2)=ty(2)
y(3)=ty(3)
FOR iii = 3 TO 4
FOR j = 1 TO 3
t(j)=et(j,iii)
b(j)=es(j+3,iii)
FOR k = 1 TO 3
a(j,k)=0
IF j=k THEN a(j,k)=es(j,iii)
NEXT k
NEXT j
c = es(7,iii)
a = ea(iii)
```

323

```
GOSUB transquad
GOSUB hit
ip=ep(iii)
k=iii+1
rp=ep(7)
IF k<7.5 THEN rp=ep(k)
GOSUB bend
NEXT iii
ddd=-x(3)/y(3)
ddd=x(2)+ddd*y(2)
IF ddd<pupil THEN mmm=mmm+1
IF ddd<pupil THEN GOTO sagloop1
x(1)=tx(1)
x(2)=tx(2)+mmm*.1
x(3)=tx(3)
y(1)=ty(1)
y(2)=ty(2)
y(3)=ty(3)
RETURN

REM
REM Subroutine to calculate sagittal negative pupil size
REM
sagittal2:
mmm=1
tx(1)=x(1)
tx(2)=x(2)
tx(3)=x(3)
ty(1)=y(1)
ty(2)=y(2)
ty(3)=y(3)
sagloop2:
x(1)=tx(1)
x(2)=tx(2)-mmm*.1
x(3)=tx(3)
y(1)=ty(1)
y(2)=ty(2)
y(3)=ty(3)
FOR iii = 3 TO 4
FOR j = 1 TO 3
t(j)=et(j,iii)
b(j)=es(j+3,iii)
FOR k = 1 TO 3
a(j,k)=0
IF j=k THEN a(j,k)=es(j,iii)
NEXT k
NEXT j
c = es(7,iii)
q = eq(iii)
GOSUB transquad
GOSUB hit
ip=ep(iii)
k=iii+1
rp=ep(7)
IF k<7.5 THEN rp=ep(k)
GOSUB bend
NEXT iii
ddd=-x(3)/y(3)
ddd=x(2)+ddd*y(2)
IF ddd>-pupil THEN mmm=mmm+1
IF ddd>-pupil THEN GOTO sagloop2
x(1)=tx(1)
x(2)=tx(2)-mmm*.1
x(3)=tx(3)
y(1)=ty(1)
y(2)=ty(2)
y(3)=ty(3)
RETURN
```

324

```
REM
REM Subroutine to calculate size of positive tangential pupil
REM
tangential1:
mmm=1
tx(1)=x(1)
tx(2)=x(2)
tx(3)=x(3)
ty(1)=y(1)
ty(2)=y(2)
ty(3)=y(3)
tanloop1:
x(1)=tx(1)+mmm*.1
x(2)=tx(2)
x(3)=tx(3)
y(1)=ty(1)
y(2)=ty(2)
y(3)=ty(3)
FOR iii = 3 TO 4
FOR j = 1 TO 3
t(j)=et(j,iii)
b(j)=es(j+3,iii)
FOR k = 1 TO 3
a(j,k)=0
IF j=k THEN a(j,k)=es(j,iii)
NEXT k
NEXT j
c = es(7,iii)
q = eq(iii)
GOSUB transquad
GOSUB hit
ip=ep(iii)
k=iii+1
rp=ep(7)
IF k<7.5 THEN rp=ep(k)
GOSUB bend
NEXT iii
ddd=-x(3)/y(3)
ddd=x(1)+ddd*y(1)
IF ddd<pupil THEN mmm=mmm+1
IF ddd<pupil THEN GOTO tanloop1
x(1)=tx(1)+mmm*.1
x(2)=tx(2)
x(3)=tx(3)
y(1)=ty(1)
y(2)=ty(2)
y(3)=ty(3)
RETURN

REM
REM Subroutine to calculate size of negative tangential pupil
REM
tangential2:
mmm=1
tx(1)=x(1)
tx(2)=x(2)
tx(3)=x(3)
ty(1)=y(1)
ty(2)=y(2)
ty(3)=y(3)
tanloop2:
x(1)=tx(1)-mmm*.1
x(2)=tx(2)
x(3)=tx(3)
y(1)=ty(1)
y(2)=ty(2)
y(3)=ty(3)
FOR iii = 3 TO 4
FOR j = 1 TO 3
```

325

```
          t(j)=et(j,iii)
          b(j)=es(j+3,iii)
          FOR k = 1 TO 3
          a(j,k)=0
          IF j=k THEN  a(j,k)=es(j,iii)
          NEXT k          .
          NEXT j
          c  =  es(7,iii)
          q  =  eq(iii)
          GOSUB transquad
          GOSUB hit
          ip=ep(iii)
          k=iii+1
          rp=ep(7)
     IF k<7.5 THEN rp=ep(k)
     GOSUB bend
     NEXT iii
     ddd=-x(3)/y(3)
     ddd=x(1)+ddd*y(1)
     IF ddd>-pupil THEN mmm=mmm+1
     IF ddd>-pupil THEN GOTO tanloop2
     x(1)=tx(1)-mmm*.1
     x(2)=tx(2)
     x(3)=tx(3)
     y(1)=ty(1)
     y(2)=ty(2)
     y(3)=ty(3)
     RETURN


     REM
     REM Computes starting position of ray
     REM
     back:
     x(1)=0
     x(2)=0
     x(3)=0
     y(1)=SIN(ooo)
     y(2)=0
     y(3)=COS(ooo)
     FOR III = 3 TO 4
     iii=7-III
     FOR j = 1 TO 3
     t(j)=-et(j,iii)
     b(j)=es(j+3,iii)
     FOR k = 1 TO 3
     a(j,k)=0
     IF j=k THEN  a(j,k)=es(j,iii)
     NEXT k
     NEXT j
     c  =  es(7,iii)
     q  =  -eq(iii)
     GOSUB transquad
     GOSUB hit
     k=iii+1
     ip=ep(k)
     rp=ep(7)
     IF k<7.5 THEN rp=ep(iii)
     GOSUB bend
     NEXT III
     x(3)=-x(3)
     y(1)=-y(1)
     y(2)=-y(2)
     RETURN
```

326

```
REM
REM Computes actual locations of refracting surfaces
REM
ultra:
FOR iii = 3 TO 7
FOR j = 1 TO 3 .
t(j)=et(j,iii)
b(j)=es(j+3,iii)
FOR k = 1 TO 3
a(j,k)=0
IF j=k THEN  a(j,k)=es(j,iii)
NEXT k
NEXT j
c = es(7,iii)
q = eq(iii)
GOSUB transquad
x(1)=0
x(2)=0
x(3)=-50
uang=.00001
y(1)=SIN(uang)
y(2)=0
y(3)=COS(uang)
GOSUB hit
PRINT surf$(iii):" location = ".x(3)
NEXT iii
RETURN


REM
REM Computes path of ray through eye
REM
path:
FOR iii = 3 TO  lensnum
FOR j = 1 TO 3
t(j)=et(j,iii)
b(j)=es(j+3,iii)
FOR k = 1 TO 3
a(j,k)=0
IF j=k THEN  a(j,k)=es(j,iii)
NEXT k
NEXT j
c = es(7,iii)
q = eq(iii)
GOSUB transquad
IF iii=5 THEN GOSUB rotquad
IF iii=6 THEN GOSUB rotquad
GOSUB hit
ip=ep(iii)
k=iii+1
rp=ep(7)
IF k<7.5 THEN rp=ep(k)
GOSUB bend
NEXT iii
RETURN


REM
REM Accepts value for a single parameter
REM
choice1:
EDIT FIELD  1,x$(1),(100,90)-(150,110)
BUTTON  1,1,"ok",(200,90)-(220,110)
response1:
reply=DIALOG(0)
IF reply <> 1 THEN GOTO response1
x$(1)=EDIT$(1)
EDIT FIELD CLOSE 1
BUTTON CLOSE 1
RETURN
```

327

```
REM
REM Accepts values for a set of X,Y,Z parameters
REM
choice3:
EDIT FIELD  1,x$(1),(100,50)-(150,70)
EDIT FIELD  2;x$(2),(100,90)-(150,110)
EDIT FIELD  3,x$(3),(100,130)-(150,150)
BUTTON  1,1,"ok",(200,90)-(220,110)
BUTTON  2,1,"X",(70,50)-(90,70)
BUTTON  3,1,"Y",(70,90)-(90,110)
BUTTON  4,1,"Z",(70,130)-(90,150)
response3:
reply=DIALOG(0)
IF reply <> 1 THEN GOTO response3
reply=DIALOG(1)
IF reply <>1 THEN GOTO response3
x$(1)=EDIT$(1)
x$(2)=EDIT$(2)
x$(3)=EDIT$(3)
EDIT FIELD CLOSE 1
EDIT FIELD CLOSE 2
EDIT FIELD CLOSE 3
BUTTON CLOSE 1
BUTTON CLOSE 2
BUTTON CLOSE 3
BUTTON CLOSE 4
RETURN

REM
REM Translates quadric
REM
transquad:
xx(1)=a(1,1)*t(1)+a(1,2)*t(1)+a(1,3)*t(1)
xx(2)=a(2,1)*t(2)+a(2,2)*t(2)+a(2,3)*t(2)
xx(3)=a(3,1)*t(3)+a(3,2)*t(3)+a(3,3)*t(3)
c=c+(xx(1)+b(1))*t(1)+(xx(2)+b(2))*t(2)+(xx(3)+b(3))*t(3)
b(1)=2*xx(1)+b(1)
b(2)=2*xx(2)+b(2)
b(3)=2*xx(3)+b(3)
RETURN

REM
REM Rotates quadric
REM
rotquad:
FOR i=1 TO 3
FOR j=1 TO 3
qq(i,j)=0
FOR k=1 TO 3
qq(i,j)=qq(i,j)+a(i,k)*r(k,j)
NEXT k
NEXT j
NEXT i
FOR i=1 TO 3
FOR j=1 TO 3
ss(i,j)=r(j,i)
NEXT j
NEXT i
FOR i=1 TO 3
FOR j=1 TO 3
a(i,j)=0
FOR k=1 TO 3
a(i,j)=a(i,j)+ss(i,k)*qq(k,j)
NEXT k
NEXT j
NEXT i
```

328

```
xx(1)=b(1)
xx(2)=b(2)
xx(3)=b(3)
b(1)=ss(1,1)*xx(1)+ss(1,2)*xx(2)+ss(1,3)*xx(3)
b(2)=ss(2,1)*xx(1)+ss(2,2)*xx(2)+ss(2,3)*xx(3)
b(3)=ss(3,1)*xx(1)+ss(3,2)*xx(2)+ss(3,3)*xx(3)
RETURN

REM
REM Sets up rotation matrix
REM
rotmat:
ccc=COS(lentilt)
sss=SIN(lentilt)
r(1,1)=ccc
r(1,2)=0
r(1,3)=-sss
r(2,1)=0
r(2,2)=1
r(2,3)=0
r(3,1)=sss
r(3,2)=0
r(3,3)=ccc
RETURN

REM
REM Calculates intersection with the quadric
REM
hit:
tt(1)=a(1,1)*y(1)+a(1,2)*y(2)+a(1,3)*y(3)
tt(2)=a(2,1)*y(1)+a(2,2)*y(2)+a(2,3)*y(3)
tt(3)=a(3,1)*y(1)+a(3,2)*y(2)+a(3,3)*y(3)
at=tt(1)*y(1)+tt(2)*y(2)+tt(3)*y(3)
xta(1)=x(1)*a(1,1)+x(2)*a(2,1)+x(3)*a(3,1)
xta(2)=x(1)*a(1,2)+x(2)*a(2,2)+x(3)*a(3,2)
xta(3)=x(1)*a(1,3)+x(2)*a(2,3)+x(3)*a(3,3)
tt(1)=2*xta(1)+b(1)
tt(2)=2*xta(2)+b(2)
tt(3)=2*xta(3)+b(3)
bt=tt(1)*y(1)+tt(2)*y(2)+tt(3)*y(3)
tt(1)=xta(1)+b(1)
tt(2)=xta(2)+b(2)
tt(3)=xta(3)+b(3)
ct=c+tt(1)*x(1)+tt(2)*x(2)+tt(3)*x(3)
erro=bt^2-4*at*ct
IF erro<0 THEN PRINT "error"
IF erro<0 THEN RETURN
d1=(-bt+SQR(erro))/(2*at)
d2=(-bt-SQR(erro))/(2*at)
ll=d1
uu=d2
IF ll>d2 THEN ll=d2
IF uu<d1 THEN uu=d1
dd=ll
IF q<0 THEN dd=uu
x(1)=x(1)+dd*y(1)
x(2)=x(2)+dd*y(2)
x(3)=x(3)+dd*y(3)
n(1)=a(1,1)*x(1)+a(1,2)*x(2)+a(1,3)*x(3)
n(2)=a(2,1)*x(1)+a(2,2)*x(2)+a(2,3)*x(3)
n(3)=a(3,1)*x(1)+a(3,2)*x(2)+a(3,3)*x(3)
n(1)=2*n(1)+b(1)
n(2)=2*n(2)+b(2)
n(3)=2*n(3)+b(3)
const=SQR(n(1)^2+n(2)^2+n(3)^2)
IF n(3)<0 THEN const=-const
```

329

```
n(1)=n(1)/const
n(2)=n(2)/const
n(3)=n(3)/const
RETURN

REM                    .
REM Calculates direction of refracted ray
REM
bend:
y1cos=ABS(y(1)*n(1)+y(2)*n(2)+y(3)*n(3))
y2cos=SQR(1-((ip^2/rp^2)*(1-y1cos^2)))
const=rp*y2cos-ip*y1cos
y(1)=(ip*y(1)+const*n(1))/rp
y(2)=(ip*y(2)+const*n(2))/rp
y(3)=(ip*y(3)+const*n(3))/rp
RETURN

REM
REM Calculate intersection of two rays
REM
inter:
t1=0
t2=0
q1=0
q2=0
p1=0
p2=0
FOR i=1 TO 3
t1=t1+y1(i)^2
t2=t2+y1(i)*y2(i)
q1=q1-y1(i)*y2(i)
q2=q2-y2(i)^2
p1=p1+x2(i)*y1(i)-x1(i)*y1(i)
p2=p2+x2(i)*y2(i)-x1(i)*y2(i)
NEXT i
aa=(p1*q2-q1*p2)/(t1*q2-q1*t2)
bb=(t1*p2-p1*t2)/(t1*q2-q1*t2)
FOR i=1 TO 3
r1(i)=x1(i)+aa*y1(i)
r2(i)=x2(i)+bb*y2(i)
NEXT i
RETURN

acos:
pip=3.1415926535897#
IF pxp>0 THEN pxp=ATN((SQR(1-pxp^2))/pxp)
IF pxp<0 THEN pxp=ATN((SQR(1-pxp^2))/pxp)+pip
IF pxp=0 THEN pxp=pip/2
RETURN

REM

REM End of program
REM
finish:
END
```

```
REM
REM PURKINJE IMAGES
REM

REM
REM Set up surface labels
REM
surf$(1)="Front Spectacle"
surf$(2)="Back Spectacle"
surf$(3)="Front Cornea"
surf$(4)="Back Cornea"
surf$(5)="Front Lens"
surf$(6)="Back Lens"
surf$(7)="Retina"

REM
REM Set up index labels
REM
ind$(1)="Spectacle"
ind$(2)="Cornea"
ind$(3)="Aqueous"
ind$(4)="Lens"
ind$(5)="Vitreous"

REM
REM Set up parameters of schematic eye
REM
DIM  ep(7),eq(7),es(7,7),et(3,7),el(3,3)
DIM  xp(7),xq(7),xs(7,7),xt(3,7),xl(3,3)
DIM  a(3,3),b(3),x(3),y(3),t(3),n(3)
DIM  p(3),tt(3),xta(3)
DIM  r(3,3),ss(3,3),qq(3,3)
DIM  purk1%(2,2),purk3%(2,2),purk4%(2,2)

REM
REM Set up gaze angle
REM
tgaz=0
gaz=0

REM
REM Specify portion of surface to be used.Anterior (+) or Posterior (-)
REM
eq(1)=1
eq(2)=-1
eq(3)=1
eq(4)=1
eq(5)=-1
eq(6)=-1
eq(7)=-1

REM
REM Specify the bilinear,linear and constant parameters
REM
es(1,1)=10
es(2,1)=10
es(3,1)=10
es(4,1)=0
es(5,1)=0
es(6,1)=0
es(7,1)=-1
es(1,2)=10
es(2,2)=10
es(3,2)=10
es(4,2)=0
es(5,2)=0
es(6,2)=0
es(7,2)=-1
```

331

```
        es(1,3)=9.01
        es(2,3)=9.01
        es(3,3)=10.4
        es(4,3)=0
        es(5,3)=0
        es(6,3)=0           .
        es(7,3)=-1
        es(1,4)=7.51
        es(2,4)=7.51
        es(3,4)=8.67
        es(4,4)=0
        es(5,4)=0
        es(6,4)=0
        es(7,4)=-1
        es(1,5)=-7.1
        es(2,5)=-7.1
        es(3,5)=4.95
        es(4,5)=0
        es(5,5)=0
        es(6,5)=0
        es(7,5)=-1
        es(1,6)=1
        es(2,6)=1
        es(3,6)=0
        es(4,6)=0
        es(5,6)=0
        es(6,6)=12
        es(7,6)=0
        es(1,7)=12.16
        es(2,7)=12.16
        es(3,7)=10.48
        es(4,7)=0
        es(5,7)=0
        es(6,7)=0
        es(7,7)=-1

        REM
        REM Specify locations
        REM
        et(1,1)=0
        et(2,1)=0
        et(3,1)=20
        et(1,2)=0
        et(2,2)=0
        et(3,2)=30
        et(1,3)=0
        et(2,3)=0
        et(3,3)=-6.8+10
        et(1,4)=0
        et(2,4)=0
        et(3,4)=-5.61+10
        et(1,5)=0
        et(2,5)=0
        et(3,5)=4.95+10
        et(1,6)=0
        et(2,6)=0
        et(3,6)=-4+10
        et(1,7)=0
        et(2,7)=0
        et(3,7)=-10.12+10

        REM
        REM Specify refractive indices
        REM
        ep(1)=1
        ep(2)=1
        ep(3)=1
        ep(4)=1.3771
        ep(5)=1.3374
```

332

```
        ep(6)=1.42
        ep(7)=1.336

        REM
        REM Specify refractive indices
        REM
        el(1,1)=0
        el(2,1)=200
        el(3,1)=-1000
        el(1,2)=0
        el(2,2)=-200
        el(3,2)=-1000
        el(1,3)=0
        el(2,3)=0
        el(3.3)=-1000

        REM
        REM Set up working variables
        REM
        FOR i=1 TO 7
        xp(i)=ep(i)
        xq(i)=eq(i)
        FOR j=1 TO 3
        xs(j,i)=es(j,i)
        xt(j,i)=et(j,i)
        NEXT j
        FOR j=4 TO 7
        xs(j,i)=es(j,i)
        NEXT j
        NEXT i
        FOR i=1 TO 3
        FOR j=1 TO 3
        xl(i,j)=el(i,j)
        NEXT j
        NEXT i

        REM
        REM Setup menus
        REM
        MENU 5,0,0,""

        REM
        REM Specify surfaces menu
        REM
        MENU 1,0,1,"SURFACES"
        MENU  1,1,1,surf$(1)
        MENU  1,2,1,surf$(2)
        MENU  1,3,1,surf$(3)
        MENU  1,4,1,surf$(4)
        MENU  1,5,1,surf$(5)
        MENU  1,6,1,surf$(6)
        MENU  1,7,1,surf$(7)

        REM
        REM Specify locations menu
        REM
        MENU 2,0,1,"LOCATIONS"
        MENU  2,1,1,surf$(1)
        MENU  2,2,1,surf$(2)
        MENU  2,3,1,surf$(3)
        MENU  2,4,1,surf$(4)
        MENU  2,5,1,surf$(5)
        MENU  2,6,1,surf$(6)
        MENU  2,7,1,surf$(7)
```

333

```
REM
REM Specify refractive indices menu
REM
MENU 3,0,1,"INDICES"
MENU 3,1,1,ind$(1)
MENU 3,2,1,ind$(2)
MENU 3,3,1,ind$(3)
MENU 3,4,1,ind$(4)
MENU 3,5,1,ind$(5)


REM
REM Specify lights and camera menu
REM
MENU 4,0,1,"TRACE"
MENU 4,1,1,"Light 1"
MENU 4,2,1,"Light 2"
MENU 4,3,1,"Camera"
MENU 4,4,1,"Gaze angle"


REM
REM Handle menu selections
REM
handle:
menuno=MENU(0)
IF menuno=0 THEN GOTO handle
IF menuno=1 THEN GOTO surfmenu
IF menuno=2 THEN GOTO locmenu
IF menuno=3 THEN GOTO indexmenu
IF menuno=4 THEN GOTO tracemenu
GOTO handle


REM
REM Handle surfaces menu
REM
surfmenu:
selectno=MENU(1)
IF selectno < 1 THEN GOTO handle
IF selectno > 7 THEN GOTO handle
x$(1)=STR$(xs(1,selectno))
x$(2)=STR$(xs(2,selectno))
x$(3)=STR$(xs(3,selectno))
GOSUB choice3
xs(1,selectno)=VAL(x$(1))
xs(2,selectno)=VAL(x$(2))
xs(3,selectno)=VAL(x$(3))
GOTO handle


REM
REM Handle locations menu
REM
locmenu:
selectno=MENU(1)
IF selectno < 1 THEN GOTO handle
IF selectno > 7 THEN GOTO handle
x$(1)=STR$(xt(1,selectno))
x$(2)=STR$(xt(2,selectno))
x$(3)=STR$(xt(3,selectno))
GOSUB choice3
xt(1,selectno)=VAL(x$(1))
xt(2,selectno)=VAL(x$(2))
xt(3,selectno)=VAL(x$(3))
GOTO handle


REM
REM Handle index menu
REM
indexmenu:
selectno=MENU(1)
```

334

```
            IF selectno < 1 THEN GOTO handle
            IF selectno > 5 THEN GOTO handle
            selectno=selectno+1
            IF selectno > 2 THEN  selectno=selectno+1
            x$(1)=STR$(xp(selectno))
            GOSUB choice1
            xp(selectno)=VAL(x$(1))
            GOTO handle

            REM
            REM Handle trace menu
            REM
            tracemenu:
            selectno=MENU(1)
            IF selectno <1 THEN GOTO handle
            IF selectno>4 THEN GOTO handle
            IF selectno=4 THEN GOTO traceskip
            x$(1)=STR$(xl(1,selectno))
            x$(2)=STR$(xl(2,selectno))
            x$(3)=STR$(xl(3,selectno))
            GOSUB choice3
            xl(1,selectno)=VAL(x$(1))
            xl(2,selectno)=VAL(x$(2))
            xl(3,selectno)=VAL(x$(3))
            GOTO handle
            traceskip:
            x$(1)=STR$(tgaz)
            GOSUB choice1
            tgaz=VAL(x$(1))
            gaz=tgaz/57.3

            REM
            REM Print out altered values
            REM
            LPRINT
            LPRINT "ALTERED PARAMETERS:-"
            LPRINT
            FOR i=1 TO 7
            flag$="off"
            FOR j=1 TO 3
            IF ABS(xs(j,i)-es(j,i)) > .0001 THEN  flag$="on"
            NEXT j
            IF flag$="on" THEN LPRINT surf$(i);" shape",xs(1,i),xs(2,i),xs(3,i)
            NEXT i
            LPRINT
            FOR i=1 TO 7
            flag$="off"
            FOR j=1 TO 3
            IF ABS(xt(j,i)-et(j,i)) > .0001 THEN  flag$="on"
            NEXT j
            IF flag$="on" THEN LPRINT surf$(i);" location",xt(1,i),xt(2,i),xt(3,i)
            NEXT i
            LPRINT
            IF ABS(xp(2)-ep(2)) > 0 THEN LPRINT ind$(1);" index",xp(2)
            IF ABS(xp(4)-ep(4)) > 0 THEN LPRINT ind$(2);" index",xp(4)
            IF ABS(xp(5)-ep(5)) > 0 THEN LPRINT ind$(3);" index",xp(5)
            IF ABS(xp(6)-ep(6)) > 0 THEN LPRINT ind$(4);" index",xp(6)
            IF ABS(xp(7)-ep(7)) > 0 THEN LPRINT ind$(5);" index",xp(7)
            LPRINT
            LPRINT "Coordinates of light 1: ";xl(1,1);" ";xl(2,1);" ";xl(3,1)
            LPRINT "Coordinates of light 2: ";xl(1,2);" ";xl(2,2);" ";xl(3,2)
            LPRINT "Coordinates of camera: ";xl(1,3);" ";xl(2,3);" ";xl(3,3)
            LPRINT "Gaze angle: ";tgaz
            LPRINT

            REM
            REM Copy current parameters
            REM
            FOR i=1 TO 7
```

335

```
        ep(i)=xp(i)
        eq(i)=xq(i)
        FOR j=1 TO 3
        IF ABS(xs(j,i))<.00001 THEN es(j,i)=0
        IF ABS(xs(j,i))<.00001 THEN GOTO avoid
        es(j,i)=1/(xs(j,i)^2)
        IF xs(j,i)<0 THEN es(j,i)=-es(j,i)
        avoid:
        et(j,i)=xt(j,i)
        NEXT j
        FOR j=4 TO 7
        es(j,i)=xs(j,i)
        NEXT j
        NEXT i
        REM
        REM Position lights and camera at a position of 1 metre
        REM
        FOR i=1 TO 3
        FOR j=1 TO 3
        el(i,j)=xl(i,j)*(-1000/(xl(3,j)))
        NEXT j
        NEXT i

        REM
        REM Carry out trace
        REM
        GOSUB rotmat
        REM
        REM Find reflection from anterior cornea of first light
        REM
        ppp=0
        eee=0
        xdist=el(1,1)-el(1,3)
        ydist=el(2,1)-el(2,3)
        corn1:
        x(1)=el(1,3)
        x(2)=el(2,3)
        x(3)=el(3,3)
        y(1)=SIN(ppp)
        y(2)=SIN(eee)*COS(ppp)
        v(3)=COS(eee)*COS(ppp)
        lensnum=3
        GOSUB path
        GOSUB reflec
        ddd=(-1000-x(3))/y(3)
        hdist=x(1)+ddd*y(1)-el(1,3)
        vdist=x(2)+ddd*y(2)-el(2,3)
        PRINT hdist,vdist
        IF hdist<xdist THEN ppp=ppp+.00001
        IF hdist>=xdist THEN ppp=ppp-.00001
        IF vdist<ydist THEN eee=eee+.00001
        IF vdist>=ydist THEN eee=eee-.00001
        IF (ABS(xdist-hdist)+ABS(ydist-vdist))>4.5 THEN GOTO corn1
        LPRINT "Anterior cornea reflection of light1:-"
        LPRINT x(1)," ",x(2)," ",x(3)
        purk1%(1,1)=INT(x(1)*40+200)
        purk1%(2,1)=INT(x(2)*40+130)

        REM
        REM Find reflection from anterior cornea of second light
        REM
        ppp=0
        eee=0
        xdist=el(1,2)-el(1,3)
        ydist=el(2,2)-el(2,3)
        corn2:
        x(1)=el(1,3)
        x(2)=el(2,3)
        x(3)=el(3,3)
```

336

```
y(1)=SIN(ppp)
y(2)=SIN(eee)*COS(ppp)
y(3)=COS(eee)*COS(ppp)
lensnum=3
GOSUB path
GOSUB reflec ·
ddd=(-1000-x(3))/y(3)
hdist=x(1)+ddd*y(1)-el(1,3)
vdist=x(2)+ddd*y(2)-el(2,3)
PRINT hdist,vdist
IF hdist<xdist THEN ppp=ppp+.00001
IF hdist>=xdist THEN ppp=ppp-.00001
IF vdist<ydist THEN eee=eee+.00001
IF vdist>=ydist THEN eee=eee-.00001
IF (ABS(xdist-hdist)+ABS(ydist-vdist))>4.5 THEN GOTO corn2
LPRINT "Anterior cornea reflection of light2:-"
LPRINT x(1)," ",x(2)," ",x(3)
purk1%(1,2)=INT(x(1)*40+200)
purk1%(2,2)=INT(x(2)*40+130)

REM
REM Find reflection from anterior lens of first light
REM
ppp=0
eee=0
xdist=el(1,1)-el(1,3)
ydist=el(2,1)-el(2,3)
antlens1:
x(1)=el(1,3)
x(2)=el(2,3)
x(3)=el(3,3)
y(1)=SIN(ppp)
y(2)=SIN(eee)*COS(ppp)
y(3)=COS(eee)*COS(ppp)
lensnum=5
GOSUB path
GOSUB reflec
GOSUB pathout
ddd=(-1000-x(3))/y(3)
hdist=x(1)+ddd*y(1)-el(1,3)
vdist=x(2)+ddd*y(2)-el(2,3)
PRINT hdist,vdist
IF hdist<xdist THEN ppp=ppp+.00001
IF hdist>=xdist THEN ppp=ppp-.00001
IF vdist<ydist THEN eee=eee+.00001
IF vdist>=ydist THEN eee=eee-.00001
IF (ABS(xdist-hdist)+ABS(ydist-vdist))>4.5 THEN GOTO antlens1
x(1)=el(1,3)
x(2)=el(2,3)
x(3)=el(3,3)
y(1)=SIN(ppp)
y(2)=SIN(eee)*COS(ppp)
y(3)=COS(eee)*COS(ppp)
lensnum=3
GOSUB path
LPRINT "Anterior lens reflection of light1:-"
LPRINT x(1)," ",x(2)," ",x(3)
purk3%(1,1)=INT(x(1)*40+200)
purk3%(2,1)=INT(x(2)*40+130)

REM
REM Find reflection from anterior lens of second light
REM
ppp=0
eee=0
xdist=el(1,2)-el(1,3)
ydist=el(2,2)-el(2,3)
antlens2:
```

```
x(1)=el(1,3)
x(2)=el(2,3)
x(3)=el(3,3)
y(1)=SIN(ppp)
y(2)=SIN(eee)*COS(ppp)
y(3)=COS(eee)*COS(ppp)
lensnum=5
GOSUB path
GOSUB reflec
GOSUB pathout
ddd=(-1000-x(3))/y(3)
hdist=x(1)+ddd*y(1)-el(1,3)
vdist=x(2)+ddd*y(2)-el(2,3)
PRINT hdist,vdist
IF hdist<xdist THEN ppp=ppp+.00001
IF hdist>=xdist THEN ppp=ppp-.00001
IF vdist<ydist THEN eee=eee+.00001
IF vdist>=ydist THEN eee=eee-.00001
IF (ABS(xdist-hdist)+ABS(ydist-vdist))>4.5 THEN GOTO antlens2
x(1)=el(1,3)
x(2)=el(2,3)
x(3)=el(3,3)
y(1)=SIN(ppp)
y(2)=SIN(eee)*COS(ppp)
y(3)=COS(eee)*COS(ppp)
lensnum=3
GOSUB path
LPRINT "Anterior lens reflection of light2:-"
LPRINT x(1)," ",x(2)," ",x(3)
purk3%(1,2)=INT(x(1)*40+200)
purk3%(2,2)=INT(x(2)*40+130)

REM
REM Find reflection from posterior lens of first light
REM
ppp=0
eee=0
xdist=el(1,1)-el(1,3)
ydist=el(2,1)-el(2,3)
postlens1:
x(1)=el(1,3)
x(2)=el(2,3)
x(3)=el(3,3)
y(1)=SIN(ppp)
y(2)=SIN(eee)*COS(ppp)
y(3)=COS(eee)*COS(ppp)
lensnum=6
GOSUB path
GOSUB reflec
GOSUB pathout
ddd=(-1000-x(3))/y(3)
hdist=x(1)+ddd*y(1)-el(1,3)
vdist=x(2)+ddd*y(2)-el(2,3)
PRINT hdist,vdist
IF hdist<xdist THEN ppp=ppp-.00001
IF hdist>=xdist THEN ppp=ppp+.00001
IF vdist<ydist THEN eee=eee-.00001
IF vdist>=ydist THEN eee=eee+.00001
IF (ABS(xdist-hdist)+ABS(ydist-vdist))>4.5 THEN GOTO postlens1
x(1)=el(1,3)
x(2)=el(2,3)
x(3)=el(3,3)
y(1)=SIN(ppp)
y(2)=SIN(eee)*COS(ppp)
y(3)=COS(eee)*COS(ppp)
lensnum=3
GOSUB path
LPRINT "Posterior lens reflection of light1:-"
```

```
        LPRINT x(1)," ",x(2)," ",x(3)
        purk4%(1,1)=INT(x(1)*40+200)
        purk4%(2,1)=INT(x(2)*40+130)

        REM
        REM Find reflection from posterior lens of second light
        REM
        ppp=0
        eee=0
        xdist=el(1,2)-el(1,3)
        ydist=el(2,2)-el(2,3)
        postlens2:
        x(1)=el(1,3)
        x(2)=el(2,3)
        x(3)=el(3,3)
        y(1)=SIN(ppp)
        y(2)=SIN(eee)*COS(ppp)
        y(3)=COS(eee)*COS(ppp)
        lensnum=6
        GOSUB path
        GOSUB reflec
        GOSUB pathout
        ddd=(-1000-x(3))/y(3)
        hdist=x(1)+ddd*y(1)-el(1,3)
        vdist=x(2)+ddd*y(2)-el(2,3)
        PRINT hdist,vdist
        IF hdist<xdist THEN ppp=ppp-.00001
        IF hdist>=xdist THEN ppp=ppp+.00001
        IF vdist<ydist THEN eee=eee-.00001
        IF vdist>=ydist THEN eee=eee+.00001
        IF (ABS(xdist-hdist)+ABS(ydist-vdist))>4.5 THEN GOTO postlens2
        x(1)=el(1,3)
        x(2)=el(2,3)
        x(3)=el(3,3)
        y(1)=SIN(ppp)
        y(2)=SIN(eee)*COS(ppp)
        y(3)=COS(eee)*COS(ppp)
        lensnum=3
        GOSUB path
        LPRINT "Posterior lens reflection of light2:-"
        LPRINT x(1)," ",x(2)," ",x(3)
        purk4%(1,2)=INT(x(1)*40+200)
        purk4%(2,2)=INT(x(2)*40+130)

        REM
        REM Draw picture
        REM
        PICTURE ON
        CALL PENSIZE(1,1)
        CALL MOVETO(200,230)
        FOR i=1 TO 730
        j=i/100
        txt%=INT(SIN(j)*100+200)
        tyt%=INT(COS(j)*100+130)
        CALL LINETO(txt%,tyt%)
        NEXT i
        REM
        REM Plot images
        REM
        FOR i=1 TO 2
        txt%=purk1%(1,i)-3
        tyt%=purk1%(2,i)
        CALL MOVETO(txt%,tyt%)
        txt%=txt%+6
```

```
        CALL LINETO(txt%,tyt%)
        txt%=purk1%(1,i)
        tyt%=purk1%(2,i)-3
        CALL MOVETO(txt%,tyt%)
        tyt%=tyt%+6
        CALL LINETO(txt%,tyt%)
        NEXT i
        FOR i=1 TO 2
        txt%=purk3%(1,i)-2
        tyt%=purk3%(2,i)-2
        CALL MOVETO(txt%,tyt%)
        txt%=txt%+4
        tyt%=tyt%+4
        CALL LINETO(txt%,tyt%)
        txt%=purk3%(1,i)+2
        tyt%=purk3%(2,i)-2
        CALL MOVETO(txt%,tyt%)
        txt%=txt%-4
        tyt%=tyt%+4
        CALL LINETO(txt%,tyt%)
        NEXT i
        FOR i=1 TO 2
        txt%=purk4%(1,i)
        tyt%=purk4%(2,i)-3
        CALL MOVETO(txt%,tyt%)
        tyt%=tyt%+3
        CALL LINETO(txt%,tyt%)
        txt%=purk4%(1,i)
        tyt%=purk4%(2,i)
        CALL MOVETO(txt%,tyt%)
        txt%=txt%-2
        tyt%=tyt%+2
        CALL LINETO(txt%,tyt%)
        txt%=purk4%(1,i)
        tyt%=purk4%(2,i)
        CALL MOVETO(txt%,tyt%)
        txt%=txt%+2
        tyt%=tyt%+2
        CALL LINETO(txt%,tyt%)
        NEXT i
        REM
        REM Save picture
        REM
        im$=PICTURE$
        OPEN "clip:picture" FOR OUTPUT AS #1 LEN=32000
        PRINT#1,im$
        CLOSE#1

        REM
        REM End of main program
        REM
        GOTO finish

        REM
        REM Computes path of ray through eye
        REM
        path:
        FOR iii = 3 TO lensnum
        FOR j = 1 TO 3
        t(j)=et(j,iii)
        b(j)=es(j+3,iii)
        FOR k = 1 TO 3
        a(j,k)=0
        IF j=k THEN a(j,k)=es(j,iii)
        NEXT k
        NEXT j
        c = es(7,iii)
        q = eq(iii)
```

340

```
        GOSUB transquad
        GOSUB rotquad
        GOSUB hit
        ip=ep(iii)
        k=iii+1
        rp=ep(7)
        IF k<7.5 THEN rp=ep(k)
        IF iii=lensnum THEN rp=io
        GOSUB bend
        NEXT iii
        RETURN

        REM
        REM Computes path of ray out through eye
        REM
        pathout:
        FOR kkk = 1 TO (lensnum-3)
        iii=lensnum-kkk
        FOR j = 1 TO 3
        t(j)=et(j,iii)
        b(j)=es(j+3,iii)
        FOR k = 1 TO 3
        a(j,k)=0
        IF j=k THEN a(j,k)=es(j,iii)
        NEXT k
        NEXT j
        c = es(7,iii)
        q = -eq(iii)
        GOSUB transquad
        GOSUB rotquad
        GOSUB hit
        n(1)=-n(1)
        n(2)=-n(2)
        n(3)=-n(3)
        k=iii+1
        ip=ep(k)
        rp=ep(iii)
        GOSUB bend
        NEXT kkk
        RETURN

        REM
        REM Accepts value for a single parameter
        REM
        choice1:
        EDIT FIELD  1,x$(1),(100,90)-(150,110)
        BUTTON  1,1,"ok",(200,90)-(220,110)
        response1:
        reply=DIALOG(0)
        IF reply <> 1 THEN GOTO response1
        x$(1)=EDIT$(1)
        EDIT FIELD CLOSE 1
        BUTTON CLOSE 1
        RETURN

        REM
        REM Accepts values for a set of X,Y,Z parameters
        REM
        choice3:
        EDIT FIELD  1,x$(1),(100,50)-(150,70)
        EDIT FIELD  2,x$(2),(100,90)-(150,110)
        EDIT FIELD  3,x$(3),(100,130)-(150,150)
        BUTTON  1,1,"ok",(200,90)-(220,110)
        BUTTON  2,1,"X",(70,50)-(90,70)
        BUTTON  3,1,"Y",(70,90)-(90,110)
        BUTTON  4,1,"Z",(70,130)-(90,150)
        response3:
        reply=DIALOG(0)
```

```
        IF reply <> 1 THEN GOTO response3
        reply=DIALOG(1)
        IF reply <>1 THEN GOTO response3
        x$(1)=EDIT$(1)
        x$(2)=EDIT$(2)
        x$(3)=EDIT$(3) .
        EDIT FIELD CLOSE 1
        EDIT FIELD CLOSE 2
        EDIT FIELD CLOSE 3
        BUTTON CLOSE 1
        BUTTON CLOSE 2
        BUTTON CLOSE 3
        BUTTON CLOSE 4
        RETURN

        REM
        REM Translates quadric
        REM
        transquad:
        xx(1)=a(1,1)*t(1)+a(1,2)*t(1)+a(1,3)*t(1)
        xx(2)=a(2,1)*t(2)+a(2,2)*t(2)+a(2,3)*t(2)
        xx(3)=a(3,1)*t(3)+a(3,2)*t(3)+a(3,3)*t(3)
        c=c+(xx(1)+b(1))*t(1)+(xx(2)+b(2))*t(2)+(xx(3)+b(3))*t(3)
        b(1)=2*xx(1)+b(1)
        b(2)=2*xx(2)+b(2)
        b(3)=2*xx(3)+b(3)
        RETURN

        REM
        REM Rotates quadric
        REM
        rotquad:
        FOR i=1 TO 3
        FOR j=1 TO 3
        qq(i,j)=0
        FOR k=1 TO 3
        qq(i,j)=qq(i,j)+a(i,k)*r(k,j)
        NEXT k
        NEXT j
        NEXT i
        FOR i=1 TO 3
        FOR j=1 TO 3
        ss(i,j)=r(j,i)
        NEXT j
        NEXT i
        FOR i=1 TO 3
        FOR j=1 TO 3
        a(i,j)=0
        FOR k=1 TO 3
        a(i,j)=a(i,j)+ss(i,k)*qq(k,j)
        NEXT k
        NEXT j
        NEXT i
        xx(1)=b(1)
        xx(2)=b(2)
        xx(3)=b(3)
        b(1)=ss(1,1)*xx(1)+ss(1,2)*xx(2)+ss(1,3)*xx(3)
        b(2)=ss(2,1)*xx(1)+ss(2,2)*xx(2)+ss(2,3)*xx(3)
        b(3)=ss(3,1)*xx(1)+ss(3,2)*xx(2)+ss(3,3)*xx(3)
        RETURN

        REM
        REM Sets up rotation matrix
        REM
        rotmat:
        r(1,1)=COS(gaz)
        r(1,2)=0
        r(1,3)=-SIN(gaz)
        r(2,1)=0
```

342

```
        r(2,2)=1
        r(2,3)=0
        r(3,1)=SIN(gaz)
        r(3,2)=0
        r(3,3)=COS(gaz)
        RETURN              .

        REM
        REM Calculates intersection with the quadric
        REM
        hit:
        tt(1)=a(1,1)*y(1)+a(1,2)*y(2)+a(1,3)*y(3)
        tt(2)=a(2,1)*y(1)+a(2,2)*y(2)+a(2,3)*y(3)
        tt(3)=a(3,1)*y(1)+a(3,2)*y(2)+a(3,3)*y(3)
        at=tt(1)*y(1)+tt(2)*y(2)+tt(3)*y(3)
        xta(1)=x(1)*a(1,1)+x(2)*a(2,1)+x(3)*a(3,1)
        xta(2)=x(1)*a(1,2)+x(2)*a(2,2)+x(3)*a(3,2)
        xta(3)=x(1)*a(1,3)+x(2)*a(2,3)+x(3)*a(3,3)
        tt(1)=2*xta(1)+b(1)
        tt(2)=2*xta(2)+b(2)
        tt(3)=2*xta(3)+b(3)
        bt=tt(1)*y(1)+tt(2)*y(2)+tt(3)*y(3)
        tt(1)=xta(1)+b(1)
        tt(2)=xta(2)+b(2)
        tt(3)=xta(3)+b(3)
        ct=c+tt(1)*x(1)+tt(2)*x(2)+tt(3)*x(3)
        erro=bt^2-4*at*ct
        IF erro<0 THEN PRINT "error"
        IF erro<0 THEN RETURN
        IF at=0 THEN d1=ct/bt
        IF at=0 THEN d2=ct/bt
        IF at=0 THEN GOTO zeroloop
        d1=(-bt+SQR(erro))/(2*at)
        d2=(-bt-SQR(erro))/(2*at)
        zeroloop:
        ll=d1
        uu=d2
        IF ll>d2 THEN ll=d2
        IF uu<d1 THEN uu=d1
        dd=ll
        IF q<0 THEN dd=uu
        x(1)=x(1)+dd*y(1)
        x(2)=x(2)+dd*y(2)
        x(3)=x(3)+dd*y(3)
        n(1)=a(1,1)*x(1)+a(1,2)*x(2)+a(1,3)*x(3)
        n(2)=a(2,1)*x(1)+a(2,2)*x(2)+a(2,3)*x(3)
        n(3)=a(3,1)*x(1)+a(3,2)*x(2)+a(3,3)*x(3)
        n(1)=2*n(1)+b(1)
        n(2)=2*n(2)+b(2)
        n(3)=2*n(3)+b(3)
        const=SQR(n(1)^2+n(2)^2+n(3)^2)
        IF n(3)<0 THEN const=-const
        n(1)=n(1)/const
        n(2)=n(2)/const
        n(3)=n(3)/const
        RETURN

        REM
        REM Calculates direction of refracted ray
        REM
        bend:
        y1cos=ABS(y(1)*n(1)+y(2)*n(2)+y(3)*n(3))
        y2cos=SQR(1-((ip^2/rp^2)*(1-y1cos^2)))
        const=rp*y2cos-ip*y1cos
        y(1)=(ip*y(1)+const*n(1))/rp
        y(2)=(ip*y(2)+const*n(2))/rp
        y(3)=(ip*y(3)+const*n(3))/rp
        RETURN
```

343

```
REM
REM Calculates direction of reflected ray
REM
reflec:
y(1)=y(1)-2*n(1)
y(2)=y(2)-2*n(2)
y(3)=y(3)-2*n(3)
const=SQR(y(1)^2+y(2)^2+y(3)^2)
y(1)=y(1)/const
y(2)=y(2)/const
y(3)=y(3)/const
RETURN

REM
REM End of program
REM
finish:
END
```

344

REFERENCES

Aebly, J. (1922) Zur frage der gestalt der vorderen hornhautflache. *Zeitschrift feur Entwicklungspsychology und Mechanischen,* 53, 223. Cited by Ludlam and Wittenberg (1966b).

Alsbirk, P.H. (1974) Optical pachymetry of the anterior chamber. A methodological study of errors of measurement using Haag Streit 900 Instruments. *Acta Ophthalmologica,* 52, 747-758.

Alpern, M. and Campbell, F.W. (1962) The behaviour of the pupil during dark adaptation. *Journal of Physiology (London),* 165, 5-7.

Ames, A. and Proctor, C.A. (1921) Dioptrics of the eye. *Journal of the Optical Society of America,* 5, 22-84.

Ashton, G.C. (1985) Segregation analysis of ocular refraction and myopia. *Human Heredity,* 35, 233-239.

Atkinson, J., Braddick, O. and French, J. (1980) Infant astigmatism: its disⱠappearance with age. *Vision Research,* 20, 891-893.

Aubert, H. (1885) Nahert sich die hornhautkrummung am meisten der ellipse? *Pfluger's Archiv fur die Gesamte Physiologie,* 35, 597-621. Cited by Ludlam and Wittenberg (1966b).

Awerbach, M.I. (1900) *The Dioptrics of Refraction* (Thesis in Russian). Moscow. Cited by Ludlam (1967).

Baldwin, W.R. (1962) Corneal curvature changes in high myopia vs corneal curvature changes in low myopia. *American Journal of Optometry & A.A.A.O.,* 39, 349-355.

Baldwin,W.R. (1964) The relationship between axial length of the eye and certain other anthropometric measurements in myopes. *American Journal of Optometry & A.A.A.O.,* 41, 513-522.

Barker, T. (1943) Ray tracing through non-spherical surfaces. *The Proceedings of the Physical Society,* 55, 361-364.

Barlow, H.B. (1972) Dark and light adaptation: Psychophysics. In Jameson, D. and Hurvich, L.M. (Eds) *Handbook of Sensory Physiology* Vol. 7/4. Springer, New York. Cited by Woodhouse and Campbell (1975).

Barrett, C.D. (1945) Sources of error and working methods in retinoscopy. *British Journal of Physiological Optics,* 5, 35-40.

Baum, G. (1956) The effect of ultrasonic radiation. *American Journal of Ophthalmology,* 42, 696-706.

Bedrossian, R.H. (1966) Treatment of progressive myopia with atropine. In *Proceedings of the XX International Congress of Ophthalmology,* Munich, pp 612-617. Exerpta Medica Foundation, New York. Cited by Young (1975).

Benedek, G.B. (1971) Theory of transparency of the eye. *Applied Optics,* 10, 459-473.

Bennett, A.G. (1951) Oblique refraction of the schematic eye. *Optician,* 121, 583-588.

Bennett, A.G. (1960) Refraction by automation? New applications of the Scheiner disc. *Optician*, **139**, 5-9.

Bennett, A.G. (1961) Appendix D. The computation of optical dimensions. In Sorsby et al. (1961) pp 55-64.

Bennett, A.G. (1968) Aspheric contact lens surface. *Ophthalmic Optician*, **8**, 1037-1040, 1297-1300, 1311 and **9**, 222-230.

Bennett, A.G. (1984) Astigmatic effect of a tilted crystalline lens. *Ophthalmic Optician*, **24**, 793-794.

Bennett, A.G. and Rabbetts, R.B. (1984) *Clinical Visual Optics*. Butterworth, London.

Berg, F. (1927) Underskningar over framre hornhinneytans form. *Akademisk Afhandling Upsala*, Gotenberg. Cited by Ludlam and Wittenberg (1966b).

Berg, F. (1929) Vergleichende messungen der form derivorderen hornhautflache mit ophthalmometer und mit photographischer method. *Acta Ophthalmology*, **7**, 386-423. Cited by Clark (1973a).

Bibby, M.M. (1976) Computer assisted photokeratoscopy and contact lens design. 1. *Optician*, **171(4423)**, 37-44, **171(4424)**, 11-17 and **171(4426)**, 15-17.

Bier, N. (1956) A study of the cornea in relation to contact lens practice. *British Journal of Physiological Optics*, **13**, 79-92.

Binder, P.S., Kohler, J.A. and Rorabaugh, D.A. (1977) Evaluation of an electric corneal pachometer. *Investigative Ophthalmology and Visual Science*, **161**, 855-858.

Blaker, J.W. (1980) Toward an adaptive model of the human eye. *Journal of the Optical Society of America*, **70**, 220-223.

Blix, M. (1880) Oftalmometriska studier. *Acta Societatis Medicorum Upsaliensis*, **15**, 349-421. Cited by Von Bahr (1948).

Bonnet, R. and Cochet, P. (1962) New method of topographic ophthalmometry - its theoretical and clinical applications (trans. Eagle, E.). *American Journal of Optometry & A.A.A.O.*, **39**, 227-251.

Borish, I.M. (1970) *Clinical Refraction*. Professional Press, Chicago.

Braddick, O., Atkinson, J., French, J. and Howland, H.C. (1979) A photorefractive study of Infant accommodation. *Vision Research*, **19**, 1319-1330.

Brown, E.V.L. (1938) Net yearly changes in refraction of atropinised eye from birth to beyond middle life. *Archives of Ophthalmology*, **37**, 587-592.

Brown, N. (1969) Slit image photography. *Transactions of the Ophthalmological Societies of the United Kingdom*, **89**, 397-408.

Brown, N. (1972) An advanced slit image camera. *British Journal of Ophthalmology*, **56**, 624-631.

Brown, N. (1973) The change in shape and internal form of the eye on accommodation. *Experimental Eye Research,* **15,** 441-460.

Bullimore, M. and Gilmartin, B. (1987) Aspects of tonic accommodation in emmetropia and late-onset myopia. *American Journal of Optometry and Physiological Optics.* In press.

Calmettes, L., Deodati, F., Huron, H. and Bechac, G. (1958) Study of the depth of anterior chamber - physiological variations with particular emphasis on ametropia (trans. Pitts, D.A. and Millodot, M.). *American Journal of Optometry & A.A.A.O.,* **43,** 765-793.

Campbell, F.W. (1957) The depth of field of the human eye. *Optica Acta,* **4,** 157-164.

Campbell, F.W. and Gregory, A.H. (1960) Effect of size of pupil on visual acuity. *Nature (London),* **187,** 1121-1123.

Campbell, F.W. and Primrose, J.A.E. (1953) The state of accommodation of the human eye in darkness. *Transactions of the Ophthalmological Society of America,* **68,** 353-361.

Carpenter, R.S. (1977) *Movements of the Eyes.* Pion, London.

Charman, W.N. (1972) Diffraction and the precision of measurement of corneal and other small radii. *American Journal of Optometry & A.A.A.O.,* **49,** 672-679.

Charman, W.N. (1980) Measurement of pupil diameter by image-doubling. *Optician,* **179,** 24-28.

Charman, W.N. (1983) The retinal image of the human eye. In Osborne, N. and Chandler, G. (Eds) *Progress in Retinal Research,* Vol. 2, Ch. 1, pp 1-50. Pergamon Press. Oxford.

Charman, W.N. and Jennings, J.A.M. (1976) Objective measurement of the longitudinal chromatic aberration of the human eye. *Vision Research,* **16,** 999-1005.

Charman, W.N. and Jennings, J.A.M. (1982) Ametropia and peripheral refraction. *American Journal of Optometry and Physiological Optics,* **59,** 922-923.

Clark, B.A.J. (1966) *The determination of corneal topography.* Master's Thesis, University of Melbourne. Cited by Clark (1973b).

Clark, B.A.J. (1971) *Topography of the normal human cornea.* Ph.D. Thesis, University of Melbourne. Cited by Clark (1973b).

Clark, B.A.J. (1972) Autocollimating photokeratoscope. *Journal of the Optical Society of America,* **62,** 169-176.

Clark, B.A.J. (1973a) Keratometry: a review. *Australian Journal of Optometry,* **56,** 94-100.

Clark, B.A.J. (1973b) Conventional keratoscopy - a critical review. *Australian Journal of Optometry,* **56,** 140-155.

Clark, B.A.J. (1974a) Topography of some individual corneas. *Australian Journal of Optometry*, **57**, 65-69.

Clark, B.A.J. (1974b) Mean topography of normal corneas. *Australian Journal of Optometry*, **57**, 107-114.

Coulombre, A.J. and Coulombre, J.L. (1956) The role of intraocular pressure in the development of the chick eye: I. Control of eye size. *Journal of Experimental Zoology*, **133**, 211-255.

Cohn, H. (1886) *The Hygiene of the eye in schools*, an English translation, Turnbull, W.P. (Ed) Simpkin, Marshall, London.

Cohn, P.M. (1961) *Solid Geometry*. Routledge, Kegan and Paul, London.

Coleman, D.J. (1967) Ophthalmic ultrasonography: comparative techniques. *International Ophthalmology Clinics*, **19**, 225-236.

Coleman, D.J. (1970) Unifed model for accommodative mechanism. *American Journal of Ophthalmology*, **69**, 1063-1079.

Cox, J.L., Farrell, R.A., Hart, R.W. and Langham, M.E. (1970) The transparency of the mammalian cornea. *Journal of Physiology (London)*, **210**, 601-616.

Crawford, H.B. (1936) The dependance of pupil size upon external light stimulus under static and variable conditions. *Proceedings of the Royal Society*, **B121**, 376-395.

Davson, H. (1980) *Physiology of the Eye*, 4th Edition. Churchill Livingstone, Edinburgh.

Dekking, H.M. (1930) Zur photography der hornhautoberflache. *Albrecht von Graefes Archiv fur Klinische und Experimentelle Ophthalmologie*, **124**, 708-730. Cited by Clark (1973b).

Deller, J.F.P., O'Connor, A.D. and Sorsby, A. (1947) X-ray measurements of the diameters of the living eye. *Proceedings of the Royal Society*, **B134**, 456-467.

Donaldson, D.D. (1966) Measurement of corneal thickness. *Archives of Ophthalmology*, **76**, 25-31.

Donders, F.C. (1864) *On the Anomalies of Accommodation and Refraction of the Eye*. New Sydenham Society, London.

Drasdo, N. and Fowler, C.W. (1974) Non-linear projection of the retinal image in a wide-angle schematic eye. *British Journal of Ophthalmology*, **58**, 709-714.

Duke-Elder, S. and Abrams, D. (1970) Ophthalmic optics and refraction. *System of Ophthalmology*, Vol. V. Kimpton, London.

Duke-Elder, S. and Wybar, K.C. (1961) The anatomy of the visual systrem. *System of Ophthalmology*, Vol. II. Kimpton, London.

Ebenholtz, S.M. (1983) Accommodative hysteresis: a precursor to induced myopia? *Investigative Ophthalmology and Visual Science*, **24**, 513-515.

Ebenholtz, S.M. (1985) Accommodative hysteresis: relation to resting focus. *American Journal of Optometry and Physiological Optics*, **62**, 755-762.

Edmund, C. and La Cour, M. (1986) Some components effecting the precision of corneal thickness measurement performed by optical pachometry. *Acta Ophthalmologica*, **64**, 499-503.

Ehlers, N. (1965) The precorneal film. *Acta Ophthalmologica Supplement*, **81**, 1-136.
El Hage, S.G. (1969) Recherche de l'equation mathematique de la cornee a partir d'une methode photokeratoscopie. *Opticien Lunetier*, **192**, 16. Cited by Clark (1973b).

El Hage, S.G. (1970) Contribution a l'etude de la forme corneenne. *Comptes Rendue Hebdomadaires des Seances de l'Acadademie des Sciences (Paris)*, **D270**, 3299-3302. Cited by Clark (1973b).

El Hage, S.G. and Berny, F. (1973) Contribution of the crystalline lens to the spherical aberration of the eye. *Journal of the Optical Society of America*, **63**, 205-211.

Ellerbrock, V.J. (1963) Developmental, congenital and hereditary anomalies of the eye. In Hirsch, M.J. and Wick, R.E. (Eds) Vision of Children, Ch.2, pp 79-98. Chilton Book Co., Philadelphia.

Emsley, H.H. (1952) *Visual Optics*, Vol. 1, Hatton, London.

Eriksen (1893) *Hornheindemaalinger*. Aarhus, Denmark. Cited by Ludlam and Wittenberg (1966b).

Evershed-Martin, L. (1959) The sanctity of corneal clarity and some contact lens fallacies. *British Journal of Physiological Optics*, **16**, 24-35.

Farrell, R.A., McCally, R.L. and Tatham, P.E.R. (1973) Wave-length dependencies of light scattering in normal and cold swollen rabbit corneae and their structural implications. *Journal of Physiology (London)*, **233**, 589-612.

Ferree, C.E. and Rand, G.(1933) Interpretation of refractive condition in the peripheral field of vision. *Archives of Ophthalmology*, **9**, 925-938.

Ferree, C.E., Rand, G. and Hardy, C. (1931) Refraction for the peripheral field of vision. *Archives of Ophthalmology*, **5**, 717-731.

Ferree, C.E., Rand, G. and Hardy, C. (1932) Refractive asymmetry in the temporal and nasal halves of the visual field. *American Journal of Ophthalmology*, **15**, 513-522.

Feuk, T. (1970) On the transparency of the stroma in the mammalian cornea. *IEE Transactions on Bio-Medical Engineering*, **BME17**, 186-190.

Fincham, E.F. (1926) The changes in the form of the crystalline lens in accommodation. *American Journal of Physiological Optics.*, **7**, 469. Cited by Watkins (1972).

Fincham, E.F. (1937) The mechanism of accommodation. *British Journal of Physiological Optics*. Monograph supplement VIII, Pulman, London.

Fischer, F.P. (1948) *Scenescence of the eye*. In Sorsby, A. (Ed) Modern Trends in Ophthalmology, Vol. 2, Ch. 6, pp 54-70. Butterworth, London.

Fisher, R.F. (1969a) The elastic constants of the human lens capsule. *Journal of Physiology (London)*, **201**, 1-20.

Fisher, R.F. (1969b) The significance of the shape of the lens and capsular energy changes in accommodation. *Journal of Physiology (London)*, **201**, 21-47.

Fisher, R.F. (1971) The elastic constants of the human lens. *Journal of Physiology (London)*, **212**, 147-180.

Fisher, R.F. and Wakely, J. (1976) The elastic constants and ultrastructural organization of a basement membrane (lens capsule). *Proceedings of the Royal Society*, **193**, 335-358.

Fledelius, H.C. (1976) Prematurity of the eye. Ophthalmic 10 year follow-up of children of low and normal birthweight. *Acta Ophthalmologica Supplement* **128**, 1-233.

Fledelius, H.C. and Stubgaard, M. (1986) Changes in refraction and corneal curvature during growth and adult life. *Acta Ophthalmologica*, **64**, 487-491.

Fletcher, M.C. and Brandon, S. (1955) Myopia and prematurity. American Journal of Ophthalmology, 40, 474-481.

Francis, J.L. (1962) Some measurements on myopic eyes. In *Transactions of the International Ophthalmic Optical Congress* 1961. pp 406-416. Hafner Publishing Company, New York.

Francois, J. and Goes, F. (1969a) Echographical study of the lens thickness as a function of the axial length in emmetropic eyes of the same age. In *Ultrasonographica Medica*, pp 531-538. Verlag der Weiner Akademie, SIDUO III.

Francois, J. and Goes, F. (1969b) Oculometry in emmetropia and ametropia. In *Ultrasonographica Medica*, pp 473-515. Verlag der Weiner Akademie, SIDUO III.

Francois, J. and Goes, F. (1977) Ultrasonographic study of 100 emmetropic eyes. *Ophthalmologica (Basel)*, **175**, 321-327.

French, C.N. and Wood, I.C.J. (1982) The Dioptron II's validity and reliability as a function of its three accuracy indices. *Ophthalmic and Physiological Optics*, **2**, 57-74.

French, C.N., Nixon, J.A. and Wood, I.C.J. (1982) Dioptron - and retinoscopy - subjective discrepencies: effect of age. *Ophthalmic and Physiological Optics*, **2**, 227-230.

Freytag (1907) Die brechungsindices der linse und der flussigen augenmedien des menschen und hoherer tiere in verschiedenen lebensaltern in vergleichenden untersuchungen. Wiesbaden. Cited by Huggert (1948).

Fry, G.A. (1959) The image forming mechanism of the eye. In Field, J. (Ed) *Handbook of Physiology*, Vol. 1, Section I. Neurophysiology, Waverley Press, Baltimore. Cited by Watkins (1972).

Fujii, T., Maruyama, S. and Ikeda, M. (1972) Determination of corneal configuration by measurement of its derivatives. *Optica Acta*, **19**, 425-430.

Fujita, S. (1980) Diurnal variation of human corneal thickness. *Japanese Journal of Ophthalmology*, **24**, 444-456.

Fulton, A.B., Dobson, V., Salem, D., Mar, C., Peterson, R. and Hansen, R. (1980) Cycloplegic refractions in infants and young children. *American Journal of Ophthalmology*, **90**, 239-247.

Gallati, J. (1923) Die relativen dickenwerte von rinde und kern der menschlichen linse in verschiedenen lebensaltern. *Zeitschrift feur Augenheilkunde*, **51**, 133-144. Cited by Brown (1973).

Gardiner, P.A. (1962) Corneal power in myopic children. *British Journal of Ophthalmology*, **46**, 138-143.

Gernet, H. (1964a) Contribution to the problem of emmetropia. *Ophthalmologica (Basel)*, **147**, 235-243.

Gernet, H. (1964b) Uber achsenlange und brechkraft emmetroper lebender augen. *Albrecht von Graefes Archiv fur Klinische und Experimentelle Ophthalmologie*, **166**, 424-431. Cited by Larsen (1971c).

Gernet, H. (1964c) Achsenlange und refraction lebender augen von neugeborenen. *Albrecht von Graefes Archiv fur Klinische und Experimentelle Ophthalmologie*, **166**, 530-536. Cited by Larsen (1971c).

Gernet, H. and Hollwich, F. (1969) Oculometrie des kindlichen glaucoms. *Berichte der Deutschen Ophthalmologischen Gesellschaft*, **69**, 341-348. Cited by Larsen (1971c).

Giglio, E.J. and Ludlam, W.M. (1967) High resolution ultrasonic equipment to measure intra-ocular distances. *Journal of the American Optometric Association*, **38**, 367-371.

Giglio, E.J. and Ludlam, W.M. (1971) A hand held probe for acoustic coupling in ultrasonic intra-ocular distance measurements of young children. *American Journal of Optometry & A.A.A.O.*, **48**, 1025-1030.

Giglio, E.J., Ludlam, W.M. and Wittenberg, S. (1968) Improvement in the measurement of intra-ocular distances using ultrasound. *Journal of the Acoustical Society of America*, **44**, 1359-1364.

Giglio, E.J. and Meyers, R.R. (1969) An automatic probe transport to the eye for ultrasound. *American Journal of Optometry & A.A.A.O.*, **46**, 275-282.

Gilmartin, B. and Hogan, R.E. (1985) The role of the sympathetic nervous system in ocular accommodation and ametropia. *Ophthalmic and Physiological Optics*, **5**, 91-93.

Gilmartin, B. and Bullimore, R.E. (1987) Sustained near-vision augments inhibitory sympathetic innervation of the ciliary muscle. *Clinical Vision Sciences*, **1**, 197-208.

Girard, L.G. (1970) *Corneal Contact Lenses*, 2nd ed., Mosby, St. Louis.

Goldmann, H. (1940) Spaltlampenphotographic und photometrie. *Ophthalmologica (Basel)*, **98**, 257-270. Cited by Bennett and Rabbetts (1984).

Goldmann, H. (1968) Biomicroscopy of the eye [The 22nd Francis I. Proctor Lecture]. *American Journal of Ophthalmology*, **66**, 789-864.

Goldmann, H. and Hagen, R. (1942) Zur direkten messung der total brechkraft des lebenden menschlichen auges. *Ophthalmologica (Basel)*, **104**, 15-22. Cited by Bennett and Rabbetts (1984).

Goldschmidt, E. (1968) On the etiology of myopia. *Acta Ophthalmologica Supplement*, **98**, 1-172.

Gordon, R.A. and Donzis, P.B. (1985) Refractive development of the human eye. *Archives of Ophthalmology*, **62**, 391-400.

Greene, P.R. (1980) Mechanical considerations in myopia - relative effects of accommodation, accommodative convergence, intraocular pressure and extra-ocular muscles. *American Journal of Optometry and Physiological Optics*, **57**, 902-914.

Grosvenor, T. (1961) Clinical use of the keratometer in evaluating corneal contour. *American Journal of Optometry & A.A.A.O.*, **38**, 237-245.

Guillon, M., Lydon, D.P.M. and Wilson, C. (1986) Corneal topography: a clinical model. *Ophthalmic and Physiological Optics*, **6**, 47-56.

Gullstrand, A. (1924) Appendices to *Physiological Optics*, Vol. 1 by Helmholtz, (trans. Southall, J.P.C.). *Optical Society of America, Rochester.*

Hallden, U. (1956) An optical explanation of Hering-Hillebrand's horopter deviation. *Archives of Ophthalmology*, **55**, 830-835.

Hart, R.W. and Farrell, R.A. (1969) Light scattering in the cornea. *Journal of the Optical Society of America*, **59**, 766-774.

Heim, M.(1941) Photographische bestimmung der tiefe und des volumens der menschlichen vorderkammer. *Ophthalmologica (Basel)*, **102**, 193-220.

Helmholtz, H. (1924) *Physiological Optics*, Vol. 1, (trans. Southall, J.P.C.) *Optical Society of America, Rochester.*

Henson, D.B. (1983) *Optometric Instrumentation.* Butterworths, London.

Hess, C. (1929) *Handbuch der Normalen und Pathologischen Physiologie*, Vol. 12. Cited by Park (1936).

Hess, E.H. (1965) Attitude and pupil size. *Scientific American*, **212**, 46-54.

Hirji, N.K. and Larke, J.R. (1978) Thickness of the human cornea measured by topographic pachometry. *American Journal of Optometry and Physiological Optics*, **55**, 97-100.

Hirsch, M.J. (1959) Changes in the refractive state after the age of 45. *American Journal of Optometry & A.A.A.O.*, **36**, 395-405.

Hirsch, M.J. (1963) Changes in astigmatism during the first eight years of school, an interim report from Ojai longitudinal study. *American Journal of Optometry & A.A.A.O.*, **40**, 127-132.

Hirsch, M.J. (1964) The longitudinal study in refraction. *American Journal of Optometry & A.A.A.O.*, **41**, 137-141.

370

Hirsch, M.J. (1966) Summary of current research on refractive anomalies. *American Journal of Optometry & A.A.A.O.*, 43, 755-762.

Hogan, R.E. (1985) Aspects of Tonic Accommodation and Tonic Vergence. Ph.D. Thesis, Aston University, Birmingham.

Holden, B.A. (1970) *The Development and control of Myopia and the Effects of Contact Lenses on Corneal Topography*. Ph.D. Thesis, The City University, London. Cited by Watkins (1972).

Hoogerheide, J., Rempt, F. and Hoogenboom, W.P.H. (1971) Acquired myopia in young pilots. *Ophthalmologica (Basel)*, 163, 209-215.

Howcroft, M.J. and Parker, J.A. (1977) Aspheric curvatures for the human lens. *Vision Research*, 17, 1217-1223.

Howland H.C. (1982) Infant eyes: optics and accommodation. *Current Eye Research*, 2, 217-224.

Howland, H.C., Atkinson, J., Braddick, O. and French, J. (1978) Infant astigmatism measured by photorefraction. *Science (New York)*, 202, 331-333.

Howland, H.C. and Sayles, N. (1984) Photorefractive measurements of astigmatism in infants and young children. *Investigative Ophthalmology and Visual Science*, 25, 93-102.

Howland, H.C. and Sayles, N. (1985) Photokeratometric and photorefractive measurements of astigmatism in infants and young children. *Vision Research*, 25, 73-81.

Huggert, A. (1948) On the form of the iso-indicial surfaces of the human crystalline lens. *Acta Ophthalmologica Supplement*, 30, 1-126.

Ingram, R.M. and Barr, A. (1979) Changes in refraction between the ages of 1 and $3\frac{1}{2}$ years. *British Journal of Ophthalmology*, 63, 339-342.

Ivanhoff, A. (1956) About the spherical aberration of the eye. *Journal of the Optical Society of America*, 46, 901-903.

Jaeger, G. (1952) Tiefenmesserung der menschlichen vorderkrammer mit plan - parallelen platten. *Albrecht von Graefes Archiv fur Klinische und Experimentelle Ophthalmologie*, 153, 120-131.

Janisse, M.P. (1973) *Pupillary Dynamics and Behaviour*. Plenum Press, New York.

Jansson, F. (1963a) Measurements of intraocular distances by ultrasound and comparison between optical and ultrasonic determinations of the depth of the anterior chamber. *Acta Ophthalmologica*, 41, 25-61.

Jansson, F. (1963b) Measurements of intraocular distances by ultrasound. *Acta Ophthalmologica Supplement*, 74, 1-51.

Jansson, F. and Kock, E. (1962) Determination of the velocity of ultrasound in human eyes and vitreous. *Acta Ophthalmologica*, 40, 420-433.

371

Jansson, F. and Sundmark, E. (1961) Determination of the velocity of ultrasound in ocular tissues at different temperatures. *Acta Ophthalmologica* , 39, 899-910.

Javal, E. (1890) *Memoires d'Ophtalmologie*. Paris, Masson. Cited by Ludlam and Wittenberg (1966a).

Jay, B.S. (1962) The effective pupillary area at varying perimetric angles. *Vision Research*, 1, 418-424.

Jenkins, T.C.A. (1963) Aberrations of the eye and their effects on vision. Part 1. *British Journal of Physiological Optics*, 20, 59-91.

Jennings, J.A.M. and Charman, W.N. (1978) Optical image quality in the human eye. *American Journal of Optometry and Physiological Optics*, 55, 582-590.

Jennings, J.A.M. and Charman, W.N. (1981) Off-axis image quality in the peripheral retina. *Vision Research*, 21, 445-455.

Juillerat, G. and Koby, F.E. (1928) Determination de l'epaisseur de la cornee sur la vivant aumoyen de la lampe a fente. *Revue Generale d'Ophtalmologie*, 42, 203-227. Cited by Von Bahr (1948).

Kabe, S. (1968) Improvement of infra-red phakometer. *Japanese Journal of Ophthalmology*, 12, 146-155.

Keeny, A.H. (1951) *Chronology of Ophthalmic Development, A Lecture Series*. Thomas, Springfield, Illinois.

Kiely, P.M., Smith, G. and Carney, L.G. (1982) The mean shape of the human cornea. *Optica Acta*, 29, 1027-1040.

Kiely, P.M., Smith, G. and Carney, L.G. (1983) Menstrual cycle variations of corneal topography and thickness. *American Journal of Physiological Optics*, 60, 822-829.

Kiely, P.M., Smith, G. and Carney, L.G. (1984) Meridional variations of corneal shape. *American Journal of Physiological Optics*, 61, 619-626.

Knapp, H. (1860) *Die Krummung der Hornhaut des Menschlichen Auges*, Heildelberg. Cited by Ludlam and Wittenberg (1966b)

Knoll, H.A. (1961a) Corneal contours in the general population as revealed by the photokeratoscope. *American Journal of Optometry & A. A. A. O.*, 38, 389-397.

Knoll, H.A. (1961b) Photokeratoscopy and corneal contours. In *Encyclopedia of Contact Lens Practice*, 9th supplement, Vol. II, Ch. VII. International Optics Publishing Co., Indiana.

Knoll, H.A. (1980) Position of the corneal apex in the normal eye. *American Journal of Physiological Optics*, 57, 124-125.

Knoll, H.A., Stimson, R.L. and Weeks, C.L. (1957) New photokeratoscope utilising a hemispherical object surface. *Journal of the Optical Society of America*, 47, 221-222.

Kooijman, A.C. (1983) Light distribution on the retina of a wide-angle theoretical eye. *Journal of the Optical Society of America*, 73, 1544-1550.

Koomen, M., Tousey, R. and Scolnik, R. (1949) The spherical aberration of the eye. *Journal of the Optical Society of America*, **39**, 370-376.

Kruse-Hansøn, F. (1971) A clinical study of the normal human central corneal thickness. *Acta Ophthalmologica*, **49**, 82-88.

Kronfield, P.C. and Devney, C. (1931) Ein beitung zur kentis der refraktionskurve. *Albrecht von Graefes Archiv fur Klinische und Experimentelle Ophthalmologie*, **126**, 487-501.

Kuck, J.F.R. (1970) Chemical constituents of the lens. In Graymore, C.N. (Ed) Biochemistry of the eye, Ch. 3, pp 183-371. Academic Press, London.

Lancaster, W.B. (1943) Terminology in ocular motility and allied subjects. *American Journal of Ophthalmology*, **26**, 122-132.

Larsen, J.S. (1971a) The sagittal growth of the eye. I. Ultrasonic measurement of the depth of the anterior chamber from birth to puberty. *Acta Ophthalmologica*, **49**, 239-262.

Larsen, J.S. (1971b) The sagittal growth of the eye. II. Ultrasonic measurement of the axial diammeter of the lens and anterior segment from birth to puberty. *Acta Ophthalmologica*, **49**, 427-440.

Larsen, J.S. (1971c) The sagittal growth of the eye. III. Ultrasonic measurement of the posterior segment from birth to puberty. *Acta Ophthalmologica*, **49**, 441-453.

Larsen, J.S. (1971d) The sagittal growth of the eye. IV. Ultrasonic measurement of the axial length from birth to puberty. *Acta Ophthalmologica*, **49**, 873-886.

Larsen, J.S. (1979) Axial length of the emmetropic eye and its relation to head size. *Acta Ophthalmologica*, **57**, 76-83.

Leary, G.A., Sorsby, A., Richards, M.J. and Chaston, J. (1963) Ultrasonographic measurement of the components of ocular refraction in life. Part 1 - technical considerations. *Vision Research*, **3**, 487-498.

Leary, G.A. and Young, F.A. (1968) A set of equations for computing the components of ocular refraction. *American Journal of Optometry & A. A. A. O.*, **45**, 743-759.

Le Grand, Y. (1967) *Form and Space Vision* (trans. Millodot, M. and Heath, C.G.). Indiana U.P., Bloomington.

Le Grand, Y. and El Hage, S.G. (1980) *Physiological Optics*. Springer-Verlag, Berlin.

Leibowitz, H.W. and Owens, D.A. (1975) Anomalous myopias and the intermediate dark focus of accommodation. *Science*, **189**, 646-648.

Levene, J.R. (1965) The true inventors of the keratoscope and photo-keratoscope. *British Journal of Historical Science*, **2**, 324-342. Cited by Bennett and Rabbetts (1984).

Lindsted, F. (1916) Uber messungen der tiefe des vorderen augenkammer mittels eines neven far klinischen gebraush bestimmten instruments. *Archiv fur Augenheilkunde*, **80**, 104-167. Cited by Stenstrom (1953).

Littman, H. (1951) Grundlegende betrchtungen zur ophthalmometrie. *Albrecht von Graefes Archiv fur Klinische und Experimentelle Ophthalmologie*, **133**, 152-156. Cited by Clark (1973a).

Lobeck, G. (1937) Uber den durchmesser der netzhautgefasse am gesuden und kranken menschen. *Albrecht von Graefes Archiv fur Klinische und Experimentelle Ophthalmologie*, **151**, 249-274. Cited by Goldmann (1968).

Long, W.F. (1974) A mathematical analysis of multi-meridional refractometry. *American Journal of Optometry and Physiological Optics*, **51**, 260-263.

Loper, L. (1959) The relationship between angle lambda and the residual astigmatism of the eye. *American Journal of Optometry & A. A. A. O.*, **36**, 365-377.

Lotmar, W, (1971) Theoretical eye model with aspherics. *Journal of the Optical Society of America*, **61**, 1522-1529.

Lotmar, W. and Lotmar, T. (1974) Peripheral astigmatism in the human eye: experimental data and theoretical model predictions. *Journal of the Optical Society of America*, **64**, 510-513.

Lowe, R.F. (1966) New instruments for measuring anterior chamber depth and corneal thickness. *American Journal of Ophthalmology*, **62**, 7-11.

Lowe, R.F. (1968) Time amplitude ultrasonography for ocular biometry. *American Journal of Ophthalmology*, **66**, 913-918.

Lowe, R.F. (1969) Central corneal thickness. *British Journal of Ophthalmology*, **53**, 824-826.

Lowe, R.F. (1970) Aetiology of the anatomical basis of primary angle closure glaucoma. *British journal of Ophthalmology*, **54**, 161-169.

Lowe, R.F. and Clark, B.A.J. (1973a) Posterior corneal curvature. Correlations in normal eyes and in eyes involved with primary angle-closure glaucoma. *British Journal of Ophthalmology*, **57**, 464-470.

Lowe, R.F. and Clark, B.A.J. (1973b) Radius of curvature of anterior lens surface. Correlations in normal eyes and in eyes involved with primary angle-closure glaucoma. *British Journal of Ophthalmology*, **57**, 471-474.

Lowenstein, O. and Lowenfeld, I.E. (1958) Electronic pupillometry: a new instrument and some clinical applications. *Archives of Ophthalmology*, **59**, 352-363.

Lowenstein, O. and Lowenfeld, I.E. (1969) The pupil. In Davson, H. (Ed) *The Eye*, Vol. 3, Ch.9, pp 255-337. Academic Press, New York.

Ludlam, W.M. (1967) Human experimentation and research on refractive state; an evaluation of in vivo ocular component metrology. In Hirsch, M.J. (Ed) Synopsis of the refractive state of the eye. *American Academy of Optometry*, Vol. 5, Ch. 3, pp 13-25, Burgess, Minneapolis.

Ludlam, W.M. and Giglio, E.J. (1966) Ultrasound - a diagnostic tool for examination of the eye. *American Journal of Optometry & A.A.A.O.*, **43**, 687-731.

Ludlam, W.M., Weinberg, S.S, Twarowski, C.J. and Ludlam, D.P. (1972) Comparison of cycloplegic and non-cycloplegic ocular component measurement in children. *American Journal of Optometry & A.A.A.O.*, **49**, 805-818.

Ludlam, W.M. and Wittenberg, S. (1966a) The effect of measuring corneal toroidicity with reference to the line of sight. *British Journal of Physiological Optics*, **23**, 178-185.

Ludlam, W.M. and Wittenberg, S. (1966b) Measurements of the ocular dioptric elements utilising photographic methods. Part II. Cornea - theoretical considerations. *American Journal of Optometry & A.A.A.O.*, **43**, 249-267.

Ludlam, W.M., Wittenberg, S. and Rosenthal, J. (1965) Measurements of the ocular dioptric elements utilising photographic methods. Part I. Errors analysis of Sorsby's photographic ophthalmophakometry. *American Journal of Optometry & A.A.A.O.*, **42**, 394-416.

Ludlam, W.M. and Wittenberg, S., Rosenthal, J. and Harris, G. (1967) Photographic analysis of the ocular dioptric elements. Part III. The acquisition, storage, retrieval and utilization of primary data in photokeratoscopy. *American Journal of Optometry & A.A.A.O.*, **44**, 276-296.

Luyckx-Bacus, J. (1966) Mesure des composantes optiques de l'oeil du nouveau-ne pour echographie ultrasonique. *Archives d'Ophtalmologie (Paris)*, **26**, 159-170. Cited by Larsen (1971c).

Luyckx-Bacus, J. and Delmarcelle, Y. (1969) Influence des alterations biometries du cristallin sur la profondeur de la chambre anterieure. *Bulletin de la Societe Belge d'Ophtalmologie*, **152**, 507-513. Cited by Weekers et al (1973).

Luyckx-Bacus, J. and Weekers, J. (1966) Etude biometrique de l'oeil humain par ultrasonographie. I. Les ametropies. *Bulletin de la Societe Belge d'Ophtalmologie*, **143**, 552-567. Cited by Weekers et al. (1973).

Lyle, W.M. (1971) Changes in corneal astigmatism with age. *American Journal of Optometry & A.A.A.O.*, **48**, 467-478.

Maddock, R.J., Millodot, M., Leat, S. and Johnson, C.A. (1981) Accommodation responses and refractive error. *Investigative Ophthalmology and Visual Science*, **20**, 387-391.

Mandell, R.B. (1960) Jesse Ramsden: an inventor of the ophthalmometer. *American Journal of Optometry & A. A. A. O.*, **37**, 633-638.

Mandell, R.B. (1962a) Reflection point ophthalmometry: a method to measure corneal contour. *American Journal of Optometry & A. A. A. O.*, **39**, 513-537.

Mandell, R.B. (1962b) Methods to measure the peripheral corneal curvature. Part 3: Ophthalmometry. *Journal of the American Optometric Association*, **33**, 889-892.

Mandell, R.B. (1964) Corneal areas utilised in ophthalmometry. *American Journal of Optometry & A. A. A. O.*, **41**, 150-153.

Mandell, R.B. (1965) Contact Lens Practice: Basic and Advanced. Thomas, Springfield, Illinois.

Mandell, R.B. (1967) Corneal contour of the human infant. *Archives of Ophthalmology*, 77, 345-348.

Mandell, R.B. (1969) Reply to comments by Ludlam (1969) on Mandell and St Helen (1969). *American Journal of Optometry & A. A. A. O.*, 46, 768-772.

Mandell, R.B. and Polse, K.A. (1969) Keratokonus: spatial variation of corneal thickness as a diagnostic test. *Archives of Ophthalmology*, 82, 182-187.

Mandell, R.B. and St. Helen, R. (1968) Stability of the corneal contour. *American Journal of Optometry & A. A. A. O.*, 45, 797-806.

Mandell, R.B. and St. Helen, R. (1969) Position and curvature of the corneal apex. *American Journal of Optometry & A. A. A. O.*, 46, 25-29.

Mandell, R.B. and St. Helen, R. (1971) Mathematical model of corneal contour. *British Journal of Physiological Optics*, 26, 183-197.

✳ MARCHAND (1978) [SEE BOTTOM OF PAGE]

Martola, E.L. and Baum, J.L. (1968) Central and peripheral corneal thickness. A clinical study. *Archives of Ophthalmology*, 79, 28-30.

Mattheissen, L. (1902) Uber aplanatische brechung und spiegelung in oberflachen zweiter ordnung und die hornhautrefraction. *Pfluger's Archiv fur die gesamte Physiology*, 91, 295-309. Cited by Ludlam and Wittenberg (1966b).

Maurice, D.M. (1957) The structure and transparency of the cornea. *Journal of Physiology (London)*, 136, 263-286.

Maurice, D.M. (1967) The use of flourescein in ophthalmological research. *Investigative Ophthalmology*, 6, 464-477.

Maurice, D.M. and Giardini, A.A. (1951) Optical apparatus for measuring the corneal thickness and average thickness of the human cornea. *British Journal of Ophthalmology*, 35, 169-177.

McBrien, N.A. (1986) Tonic accommodation and refractive error. *Ophthalmic and Physiological Optics*, 6, 443.

McBrien, N.A. and Barnes, D.A. (1984) A review and evaluation of theories of refractive error development. *Ophthalmic and Physiological Optics*, 4, 201-213.

McBrien, N.A. and Millodot, M. (1985) Clinical evaluation of the Canon Autoref R-1. *American Journal of Optometry and Physiological Optics*, 62, 786-792.

McBrien, N.A. and Millodot, M. (1986a) The effect of refractive error on the accommodative response gradient. *Ophthalmic and Physiological Optics*, 6, 145-149.

McBrien, N.A. and Millodot, M. (1986b) Amplitude of accommodation and refractive error. *Investigative Ophthalmology and Visual Science*, 27, 1187-1190.

Millodot, M. (1976) The influence of age on the chromatic aberration of the eye. *Albrecht von Graefes Archiv fur Klinische und Experimentelle Ophthalmologie*, 198, 235-243.

— MARCHAND, E. (1978) *Gradient index optics*, ACADEMIC PRESS, NEW YORK.

376

Millodot, M. (1981) Effect of ametropia on peripheral refraction. *American Journal of Optometry and Physiological Optics*, **58**, 691-695.

Millodot, M. (1984) Peripheral refraction in aphakic eyes. *American Journal of Optometry and Physiological Optics*, **61**, 586-589.

Millodot, M. and Lamont, A. (1974) Refraction in the periphery of the eye. *Journal of the Optical Society of America*, **64**, 110-111.

Millodot, M. and O'Leary, D. (1978) The discrepency between retinoscopic and subjective measurements: effect of age. *American Journal of Optometry and Physiological Optics*, **55**, 309-316.

Mishima, S. (1968) Corneal thickness. *Survey of Ophthalmology*, **13**, 57-96. Cited by Watkins (1972).

Mishima, S. and Hedbys, B.O. (1968) Measurement of corneal thickness with with the Haag-Streit Pachometer. *Archives of Ophthalmology*, **80**, 710-713.

Mohindra, I. and Held, R. (1981) Refraction in humans from birth to five years. *Documenta Ophthalmologica Proceedings Series*, 28, 19-27.

Mohindra, I., Held, R., Gwiazda, J. and Brill, S. (1978) Astigmatism in infants. *Science (New York)*, **202**, 329-331.

Mundt, G.H. and Hughes, W.F. (1956) Ultrasonics in ocular diagnostics. *American Journal of Ophthalmology*, **41**, 488-498.

Nakajima, A. (1955) Practicable methods of phakometry. *Acta Societatis Ophthalmologicaea Japonicae*, **59**, 783-790.

Nakajima, A. (1968) Refractive elements of the eye as metric traits. *Acta Societatis Ophthalmologicaea Japonicae*, **72**, 2059-2082.

Nakao, S., Fujimoto, S., Nagata, R. and Iwata, K. (1968) Model of the refractive index distribution in the rabbit crystalline lens. *Japanese Journal of Clinical Ophthalmology*, **23**, 903-906.

Nakao, S., Mine, K., Nishioka, K. and Kamiya, S. (1969a) The distribution of refractive indices in the human crystalline lens. *Japanese Journal of Clinical Ophthalmology*, **23**, 41-44.

Nakao, S., Ono, T., Nagata, R. and Iwata, K. (1969b) The distribution of refractive indices in the human crystalline lens. *Japanese Journal of Clinical Ophthalmology*, **23**, 903-906.

Nordensen, E. (1883) Recherches ophthalmometriques sur l'astigmatism de la cornee chez les ecoliers de sept a vingt ans. *Annales d'Oculistique (Paris)*, **89**, 110-138. Cited by Reading (1972).

Nordensen, J.W. (1943) Some remarks on Fincham's capsular theory of accommodation. *British Journal of Ophthalmology*, **27**, 127-131.

Nordensen, J.W. (1956) Annaherungskurven fur schitte der vorderen hornhautflache. *Albrecht von Graefes Archiv fur Klinische und Experimentelle Ophthalmologie*, **157**, 528-533. Cited by Ludlam and Wittenberg (1966b).

Noto, F. (1961) Form of the anterior corneal surface. *Acta Societatis Ophthalmologicae Japonicae*, **65**, 447-468.

Nover, A. and Grote, W. (1965) Uber die bestimmung der achsellage des menschlichen auges mit ultraschall am lebenden. *Albrecht von Graefes Archiv fur Klinische und Experimentelle Ophthalmologie*, **168**, 405-418. Cited by Larsen (1971c).

Obrig, T. (1957) Contact Lenses, 3rd ed., Chilton, Philadelphia.

Oksala, A. and Lehtinen, A. (1957) Diagnostics of detachment of the retina by means of ultrasound. *Acta Ophthalmologica*, **35**, 461-467.

Oksala, A. and Lehtinen, A. (1958) Measuremen of the velocity of sound in some parts of the eye. *Acta Ophthalmologica*, **36**, 633-639.

O'Leary, D. and Millodot, M. (1978) The discrepancy between retinoscopic and subjective measurements: effect of light polarisation. *American Journal of Optometry and Physiological Optics*, **55**, 553-556.

Olsen, T.and Ehlers, N. (1984) The thickness of the human cornea as determined by the specular method. *Acta Ophthalmologica*, **62**, 859-871.

Olsen, T., Nielson, C.B. and Ehlers, N. (1980) On the optical measurement of corneal thickness. II. The measuring conditions and sources of error. *Acta Ophthalmologica*, **58**, 975-984.

Otsuku, J., Tokoro, T. and Kabe, S. (1965) Infra-red phakometry. *Acta Societatis Ophthalmologicae Japonicae*, **69**, 970-986.

Park, G.E. (1936) An investigationof the angular relation of the visual (visierline) and optic (corneal) axes of the eye. *American Journal of Ophthalmology*, **19**, 967-974.

Parker, J.A. (1972) Aspheric optics of the human lens. *Canadian Journal of Ophthalmology*, **7**, 780-782.

Patnaik, B. (1967) A photographic study of accommodative mechanisms: changes in the lens nucleus during accommodation. *Investigative Ophthalmology*, **6**, 601-611.

Peter, R. (1924) Ueber die cornea - grosse und ihre verebung. *Albrecht von Graefes Archiv fur Klinische und Experimentelle Ophthalmologie*, **115**, 29. Cited by Borish (1970).

Phillips, R.A. (1952) Changes in corneal astigmatism. *American Journal of Optometry & A. A. A. O.*, **27**, 379-380.

Polyak, S.L. (1941) *The Retina*. University of Chicago Press.

Pomerantzeff, O., Fish, H., Govignon, J. and Schephens, C.L. (1971) Wide angle optical model of the human eye. *Annals of Ophthalmology*, **3**, 815-819.

Pomerantzeff, O., Fish, H., Govignon, J. and Schephens, C.L. (1972) Wide angle optical model of the human eye. *Optica Acta*, **19**, 387-388.

Pomerantzeff, O., Pankratov, M., Wang, G. and Dufault, P. (1984) Wide-angle optical model of the eye. *American Journal of Optometry and Physiological Optics*, **61**, 166-176.

Rabin, J., Van Sluyters, R.C. and Malach, R. (1981) Emmetropization: a vision dependent phenomenon. *Investigative Ophthalmology and Visual Science*, **20**, 561-564.

Raeder, J.G. (1922) Untersuchung uber die lage und dicke der linse im menslichen auge bei physiologen und patologischen zustanden, nach einer neuen methode gemessen. *Albrecht von Graefes Archiv fur Klinische und Experimentelle Ophthalmologie*, **110**, 73-108. Cited by Larsen (1971a).

Ramsdale, C. (1982) *Studies into some aspects of accommodation and convergence.* Ph.D. Thesis, University of Manchester.

Reading, V.M. (1972) Corneal curvatures. *Contact Lens Journal*, **3**, 23-25.

Reeves, P. (1918) Rate of pupillary dilation and contraction. *Psychological Review*, **25** 330-340.

Rempt, F., Hoogerheide, J. and Hoogenboom, W.P.H. (1971) Peripheral retinoscopy and the skiagram. *Ophthalmologica (Basel)*, **162**, 1-10.

Rosenfield, M. and Gilmartin, B. (1987) Effect of near-vision task on the response AC/A of a myopic population. *Ophthalmic and Physiological Optics*. **7**, 225-233.

Rubin, M. (1975) *Contact lens practice, visual, therapeutic and prosthetic*, 1st ed., Balliere Tindall, London.

Rushton, J. (1938) Clinical measurement of the axial length of the living eye. *Transactions of the Ophthalmological Societies of the United Kingdom*, **58**, 138-140.

Saladin, J.J. (1978) Television pupillometry via digital time processing. *Investigative Ophthalmology and Visual Science*, **17**, 702-705.

Saunders, H.J. (1981) Age-dependence of human refractive errors. *Ophthalmic and Physiological Optics*, **1**, 159-174.

Saunders, H.J. (1982) Corneal power and visual error. *Ophthalmic and Physiological Optics*, **2**, 37-45.

Saunders, H.J. (1986) A longitudinal study of the age dependence of human ocular refraction. I. Age-dependant changes in the equivalent sphere. *Ophthalmic and Physiological Optics*, **6**, 39-46.

Scammon, R.E. and Wilmer, H.A. (1950) Growth of the components of the human eyeball. *Archives of Ophthalmology*, **43**, 599-633.

Scheiner, C. (1619) *Oculus Sive Fundamentum Opticum*. Innsbruck. Cited by Ludlam (1967).

Scheimpflug, T. (1906) Der photoperspectograph and seine anwendung. *Photographische Korrespondenz*, **43**, 516 Cited by Brown (1972).

Shipley, T. and Rawlings, S.C. (1970) The nonius horopter - II. An experimental report. *Vision Research*, **10**, 1263-1299.

Slataper, F.J. (1950) Age norms of refraction and vision. *Archives of Ophthalmology*, **43**, 466-481.

Smith, J.W. (1969) The transparency of the corneal stroma. *Vision Research*, **9**, 393-396.

Smith, W.J. (1966) *Modern Optical Engineering: The Design of Optical Systems.* McGraw - Hill, New York.

Solomons, H. (1977) Kinematics of the extra-ocular muscles. Part 1 - Matrix representation of eye rotations. *The Opthalmic Optician*, **17**, 10-14.

Spooner, J.J.D. (1957) Refractive error as problems in growth and form. *British Journal Physiological Optics*, **14**, 127-137.

Sorsby, A. (1948) X-ray measurement of the diameters of the living eye. In Sorsby, A. (ed) *Modern Trends in Ophthalmology*, Vol. II, pp 103-110. Butterworth, London.

Sorsby, A. (1967) The nature of spherical refractive errors. In *Report of the Workshop on Refractive Anomalies of the Eye*. N.I.N.D.B. Monograph No.5, U.S. Department of Health, Education and Welfare, Washington, D.C..

Sorsby. A. and Benjamin, B. (1973) Modes of inheritance of errors of refraction. *Journal of Medical Genetics*, **10**, 161-164.

Sorsby. A., Benjamin, B. and Bennett, A.G. (1981) Steiger on refraction: a reappraisal. *British Journal of Ophthalmology*, **65**, 805-811.

Sorsby, A., Benjamin, B., Davey, J.B., Sheridan, M. and Tanner, J. M. (1957) Emmetropia and its aberrations. Medical Research Council Special Report Series No. 293, HMSO, London.

Sorsby, A., Benjamin, B. and Sheridan, M. (1961) Refraction and its components during growth of the eye from the age of three. Medical Research Council Special Report Series No. 301, HMSO, London.

Sorsby, A. and Leary, G.A. (1970) A longitudinal study of refraction and its components during growth. Medical Research Council Special Report Series No. 309, HMSO, London.

Sorsby, A., Leary, G.A. and Richards, M.J. (1962a) Correlation ametropia and component ametropia. *Vision Research*, **2**, 309-313.

Sorsby, A., Leary, G.A., Richards, M.J. and Chaston, J. (1963) Ultrasonographic measurement of the components of ocular refraction in life. 2. Clinical proceedures: Ultrasonic measurements compared with phakometric measurements in a series of 140 eyes. *Vision Research*, **3**, 499-505.

Sorsby, A. and O'Connor, A.D. (1945) Measurement of the diameters of the living eye by means of X-rays. *Nature (London)*, **156**, 779. Cited by Deller et al. (1947).

Sorsby, A. and Sheridan, M. (1960) The eye at birth: measurement of the principal diameters in forty-eight cadavers. *Journal of Anatomy*, **94**, 192-197.

Sorsby, A. and Sheridan, M. and Leary, G.A. (1962b) Refraction and its components in twins. Medical Research Council Special Report Series No. 303, HMSO, London.

Soper, J.W., Samson, J.W. and Girard, L.J. (1962) Corneal topography, keratometry and contact lenses. *Archives of Ophthalmology*, **67**, 753-760.

Spring, K.H. and Stiles, W.S. (1948) Apparent shape and size of the pupil viewed obliquely. *British Journal of Ophthalmology*, **32**, 347-354.

Steiger, A. (1913) *Die entstehung der spharischen refraktienen des menschlichen auges.* Karger, Berlin. Cited by Sorsby et al. (1957).

Steindorff, K. (1947) Deskriptive anatomie des auges der wirbeltiere und des menschen. *Tabulae Biologicae (Berlin)*, **22**, 166-297. Cited by Charman (1983).

Stenstrom, S. (1946) Investigation of the variation and correlation of the optical elements of human eyes [trans. (1948) Woolf, D.]. *American Journal of Optometry* Monograph 58.

Stenstrom, S. (1948a) Variation in size and shape of the eye. *Acta Ophthalmologica*, **26**, 559-567.

Stenstrom, S. (1948b) Variations and correlations of the optical components of the eye. In Sorsby, A. (Ed) Modern Trends in Ophthalmology, Vol. II, pp 87-102. Butterworth, London.

Stenstrom, S. (1953) An apparatus for the measurement of the depth of the anterior chamber based on the principle of Lindsted. *Acta Ophthalmologica*, **31**, 265-270.

Stiles, W.S. and Crawford, B.H. (1933) The luminous efficiency of rays entering the eye pupil at different points. *Proceedings of the Royal Society (London)*, **B112**, 428-450.

Stimson, R.L. (1957) Lenses for aphakics. *British Journal of Physiological Optics*, **14**, 78-89.

Stone, J. (1962) The validity of some existing methods of measuring corneal contour with suggested new methods. *British Journal of Physiological Optics*, **19**, 205-230.

Storey, J.K. and Rabie, E.P. (1983) Ultrasound - a research tool in the study of accommodation. *Ophthalmic and Physiological Optics*, **3**, 315-320.

Storey, J.K. and Rabie, E.P. (1985) Ultrasonic measurement of the transverse lens diameter during accommodation. *Ophthalmic and Physiological Optics*, **5**, 145-148.

Straub, M. (1909) Uber die aetiology der brechung-sonomalien des auges und den ursprung der emmetropie. *Albrecht von Graefes Archiv fur Klinische und Experimentelle Ophthalmologie*, **70**, 130-199.

Sulzer, D. (1892) La forme de la cornee humaine et son influence sur la vision. *Archives d'Ophtalmologie (Paris)*, **12**, 32-50. Cited by Ludlam and Wittenberg (1966b).

Tagawa, S. (1928) Uber die dispersion der brechenden medien des auges, *Archiv fur Augenheilkunde*, **99**, 587. Cited by Watkins (1972).

Taylor, S. (1977) Techniques for measuring pupil size. *Optician*, **174**, 19-20, 29.

Tomlinson, A. (1972) A clinical study of the central and peripheral thickness and curvature of the human cornea. *Acta Ophthalmologica*, **49**, 73-82.

Tomlinson, A. (1976) Contact lens and corneal topography with wear of 'softlens'. *American Journal of Physiological Optics*, **53**, 727-734.

Tomlinson, A. and Schwartz, C. (1979) The position of the corneal apex in the normal eye. *American Journal of Physiological Optics*, **56**, 236-240.

Tornqvist, R. (1953) Shallow anterior chamber in acute glaucoma. *Acta Ophthalmologica Supplement*, **39**, 1-74.

Townsley, M.G. (1967) New equipment and methods for determining the contour of the human cornea. *Contacto*, **11**, 72. Cited by Clark (1973b).

Tron, E. (1929) Variationsstatistische untersuchunge uber refraction. *Albrecht von Graefes Archiv fur Klinische und Experimentelle Ophthalmologie*, **122**, 1. Cited by Ludlam (1967).

Tron, E. (1934) Ueber die optischen grundlagen der ametropie. *Albrecht von Graefes Archiv fur Klinische und Experimentelle Ophthalmologie*, **132**, 182-223. Cited by Borish (1970).

Tschermak, A. (1942) *Introduction to Physiological Optics* [trans. Boeder, P.(1952)]. Thomas, Springfield.

Tscherning, M. (1904) Physiologic Optics [trans. Weiland, C.]. Keystone, Philadelphia.

Ulbrich, H. (1914) Messung der kammertiefe. *Klinische Monatsblatter fur Augenheilkunde*, **53**, 244. Cited by Goldmann (1968).

Van Alphen, G.W.H.M. (1961) On emmetropia and ametropia. *Ophthalmologica Supplement*, **142**, 1-92.

Van Alphen, G.W.H.M. (1967) On emmetropia and ametropia. In *Report of the Workshop on Refractive Anomalies of the Eye*. N.I.N.D.B. Monograph No.5, U.S. Department of Health, Education and Welfare, Washington, D.C.

Van Alphen, G.W.H.M. (1979) Adregenergic receptors of the ciliary muscle of the human eye. *Investigative Ophthalmology and Visual Science*, **15**, 502-505.

Van Alphen, G.W.H.M. (1986) Choroidal stress and ametropia. *Vision Research*, **26**, 723-734.

Van Den Brink, G. (1962) Measurements of the geometric aberrations of the eye. *Vision Research*, **2**, 233-234.

Van Meeteren, A. (1974) Calculations of the optical modulation transfer function of the human eye for white light. *Optica Acta*, **21**, 395-412.

Von Bahr, G. (1948) Measurements of the thickness of the cornea. *Acta Ophthalmologica (Basel)*, **26**, 247-265.

Wang, G., Pomerantzeff, O. and Pankratov, M.M. (1983) Astigmatism of oblique incidence in the human model eye. *Vision Research*, **23**, 1079-1085.

Wanko, T. and Gavin, M.A. (1958) The fine structure of the lens epithelium. *Archives of Ophthalmology*, **60**, 868-879.

Watanabe, T. and Oono, S. (1982) A solid state television pupillometer. *Vision Research*, **22**, 499-505.

Watkins, R.D. (1972) *A Finite-aperture Model of the Optical System of the Human Eye.* Ph. D. Thesis, Flinders University, Australia.

Weale, R.A. (1962) Presbyopia. *British Journal of Ophthalmology*, **46**, 660-668.

Weale, R.A. (1963) *The Aging Eye.* H.K. Lewis, London.

Weale, R.A. (1979) Sex, age and the birefringence of the human crystalline lens. *Experimental eye research*, **29**, 449-461.

Weale, R.A. (1982) *A Biography of the Eye.* H.K. Lewis, London.

Weekers, R., Delmarcelle, Y. Luyckx-Bacus, J. (1975) Biometrics of the crystalline lens. In Bellows, J.G. (Ed) *Cataract and Abnormalities of the Lens*, pp 134-147. Grune and Stratton Inc., London.

Weekers, R., Delmarcelle, Y. Luyckx-Bacus, J. and Collington, J. (1973) Morphological changes of the lens with age and cataract. *Ciba Foundation Symposium* **19**, pp 25-40. Elsevier Exerpta Medica, North Holland.

Weekers, R. and Grieten, J. (1961) Mesure de la profondeur de la chambre anterieure en clinique. *Bulletin de la Societe Belge d'Ophtalmologie*, **129**, 361-381. Cited by Larsen (1971a).

Wesley, N.K. (1969) Practical application and new concepts with the photo-electronic keratoscope. *Contacto*, **13**, 32-43.

Wittenberg, S. (1966) Appendix notes to translation of Gullstrand (1896). *American Journal of Optometry & A.A.A.O.*, **43**, 198-214.

Wittenberg, S. and Ludlam, W.M. (1970) Planar reflected imagery in photokeratoscopy. *Journal of the Optical Society of America*, **60**, 981-985.

Woodhouse, J.M. (1975) The effect of pupil size on grating detection at various contrast levels.*Vision Research*, **15**, 645-648.

Woodhouse, J.M. and Campbell, F.W. (1975) The role of the pupillery light reflex in aiding adaptation to the dark. *Vision Research*, **15**, 649-653.

Wulfeck, J.W. (1955) Infrared photography of the so-called third Purkinje image. *Journal of the Optical Society of America*, **45**, 928-930.

Yamamoto, Y., Namiki, R., Baba, M. and Kato, M. (1960) A study of the merasurement of ocular axial length by ultrasound echography. *Acta Societatis Ophthalmologicae Japonicae*, **64**, 1333-1341.

Young, F.A. (1961) The effect of restricted visual space on primate eyes. *American Journal of Ophthalmology*, **52**, 799-806.

Young, F.A. (1967) Present state of knowledge regarding mechanisms giving rise to refraction anomalies. In *Report of the Workshop on Refractive Anomalies of the Eye*. N.I.N.D.B. Monograph No.5, U.S. Department of Health, Education and Welfare, Washington, D.C.

Young, F.A. (1975) Development and control of myopia in human and subhuman primates. *Concacto*, **19**, 16-31.

Young, F.A. (1977) The nature and control of myopia. *Journal of the American Optometric Association*, **48**, 451-457.

Young, F.A. (1981) Primate myopia. *American Journal of Optometry and Physiological Optics*, **58**, 560-566.

Young, F.A. and Leary, G.A. (1972) The inheritance of ocular components. *American Journal of Optometry & A.O.O.O.*, **49**, 546-555.

Young, F.A., Leary, G.A., Baldwin, W.R., West, D.C., Box, R.A., Harris, E. and Johnson, C. (1969). The transmission of refractive errors within Eskimo families. *American Journal of Optometry & A.O.O.O.*, **46**, 676-685.

Young, F.A., Leary, G.A., Zimmerman, R.R. and Strobel, D.A. (1973). Diet and refractive characteristics. *American Journal of Optometry & A.O.O.O.*, **50**, 226-333.

Young, T. (1801) On the mechanism of the eye. *Philosophical Transactions of the Royal Society of London (Biological)*, **91**, 23-88. Cited by Millodot (1981).

Young, T. (1807) *Course of Lectures in Natural Philosophy and the Mechanical Arts*, Vol. 2, pp 588-589. Johnson, London. Cited by Charman (1983).

Zeeman, W.P.C. (1911) Linsenmessungen und emmetropisation. *Albrecht von Graefes Archiv fur Klinische und Experimentelle Ophthalmologie*, **78**, 93-128. Cited by Larsen (1971b).

Zeiss, E. (1938) Uber linsenveranderungen an herausgenommen. Rinderlinsen durch ultraschallein wirkung. *Albrecht von Graefes Archiv fur Klinische und Experimentelle Ophthalmologie*, **139**, 301-322. Cited by Leary et al. (1963).

Zinn, K.M. (1972) *The Pupil*, Thomas, Springfield, Illinois.